SPECTRUM AND POWER EFFICIENT OPTICAL OFDM FOR VISIBLE LIGHT COMMUNICATION SYSTEMS

SPECTRUM AND POWER EFFICIENT OPTICAL OFDM FOR VISIBLE LIGHT COMMUNICATION SYSTEMS

BY

RUOWEN BAI, B.Sc., M.Eng.

A THESIS

SUBMITTED TO THE DEPARTMENT OF ELECTRICAL & COMPUTER ENGINEERING

AND THE SCHOOL OF GRADUATE STUDIES

OF MCMASTER UNIVERSITY

IN PARTIAL FULFILMENT OF THE REQUIREMENTS

FOR THE DEGREE OF

DOCTOR OF PHILOSOPHY

Doctor of Philosophy (2021) McMaster University

(Electrical & Computer Engineering) Hamilton, Ontario, Canada

TITLE:	Spectrum and Power Efficient Optical OFDM for Visible Light Communication Systems
AUTHOR:	Ruowen Bai M.Eng. (Department of Electronic Engineering) Tsinghua University, Beijing, China B.Sc. (Electronic Information Science and Technology) Nankai University, Tianjin, China
SUPERVISOR:	Dr. Steve Hranilovic
NUMBER OF PAGES:	xxiv, 226

Lay Abstract

Visible light communications (VLC) integrate into the ubiquitous light-emitting diode (LED) luminaires, providing lighting and communication simultaneously. Commercially available LEDs are low-cost, simple, and have a limited modulation bandwidth. These LEDs demand that VLC orthogonal frequency division multiplexing (OFDM) modulation schemes be spectrum- and power-efficient with low complexity. Concerning these challenges, this thesis presents a novel spectrum- and power-efficient VLC OFDM scheme with low complexity. Firstly, absolute value layered asymmetrically clipped optical OFDM (ALACO-OFDM) is presented to achieve high spectral and power efficiency while requiring fewer layers. Then layered antisymmetry-constructed clipped optical OFDM (LAC-OFDM) is introduced, which requires low complexity as compared to existing layered asymmetrically-clipped optical OFDM (LACO-OFDM). Given a VLC dispersive channel, low-complexity LACO-OFDM (L-LACO) is furthermore introduced with simple equalization but generates an identical signal to the existing LACO-OFDM. Finally, for a bandlimited VLC channel, Kramers-Kronig optical OFDM (KKO-OFDM) is presented to achieve high spectral and power efficiency. The ALACO-OFDM and LAC-OFDM work in flat VLC line-of-sight links while L-LACO in VLC dispersive links and KKO-OFDM in bandlimited VLC dispersive links with simple equalizer.

Abstract

The need for wireless connectivity is ever increasing while conventional radio frequency (RF) communications are limited by the amount of available spectrum. Visible light communications (VLC) are emerging as a promising complementary to the RF wireless, thanks to the enormous available bandwidth in the visible spectrum. Moreover, VLC integrates into the ubiquitous illumination infrastructures to satisfy the need for wireless connectivity indoors.

Commercially available light-emitting diodes (LEDs) are low-cost, simple, and have a small modulation bandwidth. For the small modulation bandwidth, VLC systems must enjoy high spectral efficiency to achieve high-rate transmission. Additionally, VLC systems must have high power efficiency to help preserve the critical advantage of LEDs for illumination applications. Furthermore, since LED luminaires are constrained by cost, deployed VLC systems must be low-complexity. Indoor VLC channels are dispersive due to multipath propagation indoors and due to the limited bandwidth of the optoelectronics. However, time-domain equalization on such channels can be prohibitively expensive for long serials. These challenges motivate extensive research on optical orthogonal frequency division multiplexing (OFDM).

Given those problems and challenges, this thesis introduces novel spectrum- and

power-efficient optical OFDM modulation schemes to implement with low complexity in VLC systems. Firstly, absolute value layered asymmetrically clipped optical OFDM (ALACO-OFDM) is presented to achieve high spectral efficiency and high power efficiency with fewer layers, thus requiring low complexity. Compared to its counterparts, ALACO-OFDM can achieve higher spectral efficiency and information rate even with fewer layers.

Antisymmetry-constructed clipped optical OFDM (AC-OFDM) is then introduced as a novel low-complexity modulation scheme. To enhance the spectral efficiency and retain low-complexity, layered AC-OFDM (LAC-OFDM) is introduced, consisting of several layers of AC-OFDM signals. LAC-OFDM is shown to be less complex compared to its state-of-the-art counterparts.

Concerning a practical VLC dispersive channel, low-complexity layered ACO-OFDM (L-LACO) is introduced with simple equalization. Mathematically, L-LACO generates identical signals to the existing layered asymmetrically-clipped optical OFDM (LACO-OFDM); however, it requires only half arithmetic operations at both the transmitter and the receiver.

For a practical bandlimited VLC dispersive channel, the previous optical OFDM modulation schemes will be no longer non-negative after interpolation with $\mathrm{sinc}(t)$ pulse. This thesis presents Kramers-Kronig (KK) optical OFDM (KKO-OFDM) to enhance the spectral efficiency and power efficiency for such bandlimited VLC channels. The KKO-OFDM transmit signal is constructed to be real-valued, non-negative, and strictly bandlimited. Numerical results show that KKO-OFDM outperforms DCO-OFDM and LACO-OFDM in bandlimited VLC channels in terms of optical power efficiency.

To my family

Acknowledgments

I offer my sincere gratitude to my kind supervisor, Dr. Steve Hranilovic for his help, encouragement, and insightful comments throughout my Ph.D. study and work. I have been deeply inspired by Dr. Hranilovic's professional knowledge, insightful comments, and great ideas. Dr. Steve Hranilovic would never hesitate to spend his valuable time discussing with me and presenting our great idea. I appreciate the valuable support and kind help.

I would like to sincerely thank Dr. Tim Davidson and Dr. Shiva Kumar for serving as my supervisory committee members. I am deeply grateful for their insightful comments, professional knowledge, and kind encouragement throughout my Ph.D. research. I would like to sincerely thank Dr. Zhaocheng Wang, from Tsinghua University, for his insightful comments and kind support. I would like to sincerely thank Dr. Julian Cheng from the University of British Columbia for his professional knowledge and kind help.

I would like to sincerely thank my lab colleagues. Especially, I sincerely thank Dr. Van Thanh Pham for his valuable discussion and kind help. I sincerely thank Dr. Mohammed Mossaad for his helpful aid throughout my Ph.D. research. I sincerely appreciate the kind help from Abdallah S. Ghazy, Tau Raphael Rasethuntsa, Donghan Li, Ziqi Dou, Dr. Khaqan Majeed, Dr. Haitham S. Khallaf, Dr. Michael Taylor,

Mohamadreza Pashazanoosi, Alireza Barmaki, Mark Knez, Neelima Sreekantan Nair, Anthony Vu, and Nicholas Mateus.

I would like to sincerely thank Cheryl Gies, the graduate administrative assistant of the Department of Electrical and Computer Engineering, Tracey Coop, the accounting & academic administrative assistant, and Joe Peric, the instructional computing specialist, for their friendly accompany and kind help.

I would like to show the deepest gratitude to my parents, wife, brother, and sisters for their endless love, trust, and support. I would like to thank my family for keeping all the members closely united and connected. It is my family, friends, teachers, and people around me that shape me into whom I am now.

Contents

List of Figures

List of Tables

Abbreviations

AAO-OFDM	Asymmetrically Clipped Absolute Value Optical OFDM
AC-OFDM	Antisymmetry-Constructed Clipped Optical OFDM
ACO-OFDM	Asymmetrically-Clipped Optical OFDM
ALACO-OFDM	Absolute Value Layered ACO-OFDM
ADC	Analog-to-Digital Converter
ADO-OFDM	Asymmetrically Clipped DC-biased Optical OFDM
ASCO-OFDM	Asymmetrically and Symmetrically Clipped Optical OFDM
AVO-OFDM	Absolute Value Optical OFDM
AI	Artificial Intelligence
AWGN	Additive White Gaussian Noise
AR	Augmented Reality
BER	Bit-Error Rate
CCDF	Complementary Cumulative Distribution Function

CDF	Cumulative Distribution Function
CEO-OFDM	Clipping-Enhanced Optical OFDM
CLT	Central Limit Theorem
CP	Cyclic Prefix
CSK	Color-Shift Keying
DAC	Digital-to-Analog Converter
DC	Direct Current
DCO-OFDM	DC-biased Optical OFDM
DFT	Discrete Fourier Transform
DMT	Discrete Multitone
DSB	Double-Sideband
eACO-OFDM	Enhanced ACO-OFDM
EACO-OFDM	Enhanced ACO-OFDM
eADO-OFDM	Enhanced ADO-OFDM
EADO-OFDM	Enhanced ADO-OFDM
eU-OFDM	Enhanced U-OFDM
ePAM-DMT	Enhanced PAM-DMT
FEC	Forward Error Correction

FFT	Fast Fourier Transform
FOV	Field-of-View
FPGA	Field-Programmable Gate Array
FS	Fourier Series
GREENER-OFDM	GeneRalizEd EnhaNcEd unipolaR OFDM
HACO-OFDM	Hybrid Asymmetrically Clipped Optical OFDM
HDAP-OFDM	Hybrid DC-biased Asymmetrically clipped Pulse amplitude modulated OFDM
HLACO-OFDM	Hybrid LACO-OFDM
HS	Hermitian Symmetry
i.i.d	Independent and Identically Distributed
ICI	Inter-Carrier Interference
IDFT	Inverse Discrete Fourier Transform
IFFT	Inverse Fast Fourier Transform
IM/DD	Intensity Modulation/Direct Detection
IoT	Internet of Things
ISI	Inter-Symbol Interference

KK	Kramers-Kronig
KKO-OFDM	Kramers-Kronig Optical OFDM
L-ACO	Low-complexity ACO-OFDM
L-LACO	Low-complexity LACO-OFDM
LAC-OFDM	Layered AC-OFDM
LACO-OFDM	Layered ACO-OFDM
LCEO-OFDM	L-slots CEO-OFDM
LD	Laser Diode
LED	Light-Emitting Diode
Li-Fi	Light Fidelity
LOS	Line-of-Sight
LTE	Long Term Evolution
LPF	Low Pass Filter
MIMO	Multiple-Input/Multiple-Output
M2M	Machine-To-Machine
NLoS	Non-Line-of-Sight
NOMA	Non-Orthogonal Multiple Access
OFDM	Orthogonal Frequency-Division Multiplexing

OOB	Out-of-Band
OOK	On-Off Keying
OSNR	Optical Signal-to-Noise Ratio
OWC	Optical Wireless Communication
QAM	Quadrature-Amplitude Modulation
P/S	Parallel-to-Serial
PAM	Pulse Amplitude Modulation
PAM-DMT	Pulse-Amplitude-Modulated Discrete Multitone Modulation
PAPR	Peak-to-Average Power Ratio
PD	Photodetector
PPM	Pulse Position Modulation
PSD	Power Spectral Density
PSK	Phase-Shift Keying
RAO	Real-valued Addition Operation
RF	Radio Frequency
RMO	Real-valued Multiplication Operation
RMS	Root Mean Square
S/P	Serial-to-Parallel

SEE-OFDM	Spectrally and Energy Efficient OFDM
SFO-OFDM	Spectrally Factorized Optical OFDM
SNR	Signal-to-Noise Ratio
SSB	Single-Sideband
SSL	Solid-State Lighting
THO-OFDM	Triple-layer Hybrid Optical OFDM
THz	Terahertz
U-OFDM	Unipolar OFDM
VLC	Visible-Light Communication
VR	Virtual Reality
WDM	Wavelength Division Multiplexing
Wi-Fi	Wireless Fidelity

Chapter 1

Introduction

As new information technologies and applications arise, such as artificial intelligence (AI), the Internet-of-Things (IoT), virtual reality (VR), and augmented reality (AR), billions of mobile devices are connected, and the requirements for data transmission are escalating. According to the Cisco Annual Internet Report, it will grow to 13.1 billion mobile devices and 14.7 billion machine-to-machine (M2M) connections by 2023 [1]. This increase demands a great capacity for next-generation wireless computing and wireless communication. While conventional radio frequency (RF) communications provide an attractive solution, they are limited by the amount of available RF spectrum [2, 3]. As a consequence, optical wireless communication (OWC) has been considered as a complementary physical layer for conventional wireless communications [3]. Optical wireless communication is a type of optical communication, which leverages the huge amount of available spectrum such as infrared (IR) [4], visible light [5], or ultraviolet [6] to achieve wireless communications. Thanks to the ubiquity of LED luminaires, visible light communications (VLC) as a variant of OWC is a promising candidate for indoor wireless data transmission [2, 3].

1.1 Visible Light Communications

1.1.1 Context

Visible light communications employ the visible light spectrum between 460 THz and 790 THz (Terahertz, THz) to achieve indoor wireless data transmission [7]. This is an available bandwidth of nearly 330 THz. Visible light communications do not require any licenses worldwide, unlike conventional RF communications. In VLC systems, a light-emitting diode (LED) typically serves as the transmitter, while a photodetector (PD) serves as the receiver. LEDs are massively used in illumination thanks to their high power efficacy, long lifespan, and high colour quality [8]. LEDs are anticipated to comprise 84% of all lighting installations in The United States of America (USA) by the year 2035 [8]. Leveraging the enormous license-free optical spectrum and the ubiquity of solid-state lighting (SSL), VLC is a promising candidate for indoor situations demanding high capacity for multi-users. Power line communications (PLC) [9, 10, 11, 12, 13], power-over-Ethernet (PoE) [14, 15, 16, 17], lighting control network [18, 19, 20] are proposed as backbone networks for VLC systems to integrate into existing illumination infrastructures. In VLC systems, only the intensity of visible light is modulated to carry information and inherently does not interfere with conventional RF wireless communications. Additionally, VLC systems add a secondary communication function to the LED while simultaneously providing illumination, saving energy, and being environment-friendly. The intensity of light can be changed quickly, and the average optical power is set to a constant value such that no LED flickering will be perceptible to humans [7, 15]. Furthermore, there is no radio wave in the VLC systems compared to conventional RF wireless, which will not

cause electromagnetic pollution. Compared to conventional RF wireless, VLC systems are a more secure communication candidate, which cannot be eavesdropped on by a next-door eavesdropper since visible light will inherently not penetrate the walls of an office. While there may still exist eavesdroppers in the same room as legitimate users, secure methods such as transmit beamforming and artificial noise are proposed to enhance the secrecy rate in VLC wiretap channels [21, 22, 23, 24, 25, 26]. Compared to conventional RF wireless, VLC systems enjoy cost competitiveness since the transmitters, LEDs are less expensive than base stations employed in conventional RF wireless communication systems [7].

1.1.2 Visible Light Communication History

The first visible red LED was invented by Nick Holonyak Jr. in 1962 [27]. However, the first red LED was not sufficiently bright. In 1994, high-brightness blue LEDs were invented by Shuji Nakamura [28]. White light can be generated by coating the blue LEDs with phosphors, which is adopted in much of today's lighting industry.

The first wireless audio transmission employing VLC with white LEDs dates back to 1999 by G. Pang et al. [29]. Wireless optical communication system using white-coloured LEDs was proposed and simulated for wireless home links in the year 2000 in [30]. In 2003, M. Nakagawa *et al.* proposed to integrate power-line communication and white LED VLC systems. This integrated system was built and verified in a lab with a data rate of 1 Kb/s [31]. In 2009, D. O'Brien *et al.* verified an indoor VLC system at a rate of 100 Mb/s with a distance of 10 cm [32]. This VLC system utilized a first-order analog equalizer to expand the bandwidth to 50 MHz. Moreover, a blue filter was employed, and only the blue component of the white LED was detected

at the receiver. In 2011, J. Vučić *et al.* reported a VLC system achieving at 803 Mb/s with bit error rate (BER) below 2×10^{-3} operating at a distance of 12 cm [33]. This VLC system employed wavelength division multiplexing (WDM) and discrete multitone (DMT) modulation and utilized a RGB-type white LED. In the same year, A. M. Khalid *et al.* reported an experimental demonstration achieving 1 Gb/s with a phosphorescent white LED at a BER of 1.5×10^{-3}, which employed optimized DMT modulation and adaptive bit- and power-loading [34]. In 2012, G. Cossu *et al.* reported an experimental demonstration of a gigabit-class indoor VLC system using RGB white LEDs and leveraging DMT modulation, in which 1.5 Gbit/s with single channel and 3.4 Gbit/s by WDM transmission were demonstrated [35]. The 3-dB modulation bandwidth of an μLED is exhibited to be more than 60 MHz, much higher than the bandwidth of a conventional commercial white LED. In 2014, H. Haas *et al.* presented a VLC experiment achieving 3 Gb/s using a single μLED and employing orthogonal frequency division multiplexing (OFDM) [36]. In 2015, N. Chi *et al.* reported the highest data rate at the time of 1.6 Gb/s exploiting a cascaded pre-equalization circuit using a commercially available white phosphorescent LED [37]. In 2017, M. S. Islim *et al.* proposed a novel violet micro-LED array allowing a modulation bandwidth up to 655 MHz [38]. A transmission rate of 11.12 Gb/s was reported at the 7% FEC limit (i.e., BER = 0.0038) for an OFDM-based VLC system employing that violet micro-LED [38]. In 2019, H. Haas *et al.* demonstrated a VLC system enabling 15.73 Gb/s employing four single colour off-the-shelf commercially available LEDs working at a link-distance of 1.6 m [39]. This VLC system used forward error correction coding and the OFDM scheme with adaptive bit loading. More recently, Z. Xu *et al.* demonstrated indoor VLC systems employing off-the-shelf

red, green and blue LEDs achieving 3 Gb/s at a distance of 5 meters in 2021 [40]. The VLC systems leveraged on-off keying (OOK) modulation and imaging techniques and utilized analogue pre-equalization to extend the modulation bandwidth of the LEDs from 10 MHz to about 300 MHz [40]. In the same year, N. Chi *et al.* demonstrated an underwater VLC system employing adaptive deep-learning equalizer to tackle LED nonlinearity [41]. A data rate of 2.85 Gb/s was reported achieving a BER below 3.8×10^{-3} with reduced computation complexity [41]. In the same year, N. Chi *et al.* reported a VLC system employing InGaN/GaN-based LEDs with Si-substrate, which achieved 24.25 Gb/s transmissions using eight wavelengths at a distance of 1.2 m [42].

There is an inherent trade-off between modulation bandwidth and optical efficiency for commercially available LEDs. Additionally, the modulation bandwidth of a commercial phosphorescent LED used for illumination applications is typically several MHz [32]. In contrast, a laser diode (LD) has a high optical efficiency at high current densities and enjoys a large modulation bandwidth in the GHz range [43]. Consequently, LDs are attracting increasing interest in making the most of the visible light spectrum. In 2015, H. Haas *et al.* demonstrated an experiment employing commercially available off-the-shelf RGB-LDs achieving Gigabit-class wireless transmission and showed potential wireless access beyond 100 Gb/s considering indoor illumination constraints [43]. In 2019, D. O'Brien *et al.* reported an LD-based VLC operating over a wide area (i.e., a covering area of 39 m^2) and supporting up to 35 Gb/s data rate. This system employed four-colour multiplexed VLC transmission with a link distance of 4 m [44].

Besides these academic advancements, there are huge developments in the standards and industry, which help commercialize VLC a lot. In 2003, the visible light communications consortium (VLCC) was firstly started in Japan, working on proposing standards on VLC systems [45]. Later, Japan Electronics and Information Technology Industries Association(JEITA) presented three standards for VLC, including JEITA CP-1221 (in 2007), JEITA CP-1222 (in 2007), and JEITA CP-1223 (in 2013). In 2008, a project named as *the Home Gigabit Access* was introduced in Europe, which faces the challenge to develop VLC networks and standards [46]. Later in 2011, IEEE 802.15.7 standard was proposed for VLC systems [47]. Several VLC solution vendors worldwide include pureLiFi, Oledcomm, Outstanding Technology, Koninklijke Philips, Nakagawa Laboratories, and Nakagawa Laboratories.

1.2 Visible Light Communications Channel Model

In VLC systems, a commercially available LED is typically employed as the transmitter. Information is modulated onto the instantaneous optical intensity (i.e., intensity modulation (IM)) [3, 4, 7]. The optical intensity is well modelled as being proportional to the LED input electrical current [4]. The LED input current is required to be real-valued and non-negative. Considering the illumination requirement and dimming control, constraints are also imposed on the average amplitude of the emitted signals [3, 4, 7].

Visible light communications systems typically employ a PD as the receiver, which utilizes direct detection (DD) for simplicity. The PD generates an electrical current that is well modelled as being proportional to the effective optical power received [3, 4, 7]. Additionally, considering a quasi-static indoor environment, VLC channels

are generally assumed to be linear time-invariant (LTI) [48]. At the receiver, thermal noise and shot noise are well modelled as additive white Gaussian noise (AWGN) [4].

High-speed LEDs specifically designed for high bandwidth VLC are complex and expensive. Additionally, high-speed LDs are costly and complicated, which may also cause health concerns, i.e., irreversible injury to the skin and eye, due to laser biological effects [49]. Hence, the aforementioned high-speed LEDs and LDs in Section 1.1.2 only typically exist in the lab. The existing illumination infrastructures are generally commercially available, and affordable LEDs [8]. These commercially available off-the-shelf LEDs are less expensive and much simpler though they also have a much smaller modulation [32].

Therefore, improving spectral and power efficiency and reducing the complexity is critically essential for VLC going into people's houses soon.

1.3 Optical Orthogonal Frequency Division Multiplexing

VLC integrates into existing illumination infrastructure to provide lighting and communications simultaneously at low complexity and low cost. Visible light communications employ an IM/DD channel link, in which LED input electrical current must remain real-valued and non-negative with a constraint on the mean value. In addition, the VLC channel is dispersive due to multipath distortion from multiple reflections of light from transmitter to receiver [4, 50].

Orthogonal frequency division multiplexing (OFDM) is extensively employed as

a modulation technique in conventional radio frequency communication systems because of its resistance to inter-symbol interference (ISI) caused by dispersive channels. However, conventional OFDM cannot be employed directly in VLC systems since conventional OFDM signals are complex-valued and bipolar with an electrical power constraint. In contrast, LED input electrical current requires a real-valued and non-negative signal. Conventional OFDM has to be modified before being applied in VLC systems [51].

The Hermitian symmetry constraint is generally imposed in the frequency-domain symbol to achieve a real-valued signal in the time domain. Hence, only half of the total subcarriers are available for modulation [51]. Several methods were proposed to ensure the signal is non-negative, resulting in many optical OFDM schemes suitable for IM/DD VLC channels. This Chapter classifies these optical OFDM schemes into three main categories: *Single-layer optical OFDM*, *Dual-layer optical OFDM*, and *Multiple-layer optical OFDM*. In this thesis, the term 'layer' refers to a set of OFDM signals that are superimposed to improve the spectral efficiency of the modulation.

1.3.1 Single-layer Optical OFDM

Due to the low complexity and high spectral efficiency, the direct current (DC) biased optical OFDM (DCO-OFDM) is a popular scheme for VLC systems. In the DCO-OFDM, Hermitian symmetry (HS) is employed to generate a real-valued output of the inverse fast Fourier transform (IFFT). To make the output signal non-negative, a DC bias is added, and all the remaining negative peaks are clipped at zero [4][51]. Although spectrally efficient, DCO-OFDM requires a large DC bias that consumes much optical power. Note that the DC bias conveys no information resulting in power

inefficiency. The DC bias can also be used to help guarantee a desired illumination level [52]. In order to fit the DCO-OFDM signal into dynamic range for the LED, a clipping operation is typically done, resulting in out-of-band (OOB) distortion [53]. Alternatively, an adaptive minimum DC bias can be added to ensure non-negativity according to an OFDM symbol [54]. Although there is no OOB clipping distortion, this method may result in LED flickering for VLC systems.

Asymmetrically clipped optical OFDM (ACO-OFDM) was proposed to improve the power efficiency of ACO-OFDM at the expense of spectral efficiency [55, 56]. In ACO-OFDM, data are modulated onto odd subcarriers while the even subcarriers are set to zeros leading to the output of IFFT having an anti-symmetry. Thanks to this anti-symmetry, the negative parts can be clipped directly without any loss of information. It is shown in [55] that ACO-OFDM enjoys optical power efficiency over DCO-OFDM since no DC bias is required; however, the spectral efficiency is half as large as DCO-OFDM. In other words, ACO-OFDM sacrifices half spectral efficiency to achieve non-negative. In addition, the sharp clipping will cause OOB clipping distortion [53].

Pulse-amplitude-modulated discrete multitone modulation (PAM-DMT) was proposed in [57], in which data are modulated onto the imaginary parts of each subcarrier, leading to an anti-symmetry in the output of the IFFT. Like ACO-OFDM, clipping negative parts directly results in non-negative signals suitable for VLC channels. In addition, PAM-DMT is optically power-efficient, although its spectral efficiency is only half as large as DCO-OFDM, and there is OOB clipping distortion due to the clipping.

Unipolar OFDM (U-OFDM) was proposed in [58], which utilizes two real-valued

and non-negative samples in two adjacent OFDM frames to carry information of one sample in the original OFDM frame. The position of zero is used to indicate the sign of a sample. In this way, U-OFDM signals are real-valued and non-negative, and suitable for VLC channels. Flip-OFDM was proposed in parallel [59], in which two adjacent OFDM frames are employed to send portions of one OFDM frame depending on the sign of each sample. Similar to PAM-DMT and ACO-OFDM, U-OFDM and Flip-OFDM are optically power-efficient; however, the spectral efficiency is half as large as DCO-OFDM, and the signals are not bandlimited due to the sharp transition.

A power-efficient DCO-OFDM was proposed in [60], in which absolute value operation is employed to ensure non-negativity, unlike DCO-OFDM clipping the remaining negative peaks. At the receiver, the sign of each sample is retrieved using an iterative signs estimation algorithm (ISEA). However, high DC bias is still required, which causes power inefficiency. In addition, the proposed iterative receiver based on ISEA requires high computational complexity.

Clipping-enhanced optical OFDM (CEO-OFDM) was proposed in [61], in which a peak-power-clipped signal is transmitted using two-time slots to carry information. The clipping operation allows higher SNR thanks to using a higher modulation index while sacrificing bandwidth. In addition, it was shown that CEO-OFDM is less sensitive to the LED nonlinear transferring characteristic over other state-of-the-art OFDM. Later an L-slots CEO-OFDM (LCEO-OFDM) was proposed in [62], which transmits the clipped signal by using L time slots to improve CEO-OFDM performance further.

Although the aforementioned single-layer optical OFDM modulation schemes satisfy the non-negativity constraint, there may exist negative peaks when these modulation schemes are filtered by a low-pass filter due to the sharp transitions [53]. Alternatively, spectrally factorized optical OFDM (SFO-OFDM) was proposed in [63], which was shown to be bandwidth efficient. In SFO-OFDM, information carried is linked to the position of the roots. A bandlimited real, non-negative signal is then generated by using the autocorrelation of a complex data sequence. Though potentially high spectral efficiency, SFO-OFDM requires high complexity for a practical VLC system, which utilizes many subcarriers.

Those above single-layer optical OFDM schemes are briefly summarized and compared in the following Table 1.1.

1.3.2 Dual-layer Optical OFDM

To enhance the spectral efficiency and retain optically power-efficient at the same time, dual layers/streams of simple OFDM, such as DCO-, ACO-OFDM, PAM-DMT and U-OFDM in 1.3.1, are combined, which are termed as *Dual-layer optical OFDM* in this thesis.

Asymmetrically clipped DC-biased optical OFDM (ADO-OFDM) was proposed in [56], in which ACO-OFDM symbols are modulated onto odd subcarriers while DCO-OFDM symbols are modulated onto even subcarriers. ADO-OFDM enjoys the same spectral efficiency as DCO-OFDM; however, ADO-OFDM is more efficient in optical power thanks to employing optimal constellation combination with smaller DC bias required compared to one-stream DCO-OFDM. A novel iterative receiver

Table 1.1: Single-layer optical OFDM comparison (Spectral efficiency is with respect to DCO-OFDM, i.e., spectral efficiency of DCO-OFDM is 100%)

Modulation Scheme	**Brief Description**	**Spectral Efficiency**
DCO-OFDM [4, 51]	Adds DC bias; Clips remaining negative peaks	100%
Power-efficient DCO-OFDM [60]	Adds DC bias; Take the absolute value to meet non-negativity	100%
ACO-OFDM [55]	Modulates odd subcarriers only; Clips negative parts	50%
PAM-DMT [57]	Modulates only imaginary parts of subcarriers; Clip negative parts	50%
U-OFDM [58]	Use two OFDM frames; Sample position indicate the sign	50%
Flip-OFDM [59]	Positive and flipped negative parts transmitted in two OFDM frames;	50%
CEO-OFDM [61]	Use three OFDM frames to transmit positive parts, negative-part magnitudes, and peak-power-clipped signals	1/3
LCEO-OFDM [62]	Use $L+2$ OFDM frames to transmit positive parts, negative-part magnitudes, and peak-power-clipped signals	1/(L+2)
SFO-OFDM [63]	Root positions carry information.	100%

for ADO-OFDM was proposed in [64], in which ACO-OFDM and DCO-OFDM time-domain signals are distinguished firstly. Pairwise clipping, negative clipping, pairwise averaging are employed to reduce the effect of noise and interference caused by zero clipping in ACO-OFDM. Additionally, an optimal optical power allocation was derived ACO-OFDM component in ADO-OFDM.

Enhanced asymmetrically clipped DC biased optical OFDM (EADO-OFDM) was proposed in [65], in which ACO-OFDM symbols are modulated onto odd subcarriers while absolute valued DC biased optical OFDM (AV-DCO-OFDM) symbols are modulated onto even subcarriers. The spectral efficiency of EADO-OFDM is the same as DCO-OFDM. The DC bias required in EADO-OFDM is smaller than power-efficient DCO-OFDM, conventional DCO-OFDM and ADO-OFDM. Additionally, there is no clipping distortion in EADO-OFDM compared to DCO-OFDM and ADO-OFDM. Hence EADO-OFDM is more optical power efficient.

Enhanced ADO-OFDM (eADO-OFDM) was proposed in [66], which combines ADO-OFDM and negative ADO-OFDM (NADO-OFDM) in different time slots, i.e., time-division multiplexing to achieve various dimming levels. It was shown that eADO-OFDM could utilize the entire dynamic range of LEDs and achieve higher spectral efficiency over its conventional counterparts. An iterative receiver with interference cancellation is also employed to enhance the BER performance.

Hybrid asymmetrically clipped optical OFDM (HACO-OFDM) was proposed in [67], in which ACO-OFDM symbols are modulated onto the odd subcarriers, and PAM symbols are modulated onto the imaginary parts of the even subcarriers. The spectral efficiency of HACO-OFDM is smaller than DCO-OFDM but higher than ACO-OFDM since real parts of the even subcarrier are discarded.

Asymmetrically and symmetrically clipped optical OFDM (ASCO-OFDM) was proposed in [68]. ASCO-OFDM combines ACO-OFDM symbols modulated onto the odd subcarriers and symmetrically clipping optical OFDM (SCO-OFDM) / Flip-OFDM / U-OFDM symbols modulated onto the even subcarriers of two adjacent OFDM frames. SCO-OFDM signals using two adjacent OFDM frames carry the same information as one OFDM frame. Hence half of the even subcarriers are wasted. Theoretically, the spectral efficiency is the same as HACO-OFDM.

Asymmetrical hybrid optical OFDM (AHO-OFDM) was proposed in [69], in which either ACO-OFDM signal on odd subcarriers or PAM-DMT signal on even subcarriers is inverted. Then both signals are combined for transmission to achieve dimming control. AHO-OFDM can make the most of the dynamic range of LEDs at various dimming targets. The spectral efficiency is the same as HACO-OFDM, considering that the real parts of even subcarriers are discarded.

Asymmetrically clipped absolute value optical OFDM (AAO-OFDM) was proposed in [48]. In AAO-OFDM, ACO-OFDM symbols are modulated onto the odd subcarriers, while absolute value optical OFDM (AVO-OFDM) symbols are modulated onto the even subcarriers. In AVO-OFDM, absolute value operation is employed to ensure signal non-negative. The sign information is carried by ACO-OFDM modulated onto the odd subcarriers. It is worth noting that the sign information of AVO-OFDM signals consumes some spectral efficiency, which indicates that the spectral efficiency of AAO-OFDM can still be improved further.

Those dual-layer optical OFDM schemes are briefly compared in the following Table 1.2.

Table 1.2: Dual-layer optical OFDM comparison (Spectral efficiency is with respect to DCO-OFDM, i.e., spectral efficiency of DCO-OFDM is 100%)

Modulation Scheme	**Brief Description**	**Spectral Efficiency**
ADO-OFDM [56]	ACO-OFDM modulates odd subcarriers while DCO-OFDM modulates even subcarriers	100%
EADO-OFDM [65]	Power-efficient DCO-OFDM modulates even subcarriers while ACO-OFDM modulates odd subcarriers	100%
eADO-OFDM [66]	Transmits ADO-OFDM and NADO-OFDM in different time slots	$\approx$ 100%
HACO-OFDM [67]	ACO-OFDM modulates odd subcarriers while PAM-DMT modulates imaginary parts of even subcarriers	75%
ASCO-OFDM [68]	ACO-OFDM modulates odd subcarriers while SCO-OFDM modulates even subcarriers in two OFDM frames	75%
AHO-OFDM [69]	Replace PAM-DMT with minus PAM-DMT in HACO-OFDM with a DC bias	75%
AAO-OFDM [48]	ACO-OFDM modulates odd subcarriers while AVO-OFDM modulates even subcarriers	<100%

1.3.3 Multiple-layer Optical OFDM

To enhance the spectral efficiency and retain optically power-efficient, multiple streams of simple OFDM are combined and transmitted simultaneously, which are termed as *multiple-layer optical OFDM* in this thesis. Here, assume there are more than two layers.

Enhanced unipolar orthogonal frequency division multiplexing (eU-OFDM) was proposed in [58], which superimposes multiple depths of U-OFDM to enhance the spectral efficiency while requiring no added DC bias. A super eU-OFDM frame combines D depths of eU-OFDM for the same length, $2^D N$ where N is the number of subcarriers. In the d-th depth, each U-OFDM frame is replicated for 2^{d-1} times while N-point IFFT is required for all U-OFDM frames in all depths. As a consequence, the spectral efficiency is enhanced as big as DCO-OFDM when $D \to \infty$. It is shown in [58] eU-OFDM achieves significant electrical/optical power advantages compared to DCO-OFDM with sacrificing negligible spectral efficiency. Later, GeneRalizEd EnhaNcEd unipolaR OFDM (GREENER-OFDM) was proposed in [70], which generalize eU-OFDM for arbitrary combinations of different constellation sizes and power allocation schemes.

Enhanced PAM-DMT (ePAM-OFDM) was proposed in [71], which superimposes multiple depths of PAM-DMT signal, and no DC bias is required. The superimposition of ePAM-DMT is similar to eU-OFDM. ePAM-DMT with arbitrary power allocation factors and with arbitrary modulation order were analyzed in [71] and was demonstrated to be more electrical power efficient, however, less optical power efficient compared to conventional DCO-OFDM.

Spectrally and energy efficient OFDM (SEE-OFDM) was proposed as a multi-component/path scheme in [72]. SEE-OFDM enjoys the similar philosophy of LACO-OFDM at the transmitter; however, only one N-point FFT is required at the receiver after anti-symmetry reconstruction. Though the SEE-OFDM receiver requires less complexity compared to LACO-OFDM, its BER performance is worse due to doubled noise power for the reconstruction. A late version of SEE-OFDM was then proposed in [73], in which slicing was utilized to enhance the performance.

Layered ACO-OFDM (LACO-OFDM) was proposed in [74], in which L layers of ACO-OFDM signal are added together and transmitted simultaneously. These L ACO-OFDM layers are modulated onto disjoint sets of subcarriers, and each layer enjoys an anti-symmetry with the negative parts clipped. At the receiver, LACO-OFDM is demodulated layer by layer successively. The first layer is demodulated first because it is not distorted by any layers. Then, the clipping distortion from the first layer is estimated and removed from the received signal in the frequency domain to demodulate the second layer, the third layer, etc. There are intense research articles on LACO-OFDM, which are briefly compared and analysed in Table 1.3.

Several multi-layer OFDM schemes were proposed independently in a similar philosophy to LACO-OFDM. Asymmetrically clipped, successively decoded OFDM (AC/SD-OFDM) was proposed in [109, 110]. AC/SD-OFDM transmitter employs a single N-point IFFT for each layer while LACO-OFDM proposed in [74] employs one $N/2^{l-1}$-point IFFT for the l-th layer. In contrast, the LACO-OFDM transmitter requires less complexity. AC/SD-OFDM receiver removes the clipping distortion in the time domain, while LACO-OFDM removes clipping distortion in the frequency

Table 1.3: Recent Research on LACO-OFDM (reproduced from [75]).

Topics and Directions	**Relevant Recent Researches**
BER performance	[76] An improved receiver with residual clipping noise mitigation [77] An improved receiver using pairwise detection for noise cancellation [78] A receiver using diversity combining on both flat and frequency-selective channels [79] A diversity combining receiver achieving up to 2 dB electrical gains [80] A two-stage receiver realizing up to 2.43 dB gains [81] A multi-stage improved receiver to mitigate the clipping noise due to dynamic range of electrical and optical components
PAPR reduction	[82] Performance analysis & PAPR reduction [83] Layered/enhanced asymmetrically clipped optical single-carrier frequency-division multiplexing (L/E-ACO-SCFDM) with PAPR reduction up to 4.2 dB [84] Interleaved discrete-Fourier-transform-spread layered/enhanced ACO-OFDM (IDFTS-L/e-ACO) with PAPR reduction up to 7.5 dB [85] Cyclic shifted LACO-OFDM with PAPR reduction up to 2.5 dB
Capacity analysis	[86] Analyses, optimises and compares the achievable information rate of optical OFDM modulation schemes in an IM/DD channel with Gaussian noise [87] Proposes adaptive LACO-OFDM and analyses capacity with optimal layer [88] Analyses comparatively the capacity of unipolar OFDM schemes in Gaussian optical intensity channel [89] Analyses and optimises discrete-input continuous-output memoryless channel capacity of LACO-OFDM [53] Analyses and compares achievable rate of multi-carrier modulation schemes for bandlimited IM/DD Systems
Channel coding	[90] Pairwise coding to mitigate error propagation between layers [91] Analyses capacity and integrates forward error correction (FEC) codes to LACO-OFDM for BER improvement [92] Designs a multilayered code that trades spectral efficiency for BER improvement [93] Multilayered channel coding with experiment verification
Dimming control	[94] Dimmable LACO-OFDM with wide dimming range [95] Spatial-domain and time-domain dimming control for LACO-OFDM [96] Dimmable L/E-ACO-SCFDM [97] Dimmable reconstructed LACO-OFDM (RLACO-OFDM)
Spectrum efficient	[86, 98] Proposes ALACO-OFDM that can be more spectral efficient than LACO-OFDM with fewer layers [99] Proposes hybrid non-orthogonal multiple access (NOMA) and orthogonal multiple access (OMA) for LACO-OFDM performance improvement [100] Proposes hierarchical pre-distorted LACO-OFDM (HPD-LACO-OFDM) for NOMA performance improvement [101] Proposes flexible NOMA-based non-orthogonal hybrid optical OFDM (NOHO-OFDM) scheme
Experimental demo.	[102] Demonstrates an experiment based field-programmable gate arrays with low-complexity transmitter [100] Demonstrates a point-to-point transmission experiment [103] Demonstrates worst-case residual clipping noise power model for bit-loading in LACO-OFDM [104] Demonstrates a short-haul optical fiber link using layered/enhanced ACO-OFDM (L/E-ACO-OFDM)
Reduce complexity	[105, 72] Proposes a receiver with a single FFT sacrificing about $2-3$ dB power [102] Focuses on a high-efficient implementation from the hardware prospect and improves L/E-ACO-OFDM transmitter [106, 107] Proposes LAC-OFDM saving half arithmetic operations while achieving same BER performance as LACO-OFDM under a VLC LOS flat channel
Bandlimited signal	[108] Simulates LACO-OFDM BER performance for a strictly bandlimited VLC system [53] Analyses achievable rate of multi-carrier modulation schemes, including SEE-OFDM, and proposes filtered SEE-OFDM for bandlimited IM/DD systems

domain. AC/SD-OFDM receiver employs N-point IFFT to estimate the clipping distortion from each layer while LACO-OFDM receiver estimates the clipping distortion from the l-th layer using $N/2^{l-1}$-point IFFT. Hence, the LACO-OFDM receiver also requires less complexity. Enhanced asymmetrically clipped optical OFDM (eACO-OFDM) was proposed in [111], in which multiple depths of ACO-OFDM signals are combined. It was shown that in [111], eACO-OFDM achieves the same performance as GREENER-OFDM, and eACO-OFDM is more electrical power efficient compared to DCO-OFDM. In addition, eACO-OFDM achieves equivalent performance to DCO-OFDM for optical SNR values. Enhanced asymmetrically clipped optical OFDM (EACO-OFDM) was proposed in [112], which combines ACO-OFDM signals based on musical chords corresponding to multiple layers. With 1024-QAM modulation, EACO-OFDM was shown to achieve a 7-dB sensitivity advantage compared to DCO-OFDM.

Triple-layer hybrid optical OFDM (THO-OFDM) was proposed in [113], which combines two layers of ACO-OFDM and one layer PAM-DMT onto imaginary parts of the remaining subcarriers with the real parts discarded. It was demonstrated that THO-OFDM requires less complexity and has a 3-dB smaller PAPR compared to LACO-OFDM.

Hybrid DC-biased asymmetrically-clipped pulse-amplitude-modulated OFDM (HDAP-OFDM) was proposed in [114], in which lower-index subcarriers modulate DCO-OFDM symbols, and the remaining subcarriers modulate ACO-OFDM symbols on the odd subcarriers and modulate PAM-DMT symbols on imaginary parts of the even-index subcarriers with the real parts discarded. It was shown in [114] that HDAP-OFDM is more suitable for dimming Li-Fi systems, though not optical power

efficient due to requiring a DC bias.

Negative LACO-OFDM (NLACO-OFDM) was proposed in [115], in which positive parts of the ACO-OFDM signal are clipped in each layer. Hybrid LACO-OFDM (HLACO-OFDM) was then proposed to combine LACO-OFDM and NLACO-OFDM compromising different time slots, i.e., time-division multiplexing. It was shown that HLACO-OFDM could make the most of the dynamic range of LED and enhance spectral efficiency compared to its counterparts when achieving a dimming target.

Non-orthogonal multiple access (NOMA) based optical OFDM (NOHO-OFDM) was proposed in [101], which combines triple layers to enhance data rate. The NOHO-OFDM includes ACO-OFDM on odd subcarriers and DCO-OFDM on both odd and even subcarriers arising from NOMA. It was shown that NOHO-OFDM is superior to DCO-OFDM with respect to high power efficiency and to ACO-OFDM with respect to high spectral efficiency.

Comparison between the multiple-layer optical OFDM modulation schemes is summarized in the following Table 1.4.

1.4 Approaches to Enhance Optical OFDM BER Performance

This section introduces several approaches that enhance the BER performance of VLC systems employing the aforementioned optical OFDM schemes presented in Section 1.3.

Table 1.4: Multi-layer optical OFDM comparison (Spectral efficiency is with respect to DCO-OFDM, i.e., spectral efficiency of DCO-OFDM is 100%)

Modulation Scheme	**Brief Description**	**Spectral Efficiency**
eU-OFDM [58]	Superimposes L depths of U-OFDM to with no added DC bias.	$1-\frac{1}{2^L}$
GREENER-OFDM [70]	Generalized eU-OFDM	$1-\frac{1}{2^L}$
ePAM-OFDM [71]	Superimposes L depths of PAM-DMT with no DC bias	$1-\frac{1}{2^L}$
LACO-OFDM [74]	Superimposes L ACO-OFDM layers with no DC bias	$1-\frac{1}{2^L}$
SEE-OFDM [72]	Similar to LACO-OFDM transmitter; however, only one N-point FFT is required at the receiver	$1-\frac{1}{2^L}$
AC/SD-OFDM [109, 110]	Superimposes L ACO-OFDM layers; Bigger-size IFFT than LACO-OFDM transmitter	$1-\frac{1}{2^L}$
eACO-OFDM [111]	Independent work similar to LACO-OFDM	$1-\frac{1}{2^L}$
EACO-OFDM [112]	Independent work similar to LACO-OFDM	$1-\frac{1}{2^L}$
THO-OFDM [113]	Superimposes two-layer LACO-OFDM and PAM-DMT with no DC bias	87.5%
HDAP-OFDM [114]	Superimposes DCO-OFDM, ACO-OFDM and PAM-DMT	≈100%
HLACO-OFDM [115]	Combines LACO-OFDM and NLACO-OFDM in different time slots	$\approx 1-\frac{1}{2^L}$
NOHO-OFDM [101]	Combines ACO-OFDM and two DCO-OFDM layers	>100%

1.4.1 Clipping at Receiver for ACO-OFDM

The IM/DD VLC channel demands that the drive current of an LED be real-valued and non-negative. At the receiver, negative peaks in the received signals are results from AWGN. Hence, clipping the negative peaks at the receiver side can enhance the BER performance of an optical OFDM scheme. Clipping the negative peaks at the receiver could reduce parts of the effect of AWGN and enhance the BER performance of ACO-OFDM [116]. It was reported that approximately 25% of AWGN or about 1.25 dB electrical power of the AWGN would be reduced; hence the BER performance would be enhanced at the receiver of ACO-OFDM [116].

Remark 1. *As verified in Chapter 5, ACO-OFDM signals are not bandlimited. Hence there will exist negative peaks as well after a low-pass filter. Therefore, negative peaks of the received signals may be caused by AWGN and low-pass filtering. In a practical VLC system, this fact may decrease the gains of this method proposed in [116].*

1.4.2 Diversity Combing Receiver for ACO-OFDM

A conventional ACO-OFDM receiver detects symbols on the odd subcarriers while discarding clipping distortion falling onto even subcarriers. However, the clipping distortion also carries instructive information about the transmit signal. Employing both information carried on odd subcarriers, and even subcarriers can enhance ACO-OFDM demodulation performance. A diversity combining receiver for ACO-OFDM was proposed in [117], which combines the received signals from odd subcarriers and clipping distortion from even subcarriers with a weighting factor α. It was reported that theoretically and by simulation, up to 2.53 dB electrical gain could be achieved for a flat VLC LOS channel with AWGN.

However, it is shown in [118] that the aforementioned diversity combining ACO-OFDM is extremely sensitive to the value of the 0-th subcarrier. This value depends on the DC offset caused by biasing of the transmitter LED or the receiver PD circuit, low-frequency noise, or ambient light sources. Then, [118] proposed two novel algorithms to combat DC offset for diversity combining ACO-OFDM, which achieve the identical BER performance as the diversity combining ACO-OFDM, however, are insensitive to the value of the DC offset.

A frequency-domain diversity combining (FDDC) receiver is proposed in [119] for ACO-OFDM, which combines the received signals from odd subcarriers and clipping distortion from even subcarriers with a weighting factor β_k where k is the index number of subcarriers. The frequency-domain diversity combining (FDDC) receiver is shown to achieve better BER performance in a frequency selective channel over the aforementioned time-domain diversity combining ACO-OFDM receiver.

1.4.3 Pairwise Clipping Receiver for ACO-OFDM

Conventional ACO-OFDM receiver detects symbols using only received signals on odd subcarriers while discarding even subcarriers, which fails to exact information from even subcarriers. On the other hand, the ACO-OFDM signal has an anti-symmetry that guarantees non-negativity by clipping negative parts leading to half of the transmit samples being zero-valued. Based on this observation, [120] proposed a novel pairwise maximum likelihood receiver for ACO-OFDM to exploit the signal structure in the symbol detection fully and to enhance the BER performance. This pairwise maximum likelihood receiver fixes half of the received samples to zero by comparing each pair that enjoys anti-symmetry to mitigate some effects of noise.

This pairwise receiver outperforms the conventional ACO-OFDM receiver. Hence, simulations show the pairwise maximum likelihood receiver achieves 1.3 dB optical gain over the conventional ACO-OFDM receiver at a BER of 10^{-5} in [120].

1.4.4 Noise Filtering Receiver for Flip-OFDM

Two nonlinear noise filtering stages for the received time-domain Flip-OFDM sample were proposed in [121] to enhance the detection performance. In the first stage, a negative clipper is employed, which is similar to clipping at receiver for ACO-OFDM [116] and is shown to be able to achieve 1.25 dB electrical gain over the conventional Flip-OFDM receiver. In the second stage, a threshold-based noise filtering algorithm is employed to enhance the BER performance furthermore. After negative clipper, this threshold-based noise filtering algorithm compares two received signals inside the positive/negative subframe with the same index number to a threshold c and forces the output to three distinguish values. This threshold-based noise filtering is a generalized algorithm for pairwise clipping receiver for ACO-OFDM [120], i.e., when $c = 0$, it is the same algorithm as the pairwise clipping receiver. To conclude, it is shown that the two-stage noise filtering receiver enables to improve Flip-OFDM receiver by almost 3 dB electrical gains.

1.4.5 Iterative Receivers

Iterative Receiver for ACO-OFDM

In ACO-OFDM, signals on the even subcarriers can be viewed as data-dependent linear precoded OFDM [122]. Hence, a novel iterative receiver for ACO-OFDM is proposed to collect this additional diversity and coding gains in [122]. This novel receiver

extracts information carried by all the subcarriers and the structure of the clipping distortion. It is shown that this novel iterative receiver is based on the minimum mean square error (MMSE), which is shown to be superior over diversity combining receiver proposed in [117] and pairwise maximum likelihood (ML) receiver proposed in [120]. It was reported that SNR gain could exceed 3 dB over the conventional ACO-OFDM receiver in a non-flat frequency selectivity channel [122].

Iterative Receiver for PAM-DMT

Conventional PAM-DMT receiver detects symbols on the imaginary parts of the subcarriers while discarding the real parts on which the clipping distortion falls. However, the clipping distortion of PAM-DMT also carries information that can be extracted to enhance PAM-DMT performance. A novel iterative receiver for PAM-DMT is proposed to improve the BER performance in [123], which exploits both real and imaginary parts of all the subcarriers. It is shown that this iterative receiver improves the transmission performance by about 2 dB.

Iterative Receiver for Flip-OFDM

To achieve real-valued and non-negativity, Flip-OFDM employs Hermitian symmetry and then transmits positive parts and negative parts of a bipolar signal over two adjacent OFDM frames. The Flip-OFDM receiver detects symbols by exploiting the results of subtracting the negative subframe from the positive subframe that increases the noise variance and does not fully exploit the special structure. It is shown in [124] that the special structure of Flip-OFDM contains information and proposes

a novel iterative receiver in a similar philosophy to the iterative receiver for PAM-DMT [123]. About 2 dB electrical gain is achieved over the conventional Flip-OFDM receiver.

Iterative Receiver for eU-OFDM

Working in a similar way to iterative receiver for ACO-OFDM [122] and for Flip-OFDM [123], a novel iterative receiver for eU-OFDM is proposed in [125], which exploits the special structure of the transmit signal iteratively. It is shown that up to 3 dB gain is achieved over the conventional eU-OFDM in the high SNR regime.

Iterative Receiver for ADO-OFDM

ADO-OFDM transmits ACO-OFDM signals on the odd subcarriers and DCO-OFDM signals on the even subcarriers and is shown to be spectrum-efficient and energy-efficient [56]. ACO-OFDM signals have an anti-symmetry and are clipped at zero, leading to half samples being zeros while DCO-OFDM signals have symmetry. Conventional ADO-OFDM receiver fails to exploit this particular structure thus suffers from high noise power. A novel iterative receiver is proposed in [64], which distinguishes ACO-OFDM signals from DCO-OFDM signals in the time domain firstly. Then pairwise clipping for ACO-OFDM signal, negative clipping for ACO-OFDM and DCO-OFDM signals, and pairwise averaging for DCO-OFDM are employed in each iteration to reduce the effect of noise. In addition, an optimal optical power allocation factor is derived to enhance ADO-OFDM BER performance further.

Iterative Receiver for HACO-OFDM

HACO-OFDM transmits ACO-OFDM signals on the odd subcarriers and PAM-DMT signals simultaneously on imaginary parts of the even subcarriers. Both ACO-OFDM and PAM-DMT have an anti-symmetry and are clipped at zero to meet non-negativity, resulting in half of the samples being zeros in the time domain. Conventional HACO-OFDM receiver fails to exploit this special structure of ACO-OFDM and PAM-DMT components. An iterative receiver is proposed in [126] to enhance HACO-OFDM detection performance at the receiver. In this iterative receiver, ACO-OFDM signals and PAM-DMT signals are distinguished in the time domain firstly. Then pairwise clipping is employed to force half received samples of ACO-OFDM components and PAM-DMT components to be zero, which reduces up to half of the noise power. In addition, unequal power allocation is investigated to guarantee similar performance between ACO-OFDM and PAM-DMT signals. Simulations show that less than 3 dB electrical gains are achieved over the conventional HACO-OFDM receiver.

Iterative Receiver for LACO-OFDM

LACO-OFDM transmits L layers of ACO-OFDM signal simultaneously and detects each layer successively. Pairwise clipping can be employed to each ACO-OFDM signal layer to reduce noise and enhance LACO-OFDM performance. Therefore, an improved receiver for LACO-OFDM is then proposed in [77] to reduce noise and inter-layer interference. This improved receiver distinguishes all ACO-OFDM layers first in the time domain, and pairwise clipping is employed in each layer to fully exploit

each ACO-OFDM layer's special structure. Simulations show that the improved receiver can achieve more than 2 dB electrical gain over the conventional LACO-OFDM receiver.

1.5 Open Challenges in the Optical OFDM

LEDs are ubiquitously employed for indoor illumination, thanks to many strengths mentioned above. Visible light communications are integrating into these existing illumination infrastructures; thus, signalling design should consider the characteristics of these LEDs. The LEDs that are commercially available off-the-shelf products for illumination applications are low-cost, simple, and have an LPF property [32]. Hence, these LEDs demand optical OFDM signalling design to achieve high spectral efficiency and power efficiency and retain low computation complexity. Generally, there exists a trade-off.

1.5.1 Enhancing Spectrum Efficiency

The commercially available off-the-shelf LEDs have an LPF transferring characteristic and have a small modulation bandwidth of several MHz [32] though there exits more than 340 THz license-free visible light spectrum. However, the demand for high capacity data transmission is ever-growing, as mentioned at the beginning of this Chapter. This means VLC signalling design should have high spectral efficiency to make the most of this small modulation bandwidth to meet the high-rate transmission demand. Hence, enhancing spectrum efficiency is an essential open challenge and is a persistent pursuit for VLC OFDM systems.

1.5.2 Enhancing Power Efficiency

As aforementioned, LEDs are incredibly popular for illumination that they will comprise 84% of all lighting installations in the USA by the year 2035 [8]. The main reason behind LEDs' popularity is the high energy efficiency that helps save tremendous electrical energy and cost. In addition, saving electrical energy is positive for the Earth's environment and will help people combat climate-changing challenges [127]. Furthermore, VLC is considered a green technology, implying that data transmission should not decrease the high power efficiency of the LEDs [128]. Hence, VLC OFDM systems should integrate into the existing illumination infrastructures and be designed with high power efficiency to retain LEDs' popularity. Therefore, enhancing power efficiency is a critical open challenge for the implementation of VLC OFDM systems.

1.5.3 Decreasing Computational Complexity

To retain popularity, luminaires must be inexpensive and thus widely deployed VLC systems must remain simple. This means high computation complexity at optical OFDM transmitters should be avoided. In addition, multiple luminaires are typically sued to illuminate a room and to transmit data. The cost would be prohibitively high if complex drive electronics are utlized at each luminaire. Hence, avoiding high computation complexity that requires complex drive electronics is another significant open challenge at the luminaire.

1.5.4 Decreasing Peak-to-Average Power Ratio

Commercially available LEDs are low-cost and simple, with a narrow linear dynamic range. If signals go beyond this dynamic range, there will incur in-band nonlinear signal distortion and degrade the detected BER performance. This means large PAPR should be avoided in the signalling design. However, large PAPR is a notorious shortcoming for conventional OFDM signals. Hence, decreasing PAPR is an open challenge when modifying and redesigning conventional OFDM in VLC systems.

1.6 Thesis Layout

This thesis presents spectrum- and power-efficient optical OFDM schemes with low computational complexity and small PAPR to solve the problems and challenges mentioned above.

This thesis assumes that channel state information is known at both transmitter and receiver for simplicity since pilot symbols can be utilized to estimate channel state information. Furthermore, a standard model for noise in indoor VLC systems [4, 129] is assumed in this thesis. The noise is added to the photocurrent, which is the electric current through a photosensitive device, such as a photodiode (PD), arising from optical wireless radiation [4]. There are two main kinds of noise, including shot and thermal noise. At the receiver, photo-generated shot noise arises due to both the transmitted desired signal and the ambient light. Typically, the high-intensity shot noise results from the summation of many independent, Poisson distributed random variables. According to the central limit theorem (CLT), that summation approach a Gaussian distribution. Hence, the shot noise source in many indoor optical

wireless channels can be well modelled as signal-independent white Gaussian noise [4, 129]. Additionally, the thermal noise at the receiver can also be modelled as signal-independent Gaussian noise [4, 129]. Therefore, this thesis assumes a signal-independent Gaussian noise.

The optical signal-to-noise ratio (OSNR) is defined as the ratio between the average optical power of the signal and the standard deviation of the noise in this thesis. It was shown in [130] and [131] that the capacity bound for an optical wireless channel with optical power constraint is a function of the OSNR. Therefore, this thesis derives the BER and data rate that are a function of OSNR, e.g., (2.4.21). Additionally, for the sake of comparison with previous work, this thesis employs OSNR when carrying out Monte Carlo simulations.

This thesis is formalized according to regulations for a 'sandwich' format. The thesis layout is shown in Fig. 1.1 The body of this thesis contains four self-contained chapters. Every Chapter comprises sections of abstract, introduction, body and conclusions. An appendix is appended after the thesis body. All chapters are referenced and cite recent literature, which is listed in the order in **Bibliography** at the end of the document. The balance of this thesis is organized as follows.

Chapter 2 presents absolute value layered ACO-OFDM (ALACO-OFDM) that achieves higher spectral efficiency and higher power efficiency without any added DC bias even for fewer layers compared to its counterparts [98, 86].

In ALACO-OFDM, ACO-OFDM signals are transmitted at the first L layers, and AVO-OFDM is modulated onto the remaining subcarriers, and both signals are transmitted simultaneously. Spectral efficiency is analyzed and compared to its counterparts. Achievable information rates of ALACO-OFDM and related LACO-OFDM

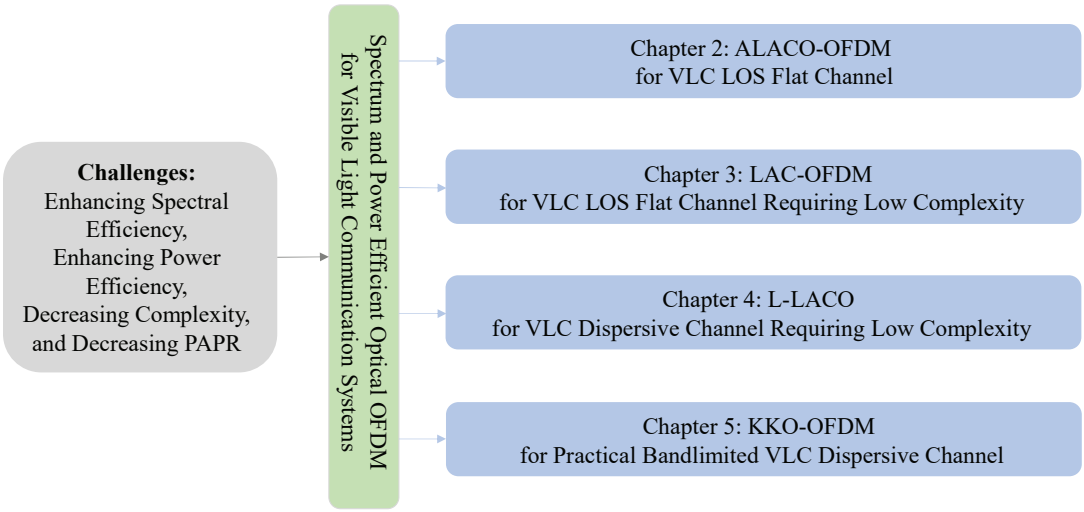

Figure 1.1: Thesis layout.

are derived theoretically. The comparison shows that ALACO-OFDM achieves higher spectral efficiency and information rate even with fewer layers than LACO-OFDM and eU-OFDM. In addition, two optical power allocation schemes over the layers of ALACO-OFDM are developed to optimize uncoded transmission performance and the achievable information rate, respectively. Furthermore, a theoretical bound on the uncoded BER of ALACO-OFDM is derived, which is verified by Monte Carlo simulation results. In terms of the peak-to-average power ratio (PAPR), ALACO-OFDM is also shown to have a lower PAPR compared to existing LACO-OFDM and eU-OFDM.

Chapter 3 introduces layered antisymmetry-constructed clipped optical OFDM (LAC-OFDM) that requires lower computational complexity than existing LACO-OFDM and eU-OFDM [107, 106].

This Chapter presents antisymmetry-constructed clipped optical OFDM (AC-OFDM) as a low-complexity optical OFDM scheme for VLC systems. In AC-OFDM,

an anti-symmetry is directly constructed in one time-domain OFDM frame. AC-OFDM is shown to achieve the same spectral efficiency and PAPR as conventional ACO-OFDM, however, is less complex to implement. LAC-OFDM is then introduced to enhance spectral efficiency, consisting of L layers of AC-OFDM signals and transmitting them simultaneously. The computational complexity of LAC-OFDM and its state-of-the-art counterparts are analyzed, showing LAC-OFDM enjoys low complexity by requiring less than half the multiplication and addition operations compared to LACO-OFDM at both the transmitter and the receiver. In addition, a theoretical BER expression for LAC-OFDM is derived theoretically, which is aligned well with simulated BER in the high SNR regime. The PAPR of LAC-OFDM and its counterparts are also evaluated and compared, which shows the PAPR of LAC-OFDM equals LACO-OFDM and is smaller than eU-OFDM with the same number of layers/streams and subcarriers. Furthermore, a pairwise iterative receiver for LAC-OFDM is introduced for LAC-OFDM to enhance power efficiency by exploiting the anti-symmetry. The computational complexity of this pairwise iterative receiver is also analyzed and compared to an existing improved receiver for LACO-OFDM. This pairwise iterative receiver can achieve better performance over an improved receiver of LACO-OFDM at the same computational complexity.

Chapter 4 presents low-complexity layered ACO-OFDM (termed as L-LACO) that generates identical signals, however, requires only half arithmetic operations compared to LACO-OFDM [75]. LAC-OFDM in **Chapter 3** works in a VLC line-of-sight flat channel and requires low computational complexity. In contrast, L-LACO works in a VLC line-of-sight flat channel and a more practical VLC dispersive channel as well, which still has low computational complexity.

L-LACO mathematically generates identical signals to LACO-OFDM; however, it requires half-size IFFT and FFT in each layer at the transmitter and receiver. LACO-OFDM classically achieves anti-symmetry in each layer by modulating data onto odd subcarriers, which requires high computational complexity. In contrast, L-LACO constructs anti-symmetry in the time domain directly. Consequently, LACO-OFDM requires nearly two times more real-valued multiplication operation (RMO) and real-valued addition operation (RAO) than the proposed L-LACO at both transmitter and receiver. It is worth mentioning that L-LACO generates an identical signal to LACO-OFDM mathematically, thus achieving the same spectral efficiency, PAPR and BER performance. However, it requires about half arithmetic operations. Additionally, the power saving thanks to the saved arithmetic operations is analyzed. Furthermore, the BER of L-LACO is simulated under a line of sight (LOS) flat channel with AWGN and under a VLC dispersive low pass filter (LPF) channel, respectively, which is shown to be identical to LACO-OFDM. Therefore, L-LACO is more suitable to low-complexity and low-cost LED luminaires employed in VLC systems due to requiring fewer arithmetic operations.

Chapter 5 introduces Kramers-Kronig Optical OFDM (KKO-OFDM) that achieves high spectral efficiency and high power efficiency for a more realistic and strictly bandlimited VLC system [108].

As discussed before, realistic VLC links are dispersive channels. Hence, the transmit signals must be strictly bandlimited such that no in-band distortion will happen. Interpolation can help generate a continuous analog signal using the discrete samples before being fed into a low pass filter. However, the previously mentioned modulation approaches, including ALACO-OFDM, LAC-OFDM, and L-LACO, will be no longer

non-negative when interpolation with sinc(t) pulse is utilized though the samples are strictly non-negative. A non-negative rectangular pulse can alternatively be used for interpolation; however, the generated analog signal will not be bandlimited. To solve these problems and challenges, in this Chapter, we directly generate bandlimited non-negative OFDM signals constrained in the mean.

In KKO-OFDM, a minimum phase single-sideband (SSB) signal is utilized to carry information, and its double-sideband (DSB) squared amplitude is used to drive an LED. Mathematically, the transmit signal is constructed to be real-valued, non-negative and strictly bandlimited, which is suitable for IM/DD VLC channels employing low-cost commercially available LEDs. The KKO-OFDM transmitter is shown to be low complexity as well and fits the low-cost, simple LEDs. KK relations are employed at the receiver to retrieve the minimum phase SSB signal phase. The required DC bias is analyzed and is compared to the complementary cumulative distribution function (CCDF) of the minimum of the signal. The average electrical SNR and BER are analyzed based on the first-order Taylor series approximation, supported by Monte Carlo simulations. The information rate is approximated by a closed-form, which is aligned well with mutual information numerical results. KKO-OFDM achieves the same spectral efficiency as DCO-OFDM, however, realizes about 1 dB optical gain at a BER= 10^{-4} in a VLC line-of-sight (LOS) channel and realizes about 1.3 dB optical gain over DCO-OFDM in a VLC dispersive LPF channel.

In **Chapter 6**, conclusions are drawn for the thesis, and future research plans are outlined.

1.7 Description of Contributions to Publications

The thesis is prepared in the format of "sandwich thesis". Chapters 2 has been published in *IEEE Transactions on Communications* [86]. Chapter 3 has been published in *Optics Express* [106]. Chapter 4 is under major review in *IEEE Transactions on Green Communications and Networking* [75]. Chapter 5 has been published in *Journal of Lightwave Technology* [108]. The contribution of each of the co-authors is described below.

Chapter 2: **Absolute Value Layered ACO-OFDM for Intensity-Modulated Optical Wireless Channels**

Authors: Ruowen Bai, and Steve Hranilovic

Ruowen Bai and Dr. Steve Hranilovic came up with the idea of ALACO-OFDM during a supervisory meeting in Fall 2018. Dr. Steve Hranilovic encouraged Ruowen Bai to present the idea elaborately. Ruowen Bai designed the block diagram for ALACO-OFDM transmitter and receiver, did signal analysis, carried out Monte Carlo simulations and plotted all the figures based on valuable comments and feedback from Dr. Steve Hranilovic. Additionally, Ruowen Bai wrote a draft of ALACO-OFDM paper while Ruowen Bai and Dr. Steve Hranilovic revised and edited the draft together. This work was presented in part at the *2019 IEEE Int. Conference on Communications (ICC 2019)* [98]. All materials have been published in *IEEE Transactions on Communications* (Volume: 68, Number: 11, Pages: 7098–7110, November 2020) [86]. The copyright of the materials is held by the IEEE, which is re-used with the permission of the IEEE. This statement follows IEEE's request.

Chapter 3: **Layered antisymmetry-constructed clipped optical OFDM for**

low-complexity VLC systems

Authors: Ruowen Bai, and Steve Hranilovic

Ruowen Bai and Dr. Steve Hranilovic came up with the idea of LAC-OFDM during a supervisory meeting in Spring 2019. Ruowen Bai designed the transmitter and receiver of LAC-OFDM, did computational complexity analysis, carried out Monte Carlo simulations and plotted all the figures while receiving valuable comments and feedback from Dr. Steve Hranilovic. Additionally, Ruowen Bai wrote a draft of LAC-OFDM paper. Ruowen Bai and Dr. Steve Hranilovic revised and edited the draft together. Furthermore, Ruowen Bai and Dr. Steve Hranilovic would like to thank Prof. Zhaocheng Wang for insightful discussions and for providing sample code on an improved receiver for LACO-OFDM to aid in comparison with [77]. This work was presented in part at the *2019 IEEE Global Communications Conference (GLOBECOM 2019)* [107]. All materials have been published in *Optics Express* (Volume: 29, Number: 7, Pages: 10613–10630, March 2021) [106]. The copyright of the materials is held by IEEE and Optica (formerly OSA). All materials are re-used with the permission of IEEE and Optica. This statement is following IEEE's and Optica's requests.

Chapter 4: **Low-Complexity Layered ACO-OFDM for Power-Efficient Visible Light Communications**

Authors: Ruowen Bai, Steve Hranilovic, and Zhaocheng Wang

Ruowen Bai and Dr. Steve Hranilovic came up with the basic idea of L-LACO during a supervisory meeting in Spring 2020. Ruowen Bai designed the transmitter and receiver of L-LACO, did computational complexity analysis, carried out Monte Carlo

simulations and plotted all the figures while receiving valuable comments and insightful feedback from Dr. Steve Hranilovic and Dr. Zhaocheng Wang. Dr. Zhaocheng Wang also helped with comparing L-LACO with his previous work LACO-OFDM. Additionally, Ruowen Bai wrote a draft of LAC-OFDM paper. Ruowen Bai, Dr. Steve Hranilovic, and Dr. Zhaocheng Wang revised and edited the draft. The work in this Chapter is under major revision in *IEEE Transactions on Green Communications and Networking* [75].

Chapter 5: **Kramers-Kronig Optical OFDM for Bandlimited Intensity Modulated Visible Light Communications**

Authors: Ruowen Bai, and Steve Hranilovic

Ruowen Bai and Dr. Steve Hranilovic came up with the idea of KKO-OFDM during a supervisory meeting in Fall 2019. Ruowen Bai designed the block diagrams for KKO-OFDM transceiver, did signal analysis, carried out Monte Carlo simulations and plotted all the figures based on valuable comments and feedback from Dr. Steve Hranilovic. In addition, Ruowen Bai wrote a draft of KKO-OFDM paper while Ruowen Bai and Dr. Steve Hranilovic revised and edited the draft together. All materials have been published in *Journal of Lightwave Technology* (doi: 10.1109/JLT.2021.3110661, Sep. 2021) [108].

Chapter 2

Absolute Value Layered ACO-OFDM for Intensity-Modulated Optical Wireless Channels

Research work in this chapter appears in the following two papers [98, 86]; however, minor modifications are made according to thesis format.

- R. Bai and S. Hranilovic, "Absolute value layered ACO-OFDM for intensity-modulated optical wireless channels," in *ICC 2019 - 2019 IEEE International*

Conference on Communications (ICC), 2019, pp. 1-6.

- R. Bai and S. Hranilovic, "Absolute value layered ACO-OFDM for intensity-modulated optical wireless channels," *IEEE Transactions on Communications*, vol. 68, no. 11, pp. 7098-7110, 2020.

As pointed out in Section 1.5.1, enhancing spectral efficiency and energy efficiency is a key challenge in VLC systems using commercially available LEDs are low-cost and simple with a small modulation bandwidth. Given this problem and challenge, absolute value layered asymmetrically clipped optical OFDM (ALACO-OFDM) is introduced to enhance spectral efficiency and energy efficiency in this chapter.

In ALACO-OFDM, asymmetrically clipped optical OFDM (ACO-OFDM) modulates the first L layers while absolute value optical OFDM (AVO-OFDM) modulates the remaining subcarriers. In this way, ALACO-OFDM uses all available subcarriers to carry information while generating a real-valued and non-negative signal suitable for IM/DD VLC links. In the existing LACO-OFDM, there are still some subcarriers remaining unused. Hence, ALACO-OFDM achieves higher spectral efficiency even with fewer layers than the state-of-the-art counterparts, LACO-OFDM and eU-OFDM. Thanks to the smaller number of layers, the required computational complexity is slightly lower compared to existing LACO-OFDM. Because no explicit DC bias is added, ALACO-OFDM achieves high energy efficiency as well. Additionally, the achievable information rate of ALACO-OFDM and its counterparts are analysed, which shows ALACO-OFDM's superior over existing LACO-OFDM. Optical power allocation is optimized by convex optimization techniques to enhance the energy efficiency and information rate further. Furthermore, ALACO-OFDM is more robust to

LED non-linear transferring characteristics thanks to a lower PAPR than its counterparts, including eU-OFDM, LACO-OFDM, and ACO-OFDM.

Abstract Enhanced unipolar orthogonal frequency division multiplexing (eU-OFDM) and layered asymmetrically clipped optical OFDM (LACO-OFDM) are spectrally efficient modulation techniques for intensity modulated systems which layer multiple non-negative signals. In this paper, we propose *absolute value layered asymmetrically clipped optical OFDM* (ALACO-OFDM), which further improves the spectral efficiency while using a smaller number of layers and no explicit direct current (DC) bias. In ALACO-OFDM, asymmetrically clipped optical OFDM (ACO-OFDM) signals are sent at the first L layers and absolute value optical OFDM (AVO-OFDM) is used for the remaining subcarriers and transmitted simultaneously. Analysis indicates that ALACO- achieves higher spectral efficiency than eU- or LACO-OFDM while using a smaller number of layers. Bounds on achievable information rates of ALACO-OFDM and related layered ACO-OFDM techniques are also developed. Two optical power allocation schemes over the layers of ALACO-OFDM are developed with the objective of optimizing uncoded transmission performance and the achievable information rate respectively. Additionally, a theoretical bound on the uncoded BER of ALACO-OFDM is derived. Monte Carlo simulation results indicate ALACO-OFDM with the optimum power allocation achieves significant uncoded BER performance gains compared to its counterparts at the same spectral efficiency while having a smaller peak-to-average power ratio.

2.1 Introduction

While a majority of wireless communications systems operate in the radio bands, optical wireless communications (OWC) has recently emerged as an attractive complementary link due to the ubiquity of solid-state illumination and the availability

of large amounts of unregulated spectrum [3, 4]. Data are conveyed by modulating the instantaneous optical intensity (i.e., intensity modulation (IM)) and detecting the received signal power using a photodiode (i.e., direct detection (DD)). Such IM/DD links impose constraints on the non-negativity of all emitted signals and constrain the average amplitude [3, 4, 48].

Many of these optical wireless channels, especially those that arise due to visible light communications (VLC), are bandwidth limited. In this context, spectrally efficient orthogonal frequency division multiplexing (OFDM) has been investigated for OWC to enhance the data rate while satisfying IM/DD amplitude constraints. To generate a real-value time-domain signal, Hermitian symmetry in the spectrum is required [51]. However, many approaches exist to ensure amplitude non-negativity. In direct current (DC) biased optical OFDM (DCO-OFDM) a conventional OFDM signal is biased to ensure non-negativity. Although this preserves its high spectral efficiency, the addition of a large DC bias makes this approach power inefficient [51]. Approaches such as asymmetrically clipped optical OFDM (ACO-OFDM) [56] and unipolar OFDM (U-OFDM) [58] are more power efficient and ensure amplitude non-negativity at a cost of half of the spectral efficiency. To address this spectral efficiency loss, enhanced U-OFDM (eU-OFDM) superimposing multiple streams of U-OFDM [58], and layered ACO-OFDM (LACO-OFDM), superimposing multiple layers of ACO-OFDM [109, 132, 74, 111, 102], have been proposed. In general, both approaches work by layering a number of non-negative signals and performing successive detection at the receiver. In theory, the spectral efficiency of eU- and LACO-OFDM approaches that of DCO-OFDM as the number of layers or streams increases. However, using a large number of layers incurs high computational complexity and latency

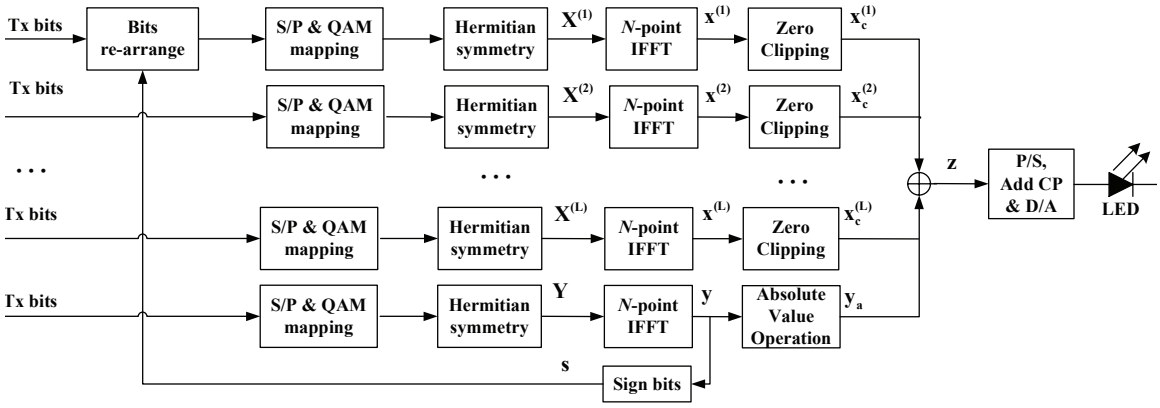

Figure 2.1: Transmitter design block diagram for ALACO-OFDM.

in the demodulator. Recently, asymmetrically clipped absolute value optical OFDM (AAO-OFDM) [48] has been proposed to enhance the spectral efficiency, in which no explicit DC bias is required. Although AAO-OFDM has only two streams, the spectral efficiency is still 0.5 bits/channel use smaller than that of DCO-OFDM.

In this work we present *absolute value layered ACO-OFDM* (ALACO-OFDM), which has a spectral efficiency approaching that of DCO-OFDM while preserving power efficiency [98]. Different from dual-stream AAO-OFDM [48], in ALACO-OFDM, ACO-OFDM signals are sent in the first L layers and absolute value optical OFDM (AVO-OFDM) [48] is used over the remaining subcarriers. These streams are superimposed in the time domain and transmitted simultaneously with no explicit DC bias. Thus, AAO-OFDM in [48] is a special case of ALACO-OFDM with $L = 1$. At the receiver, the L layers of ACO-OFDM symbols are first demodulated layer-by-layer as in LACO-OFDM [74] and then the AVO-OFDM symbols are demodulated with the aid of sign information carried in the first layer. In order to design an ALACO-OFDM system, two optimal power allocations over the layers are derived which optimize uncoded bit error rate (BER) and information rate, respectively. Our analysis indicates

that for the same spectral efficiency, ALACO-OFDM requires fewer layers, and is less complex than LACO-OFDM in terms of the number of real-valued multiplication operations and real-valued addition operations. Additionally, ALACO-OFDM achieves higher information rate than ACO-, AAO- and LACO-OFDM at moderate to high signal-to-noise ratios (SNRs). Furthermore, a theoretical bound on the BER of ALACO-OFDM is derived, which is close to the simulation results in high SNR regime. A BER performance comparison indicates uncoded ALACO-OFDM achieves significant gains over AAO-, LACO- and eU-OFDM. In terms of peak-to-average power ratio (PAPR), ALACO-OFDM is also shown to have a lower PAPR than ACO-, AAO-, LACO- or eU-OFDM.

Section 2.2 defines the ALACO-OFDM transmitter and receiver. The spectral efficiency and complexity of the ALACO-OFDM are analyzed and compared to its counterparts in Sec. 2.3. Two optimal optical power allocation schemes are designed with respect to uncoded BER and achievable information rate in Sec. 2.4. The BER and PAPR performance of ALACO-OFDM are presented and compared to its counterparts in Sec. 2.5. Finally, conclusions are drawn in Sec. 2.6.

2.2 Definition of ALACO-OFDM

2.2.1 Transmitter

The transmitter block diagram for an ALACO-OFDM based IM/DD system with N subcarriers is shown in Fig. 2.1, where N is assumed to be a power of 2. The ALACO-OFDM signal consists of L layers of ACO-OFDM [74] and a single layer of AVO-OFDM [48].

Transmitted bits are serial-to-parallel (S/P) converted and mapped to quadrature amplitude modulation (QAM) constellation symbols. To obtain a real-valued time-domain signal, Hermitian symmetry is imposed on the N subcarriers, where $X_k = X^*_{N-k}$, and X_0 and $X_{N/2}$ are set to zero [51].

For the first layer of ACO-OFDM, the constellation symbols are mapped onto odd subcarriers, i.e., X_{2k+1} for $k = 0, 1, 2, \cdots, N/4-1$), in a frame and unused subcarriers are set to zero. After applying Hermitian symmetry, the frequency-domain symbol vector $\mathbf{X}^{(1)}$ is given by

$$\mathbf{X}^{(1)} = \left[0, X_1, 0, X_3, 0, \cdots, X_{N/2-1}, 0, X^*_{N/2-1}, \cdots, 0, X^*_1\right]. \tag{2.2.1}$$

In general, for the l-th layer ACO-OFDM ($l = 1, \cdots, L$ and $L < \log_2 N - 1$), define the index set of data bearing carriers (before Hermitian symmetry) as $\mathbb{K}^{(l)}_{\text{ACO}} = \{2^{l-1}(2q+1), q = 0, 1, \cdots, \phi(l) - 1\}$ where

$$\phi(l) \triangleq \frac{N}{2^{l+1}}. \tag{2.2.2}$$

Therefore, for the l-th layer the constellation symbols are mapped onto X_k for $k \in \mathbb{K}^{(l)}_{\text{ACO}}$, Hermitian symmetry is imposed and all other subcarriers are set to zero resulting in the frequency domain symbol

$$\mathbf{X}^{(l)} = [0, \cdots, 0, X_{2^{l-1}}, 0, \cdots, 0, X_{3\cdot 2^{l-1}}, 0, \cdots, 0, X^*_{2^{l-1}}, 0, \cdots, 0] \tag{2.2.3}$$

where there are $(2^l - 1)$ zeros in between two adjacent non-zero symbols.

Next, an N-point inverse fast Fourier transform (IFFT) is performed on $\mathbf{X}^{(l)}$ at

l-th layer to obtain a bipolar time-domain signal vector $\mathbf{x}^{(l)}$, where the n-th element is defined as

$$x_n^{(l)} = \frac{1}{\sqrt{N}} \sum_{k=0}^{N-1} {X_k}^{(l)} \exp\left(j\frac{2\pi}{N}nk\right),\ 0 \le n \le N-1. \tag{2.2.4}$$

As shown in [74], $\mathbf{x}^{(l)}$ is a real-valued bipolar vector with a period of $4\phi(l) = \frac{N}{2^{l-1}}$, and has an anti-symmetry as

$$x_n^{(l)} = -x_{n+2\phi(l)}^{(l)},\ 0 \le n \le 2\phi(l)-1. \tag{2.2.5}$$

Therefore, the negative part of $\mathbf{x}^{(l)}$ can be directly clipped without losing any information leading to ACO-OFDM time-domain signal $\mathbf{x}_c^{(l)}$, which is given by [56]

$$x_{c,n}^{(l)} = \frac{1}{2}x_n^{(l)} + \frac{1}{2}\left|x_n^{(l)}\right| \tag{2.2.6}$$

where $|\cdot|$ denotes absolute value operation.

After L layers of ACO-OFDM, there remain $2\phi(L)$ subcarriers that are unused. In this work, AVO-OFDM [48] is employed to send data on these unused carriers. Note that L is a variable that must be designed to optimize the performance of ALACO-OFDM as shown in Sec. 2.4. Define $\mathbb{K}_{\text{AVO}} = \{q2^L, q = 1, \cdots, \phi(L)-1\}$ as the index set of data bearing carriers (before Hermitian symmetry) for AVO-OFDM. Specifically, QAM symbols are mapped onto Y_k for $k \in \mathbb{K}_{\text{AVO}}$ with other subcarriers set to zero. After Hermitian symmetry, the frequency-domain symbol vector $\mathbf{Y}$ is given as

$$\mathbf{Y} = [0, \cdots, 0, Y_{2^L}, 0, \cdots, 0, Y_{2\cdot 2^L}, 0, \cdots, 0, Y_{2^L}^*, 0, \cdots, 0] \tag{2.2.7}$$

where there are $(2^L - 1)$ zeros in between two adjacent non-zero symbols. The time-domain signal y_n is obtained via the IFFT to give

$$y_n = \frac{1}{\sqrt{N}} \sum_{k=0}^{N-1} Y_k \exp\left(j\frac{2\pi}{N}nk\right),\ 0 \le n \le N-1. \tag{2.2.8}$$

Substituting (2.2.7) into (2.2.8) gives

$$y_n = \frac{1}{\sqrt{N}} \sum_{q=0}^{2\phi(L)-1} Y_{q2^L} \exp\left(j\frac{2\pi}{2\phi(L)}qn\right) \tag{2.2.9}$$

where $0 \le n \le N-1$. From (2.2.9), notice that $\mathbf{y}$ has a period of $2\phi(L)$, i.e.,

$$y_n = y_{n+2\phi(L)}. \tag{2.2.10}$$

To ensure non-negativity, define $y_{a,n}$ as

$$y_{a,n} = |y_n|,\ 0 \le n \le N-1. \tag{2.2.11}$$

Considering $\mathbf{y}$ has a period of $2\phi(L)$, only $2\phi(L)$ sign bits need to be transmitted to reconstruct the original AVO-OFDM signal. Let the vector of sign bits be denoted as $\mathbf{s}$, with components [48]

$$s_n = \begin{cases} 0, & y_n \le 0; \\ 1, & y_n > 0, \end{cases} \tag{2.2.12}$$

where $0 \le n \le 2\phi(L) - 1$. These sign bits are inserted uniformly over transmitting symbols mapped to symbol vector $\mathbf{X}^{(1)}$, which is transmitted by the first layer ACO-OFDM.

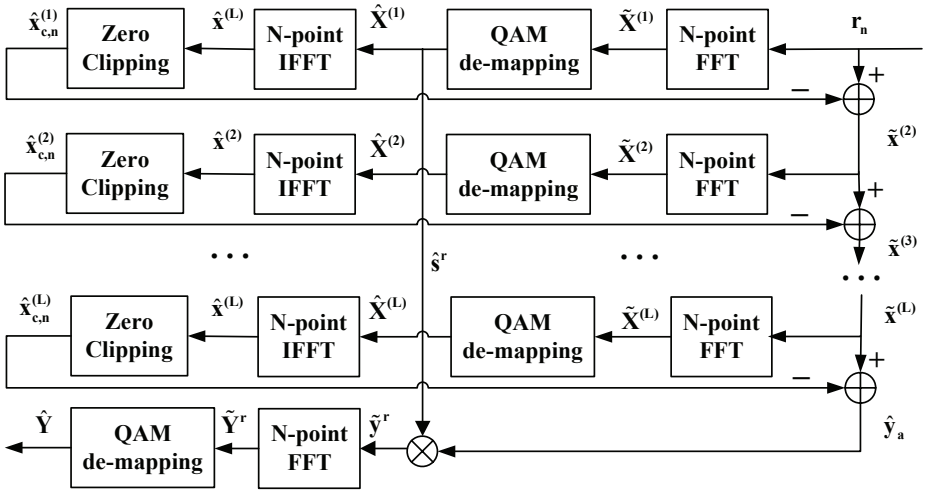

Figure 2.2: Receiver design block diagram for ALACO-OFDM.

Adding together the L layer ACO-OFDM signals $\mathbf{x}_c^{(l)}$ and the AVO-OFDM signal $\mathbf{y}_a$, the discrete time-domain transmitted signal vector is denoted $\mathbf{z}$ with components

$$z_n = \sum_{l=1}^{L} x_{c,n}^{(l)} + y_{a,n},\ 0 \leq n \leq N-1. \tag{2.2.13}$$

Finally, after parallel-to-serial (P/S) conversion and the addition of a cyclic prefix (CP), $\mathbf{z}$ is fed into a digital-to-analog (D/A) converter before driving an LED.

2.2.2 Receiver

At the receiver, a photo-diode (PD) converts the received optical signal into an electrical current. The shot noise and thermal noise are modelled as additive white Gaussian noise (AWGN) [74, 56]. As this paper focuses on transceiver design, here we consider a flat channel with perfect equalization and synchronization are assumed and the channel gain from the LED to the PD is assumed to be unity [58, 56].

The receiver block diagram is depicted in Fig. 2.2. After S/P conversion, analog-to-digital (A/D) conversion and removal of the CP, the received signal r_n is

$$r_n = z_n + w_n,\ 0 \leq n \leq N-1 \tag{2.2.14}$$

where w_n is zero mean AWGN with variance σ_w^2.

It is well known that the clipping distortion of l-th ($1 \leq l \leq L$) layer ACO-OFDM falls on subcarriers of higher layers; i.e., the l-th layer ACO-OFDM must be demodulated before the $(l+1)$-th layer [74]. It can also be shown that the AVO-OFDM layer has components solely at frequencies indices in $\mathbb{K}_{\text{AVO}}$ and Hermitian symmetric components and thus does not interfere with any of the ACO-OFDM layers [98]. Thus, demodulation starts at the first ACO-OFDM layer and clipping noise is successively removed from lower layer signals.

For the demodulation of the first layer, $\mathbf{r}$ is fed into a fast Fourier transform (FFT) module to generate its DFT symbol vector, denoted as $\widetilde{\mathbf{X}}^{(1)}$ in Fig. 2.2 with elements

$$\widetilde{X}_k^{(1)} = \frac{1}{\sqrt{N}} \sum_{n=0}^{N-1} r_n \exp\left(-j\frac{2\pi}{N}nk\right),\ 0 \leq k \leq N-1. \tag{2.2.15}$$

This vector is then utilized to detect the modulated symbols at the first layer as

$$\widehat{X}_k^{(1)} = \arg \min_{X \in \Omega_X^{(1)}} \left\| X - 2\widetilde{X}_k^{(1)} \right\|^2,\ k = 1, 3, \cdots, N/2-1 \tag{2.2.16}$$

where $\Omega_X^{(1)}$ denotes the constellation set of symbols at the first layer and the scalar 2 is due to the zero clipping loss [74].

An ACO-OFDM time-domain signal local estimation $\widehat{x}_{c,n}^{(1)}$ can be generated using an IFFT and clipping, as shown in Fig. 2.2. The signal $\widehat{x}_{c,n}^{(1)}$ is subtracted from the

received signal r_n leading to $\widetilde{x}_n^{(2)}$ that is employed to demodulate the symbols at the second layer.

Demodulation of the subsequent ACO-OFDM layers proceeds in a similar fashion where at layer l, QAM symbols are detected to the DFT symbol vector $\widetilde{\mathbf{X}}^{(l)}$ which arises as the FFT of $\widetilde{\mathbf{x}}^{(l)} = \widetilde{\mathbf{x}}^{(l-1)} - \widehat{\mathbf{x}}_c^{(l-1)}$, i.e., the impact of the detected symbols in the previous layers is removed from subsequent layers.

After the L-th ACO-OFDM layer is detected, the clipping noise on the carriers in $\mathbb{K}_{\text{AVO}}$ can be removed by computing the local estimate of $\widehat{\mathbf{x}}_c^{(L)}$ and subtracting it from the remaining signal vector $\widetilde{\mathbf{x}}^{(L)}$. More compactly, an estimate of the AVO-OFDM signal $\widehat{\mathbf{y}}_a = \widetilde{\mathbf{x}}^{(L)} - \widehat{\mathbf{x}}_c^{(L)}$.

In order to be able to demodulate the data in the AVO-OFDM signal, the sign information must be extracted from the first layer of ACO-OFDM. Let $\widehat{s}_n$ denote the detected sign information of the AVO-OFDM signal that is transmitted in layer one. Furthermore, let $\widehat{s}_n^r \in \{-1, 1\}$ denote the sign of the $\widehat{y}_{a,n}$ which is extracted for the first $2\phi(L)$ symbols by

$$\widehat{s}_n^r = \begin{cases} 1, & \widehat{s}_n = 1; \\ -1, & \widehat{s}_n = 0, \end{cases} \tag{2.2.17}$$

where $n = 0, \cdots, 2\phi(L) - 1$. As noted in (2.2.10), the AVO-OFDM signal is periodic with period $2\phi(L)$ and thus, $\widehat{s}_n^r$ can be readily extended for all $n = 0, \cdots, N-1$.

The AVO-OFDM time-domain signal can be reconstructed as

$$\widehat{y}_n^r = \widehat{s}_n^r \widehat{y}_{a,n}, \ n = 0, 1, 2, \cdots, N-1. \tag{2.2.18}$$

After an N-point FFT module, the AVO-OFDM symbols can be detected using

$$\widehat{Y}_k = \arg \min_{Y \in \Omega_Y} \left\| Y - \widehat{Y}_k^r \right\|^2 \tag{2.2.19}$$

where Ω_Y denotes the constellation set of AVO-OFDM, $\widehat{Y}_k^r$ denotes the DFT of $\widehat{y}_n^r$ and $k \in \mathbb{K}_{\text{AVO}}$.

2.3 ALACO-OFDM Signal Analysis

In this section, the spectral efficiency and computational complexity of ALACO- are analyzed and compared to eU- [58], LACO- [74] and AAO-OFDM [48].

2.3.1 Spectral Efficiency

In this work, the spectral efficiency is defined as information rate per channel use. Hence, the spectral efficiency of DCO-OFDM with QAM constellation size M, Υ_{DCO}, can be written as

$$\Upsilon_{\text{DCO}} = \frac{1}{2} \log_2 M \text{ bits/channel use.} \tag{2.3.1}$$

The spectral efficiency of eU-OFDM with L streams, $\Upsilon_{\text{eU}}^{(L)}$, and of LACO-OFDM with L layers, $\Upsilon_{\text{LA}}^{(L)}$, are equal, and take the form [58, 74]

$$\Upsilon_{\text{LA}}^{(L)} = \frac{1}{2} \log_2 M - \frac{1}{2^{L+1}} \log_2 M \text{ bits/channel use,} \tag{2.3.2}$$

in which each stream/layer is assumed to use the same constellation size M.

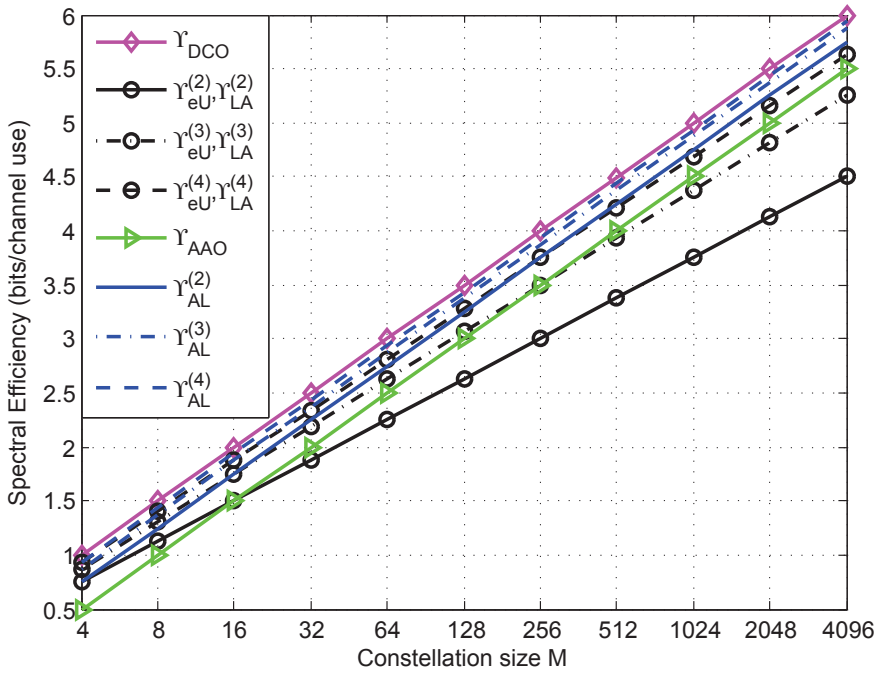

Figure 2.3: The spectral efficiency comparison between ALACO-OFDM and its counterparts with different constellation sizes.

The spectral efficiency of AAO-OFDM, Υ_{AAO}, can be calculated by [48]

$$\Upsilon_{\text{AAO}} = \frac{1}{4}(\log_2 M_1 + \log_2 M_2) - \frac{1}{2} \text{ bits/channel use}, \tag{2.3.3}$$

in which the constellation size M_1 and M_2 are assumed for AVO-OFDM and ACO-OFDM component parts, respectively. In the case of $M_1 = M_2 = M$

$$\Upsilon_{\text{AAO}} = \frac{1}{2}\log_2 M - \frac{1}{2} \text{ bits/channel use}. \tag{2.3.4}$$

For ALACO-OFDM, for the l-th ($1 \leq l \leq L$) layer ACO-OFDM, let M_l denote the size of the constellation sent on each ACO-OFDM layer. Note that there are

$\phi(l) = \frac{N}{2^{l+1}}$ effective complex symbols before Hermitian symmetry for each ACO-OFDM layer l. For AVO-OFDM, the constellation size is denoted M_v and there are $\phi(L)-1 = \frac{N}{2^{L+1}}-1$ effective complex symbols before Hermitian symmetry. Notice also that $2\phi(L) = \frac{N}{2^L}$ sign bits of AVO-OFDM time-domain signals are inserted uniformly into transmitting symbols at the first layer.

Hence, the spectral efficiency of ALACO-OFDM with L layers, denoted by $\Upsilon_{\text{AL}}^{(L)}$, is

$$\begin{aligned}\Upsilon_{\text{AL}}^{(L)} &= \frac{1}{N}\left(\sum_{l=1}^{L}\frac{N}{2^{l+1}}\log_2 M_l + \left(\frac{N}{2^{L+1}}-1\right)\log_2 M_v - \frac{N}{2^L}\right)\\ &\approx \sum_{l=1}^{L}\frac{1}{2^{l+1}}\log_2 M_l + \frac{1}{2^{L+1}}\log_2 M_v - \frac{1}{2^L}\end{aligned} \tag{2.3.5}$$

where the approximation holds for large N.

If $M_l = M_v = M$, $\Upsilon_{\text{AL}}^{(L)}$ can be rewritten as

$$\Upsilon_{\text{AL}}^{(L)} = \frac{1}{2}\log_2 M - \frac{1}{2^L} \text{ bits/channel use.} \tag{2.3.6}$$

Notice that AAO-OFDM is a special case of ALACO-OFDM with $L = 1$ according to (2.3.4) and (2.3.6).

The spectral efficiency comparison between ALACO- and DCO-, eU-, LACO- and AAO-OFDM for large N is depicted with different constellation sizes in Fig. 2.3. It can be seen that Υ_{AAO}, $\Upsilon_{\text{AL}}^{(2)}$, $\Upsilon_{\text{AL}}^{(3)}$, $\Upsilon_{\text{AL}}^{(4)}$ and Υ_{DCO} are parallel, which indicates a constant gap between them. Additionally, notice that ALACO-OFDM is closest to the spectral efficiency of DCO-OFDM. The difference in spectral efficiency between ALACO- and DCO-OFDM decreases with increasing L as $1/2^L$. For example, for $L = 2$ ALACO-OFDM 0.25 bits/channel use less than DCO-OFDM, while at $L = 4$ the difference is only 0.0625 bits/channel use. For eU-OFDM and LACO-OFDM,

the larger the constellation size, the larger the spectral-efficiency gap compared to DCO-OFDM. When $M > 256$, ALACO-OFDM with $L = 2$ achieves larger spectral efficiency than eU-OFDM and LACO-OFDM with $L = 4$. For the same layer number L, the spectral efficiency of ALACO-OFDM is

$$\frac{\log_2 M - 2}{2^{L+1}} \quad \text{bits/channel use}$$

larger than eU-OFDM and LACO-OFDM.

2.3.2 Computational Complexity

For an N-point (N a power of 2) IFFT or FFT module using the Cooley-Tukey decomposition, $M(N)$ real-valued multiplication operations (RMOs) and $A(N)$ real-valued addition operations (RAOs) are required where [133]

$$M(N) = 2N \log_2(N) - 4N + 4 \tag{2.3.7}$$

and

$$A(N) = 3N \log_2(N) - 2N + 2. \tag{2.3.8}$$

In the subsequent analysis, we assume that operations such as zero clipping, taking the sign bits, and absolute value operation do not require any arithmetic operations as they can be efficiently implemented via switching logic. In addition, the complexity of detecting QAM symbols on carriers is the same for all schemes thus is not included in this analysis.

Though the N-point IFFT and FFT in Fig. 2.1 and 2.2 are useful in depicting

the basic idea of ALACO-OFDM transceiver design, more efficient approaches have been documented in the literature. For LACO- and ALACO-OFDM, to reduce the complexity, a $4\phi(l)$-point IFFT can be employed and repeated 2^{l-1} times for l-th ACO-OFDM layer as shown in [74]. A $2\phi(L)$-point IFFT can similarly to used and repeated 2^L times for AVO-OFDM layer due to the periodic property of $\mathbf{y}$. At the receiver, averaging is required in the time domain over 2^{l-1} periods for l-th ACO-OFDM layer and over 2^L periods for AVO-OFDM layer to enhance the performance. These two approaches to the implementation layered ACO-OFDM have been included in the following analysis.

Transmitter

For DCO-OFDM, an N-point IFFT module is required at transmitter and it requires $M_{\text{DCO}}^{(t)}(N) = M(N)$ RMOs and $A_{\text{DCO}}^{(t)}(N) = A(N)$ RAOs.

For ALACO-OFDM, the required RMOs and RAOs of ALACO-OFDM can be written as

$$\begin{aligned} M_{\text{AL}}^{(t)}(L,N) &= \sum_{l=1}^{L} M\left(\frac{N}{2^{l-1}}\right) + M\left(\frac{N}{2^L}\right) \\ &= \left(1 - \frac{1}{2^{L+1}}\right) 4N\log_2(N) - \left(12 - \frac{L+4}{2^{L-1}}\right) N + 4L + 4 \end{aligned} \tag{2.3.9}$$

and

$$\begin{aligned} A_{\text{AL}}^{(t)}(L,N) &= \sum_{l=1}^{L} A\left(\frac{N}{2^{l-1}}\right) + A\left(\frac{N}{2^L}\right) + LN \\ &= \left(1 - \frac{1}{2^{L+1}}\right) 6N\log_2(N) - \left(11 - L - \frac{3L+8}{2^L}\right) N + 2L + 2. \end{aligned} \tag{2.3.10}$$

Similarly, for LACO-OFDM with N subcarriers and L layers, the required RMOs and RAOs are given by

$$\begin{aligned} M_{\mathrm{LA}}^{(t)}(L,N) &= \sum_{l=1}^{L} M\left(\frac{N}{2^{l-1}}\right) \\ &= \left(1-\frac{1}{2^L}\right) 4N\log_2(N) - \left(12-\frac{2L+6}{2^{L-1}}\right) N + 4L \end{aligned} \tag{2.3.11}$$

and

$$\begin{aligned} A_{\mathrm{LA}}^{(t)}(L,N) &= \sum_{l=1}^{L} A\left(\frac{N}{2^{l-1}}\right) + (L-1)N \\ &= \left(1-\frac{1}{2^L}\right) 6N\log_2(N) - \left(11-L-\frac{3L+5}{2^{L-1}}\right) N + 2L. \end{aligned} \tag{2.3.12}$$

For eU-OFDM with N subcarriers and L streams, there are 2^L OFDM frames included in one super frame. Hence, RMOs and RAOs averaged over a super frame are [107]

$$M_{\mathrm{eU}}^{(t)}(L,N) = \left(1-\frac{1}{2^L}\right)(2N\log_2(N) - 4N + 4) \tag{2.3.13}$$

and

$$A_{\mathrm{eU}}^{(t)}(L,N) = \left(1-\frac{1}{2^L}\right)(3N\log_2(N) - 2N + 2) + (L-1)N. \tag{2.3.14}$$

Receiver

For DCO-OFDM, an N-point FFT module is required at receiver and requires $M_{\mathrm{DCO}}^{(r)}(N) = M(N)$ RMOs and $A_{\mathrm{DCO}}^{(r)}(N) = A(N)$ RAOs.

For ALACO-OFDM, to detect the l-th layer of the ACO-OFDM signal ($1 \le l \le L$), an $4\phi(l)$-point FFT is required followed by an $4\phi(l)$-point IFFT for signal reconstruction. For AVO-OFDM layer, $2\phi(L)$-point FFT is required only for demodulation.

Hence ALACO-OFDM requires $M_{\mathrm{AL}}^{(r)}(L,N)$ RMOs as

$$\begin{aligned} M_{\mathrm{AL}}^{(r)}(L,N) &= 2\sum_{l=1}^{L} M\left(\frac{N}{2^{l-1}}\right) + M\left(\frac{N}{2^{L}}\right) \\ &= \left(1-\frac{3}{2^{L+2}}\right) 8N\log_2(N) - \left(24-\frac{3L+10}{2^{L-1}}\right) N + 8L + 4 \end{aligned} \tag{2.3.15}$$

and RAOs as

$$\begin{aligned} &A_{\mathrm{AL}}^{(r)}(L,N) = \\ &2\sum_{l=1}^{L} A\left(\frac{N}{2^{l-1}}\right) + A\left(\frac{N}{2^{L}}\right) + \underbrace{\sum_{l=1}^{L}\left(2^{l-1}-1\right)\frac{N}{2^{l-1}} + \left(2^{L}-1\right)\frac{N}{2^{L}}}_{\text{Averaging for } L \text{ ACO layers and AVO}} + \underbrace{LN}_{\text{Removing low layers}} \\ &= \left(1-\frac{3}{2^{L+2}}\right) 12N\log_2(N) - \left(21-2L-\frac{9L+19}{2^{L}}\right) N + 4L + 2. \end{aligned} \tag{2.3.16}$$

The conventional LACO-OFDM receiver [74] removes interference from lower layers in the frequency domain. In contrast, the receiver in Fig. 2.2 removes interference between layers at the receiver directly in the time domain. This approach requires fewer N-point FFTs than the receiver in [74] and is thus less complex. For the sake of fair comparison, the receiver for LACO-OFDM is computed when the interference is removed in the time domain (as shown for the first L layers in Fig. 2.2). The number of RMOs and RAOs for LACO-OFDM when interference is removed in time domain are

$$\begin{aligned} M_{\mathrm{LA}}^{(r)}(L,N) &= 2\sum_{l=1}^{L-1} M\left(\frac{N}{2^{l-1}}\right) + M\left(\frac{N}{2^{L-1}}\right) \\ &= \left(1-\frac{3}{2^{L+1}}\right) 8N\log_2(N) - \left(24-\frac{6L+14}{2^{L-1}}\right) N + 8L - 4 \end{aligned} \tag{2.3.17}$$

and

$$A_{\mathrm{LA}}^{(r)}(L,N) = 2\sum_{l=1}^{L-1} A\left(\frac{N}{2^{l-1}}\right) + A\left(\frac{N}{2^{L-1}}\right) + \underbrace{\sum_{l=1}^{L}\left(2^{l-1}-1\right)\frac{N}{2^{l-1}}}_{\text{Averaging for } L \text{ ACO layers}} + \underbrace{(L-1)N}_{\text{Removing low layers}}$$
$$= \left(1-\frac{3}{2^{L+1}}\right)12N\log_2(N) - \left(23-2L-\frac{9L+10}{2^{L-1}}\right)N + 4L - 2. \tag{2.3.18}$$

For eU-OFDM with N subcarriers and L streams, the number of RMOs and RAOs on average over a super frame are [107]

$$M_{\mathrm{eU}}^{(r)}(L,N) = \left(1-\frac{3}{2^{L+1}}\right)(4N\log_2(N) - 8N + 8) \tag{2.3.19}$$

and

$$A_{\mathrm{eU}}^{(r)}(L,N) = \left(1-\frac{3}{2^{L+1}}\right)6N\log_2(N) - \left(6-2L-\frac{7}{2^L}\right)N + 4 - \frac{6}{2^L}. \tag{2.3.20}$$

Fig. 2.4 presents a comparison of the RMOs and RAOs for ALACO-, LACO- and eU-OFDM. Although for the same L, ALACO-OFDM requires slightly more RMOs and RAOs than LACO-OFDM, given the same *spectral efficiency* LACO-OFDM requires more layers and is more complex as compared to ALACO-OFDM. For example, ALACO-OFDM with $L = 2$ and $M = 256$ and LACO-OFDM with $L = 4$ and $M = 256$ achieve the same spectral efficiency of 3.75 bits/channel use. From Fig. 2.4, at transmitter, LACO-OFDM with $L = 4$ requires about 5% more RMOs and 7% more RAOs than ALACO-OFDM with $L = 2$. At receiver, LACO-OFDM requires about 9% more RMOs and 11% more RAOs than ALACO-OFDM when operating at the same spectral efficiency.

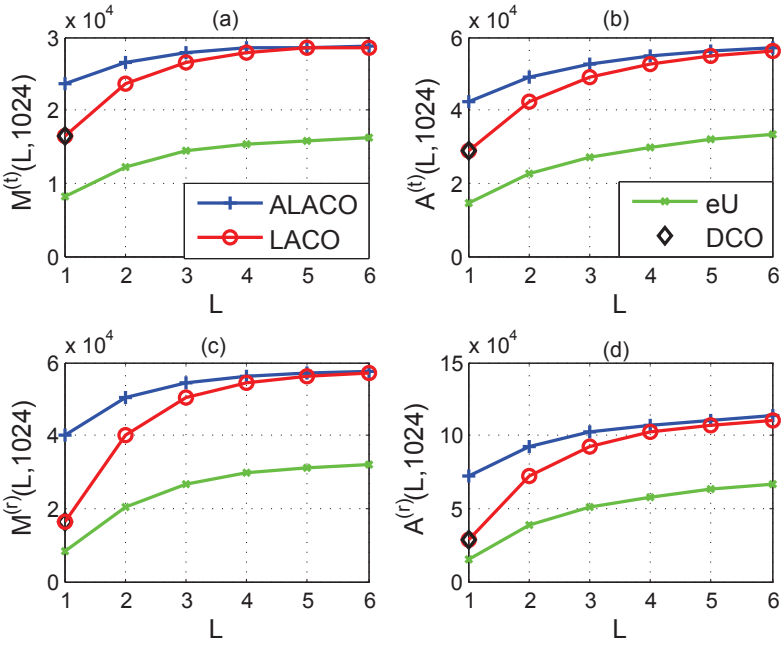

Figure 2.4: Computational complexity comparison between ALACO-OFDM and its counterparts for different L ($N = 1024$ in all cases).

2.4 Design of ALACO-OFDM Systems

Given that signals from different layers in ALACO-OFDM are combined to make the emitted signal, an open question is the allocation of optical power amongst the layers to ensure optimal performance. In this section, two optical power allocation schemes over the layers of ALACO-OFDM are discussed to optimize uncoded transmission performance and achievable information rates, respectively.

2.4.1 Signal Distributions, Optical and Electrical Power

Using the central limit theorem (CLT), the probability density function (PDF) of ACO-OFDM signal in the l-th layer is given by [56, 82, 134, 115, 110]

$$f_l(w) = \frac{1}{\sqrt{2\pi}\sigma_l}\exp\left(\frac{-\xi^2}{2\sigma_l^2}\right)u(\xi) + \frac{1}{2}\delta(\xi) \tag{2.4.1}$$

where σ_l is the standard deviation of the ACO-OFDM signal in the l-th layer before clipping, (see $\mathbf{x}^{(l)}$ in Fig. 2.1), $u(\xi)$ is a unit step function and $\delta(\xi)$ is a unit impulse funtion. The average optical and electrical power of ACO-OFDM signal in the l-th layer can be calculated as [82, 115]

$$P_{o,l} = \frac{\sigma_l}{\sqrt{2\pi}} \quad \text{and} \quad P_{e,l} = \frac{\sigma_l^2}{2}. \tag{2.4.2}$$

For AVO-OFDM, the PDF of $y_{\mathrm{a},n}$ is a truncated Gaussian [48]

$$f_v(\xi) = \frac{2}{\sqrt{2\pi}\sigma_v}\exp\left(\frac{-\xi^2}{2\sigma_v^2}\right)u(\xi) \tag{2.4.3}$$

where σ_v is the standard deviation of AVO-OFDM signal before absolute value operation (see $\mathbf{y}$ in Fig. 2.1). Additionally, the average optical and electrical power of AVO-OFDM signal are [48]

$$P_{o,v} = \frac{2\sigma_v}{\sqrt{2\pi}} \quad \text{and} \quad P_{e,v} = \sigma_v^2. \tag{2.4.4}$$

Thus, the average optical power of ALACO-OFDM signal z_n in Fig. 2.1 is can be

calculated by

$$P_{o,\mathrm{AL}} = \sum_{l=1}^{L} E\{x_{c,n}^{(l)}\} + E\{y_{a,n}\} = \frac{1}{\sqrt{2\pi}} \left(\sum_{l=1}^{L} \sigma_l + 2\sigma_v \right) \tag{2.4.5}$$

where E$\{\cdot\}$ denotes the expectation operator.

After clipping, the transmitted signal for each layer in frequency domain can be decomposed into two orthogonal components following (2.2.6), as

$$X_{c,k}^{(l)} = \frac{1}{2} X_k^{(l)} + \frac{1}{2} X_{a,k}^{(l)} \tag{2.4.6}$$

where $\frac{1}{2}X_k^{(l)}$, $k \in \mathbb{K}_{\mathrm{ACO}}^{(l)}$ is the useful transmitted signal and $\frac{1}{2}X_{a,k}^{(l)}$ is clipping distortion.

After some straightforward manipulation, the average electrical power of data symbols falling onto each subcarrier in the l-th layer ACO-OFDM is given by (ignoring Hermitian symmetric components)

$$E\left\{ \left| \frac{1}{2} X_k^{(l)} \right|^2 \right\} = \begin{cases} 2^{l-2}\sigma_l^2, & k \in \mathbb{K}_{\mathrm{ACO}}^{(l)}, \\ 0, & \text{otherwise.} \end{cases} \tag{2.4.7}$$

Similarly, assuming that the sign information is recovered correctly, the average electrical power of data symbol in k-th subcarrier in AVO-OFDM is given by

$$E\{|Y_k|^2\} = \begin{cases} 2^L \sigma_v^2, & k \in \mathbb{K}_{\mathrm{AVO}}, \\ 0, & \text{otherwise.} \end{cases} \tag{2.4.8}$$

2.4.2 Optical Power Allocation - Uncoded Transmission

Consider an ALACO-OFDM system which operates under a fixed average optical power constraint, $P_{o,\mathrm{AL}}$. Such systems arise in VLC links with dimming constraints. Assume that the clipping distortion from lower layers is completely removed from higher layers which is reasonable at high SNRs. Additionally, assume a flat channel with AWGN noise in each subcarrier with variance σ_w^2. Let SNR_k denote the electrical SNR of the k-th subcarrier from (2.4.7) and (2.4.8) which governs the uncoded BER performance.

Here we consider the optimal allocation of optical power to each ALACO-OFDM layer subject to an average optical power constraint with the objective of optimizing the uncoded BER. In particular, the optimal power allocation is the one which selects σ_l and σ_v over ALACO-OFDM layers which maximizes the minimum SNR over all data-bearing subcarriers while satisfying the average optical power constraint (2.4.5). More precisely,

$$\mathbf{P1}: \max_{\sigma_l,\, \sigma_v} \quad \min_k \mathrm{SNR}_k \tag{2.4.9a}$$

$$\text{s.t.} \quad \mathrm{SNR}_k = \begin{cases} \frac{2^{l-2}\sigma_l^2}{\sigma_w^2}, & k \in \mathbb{K}_{\mathrm{ACO}}^{(l)},\ 1 \le l \le L, \\ \frac{2^{L}\sigma_v^2}{\sigma_w^2}, & k \in \mathbb{K}_{\mathrm{AVO}}, \end{cases} \tag{2.4.9b}$$

$$\sum_{l=1}^{L} \sigma_l + 2\sigma_v = \sqrt{2\pi} P_{o,\mathrm{AL}}, \tag{2.4.9c}$$

$$\sigma_l \ge 0,\ 1 \le l \le L, \tag{2.4.9d}$$

$$\sigma_v \ge 0. \tag{2.4.9e}$$

Since $\mathrm{SNR}_k \ge 0$, taking the square root of SNR_k linearizes the optimization

problem as

$$\mathbf{P2}: \min_{\sigma_l, t} \quad -t \tag{2.4.10a}$$

$$\text{s.t.} \quad 2^{\frac{l-2}{2}} \frac{\sigma_l}{\sigma_w} \geq t, \qquad k \in \mathbb{K}_{\text{ACO}}^{(l)},\ 1 \leq l \leq L, \tag{2.4.10b}$$

$$2^{\frac{L}{2}} \frac{\sigma_v}{\sigma_w} \geq t, \qquad k \in \mathbb{K}_{\text{AVO}}, \tag{2.4.10c}$$

$$(2.4.9\text{c}) - (2.4.9\text{e}). \tag{2.4.10d}$$

The objective function and constraints of **P2** are affine, which can be solved easily through Karush-Kuhn-Tucker (KKT) method. The solutions are given as

$$\sigma_l^\star = \frac{2^{-\frac{l-2}{2}} \sqrt{\pi} P_{o,\text{AL}}}{A},\ 1 \leq l \leq L, \tag{2.4.11a}$$

$$\sigma_v^\star = \frac{2^{-\frac{L}{2}} \sqrt{\pi} P_{o,\text{AL}}}{A} \tag{2.4.11b}$$

where for readability, $A \triangleq 2 + \sqrt{2} - 2^{-(L-2)/2}$. Substituting (2.4.11) into (2.4.2) and (2.4.4), we can obtain the optimal optical power $P_{o,l}^\star$ and $P_{o,v}^\star$.

Notice that using the optimum power allocation $\sigma_l^\star$ and $\sigma_v^\star$ yields the same SNR_k for all data bearing subcarriers regardless of their layer, that is

$$\text{SNR}_k = \frac{\pi}{A^2} \frac{P_{o,\text{AL}}^2}{\sigma_w^2}. \tag{2.4.12}$$

This result corresponds to the empirically chosen power allocations used in previous work [74, 82]. Section 2.5 presents numerical investigation of (2.4.11) over different choices of power allocation.

Define power allocation factor α as the ratio between optical power of adjacent

ACO-OFDM layers, i.e.,

$$\alpha \triangleq \frac{P_{o,l}}{P_{o,l+1}},\ 1 \leq l \leq L-1. \tag{2.4.13}$$

Notice that using the optimum power allocation $\sigma_l^\star$ and $\sigma_v^\star$ in (2.4.11), $\alpha = \sqrt{2}$ and $P_{o,v} = P_{o,L}$. This result matches previous empirically derived power allocations in [74, 82, 135, 136, 84] and [48] for LACO- and AAO-OFDM respectively. In a related context, [115] also conclude that LACO-OFDM achieves optimal power allocation with $\alpha = \sqrt{2}$ under an electrical power constraint.

2.4.3 Optical Power Allocation - Information Rate

Here, the optical power allocation amongst ALACO-OFDM layers is done to maximize the overall achievable information rate under an average optical power constraint.

Achievable information rate of ALACO-OFDM

For the l-th layer ACO-OFDM, an optical power constraint leads to an electrical power constraint according to (2.4.2) and (2.4.7), hence Shannon capacity formula in [137] can be employed [134]. In addition, there are $\frac{N}{2^{l+1}}$ out of N subcarriers bearing data symbols before Hermitian symmetry. The achievable information rate for l-th ACO-OFDM layer was first derived in [88] as

$$C_l = \frac{1}{2^{l+1}} \log\left(1 + \frac{2^{l-2}\sigma_l^2}{\sigma_w^2}\right) \text{ bits/channel use.} \tag{2.4.14}$$

For the AVO-OFDM layer, consider the following theorem.

Theorem 1. *Consider an absolute-value Gaussian random variable channel, i.e., $z = y + w$, where $y = |x|$, x is real and Gaussian distributed with zero mean and variance of σ_x^2, and w is AWGN with variance of σ_w^2. The achievable information rate of this absolute-value Gaussian channel is*

$$C_v = \frac{1}{2}\log\left(1 + \frac{\sigma_x^2}{\sigma_w^2}\right) - (1 - D) \tag{2.4.15}$$

where D is a monotonically decreasing function of $\gamma = \sigma_x/\sigma_w$, $0 < D \leq 1$ and $D \to 0$ as $\gamma \to \infty$.

Proof. See Appendix A. □

For AVO-OFDM, $\phi(L)$ out of N complex channels bear data (before Hermitian symmetry). Hence, according to Thm. 1, the achievable information rate for AVO-OFDM is

$$C_{\text{avo}} = \frac{1}{2^{L+1}}\log\left(1 + \frac{2^L\sigma_v^2}{\sigma_w^2}\right) - \frac{1}{2^L}(1 - D) \text{ bits/channel use.} \tag{2.4.16}$$

The achievable information rate of ALACO-OFDM can be bounded by the sum of achievable information rates of L layers of ACO-OFDM, the AVO-OFDM layer and subtracting the sign bits carried in the first layer to give

$$\begin{aligned} C_{\text{AL}}^{(L)} &= \sum_{l=1}^{L} C_l + C_{\text{avo}} - \frac{1}{2^L} \\ &= \sum_{l=1}^{L} \frac{1}{2^{l+1}}\log\left(1 + \frac{2^{l-2}\sigma_l^2}{\sigma_w^2}\right) + \frac{1}{2^{L+1}}\log\left(1 + \frac{2^L\sigma_v^2}{\sigma_w^2}\right) - \frac{1}{2^{L-1}} + \frac{D}{2^L}, \quad C_1 \geq \frac{1}{2^L}. \end{aligned} \tag{2.4.17}$$

Optimization problem

Most VLC channels operate in the high SNR regime [138, 139]. At high SNRs, $C_{\mathrm{AL}}^{(L)}$ can be approximated as

$$\tilde{C}_{\mathrm{AL}}^{(L)} \approx \sum_{l=1}^{L} \frac{1}{2^l} \log\left(\frac{2^{\frac{l-2}{2}}\sigma_l}{\sigma_w}\right) + \frac{1}{2^L}\log\left(\frac{2^{\frac{L}{2}}\sigma_v}{\sigma_w}\right) - \frac{1}{2^{L-1}} \tag{2.4.18}$$

since at high SNR $D \to 0$ according to Thm. 1.

Consider an optimal power allocation over the ALACO-OFDM layers to maximize the capacity at high SNR, as approximated by $\tilde{C}_{\mathrm{AL}}^{(L)}$, given formally as

$$\mathbf{P3}: \max_{\sigma_l, \sigma_v} \quad \tilde{C}_{\mathrm{AL}}^{(L)} \tag{2.4.19a}$$

$$\text{s.t.} \quad (2.4.9\text{c}) - (2.4.9\text{e}). \tag{2.4.19b}$$

The objective is the sum of concave functions and is thus also concave with the constraints are affine. Hence, an optimal solution can be obtained by solving the KKT conditions as

$$\tilde{\sigma}_l = \frac{\sqrt{2\pi}P_{o,\mathrm{AL}}}{2^l},\ 1 \le l \le L, \tag{2.4.20a}$$

$$\tilde{\sigma}_v = \frac{\sqrt{2\pi}P_{o,\mathrm{AL}}}{2^{L+1}}. \tag{2.4.20b}$$

Notice that the optical power allocation factor, defined in (2.4.13), for the capacity optimal power allocation is $\alpha = 2$ which is similar to the result reported in [53, 88]. Substituting (2.4.20) into (2.4.2) and (2.4.4), the optimal optical power $\tilde{P}_{o,l}$ and $\tilde{P}_{o,v}$ can also be obtained.

Substituting (2.4.20) into (2.4.17), a lower bound on the achievable information rate of ALACO-OFDM is

$$\hat{C}_{\mathrm{AL}}^{(L)} = \sum_{l=1}^{L} \frac{1}{2^{l+1}} \log\left(1 + \frac{\pi P_{o,\mathrm{AL}}^2}{2^{l+1}\sigma_w^2}\right) - \frac{1}{2^{L-1}} + \frac{1}{2^{L+1}} \log\left(1 + \frac{\pi P_{o,\mathrm{AL}}^2}{2^{L+1}\sigma_w^2}\right) + \frac{D}{2^L} \quad \text{bits/channel use.} \tag{2.4.21}$$

Similarly, the achievable information rate of LACO-OFDM with $\alpha = 2$ can be bounded by the sum of the rates of L layers of ACO-OFDM as

$$C_{\mathrm{LA}}^{(L)} = \sum_{l=1}^{L} \frac{1}{2^{l+1}} \log\left(1 + \frac{\pi P_{o,\mathrm{AL}}^2}{2^{l-1}\left(2 - 2^{-(L-1)}\right)^2 \sigma_w^2}\right). \tag{2.4.22}$$

Note that in the limiting case for large L and at high SNRs, the capacities of LACO- and ALACO-OFDM are equal according to (2.4.21) and (2.4.22) and approach

$$C_{\alpha=2} = \frac{1}{2} \log\left(\frac{\pi P_{o,\mathrm{AL}}^2}{8\sigma_w^2}\right) \text{ bits/channel use.} \tag{2.4.23}$$

This asymptotic result has also been presented in [88].

2.4.4 Comparison Between Power Allocation Schemes

For the sake of comparison with previous work, define the optical SNR (OSNR) as in [139, 140, 53, 88]

$$\mathrm{OSNR(dB)} = 10 \log_{10}\left(\frac{P_{o,\mathrm{AL}}}{\sigma_w}\right). \tag{2.4.24}$$

From Sec. 2.4.2, ALACO-OFDM achieves optimal uncoded transmission performance with $\alpha = \sqrt{2}$ while the high SNR information optimal allocations has $\alpha = 2$

according to Sec. 2.4.3.

Substituting (2.4.11) into (2.4.17), the achievable information rate of ALACO-OFDM with $\alpha = \sqrt{2}$ is

$$C_{\mathrm{AL}}^{(L)} = \frac{1}{2}\log\left(1 + \frac{\pi}{A^2}\frac{P_{o,\mathrm{AL}}^2}{\sigma_w^2}\right) - \frac{1}{2^{L-1}} + \frac{D}{2^L} \text{ bits/channel use.} \tag{2.4.25}$$

Similarly, for LACO-OFDM with $\alpha = \sqrt{2}$,

$$C_{\mathrm{LA}}^{(L)} = \left(\frac{1}{2} - \frac{1}{2^{L+1}}\right)\log\left(1 + \frac{\pi}{B^2}\frac{P_{o,\mathrm{LA}}^2}{\sigma_w^2}\right) \text{ bits/channel use} \tag{2.4.26}$$

where $B \triangleq 2 + \sqrt{2} - 2^{-(L-2)/2} - 2^{-(L-1)/2}$.

In the limit of large L and OSNR, the performance of LACO- and ALACO-OFDM with $\alpha = \sqrt{2}$ are identical and are given as

$$C_{\alpha=\sqrt{2}} = \frac{1}{2}\log\left(1 + \frac{\pi}{6+4\sqrt{2}}\frac{P_{o,\mathrm{AL}}^2}{\sigma_w^2}\right) \text{ bits/channel use.} \tag{2.4.27}$$

Subtracting (2.4.27) from (2.4.23), the asymptotic gap in information rate between the both optical power allocation schemes, i.e., $\alpha = 2$ and $\alpha = \sqrt{2}$, is

$$\triangle C \approx \frac{1}{2}\log\left(\frac{6+4\sqrt{2}}{8}\right) = 0.27 \text{ bits/channel use.} \tag{2.4.28}$$

Figure 2.5 presents a comparison of the information rate among ACO-, LACO-, ALACO-, and AAO-OFDM for different OSNR and power allocation schemes. Note that AAO-OFDM is a special case of ALACO-OFDM with $L = 1$, i.e., the information rate of AAO-OFDM is given by $C_{\mathrm{AL}}^{(1)}$. An upper bound on capacity of IM/DD optical channel based on sphere packing [130] and a lower bound based on entropy

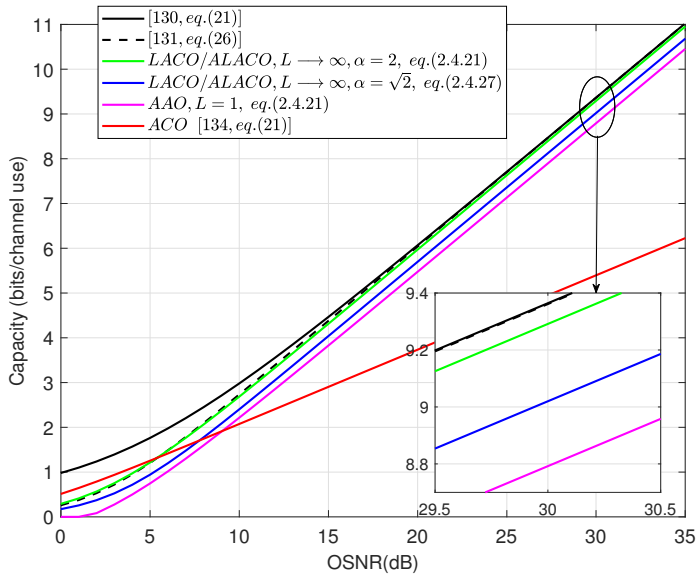

Figure 2.5: Achievable information rate comparison among ACO-, LACO-, ALACO- and AAO-OFDM for different OSNR.

power inequality (EPI) and exponentially distributed input [131] are added as the benchmarks. It can be seen ALACO- and LACO-OFDM with $\alpha = 2$ achieves higher information rate than that with $\alpha = \sqrt{2}$. And the gap is about 0.27 bits/channel use at OSNR= 30 dB that agrees well with (2.4.28). Although ALACO- and LACO-OFDM with $\alpha = 2$ can achieve higher capacity at high OSNR, its uncoded BER performance is worse than that with $\alpha = \sqrt{2}$, which is shown in Fig. 2.7.

Figure 2.6 presents the achievable information rate comparison between ALACO- and LACO-OFDM for different number of layers and OSNRs. It is evident that ALACO-OFDM achieves higher rate than LACO-OFDM with a smaller number of layers at high OSNR.

Specifically, for $\alpha = \sqrt{2}$, when OSNR = 20 dB, ALACO-OFDM with $L = 3$ achieves 5.8 bits/channel use, which is higher than the highest achievable information

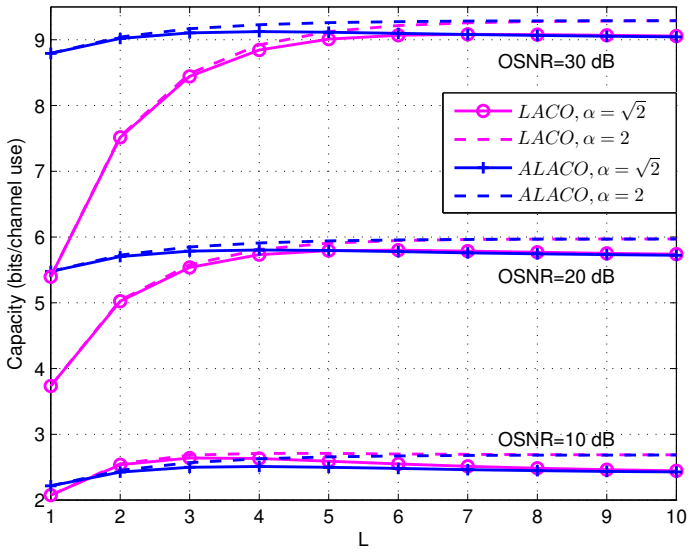

Figure 2.6: Achievable information rate comparison between ALACO- and LACO-OFDM for different OSNRs and L layers (Note: L denotes the number of ACO-OFDM layers used).

rate of LACO-OFDM with $L = 6$. When OSNR $= 30$ dB, ALACO-OFDM achieves the highest achievable information rate with $L = 4$, which is larger than the highest achievable information rate of LACO-OFDM with $L = 7$. However, when OSNR $=$ 10 dB, LACO-OFDM achieve highest achievable information rate with $L = 3$ and is slightly higher than ALCO-OFDM. This is because of the increased overhead in transmitting the sign information in the first layer. Similar conclusions hold for $\alpha = 2$ where ALACO- can still achieve higher rate than LACO-OFDM with fewer number of layers.

Notice that the difference between the achievable information rates of ALACO- and LACO-OFDM becomes smaller as number of layers increases. This is because ALACO-OFDM is defined to use all the available subcarriers, and the number of unused subcarriers in LACO-OFDM approaches zero as L becomes large.

2.5 Numerical Results

2.5.1 BER Performance

In this section, uncoded BER performance of ALACO-OFDM is analyzed and compared to its counterparts in terms of OSNR. A flat channel with AWGN is assumed and the channel gain from an LED to a PD is assumed to be unity [56, 58]. Considering a flat channel and mitigating the effect of error propagation in layered OFDM schemes, the sign bits of the AVO-OFDM layer are uniformly inserted into the bits modulated in the first ACO-OFDM layer. The total number of subcarriers is set to $N = 1024$ and M-QAM constellations with gray labeling are utilized.

The overall BER performance of ALACO-OFDM with $M = 16$ and $L = 3$ for different α are shown in Fig. 2.7. It can be seen ALACO-OFDM with power allocation factor $\alpha = \sqrt{2}$ achieves optimal BER performance in high OSNR regime. ALACO with $\alpha = \sqrt{2}$ achieves about 1.3 dB gains compared to that with $\alpha = 2$ at BER= 10^{-5}. Hence, the optical power allocation factor is set to $\alpha = \sqrt{2}$ for ALACO-, LACO- and eU-OFDM in Fig. 2.8, Fig. 2.9, Fig. 2.10 and Fig. 3.10.

Using the formula for calculating the BER of QAM [82, 141], a theoretical bound on the BER of ALACO-OFDM can be given by

$$\mathrm{BER}_{\mathrm{AL}} = \frac{\sum_{l=1}^{L} \mathrm{BER}_{\mathrm{ACO}}^{(l)} 2^{-l} \log_2 M_l + \mathrm{BER}_{\mathrm{AVO}} 2^{-L} \log_2 M_v}{\sum_{l=1}^{L} 2^{-l} \log_2 M_l + 2^{-L} \log_2 M_v} \tag{2.5.1}$$

where $\mathrm{BER}_{\mathrm{ACO}}^{(l)}$ is BER of l-th layer ACO-OFDM, given by

$$\mathrm{BER}_{\mathrm{ACO}}^{(l)} \approx \frac{4(\sqrt{M_1} - 1)}{\sqrt{M_1} \log_2 M_1} Q\left(\sqrt{\frac{3}{M_1 - 1} \frac{2^{l-2}\sigma_l^2}{\sigma_w^2}}\right), \tag{2.5.2}$$

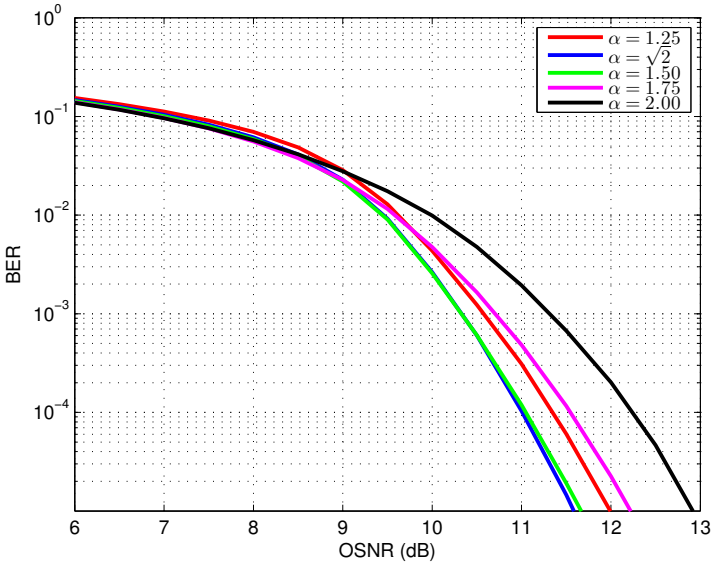

Figure 2.7: Overall uncoded BER performance of ALACO-OFDM with different optical power allocation factor α with $L = 3$ and $M = 16$ used.

and $\mathrm{BER}_{\mathrm{AVO}}$ is BER of AVO-OFDM, given by

$$\mathrm{BER}_{\mathrm{AVO}} \approx \frac{4(\sqrt{M_v}-1)}{\sqrt{M_v}\log_2 M_v} Q\left(\sqrt{\frac{3}{M_v-1}\frac{2^L\sigma_v^2}{\sigma_w^2}}\right). \tag{2.5.3}$$

"$\approx$" is used in (2.5.2) and (2.5.3) since we assume the interference from lower layers is removed completely.

Theoretical and simulated overall BER with sign bits in first layer and in second layer are shown in Fig. 2.8, in which $L = 3$, $\alpha = \sqrt{2}$ and $M = 16$ are used. It can be seen ALACO-OFDM with sign bits carried in first layer slightly outperforms that with sign bits in second layer in low OSNR regime, while both perform nearly the same in high OSNR regime. This is because sign bits carried in second layer are distorted by AWGN and estimation error accumulated from the first layer, which slightly worsens the overall BER performance. As OSNR increases, the estimation

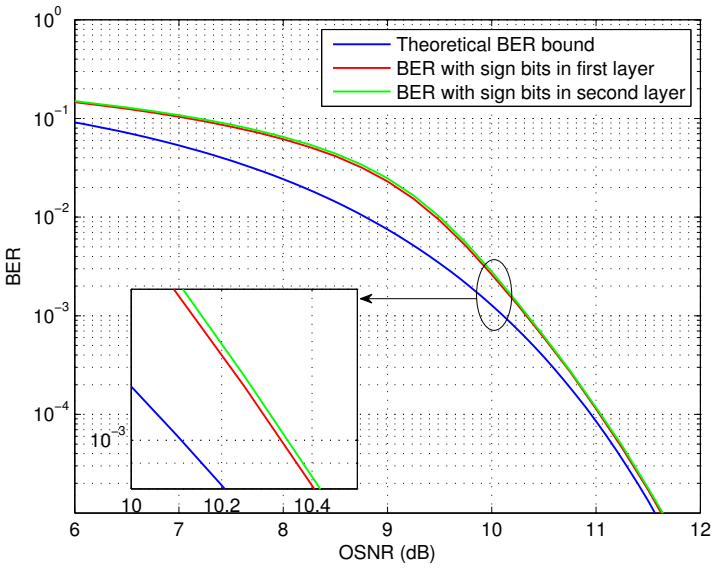

Figure 2.8: Theoretical and simulated overall BER with sign bits in first layer and in second layer with $L = 3$ and $M = 16$ used.

error in first layer becomes negligible [98]. The theoretical bound on BER is also shown in Fig. 2.8, which is close to the simulated overall BER in high OSNR regime.

The BER performance of ALACO- is compared to eU-, LACO- and AAO-OFDM is shown in Fig. 2.9 with the same spectral efficiency and a finite number of layers. Notice that AAO-OFDM is the special case of the ALACO-OFDM with $L = 1$ and the both share the same performance. For ALACO-OFDM, $M = 256$ with $L = 2$, 3 or 4 is employed, of which has spectral efficiency is $\Upsilon_{\mathrm{AL}}^{(L)} = 3.75$, 3.875 or 3.9375 bits/channel use according to (2.3.6). For eU- and LACO-OFDM, combinations of $M = 1024$ with $L = 2$, $M = 512$ with $L = 3$ and $M = 256$ with $L = 4$ are utilized, of which the spectral efficiency is respectively 3.75, 3.9375 and 3.75 bits/channel use based on (2.3.2). For AAO-OFDM, $M_1 = 512$ with $M_2 = 1024$ is employed, of which the spectral efficiency is $\Upsilon_{\mathrm{AAO}} = 3.75$ bits/channel use according to (2.3.3). It can be

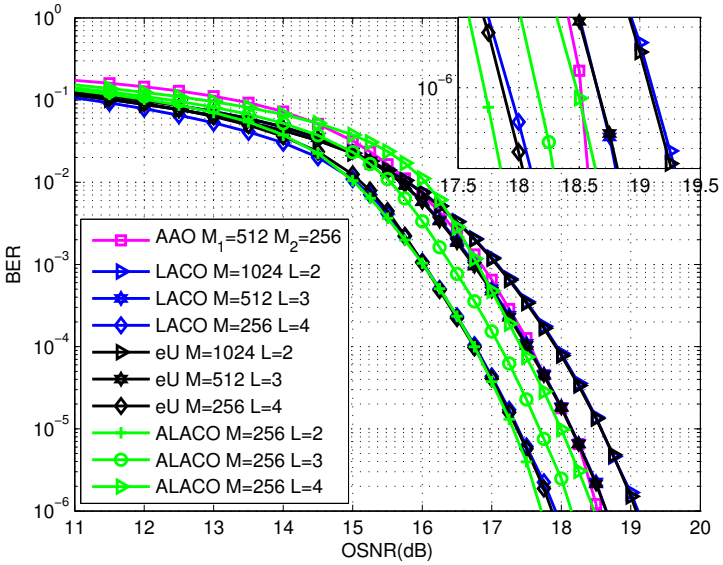

Figure 2.9: Uncoded BER performance comparison between ALACO-OFDM and its counterparts with the same or close spectral efficiency (Set $\Upsilon_{\mathrm{AAO}} = \Upsilon_{\mathrm{eU}}^{(2)} = \Upsilon_{\mathrm{LA}}^{(2)} = \Upsilon_{\mathrm{AL}}^{(2)} = \Upsilon_{\mathrm{eU}}^{(4)} = \Upsilon_{\mathrm{LA}}^{(4)} = 3.75$ bits/channel use, $\Upsilon_{\mathrm{eU}}^{(3)} = \Upsilon_{\mathrm{LA}}^{(3)} = \Upsilon_{\mathrm{AL}}^{(4)} = 3.9375$ bits/channel use, and $\Upsilon_{\mathrm{AL}}^{(3)} = 3.875$ bits/channel use).

seen that eU- and LACO-OFDM have the similar BER performance with the same layer number and constellation size, in which the spectral efficiencies of the both schemes are the same.

Consider comparing schemes with the same spectral efficiency and number of layers. Fig. 2.9 indicates that ALACO- with $M = 256$ and $L = 2$ has the best BER performance compared to eU- with $M = 1024$ and $L = 2$, LACO- with $M = 1024$ and $L = 2$ and AAO-OFDM with $M_1 = 512$ and $M_2 = 1024$ at the same spectral efficiency of 3.75 bits/channel use. When the BER approaches 10^{-6}, ALACO-OFDM achieves about 1.3, 1.4 and 0.8 dB performance gains over eU-, LACO- and AAO-OFDM, respectively. This is because ALACO-OFDM can employ smaller constellation size M to achieve the same spectral efficiency compared to the other three schemes.

Considering only the spectral efficiency, from Sec. 2.3.1, increasing L improves the spectral efficiency of ALACO-, eU- and LACO-OFDM. Notice that ALACO- with $M = 256$ and $L = 2$ has about 0.2 dB gain over eU- and LACO-OFDM with $M = 256$ and $L = 4$ at BER=10^{-6}. The spectral efficiencies of all schemes noted are the same, however, ALACO-OFDM is able to provide a gain while operating with less complexity and latency (i.e., smaller L). Similarly at a higher spectral efficiency, ALACO-OFDM with $M = 256$ and $L = 4$ achieves about 0.2 dB gain at BER= 10^{-6} compared to eU- and LACO-OFDM with $M = 512$ and $L = 3$ at the spectral efficiency of 3.9375 bits/channel use. Thus, ALACO-OFDM provides higher spectral efficiencies over earlier approaches while retaining the power efficiency of ACO-OFDM schemes.

2.5.2 Probability Density Function

In this section, the PDF of ALACO-OFDM time-domain signal for different number of layers is investigated. In ALACO-OFDM, L layers of ACO-OFDM time-domain signal are independent. Although first layer ACO-OFDM signal carries sign bits of AVO-OFDM signal, the both are independent [48]. Hence, the PDF of ALACO-OFDM can be calculated by convolving the PDFs of L layers of ACO-OFDM and the PDF of AVO-OFDM. Then the PDF of ALACO-OFDM is given by

$$f_{\mathrm{AL}}^{(L)}(\xi) = f_1(\xi) \otimes \ldots \otimes f_L(\xi) \otimes f_v(\xi) \tag{2.5.4}$$

where $\otimes$ denotes convolution operation and $f_l(\xi)$ and $f_v(\xi)$ are given by (2.4.1) and (2.4.3).

The simulated and theoretical PDF of ALACO-OFDM are shown in Fig. 2.10, in

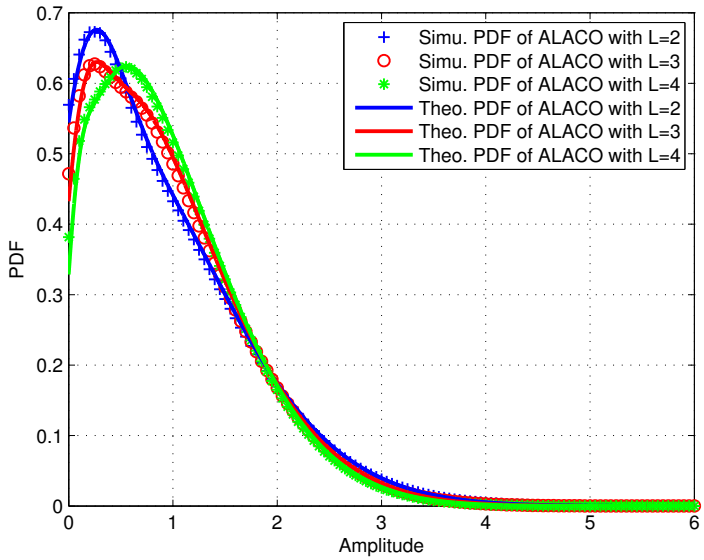

Figure 2.10: Simulated and theoretical PDF of ALACO-OFDM with $L = 2,\ 3,$ and 4 ('Simu.' and 'Theo.' denote 'Simulated' and 'Theoretical', respectively).

which the total optical power is set to unity and $\alpha = \sqrt{2}$. For the simulated PDF, $N = 1024$ subcarriers and 16-QAM are utilized. It can be seen the simulated and theoretical PDF of ALACO-OFDM are aligned well.

2.5.3 PAPR Comparison

In this section, the PAPR of ALACO-OFDM is compared versus its counterparts. Define the PAPR of a discrete time-domain signal z_n as [142]

$$\text{PAPR} = \frac{\max\limits_{0 \le n \le N-1} z_n^2}{\text{E}\{z_n^2\}}. \tag{2.5.5}$$

The complementary cumulative distribution function (CCDF) of PAPR is defined

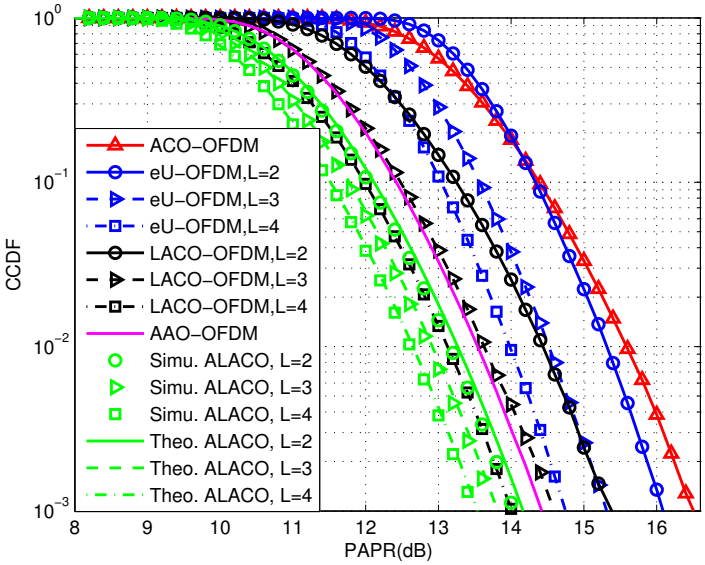

Figure 2.11: PAPR comparison between ALACO-OFDM and its counterparts with $N = 1024$ subcarriers ($\alpha = \sqrt{2}$ is used for ALACO, LACO-, and eU-OFDM).

as

$$\mathrm{CCDF}(\gamma) = 1 - \Pr\{\mathrm{PAPR} \leq \gamma\} \tag{2.5.6}$$

where $\Pr\{\Psi\}$ denotes the probability of an event Ψ.

Following the method calculating the CCDF of LACO-OFDM in [82], the $\mathrm{CCDF}(\gamma)$ can be well approximated using its PDF as

$$\mathrm{CCDF}(\gamma) \approx 1 - \left(2\int_{-\infty}^{\sqrt{\gamma \mathrm{E}\{z_n^2\}}} f_{\mathrm{AL}}^{(L)}(\xi)d\xi - 1\right)^{N/2}. \tag{2.5.7}$$

The CCDF of PAPR in ALACO- with different total layer number L is analyzed and compared to ACO-, eU-, LACO- and AAO-OFDM as shown in Fig. 3.10 for $N = 1024$. It can be seen the theoretical CCDFs of ALACO-OFDM approximated by (2.5.7) agree well with the simulated results for different number of layers. It is

evident that ACO-OFDM has the worst PAPR performance. For eU-, LACO- and ALACO-OFDM, the PAPR performance becomes better as the total layer number L increases from 2 to 4. This trend was also noticed in earlier work [82]. When CCDF $= 10^{-3}$, the PAPR of ALACO- with $L = 2$ is about 0.4 dB, 1.3 dB, 2.1 dB and 2.5 dB smaller compared to AAO-, LACO- with $L = 2$, eU- with $L = 2$ and ACO-OFDM, respectively. This is because for the same peak value, the average electrical power of ALACO-OFDM is bigger, which leads to a smaller PAPR according to (3.5.9). When CCDF approaches 10^{-3}, the PAPR of ALACO- with $L = 4$ is about 0.9 dB, 0.5 dB, 1.3 dB and 3.1 dB smaller compared to AAO-, LACO- with $L = 4$, eU- with $L = 4$ and ACO-OFDM, respectively. The analysis and comparison between ALACO-OFDM and its counterparts suggests that ALACO-OFDM, with its lower PAPR, may be less sensitive to LED nonlinearity.

2.6 Conclusions

In this paper, ALACO-OFDM is proposed to enhance the spectral efficiency for IM/DD OFDM communications while retaining power efficiency. Signal analysis indicates the spectral efficiency gap between ALACO- and DCO-OFDM can be made negligible even with a small number of layers. Notice that ALACO-OFDM is a generalization of AAO-OFDM and has a spectral efficiency that is $\frac{\log_2 M-2}{2^{L+1}}$ bits/channel use larger than eU- or LACO-OFDM with the same layer number L. Two optical power allocation schemes are discussed over the layers of ALACO-OFDM with the objective of optimizing uncoded transmission performance and the achievable information rate respectively. ALACO-OFDM with optical power allocation factor $\alpha = 2$ achieves optimal rate while the optimal uncoded BER performance is achieved when $\alpha = \sqrt{2}$.

A theoretical bound on the uncoded BER of ALACO-OFDM is also derived, which matches the simulated BER in high SNR regime. The information rate analysis also indicates ALACO- can achieve higher rate with even smaller number of layers than LACO-OFDM. In addition, ALACO- has smaller PAPR compared to eU-, LACO- and AAO-OFDM, which suggests better performance on nonlinear LED channels. Complexity analysis indicates the computational complexity of ALACO-OFDM is on the same order at LACO- and eU-OFDM while realizing performance gains. Monte Carlo simulation of BER performance is analyzed and compared, from which it can be concluded that ALACO- has the best BER performance over layered ACO-OFDM approaches with the same spectral efficiency while using a smaller number of layers.

This paper focuses on transceiver design for ALACO-OFDM and shows its advantage with a smaller number of layers over its counterparts operating at a given spectral efficiency. Future investigation include integrating ALACO-OFDM with error control coding, PAPR suppressing approaches, specially designed low-complex FFTs/IFFTs for ACO- and AVO-OFDM as well as the use of alternate transforms such as the Harley transform.

Chapter 3

Layered Antisymmetry-Constructed Clipped Optical OFDM for Low-Complexity VLC Systems

Research work in this chapter appears in the following two papers [107, 106] while minor modifications are made according to thesis format.

- R. Bai and S. Hranilovic, "Layered antisymmetry-constructed clipped optical OFDM for IM/DD systems," *in 2019 IEEE Global Communications Conference*

(GLOBECOM). IEEE, Nov. 2019, pp. 1-6.

- R. Bai and S. Hranilovic, "Layered antisymmetry-constructed clipped optical OFDM for low-complexity VLC systems," *Optics Express*, vol. 29, no. 7, pp. 10613-10630, 2021.

According to the discussions in Section 1.5.1, decreasing required computational complexity is another important challenge in VLC systems. Given this challenge, antisymmetry-constructed clipped optical orthogonal frequency division multiplexing (AC-OFDM) and layered AC-OFDM (LAC-OFDM) are presented for VLC systems in this chapter.

In ACO-OFDM, signals have an anti-symmetry, and the negative parts are clipped to satisfy the non-negativity constraint without any loss of information [51]. Inspired by ACO-OFDM, an anti-symmetry is constructed in an OFDM frame, and negative parts are clipped at zero in AC-OFDM. However, ACO-OFDM's anti-symmetry arises by modulating odd subcarriers only and setting even subcarriers to be zero in the frequency domain. In contrast, AC-OFDM directly constructs an anti-symmetry in one frame in the time domain. In this way, AC-OFDM requires half-size inverse fast Fourier transform (IFFT) at the transmitter and half-size fast Fourier transform (FFT) at the receiver, respectively. Hence, AC-OFDM enjoys low complexity to implement at both the transmitter and the receiver. Though low-complexity to implement, AC-OFDM achieves the same spectral efficiency, BER performance and PAPR performance as conventional ACO-OFDM.

To enhance the spectral efficiency, LAC-OFDM is further developed by combining and transmitting L layers of AC-OFDM signals simultaneously in philosophy similar

to LACO-OFDM [74] and eU-OFDM [143]. At the receiver, the first layer is demodulated first and is reconstructed. Then, the reconstructed signal is removed from the received signal before demodulating the next layer. In this way, LAC-OFDM is demodulated layer by layer. The required IFFT and FFT sizes are halved in each layer at both the transmitter and the receiver. The required real-valued multiplication and addition operations are computed and compared to the existing LACO-OFDM and eU-OFDM. Numerical results show LAC-OFDM achieves the same BER performance as LACO-OFDM and eU-OFDM in a VLC LOS flat channel. However, LAC-OFDM is superior in requiring fewer arithmetic operations to implement at both the transmitter and receiver. It is worth mentioning that for non-flat channels, the time-domain processing in LAC-OFDM makes equalization at the receiver more complex.

Abstract In this paper, antisymmetry-constructed clipped optical orthogonal frequency division multiplexing (AC-OFDM) is proposed for visible light communications (VLC) systems, in which an antisymmetry property is imposed directly in time domain. AC-OFDM has nearly the same spectral efficiency and peak-to-average power ratio (PAPR) as traditional asymmetrically clipped optical OFDM (ACO-OFDM) but is less complex to implement. Layered AC-OFDM (LAC-OFDM) is then proposed as an extension to further improve spectral efficiency, where different layers of AC-OFDM signals are added in the time domain and transmitted simultaneously. Computational complexity analysis and numerical results show that LAC-OFDM has nearly the same spectral efficiency as layered asymmetrically clipped optical OFDM (LACO-OFDM) and enhanced unipolar OFDM (eU-OFDM) but is less complex. Specifically, LAC-OFDM requires less than half the multiplication and addition operations compared to the comparable LACO-OFDM scheme. Additionally, a pairwise iterative receiver for LAC-OFDM is proposed and its computational complexity is analysed. Monte Carlo simulation results show that LAC-OFDM requires nearly the same optical signal-to-noise ratio (OSNR) to achieve the same BER performance as LACO- and eU-OFDM.

3.1 Introduction

Visible light communications (VLC) adds a secondary communication channel to ubiquitous solid-state illumination devices [2, 3, 4, 144] and is a candidate for future indoor broadband distribution. In VLC, data are modulated onto the instantaneous optical intensity emitted by a light-emitting diode (LED), i.e., intensity modulation (IM), and are detected by a photodiode (PD), i.e., direct detection (DD). As a result,

all signals for VLC channels must be real, non-negative and have a bounded mean value [2, 3, 4, 48, 145, 144].

The use of orthogonal frequency division multiplexing (OFDM) in VLC channels has been popular since illumination LEDs are typically low pass in nature. In order to make OFDM compatible with IM/DD VLC channels, direct current (DC) biased optical OFDM (DCO-OFDM) adds a DC bias to a conventional OFDM signal, consuming optical power while conveying no information [51]. To improve optical power efficiency, asymmetrically clipped optical OFDM (ACO-OFDM) [146], unipolar OFDM (U-OFDM) [143] and Flip-OFDM [121] were proposed, however, at a cost of half of the spectral efficiency. Enhanced U-OFDM (eU-OFDM) [143], layered ACO-OFDM (LACO-OFDM) [74], enhanced ACO-OFDM (eACO-OFDM) [147], spectral and energy efficient OFDM (SEE-OFDM) [132], and enhanced ACO-OFDM (EACO-OFDM) [102] were then proposed to retain the power efficiency of early approaches (i.e., no added DC bias) while improving spectral efficiency. LACO-OFDM and eU-OFDM work by combining different streams or layers of non-negative time-domain signals at the transmitter and successively detecting the modulated symbols at the receiver. The achievable information rate and optimal optical power allocation of LACO-OFDM are recently studied in [88, 53, 148, 86], indicating that LACO-OFDM has a small gap to the capacity for the Gaussian optical intensity channels. Although eU- and LACO-OFDM have the advantages aforementioned, they suffer from high computational complexity to generate and demodulate streams or layers which may limit their application in simple and energy efficient luminaires [149]. A low-complexity single-FFT receiver for LACO-OFDM was proposed and investigated in [105], which can reduce the computational complexity of the receiver. However, the

reduction in complexity comes at the expense of approximately 2 dB power penalty at a bit error rate (BER) of 10^{-3} [105]. Reducing the complexity at both transmitter and receiver and retaining power efficiency remains a challenge for LACO-OFDM.

This paper proposes *antisymmetry-constructed clipped optical OFDM* (AC-OFDM) and layered AC-OFDM (LAC-OFDM) for VLC systems, extending our previous work in [107]. In AC-OFDM, an antisymmetric time domain signal is constructed, as in ACO-OFDM, however, all processing is done in time domain. Different from Flip-OFDM, which employs two OFDM frames to send portions of one OFDM symbol depending on their sign [121], AC-OFDM imposes anti-symmetry directly in time domain in a single OFDM frame. AC-OFDM employs a half-size inverse fast Fourier transform (IFFT) and a half-size fast Fourier transform (FFT) compared to ACO-OFDM and Flip-OFDM. Recently, and in parallel, an approach with a half-size FFT was proposed to reduce the complexity of only the receiver for hybrid asymmetrically clipped optical OFDM (HACO-OFDM) [150]. While [150] is similar in philosophy to our earlier work on AC-OFDM [107], in this work we present a general framework which applies at both the transmitter and the receiver as well as developing a layered modulation to improve spectral efficiency. LAC-OFDM sends information in different layers of AC-OFDM signals that are superimposed and detected successively. The spectral efficiency of LAC-OFDM is nearly two times bigger than ACO-OFDM, AC-OFDM and Flip-OFDM. Though LAC-OFDM is similar in philosophy to LACO-OFDM, it is shown to have a much simpler implementation which is more amenable to low cost, energy efficient, luminaires employed in VLC systems.

Compared to our previous conference paper [107], in this paper theoretical BER expressions for LAC-OFDM are derived to evaluate the reliability, which is aligned

well with numerical results in the high signal-to-noise ratio (SNR) regime. The PAPR performance of LAC-OFDM is also evaluated and compared with its counterparts, which shows that the PAPR of LAC-OFDM is nearly the same as LACO-OFDM, and is smaller than that of eU-OFDM with the same number of layers/streams. Furthermore, a pairwise iterative receiver is proposed to further improve BER performance of AC-OFDM and LAC-OFDM. In the proposed pairwise iterative receiver, pairwise clipping is utilized in each AC-OFDM layer. This pairwise iterative receiver concept has also been extended to the case of eU-OFDM to improve BER performance. A computational complexity analysis is presented to compare this pairwise iterative receiver for LAC-OFDM to an improved receiver for LACO-OFDM [77] and to the pairwise iterative receiver for eU-OFDM. It is shown that LAC-OFDM is less complex for the same number of layers and the same number of iterations. Thus, for the same complexity, the pairwise iterative receiver for LAC-OFDM can employ more iterations and thus achieve greater BER gains compared to LACO-OFDM.

The balance of this paper is organized as follows. Section 3.2 introduces AC- and LAC-OFDM and makes connections to existing ACO-OFDM, eU-OFDM and LACO-OFDM techniques. The computational complexity and spectral efficiency of LAC-OFDM are analysed in Section 3.3 and a pairwise iterative receiver for LAC-OFDM is presented in Section 3.4. Numerical results of the computational complexity, BER, and PAPR performance are presented in Section 3.5. Finally, conclusions are drawn in Section 3.6.

3.2 System Description

3.2.1 Background

In an ACO-OFDM system with N subcarriers, data symbols are only modulated onto the odd subcarriers, while the even subcarriers are set to zero [146]. Considering the Hermitian symmetry necessary to have a real-valued output, the input symbol vector to the inverse fast Fourier transform (IFFT) is

$$\mathbf{X}_{\text{ACO}} = [0, X_1, 0, X_3, 0, \cdots, 0, X_3^*, 0, X_1^*]^T \tag{3.2.1}$$

where $X_k, 1 \leq k \leq N-1$, is a complex symbol chosen from a quadrature amplitude modulation (QAM) constellation and $(\cdot)^T$ denotes the transpose operation. A consequence of using odd carriers only is that the output ACO-OFDM signal vector $\mathbf{x}$ of the IFFT is antisymmetric [146], i.e.,

$$x_n = -x_{n+N/2},\ 0 \leq n \leq N/2-1. \tag{3.2.2}$$

It has been shown that the non-negativity constraint can be satisfied by clipping the negative part of $\mathbf{x}$ directly with no distortion to the data being transmitted. The clipping distortion consists only of components at even subcarriers in the frequency domain and hence at the receiver side, symbols can be detected directly on the odd subcarriers [146].

Although, ACO-OFDM is optically power efficient, it has half of the spectral efficiency of traditional DCO-OFDM. To improve the spectral efficiency, LACO-OFDM

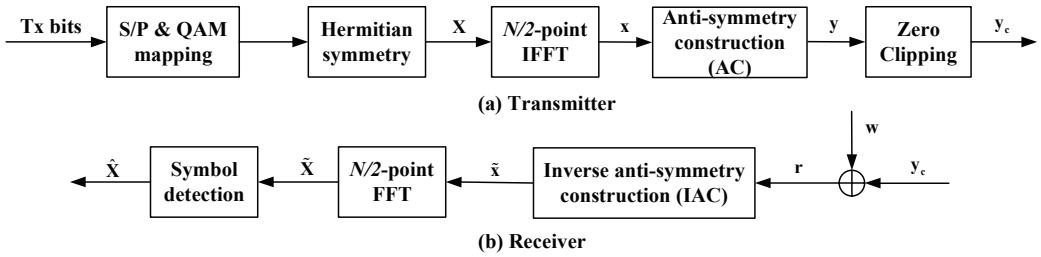

Figure 3.1: Transceiver design block diagram for AC-OFDM.

was proposed where different layers of ACO-OFDM signals are summed in time domain and transmitted simultaneously [74]. In the l-th layer, LACO-OFDM modulates data onto subcarriers with index $2^{l-1}(2k+1), (k = 0, 1, \ldots, N/2^{l+1} - 1)$. Notice that for each layer, the sets of subcarriers used are disjoint. The output signal vector of the IFFT of each layer shares the antisymmetric property of ACO-OFDM and thus zero clipping is used to make the signal non-negative. The clipping distortion for a given layer distorts all higher layers and hence, the LACO-OFDM receiver demodulates lower layer ACO-OFDM symbols before higher layers.

3.2.2 Antisymmetry-constructed clipped optical OFDM

For an N-subcarrier AC-OFDM system, the transceiver block diagram is shown in Fig. 3.1.

At the transmitter, bits are mapped to QAM constellation symbols after serial-to-parallel (S/P) conversion. After Hermitian symmetry, the input symbol vector to the $N/2$-point IFFT is given by

$$\mathbf{X} = \left[0, X_1, X_2 \cdots, X_{N/4-1}, 0, X^*_{N/4-1}, \cdots, X^*_2, X^*_1\right]^T. \tag{3.2.3}$$

Notice that the AC-OFDM frame is of length $N/2$, rather than N for ACO-OFDM

in (3.2.1), and that there is no requirement to use only odd subcarriers. The output of the $N/2$-point IFFT is given as

$$x_n = \frac{1}{\sqrt{N/2}} \sum_{k=0}^{N/2-1} X_k \exp\left(j\frac{2\pi}{N/2}nk\right),\ 0 \le n \le \frac{N}{2} - 1. \tag{3.2.4}$$

Prior to zero clipping, consider constructing the time-domain signal vector $\mathbf{y}$ using a process termed here as *antisymmetry construction* (AC) as

$$\mathbf{y} = [\mathbf{x}^T, -\mathbf{x}^T]^T. \tag{3.2.5}$$

Notice that $\mathbf{y}$ is antisymmetric, as in ACO-OFDM, i.e.,

$$y_n = -y_{n+N/2},\ 0 \le n \le N/2 - 1. \tag{3.2.6}$$

Similar to ACO-OFDM, the negative part of $\mathbf{y}$ can be clipped without any loss of information. Hence, applying zero clipping to $\mathbf{y}$ leads to the AC-OFDM signal

$$y_{c,n} = \frac{1}{2}(y_n + |y_n|),\ 0 \le n \le N - 1 \tag{3.2.7}$$

where $|y_n|$ is the clipping distortion and $|\cdot|$ denotes the absolute value operation. Using (3.2.5) and (3.2.7), $\mathbf{y}_c$ can be written as

$$\mathbf{y}_c = \left[\frac{1}{2}\mathbf{x}^T + \frac{1}{2}|\mathbf{x}|^T, -\frac{1}{2}\mathbf{x}^T + \frac{1}{2}|\mathbf{x}|^T\right]^T. \tag{3.2.8}$$

Notice that $\mathbf{x}$ can be retrieved from $\mathbf{y}_c$ through the an *inverse antisymmetry construction* (IAC) operation

$$x_n = y_{c,n} - y_{c,n+N/2},\ 0 \leq n \leq N/2-1. \tag{3.2.9}$$

It is straightforward to show that the IAC operation proposed here also appears implicitly in the demodulation of traditional ACO-OFDM, however, it requires an N-point FFT. After a cyclic prefix (CP) is added to each OFDM symbol, a digital to analog converter (DAC) is employed. The resulting analog signal $y_c(t)$ is utilized to modulate an LED.

At the receiver, shot noise and thermal noise are well modelled as additive white Gaussian noise (AWGN) [146, 4]. After sampling and discarding CP, the received signal is then given by

$$r_n = y_{c,n} + w_n,\ 0 \leq n \leq N-1 \tag{3.2.10}$$

where w_n is a sample of AWGN with standard deviation σ_w. Based on (3.2.9), an estimate of x_n can be obtained through the IAC operation as

$$\tilde{x}_n = r_n - r_{n+N/2}, 0 \leq n \leq N/2-1. \tag{3.2.11}$$

Define $\tilde{\mathbf{X}}$ as the $N/2$-point FFT of the received vector $\tilde{\mathbf{x}}$.

Finally, AC-OFDM can be detected symbol-by-symbol, i.e.,

$$\widehat{X}_k = \arg\min_{X\in\Omega_X} \left\| X - \widetilde{X}_k \right\|^2,\ k = 1, 2, \cdots, N/4-1 \tag{3.2.12}$$

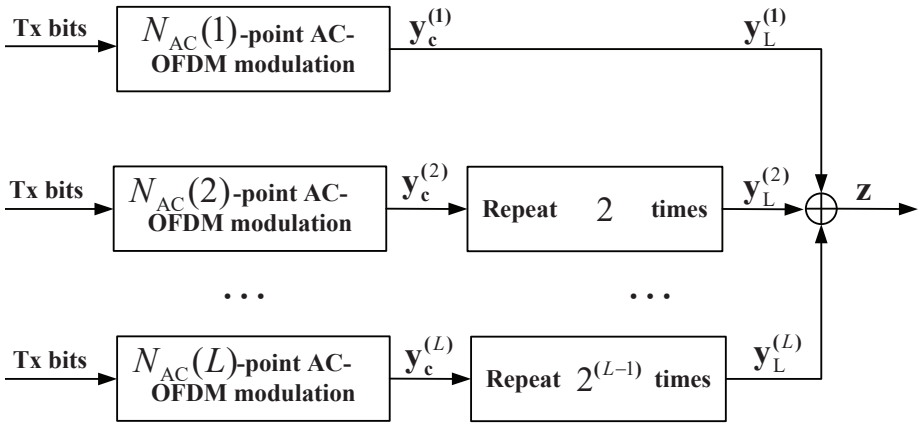

Figure 3.2: Transmitter design block diagram for LAC-OFDM.

where Ω_X denotes the constellation and $\|\cdot\|$ denotes the magnitude of a complex value.

Although a line-of-sight (LOS), flat VLC channel is assumed in this paper to aid in presenting the core idea and to compare with earlier work [146, 53, 143, 147, 132, 105, 77], AC-OFDM and later LAC-OFDM are applicable to dispersive channels. An equalization approach similar to those proposed for eU-OFDM [141] would be equivalently be applicable to AC- and LAC-OFDM.

3.2.3 Layered AC-OFDM

The transmitter block diagram for the proposed LAC-OFDM is shown in Fig. 3.2. Similar to traditional LACO-OFDM [74], different layers of AC-OFDM signals are added in the time domain and transmitted simultaneously to improve spectral efficiency.

In the l-th layer LAC-OFDM, an $N_{\mathrm{AC}}(l)$-point IFFT is utilized where

$$N_{\mathrm{AC}}(l) = \frac{N}{2^l}. \tag{3.2.13}$$

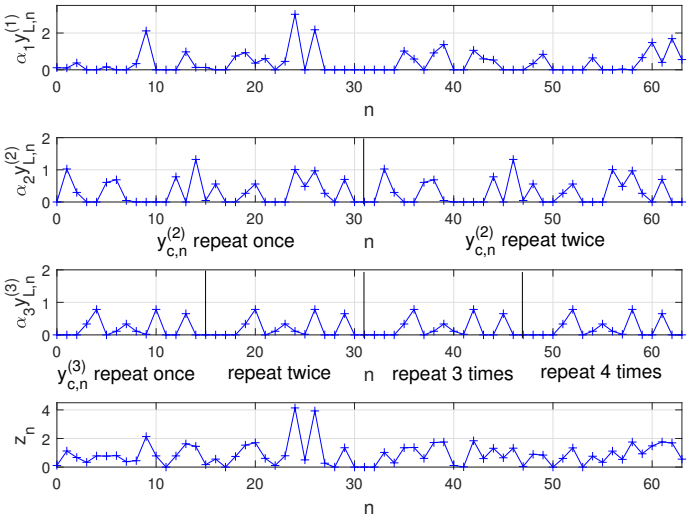

Figure 3.3: An example of LAC-OFDM signal with $L = 3$ layers and $N = 64$ subcarriers (16 QAM is used and α_l defined in (3.5.3)).

At each layer, AC-OFDM modulation is performed including an $N_{\text{AC}}(l)$-point IFFT (3.2.4), antisymmetry construction (3.2.5) and zero clipping (3.2.7), resulting in the signal, $\mathbf{y}_c^{(l)}$, with length $2N_{\text{AC}}(l)$. Notice that, in contrast, a $2N_{\text{AC}}(l)$-point IFFT is used at layer l in the traditional LACO-OFDM. Similar to traditional LACO-OFDM [74], repeating $\mathbf{y}_c^{(l)}$ for 2^{l-1} times gives the l-th layer signal in LAC-OFDM

$$\mathbf{y}_L^{(l)} = [\underbrace{\mathbf{y}_c^{(l)^T}, \cdots, \mathbf{y}_c^{(l)^T}}_{\text{repeated } 2^{l-1} \text{ times}}]^T. \tag{3.2.14}$$

The LAC-OFDM signal vector, $\mathbf{z}$ is the summation of the L layers,

$$\mathbf{z} = \sum_{l=1}^{L} \alpha_l \mathbf{y}_L^{(l)} \tag{3.2.15}$$

where α_l is power allocation factor for each layer. To illustrate the core concepts, Fig.

3.3 presents an example of the waveforms at all layers for LAC-OFDM with $L = 3$ and $N = 64$. Though not explicitly shown in Fig. 3.2, this scaling is done to ensure that each layer has the same BER performance as discussed in Sec. 3.5.

At the receiver, LAC-OFDM is demodulated layer-by-layer in an analogous fashion to LACO-OFDM, as shown in Fig. 3.4. Since the clipping distortion of l-th layer only affects layers higher than l, symbols in lower layers are detected first. Specifically, symbols $\widehat{\mathbf{X}}^{(1)}$ in the first layer are detected first through an $N/2$-point AC-OFDM demodulation including inverse antisymmetry construction (3.2.11), $N/2$-point FFT and symbol detection (3.2.12). Then the first layer AC-OFDM signal $\hat{\mathbf{y}}_L^{(1)}$ is reconstructed through $N/2$-point AC-OFDM modulation including $N/2$-point IFFT (3.2.4), antisymmetry construction (3.2.5) and zero clipping (3.2.7). The signal $\hat{\mathbf{y}}_L^{(1)}$ is subtracted from $\mathbf{r}$ leading to $\tilde{\mathbf{y}}_L^{(2)}$, which is used to demodulate the symbols $\widehat{\mathbf{X}}^{(2)}$ in the second layer.

For $l \geq 2$, as seen in Figs. 3.2 and 3.3, notice that $\mathbf{y}_c^{(l)}$ is repeated 2^{l-1} times in each frame. Taking advantage of this inherent repetition code in the frame of the LAC-OFDM signal, an estimate of the AC-OFDM signal $\tilde{\mathbf{y}}_c^{(l)}$ can be found by averaging over the repetitions in the frame as

$$\tilde{y}_{c,n}^{(l)} = \frac{1}{2^{l-1}} \sum_{q=0}^{2^{l-1}-1} \tilde{y}_{L,n+2qN_{\mathrm{AC}}(l)}^{(l)},\ 0 \leq n \leq 2N_{\mathrm{AC}}(l) - 1. \tag{3.2.16}$$

This repetition in the structure of the LAC-OFDM signal is also exploited in LACO-OFDM through the use of the N-point FFT operation. The remaining detection process is similar to the case for layer 1 described earlier with the signals reconstructed at each layer and subtracted from the received signal. To distinguish this receiver from the pairwise iterative receiver in Sec. IV.A, we denote this receiver as *simple*

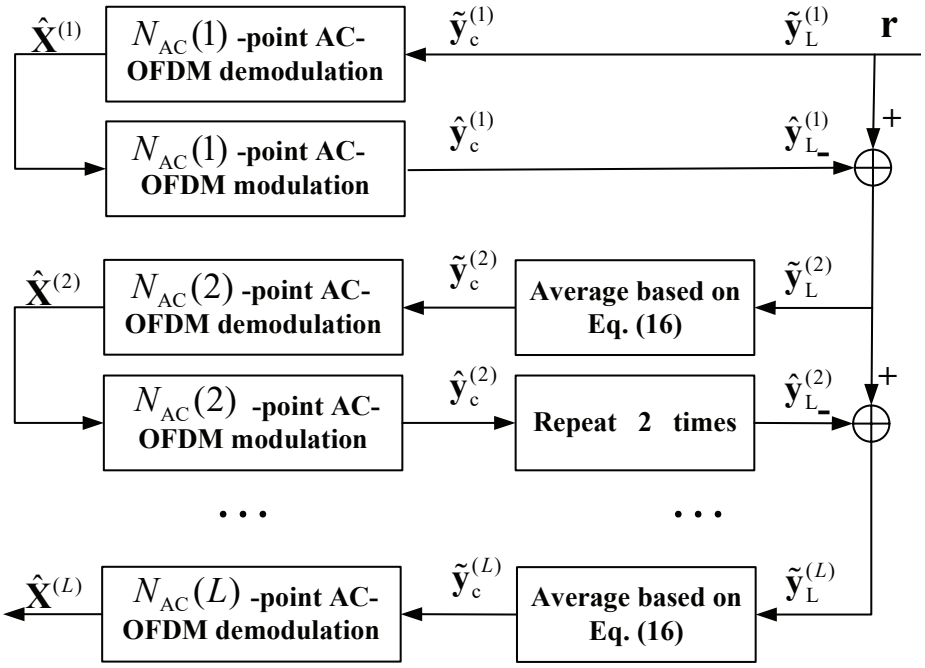

Figure 3.4: Receiver design block diagram for LAC-OFDM.

receiver for LAC.

It is interesting to note that this receiver structure combines the layered approach of LACO-OFDM [74] with the time-domain processing of the receiver from eU-OFDM [143].

3.3 Complexity Analysis

3.3.1 Computational Complexity Assumptions

In this section, the computational complexity of LAC-OFDM is quantified by counting the number of real-valued multiplication and addition operations required and comparing them to the requirements for LACO- and eU-OFDM.

According to [133], for an N-point IFFT or FFT module using Cooley-Tukey decomposition and N a power of 2, $M(N)$ real-valued multiplication operations (RMOs) and $A(N)$ real-valued addition operations (RAOs) are required where

$$M(N) = 2N\log_2(N) - 4N + 4 \tag{3.3.1}$$

and

$$A(N) = 3N\log_2(N) - 2N + 2. \tag{3.3.2}$$

In the subsequent analyses, our underlying assumption is that operations such as clipping or antisymmetry construction (3.2.5) do not require any arithmetic operations as they can be efficiently implemented via switching logic. Additionally, the complexity of detecting individual symbols on carriers is not included in this analysis and will be the same for all schemes considered.

3.3.2 Computational Complexity: Transmitter

At the LAC-OFDM transmitter, each layer requires an FFT of length $\frac{N}{2^l}$. Hence, the number of required RMOs and RAOs for an N-subcarrier LAC-OFDM system with L layers are

$$M_{\text{LAC}}^{(t)}(L,N) = \sum_{l=1}^{L} M\left(\frac{N}{2^l}\right) = \left(1 - \frac{1}{2^L}\right) 2N\log_2(N) - \left(8 - \frac{L+4}{2^{L-1}}\right) N + 4L \tag{3.3.3}$$

and

$$A_{\mathrm{LAC}}^{(t)}(L,N)=\sum_{l=1}^{L}A\left(\frac{N}{2^l}\right)+(L-1)N=\left(1-\frac{1}{2^L}\right)3N\log_2(N) \\ -\left(9-L-\frac{3L+8}{2^L}\right)N+2L. \tag{3.3.4}$$

Using a similar analysis, for traditional LACO-OFDM with N subcarriers and L layers, the RMOs and AMOs are [86]

$$M_{\mathrm{LACO}}^{(t)}(L,N)=\sum_{l=1}^{L}M\left(\frac{N}{2^{l-1}}\right)=\left(1-\frac{1}{2^L}\right)4N\log_2(N)-\left(12-\frac{2L+6}{2^{L-1}}\right)N+4L \tag{3.3.5}$$

and

$$A_{\mathrm{LACO}}^{(t)}(L,N)=\sum_{l=1}^{L}A\left(\frac{N}{2^{l-1}}\right)+(L-1)N=\left(1-\frac{1}{2^L}\right)6N\log_2(N) \\ -\left(11-L-\frac{3L+5}{2^{L-1}}\right)N+2L. \tag{3.3.6}$$

For eU-OFDM with N subcarriers and L streams, the RMOs and RAOs averaged over an OFDM super frame are [86]

$$M_{\mathrm{eU}}^{(t)}(L,N)=\frac{1}{2^L}\sum_{l=1}^{L}2^{L-l}M(N)=\left(1-\frac{1}{2^L}\right)(2N\log_2(N)-4N+4) \tag{3.3.7}$$

and

$$A_{\mathrm{eU}}^{(t)}(L,N)=\frac{1}{2^L}\left(\sum_{l=1}^{L}2^{L-l}A(N)+(L-1)2^LN\right) \\ =\left(1-\frac{1}{2^L}\right)(3N\log_2(N)-2N+2)+(L-1)N. \tag{3.3.8}$$

Comparing the dominant terms of $M_{\mathrm{LAC}}^{(t)}(L,N)$ and $A_{\mathrm{LAC}}^{(t)}(L,N)$ to $M_{\mathrm{LACO}}^{(t)}(L,N)$

and $A^{(t)}_{\text{LACO}}(L,N)$, LAC-OFDM requires only half the RMOs and half the RAOs as traditional LACO-OFDM. Though the complexity of LAC-OFDM and the averaged complexity eU-OFDM are comparable, LAC-OFDM has the advantage of lower latency since the transmitting signal is N-samples long while eU-OFDM transmits a signal of length $2^L N$-samples. Numerical comparisons of complexity are presented in Sec. 3.5.

3.3.3 Computational Complexity: Receiver

To detect the l-th layer of the AC-OFDM signal ($1 \leq l \leq L-1$), an $N_{\text{AC}}(l)$ point FFT is required followed by an $N_{\text{AC}}(l)$ point IFFT. For the last layer, i.e., $l = L$, only an $N_{\text{AC}}(L)$ point FFT is required since signal reconstruction is not necessary. Thus, LAC-OFDM requires $M^{(r)}_{\text{LAC}}(L,N)$ RMOs where

$$\begin{aligned} M^{(r)}_{\text{LAC}}(L,N) &= 2\sum_{l=1}^{L-1} M\left(\frac{N}{2^l}\right) + M\left(\frac{N}{2^L}\right) \\ &= \left(1-\frac{3}{2^{L+1}}\right) 4N\log_2(N) - \left(16-\frac{3L+10}{2^{L-1}}\right) N + 8L - 4. \end{aligned} \tag{3.3.9}$$

Similarly, the number of RAOs can be computed, however, three additional steps are required. Averaging of the received samples is done in each layer following (3.2.16) to take advantage of the structure of each layer followed by the IAC operation, defined in (3.2.9). Also, the interference of lower layers must be removed from higher layers.

The resulting number of real additions required is

$$\begin{aligned}
&A_{\mathrm{LAC}}^{(r)}(L,N) \\
&= 2\sum_{l=1}^{L-1} A\left(\frac{N}{2^l}\right) + A\left(\frac{N}{2^L}\right) + \underbrace{\sum_{l=1}^{L}\left(1-\frac{1}{2^{l-1}}\right)N}_{\text{Averaging (3.2.16)}} + \underbrace{\sum_{l=1}^{L}\frac{N}{2^l}}_{\text{IAC (3.2.9)}} + \underbrace{N(L-1)}_{\text{Subtraction of lower layers}} \\
&= \left(1-\frac{3}{2^{L+1}}\right)6N\log_2(N) - \left(18-2L-\frac{9L+19}{2^L}\right)N \quad + 4L - 2.
\end{aligned} \tag{3.3.10}$$

For LACO-OFDM with receiver proposed in [74], in which inter-layer interference (ILI) is removed in frequency domain, the total number of real arithmetic operations are

$$\begin{aligned}
&M_{\mathrm{LACO}}^{(r)}(L,N) = \\
&2\sum_{l=1}^{L-1} M\left(\frac{N}{2^{l-1}}\right) + M(N) = \left(1-\frac{\frac{8}{5}}{2^L}\right)10N\log_2(N) - \left(28-\frac{L+2}{2^{L-4}}\right)N + 8L - 4
\end{aligned} \tag{3.3.11}$$

and

$$\begin{aligned}
&A_{\mathrm{LACO}}^{(r)}(L,N) = \\
&2\sum_{l=1}^{L-1} A\left(\frac{N}{2^{l-1}}\right) + A(N) + \sum_{l=1}^{L-1}\frac{N}{2^l} = \left(1-\frac{\frac{8}{5}}{2^L}\right)15N\log_2(N) - \left(21-\frac{12L+7}{2^{L-1}}\right)N \\
&+ 4L - 2.
\end{aligned} \tag{3.3.12}$$

As shown in [86], the complexity of LACO-OFDM receiver can be reduced by removing ILI from the lower layers in the time domain before demodulating each

layer. The required RMOs and RAOs in this case are

$$M_{\mathrm{LA}}^{(r)}(L,N)=\left(1-\frac{3}{2^{L+1}}\right)8N\log_2(N)-\left(24-\frac{6L+14}{2^{L-1}}\right)N+8L-4 \tag{3.3.13}$$

and

$$A_{\mathrm{LA}}^{(r)}(L,N)=\left(1-\frac{3}{2^{L+1}}\right)12N\log_2(N)-\left(23-2L-\frac{9L+10}{2^{L-1}}\right)N+4L-2. \tag{3.3.14}$$

For the same N and L, $M_{\mathrm{LA}}^{(r)}(L,N)$ and $A_{\mathrm{LA}}^{(r)}(L,N)$ are smaller than $M_{\mathrm{LACO}}^{(r)}(L,N)$ and $A_{\mathrm{LACO}}^{(r)}(L,N)$, respectively, since an N-point FFT is used once in the receiver to remove ILI in the time domain while it is used twice in the receiver with removing ILI in the frequency domain.

For eU-OFDM, the RMOs and RAOs averaged over an OFDM super frame are [86]

$$\begin{aligned}&M_{\mathrm{eU}}^{(r)}(L,N)\\&=\frac{1}{2^L}\left(2\sum_{l=1}^{L-1}2^{L-l}M(N)+M(N)\right)=\left(1-\frac{3}{2^{L+1}}\right)(4N\log_2(N)-8N+8)\end{aligned} \tag{3.3.15}$$

and

$$\begin{aligned}&A_{\mathrm{eU}}^{(r)}(L,N)=\\&\frac{1}{2^L}\left(2\sum_{l=1}^{L-1}2^{L-l}A(N)+A(N)+\sum_{l=1}^{L}\left(2^{l-1}-1\right)\frac{2^LN}{2^{l-1}}+\sum_{l=1}^{L}2^{L-l}N+2^L(L-1)N\right)\\&=\left(1-\frac{3}{2^{L+1}}\right)6N\log_2(N)-\left(6-2L-\frac{7}{2^L}\right)N+4-\frac{6}{2^L}.\end{aligned} \tag{3.3.16}$$

Observing the dominant terms of $M_{\mathrm{LAC}}^{(r)}(L,N)$ and $A_{\mathrm{LAC}}^{(r)}(L,N)$ with $M_{\mathrm{LACO}}^{(r)}(L,N)$

and $A^{(r)}_{\text{LACO}}(L,N)$, the proposed receiver for LAC-OFDM requires less than half complexity than the traditional LACO-OFDM. As is the case with the transmitter, the receiver of LAC-OFDM requires nearly the same complexity as eU-OFDM on average. However, LAC-OFDM also has an advantage of lower latency at the receiver since each symbol can be decoded from N received samples while eU-OFDM requires $2^L N$ received samples for demodulation [143].

3.3.4 Spectral Efficiency Analysis

In LAC-OFDM, L layers of AC-OFDM signals are added together in the time domain and transmitted simultaneously. The spectral efficiency can be calculated by

$$\Upsilon^{(L)}_{\text{LAC}} = \frac{\sum_{l=1}^{L}\left(\frac{N}{2^{l+1}}-1\right)\log_2 M_l}{N+N_{\text{CP}}} \tag{3.3.17}$$

where M_l is constellation size of QAM utilized in l-th layer and N_{CP} is assumed to be length of CP. If the constellation size for each layer is set to be the same, $M_l = M$, (3.3.17) can be rewritten as

$$\Upsilon^{(L)}_{\text{LAC}} = \frac{1}{2}\left(1-\frac{1}{2^L}\right)\frac{N}{N+N_{\text{CP}}}\log_2(M) - \frac{L}{N+N_{\text{CP}}}\log_2(M). \tag{3.3.18}$$

For LACO-OFDM, the spectral efficiency is given by [74]

$$\Upsilon^{(L)}_{\text{LACO}} = \frac{1}{2}\left(1-\frac{1}{2^L}\right)\frac{N}{N+N_{\text{CP}}}\log_2(M) \tag{3.3.19}$$

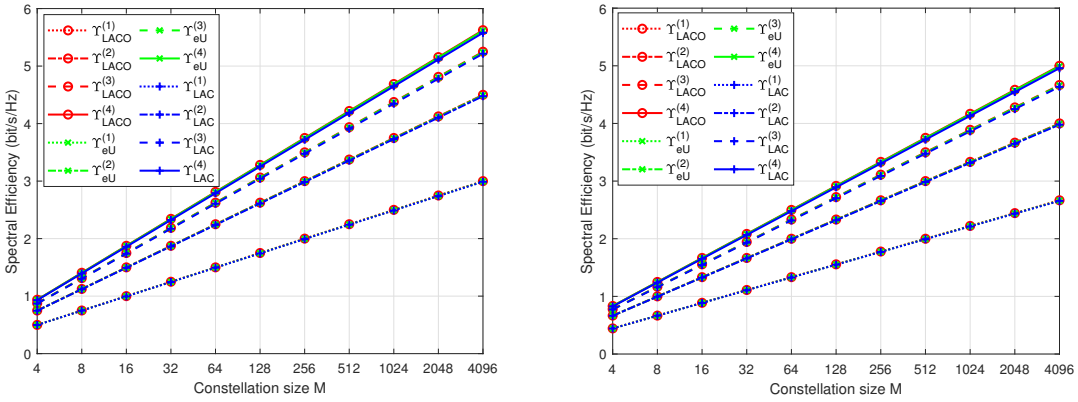

(a) $N_{\text{CP}} = 0$. (b) $N_{\text{CP}} = N/8$

Figure 3.5: Spectral efficiency comparison between LAC-OFDM and its counterparts.

while for eU-OFDM with N subcarriers and L streams, spectral efficiency is [143]

$$\Upsilon^{(L)}_{\text{eU}} = \frac{1}{2}\left(1 - \frac{1}{2^L}\right)\frac{N-2}{N+N_{\text{CP}}}\log_2(M). \tag{3.3.20}$$

For LACO-OFDM and LAC-OFDM, the number of layers L cannot be greater than $\log_2 N - 1$. For a given N and $L \leq \log_2 N - 1$, LACO-OFDM has the largest spectral efficiency while LAC-OFDM has the smallest spectral efficiency. However, in the case when N is large

$$\lim_{N\longrightarrow\infty} \frac{L}{N}\log_2(M) = 0 \tag{3.3.21}$$

and $\Upsilon_{\text{LAC}} \to \Upsilon_{\text{LACO}}$. Hence, for large N

$$\Upsilon^{(L)}_{\text{LAC}} \approx \Upsilon^{(L)}_{\text{eU}} \approx \Upsilon^{(L)}_{\text{LACO}} = \frac{1}{2}\left(1 - \frac{1}{2^L}\right)\frac{N}{N+N_{\text{CP}}}\log_2(M). \tag{3.3.22}$$

Spectral efficiency comparisons between LAC-OFDM and its counterparts for different constellation sizes is shown in Fig. 3.5, where $N = 1024$. It can be seen that the spectral efficiency of LAC-OFDM is nearly the same as eU- and LACO-OFDM when the same constellation size and the same number of layers/streams are employed.

3.4 Pairwise Iterative Receiver

3.4.1 Pairwise Iterative Receiver Design

To fully exploit the antisymmetric characteristics of the AC-OFDM signal and to enhance the BER performance, a pairwise iterative receiver for LAC-OFDM is proposed. In this pairwise receiver, AC-OFDM layers are distinguished from each other and pairwise detection on antisymmetric clipped samples is performed to mitigate the effect of noise (analogous to [120, 77] which were developed in the context of ACO-OFDM).

For the l-th AC-OFDM layer, due to the antisymmetry (3.2.6) and zero clipping (3.2.7), there exists one prior knowledge that one component inside the pair $\left(\tilde{y}_{c,n}^{(l)}, \tilde{y}_{c,n+N_{\mathrm{AC}}(l)}^{(l)}\right)$ $(0 \leq n \leq N_{\mathrm{AC}}(l) - 1)$ is necessarily zero. As given in [120], the impact on noise can be theoretically cut in half by detecting which sample was clipped at the transmitter and setting it to zero at the receiver. Specifically, after imposing pairwise detection of $\tilde{y}_{c,n}^{(l)}$, an estimate of the l-th layer AC-OFDM signal is given by

$$\left(\tilde{y}_{p,n}^{(l)}, \tilde{y}_{p,n+N_{\mathrm{AC}}(l)}^{(l)}\right) = \begin{cases} (\tilde{y}_{c,n}^{(l)}, 0), & \tilde{y}_{c,n}^{(l)} \geq \tilde{y}_{c,n+N_{\mathrm{AC}}(l)}^{(l)} \\ (0, \tilde{y}_{c,n}^{(l)}), & \tilde{y}_{c,n}^{(l)} < \tilde{y}_{c,n+N_{\mathrm{AC}}(l)}^{(l)} \end{cases}, 0 \leq n \leq N_{\mathrm{AC}}(l) - 1. \quad (3.4.1)$$

Employing pairwise detection following (3.4.1), Algorithm 1 presents the pseudocode for this pairwise iterative receiver. Note that a subscript "(i)" is added to all signals to denote the iteration number. As in [77], in the i-th iteration, a more precise estimate of l-th layer AC-OFDM signal is obtained using the pairwise detection (3.4.1). Subsequent layers are then updated by removing interference from this layer using this pairwise detected estimate according to (3.4.2).

Algorithm 1 Pairwise iterative receiver for LAC-OFDM

Input: Received signals, r_n; Number of layers, L; Constellation set, Ω_X; Maximum number of iterations, I_{m};

Output: Detected symbols, $\hat{\mathbf{X}}^{(l),(I_{\mathrm{m}})}$;

1: Calculate $\hat{\mathbf{X}}^{(l),(0)}$ and $\hat{\mathbf{y}}_L^{(l),(0)}$, $l \in [1\ L]$, by using the simple LAC receiver introduced in Sec. II.C (i.e., 0-th iteration)
2: **for** $i = 1 : I_{\mathrm{m}}$ **do**
3: **for** $l = 1 : L$ **do**
4: Create an estimate of layer signal $\widehat{\mathbf{y}'}_L^{(l)}$ by removing previously detected layer signals

$$\widehat{y'}_{L,n}^{(l),(i)} = r_n - \sum_{\nu=1}^{l-1} \alpha_\nu \hat{y}_{L,n}^{(\nu),(i)} - \sum_{\nu=l+1}^{L} \alpha_\nu \hat{y}_{L,n}^{(\nu),(i-1)}. \tag{3.4.2}$$

5: Generate $\mathbf{y'}_c^{(l)}$ by averaging according to (3.2.16);
6: Calculate $\tilde{\mathbf{y}'}_p^{(l)}$ according to pairwise detector (3.4.1);
7: Update $\hat{\mathbf{X}}^{(l),(i)}$ by AC-OFDM demodulation;
8: Update $\hat{\mathbf{y}}_c^{(l),(i)}$ using AC-OFDM modulation;
9: Update $\hat{\mathbf{y}}_L^{(l),(i)}$ by repeating $2^{(l-1)}$ times of $\hat{\mathbf{y}}_c^{(l),(i)}$;
10: **end for**
11: **end for**
12: **return** $\hat{\mathbf{X}}^{(l),(I_{\mathrm{m}})}$;

As shown in Sec. 3.5, as the number of iterations increases the performance of this pairwise receiver converges. In practice, the number of iterations is fixed and denoted I_{m}.

3.4.2 Computational Complexity: Pairwise Iterative Receiver

In each iteration of this pairwise iterative receiver, an additional simple LAC-OFDM receiver step is required in addition to pairwise detection and an additional $N_{\mathrm{AC}}(L)$-point AC-OFDM modulation for the L-th layer. The complexity of pairwise detection is not included in this analysis, since it can be implemented efficiently by logic operations. Hence, the pairwise iterative receiver with I_{m} iterations requires RMOs and RAOs as

$$M_{\mathrm{LAC}}^{(\mathrm{PR})}(L,N,I_{\mathrm{m}}) = M_{\mathrm{LAC}}^{(r)}(L,N) + I_{\mathrm{m}}\left(M_{\mathrm{LAC}}^{(r)}(L,N) + M\left(\frac{N}{2^L}\right)\right), \tag{3.4.3}$$

$$A_{\mathrm{LAC}}^{(\mathrm{PR})}(L,N,I_{\mathrm{m}}) = A_{\mathrm{LAC}}^{(r)}(L,N) + I_{\mathrm{m}}\left(A_{\mathrm{LAC}}^{(r)}(L,N) + A\left(\frac{N}{2^L}\right)\right). \tag{3.4.4}$$

For the improved receiver of LACO-OFDM in [77], pairwise detection is also required. The complexity can be similarly derived as,

$$M_{\mathrm{LA}}^{(\mathrm{IR})}(L,N,I_{\mathrm{m}}) = M_{\mathrm{LA}}^{(r)}(L,N) + I_{\mathrm{m}}\left(M_{\mathrm{LA}}^{(r)}(L,N) + M\left(\frac{N}{2^{L-1}}\right)\right), \tag{3.4.5}$$

$$A_{\mathrm{LA}}^{(\mathrm{IR})}(L,N,I_{\mathrm{m}}) = A_{\mathrm{LA}}^{(r)}(L,N) + I_{\mathrm{m}}\left(A_{\mathrm{LA}}^{(r)}(L,N) + A\left(\frac{N}{2^{L-1}}\right)\right). \tag{3.4.6}$$

A similar pairwise detector can be applied to the detection of eU-OFDM using the approach in Sec.3.4.1 recognizing that half of the samples in the transmitted signal are zero in each layer. In addition, an iterative detector can be implemented using

the framework in Algorithm 1 to yield complexity

$$M_{\mathrm{eU}}^{(\mathrm{PR})}(L,N,I_{\mathrm{m}}) = M_{\mathrm{eU}}^{(r)}(L,N) + I_{\mathrm{m}}\left(M_{\mathrm{eU}}^{(r)}(L,N) + \frac{M(N)}{2^L}\right), \tag{3.4.7}$$

$$A_{\mathrm{eU}}^{(\mathrm{PR})}(L,N,I_{\mathrm{m}}) = A_{\mathrm{eU}}^{(r)}(L,N) + I_{\mathrm{m}}\left(A_{\mathrm{eU}}^{(r)}(L,N) + \frac{A(N)}{2^L}\right). \tag{3.4.8}$$

In contrast to an earlier iterative receiver for eU-OFDM in [125], this approach is likely less complex since it does not require matrix inversion operations in each iteration.

3.5 Numerical results

3.5.1 Computational Complexity Comparisons

Computational complexity comparisons among the transmitters of LAC- and LACO- and eU-OFDM with different subcarrier number N and layer number L is shown in Fig. 3.6 and are plotted using the expressions derived in Sec. 3.3.2. In Fig. 3.6 (a) and (b), the layer number $L = 4$ and in Fig. 3.6 (c) and (d), $N = 1024$. It is evident the transmitter of traditional LACO-OFDM requires the most RMOs as well as RAOs, which is more than twice as the proposed LAC-OFDM. Notice also that the transmitter of eU-OFDM requires slightly more operations than LAC-OFDM.

Computational complexity comparison among receivers is computed using the expressions in Sec. 3.3.3 and is shown in Fig. 3.7. In Fig. 3.7 (a) and (b), L is set to 4, while in Fig. 3.7 (c) and (d), N is set to 1024. As is the case in the transmitter, the relative complexity of LAC-OFDM is the least amongst the techniques considered. Additionally, Fig. 3.7 demonstrates that the receiver for LACO-OFDM which removes

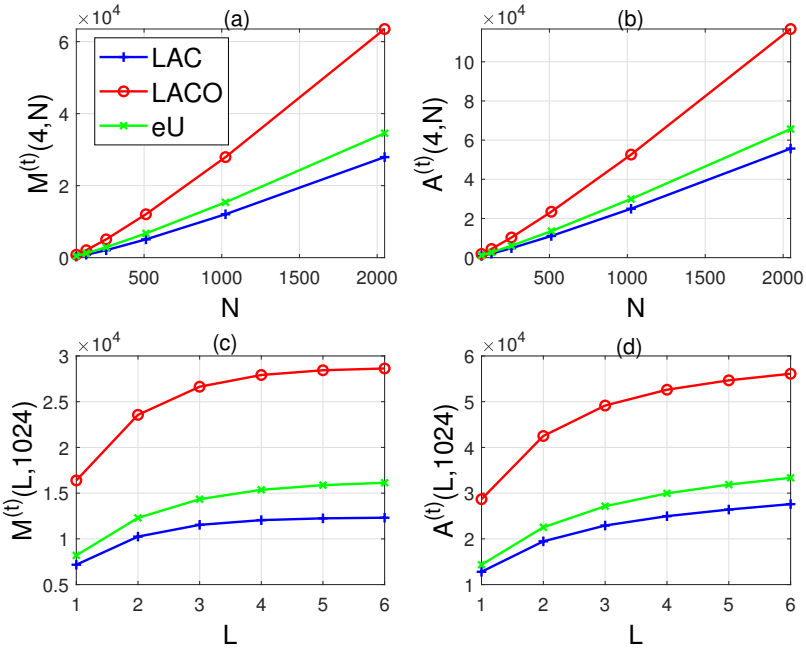

Figure 3.6: Transmitter Complexity Comparison.

ILI in the time domain is less complex than the receiver for LACO-OFDM removing ILI in the frequency domain. Notice also that the complexity of all receivers is sensitive to N as the dominant term in the complexity analysis arises due to the size of the FFT/IFFT operations. Since LAC-OFDM uses a smaller FFT size, it benefits from reduced complexity. In addition, the complexity saturates with increasing L since the number of degrees of freedom, either in frequency (e.g., LAC- or LACO-OFDM) or in time (e.g., eU-OFDM), in all IM/DD OFDM techniques considered here reduces by half with each increase in layer number. Thus, the incremental increase in complexity must saturate for increasing L.

Consider the case of $N = 1024$ and $L = 4$ for example. Table 3.1 provides a summary of the number of real addition and multiplication operations required for each IM/DD OFDM approach. Clearly, LACO-OFDM requires the most operations

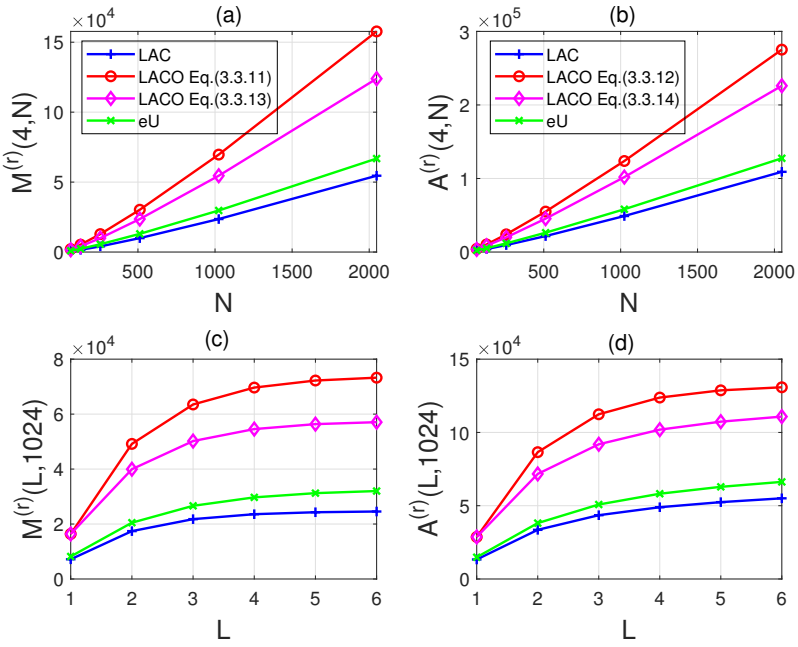

Figure 3.7: Receiver Complexity Comparison.

Table 3.1: Complexity comparison of LAC-, LACO- and eU-OFDM ($N = 1024$ and $L = 4$)

	$M^{(t)}$	$A^{(t)}$	$M^{(r)}$	$A^{(r)}$
LAC	12048	24968	23580	48974
LACO	27920	52616	69660	123790
eU	15364	29954	29703	58180

while LAC-OFDM requires the smallest number. Notice that the transmitter for LACO-OFDM requires more than twice the number of RMOs as LAC-OFDM while for the receiver LAC-OFDM requires nearly one-third of the number of RMOs as LACO-ODFM with receiver designed in [74] according to (3.3.11).

Computational complexity comparison among the pairwise iterative receivers for different number of iterations are computed according to the expressions in Sec. 3.4.2 and is shown in Fig. 3.8, where $L = 4$ and $N = 1024$. The complexity of the simple

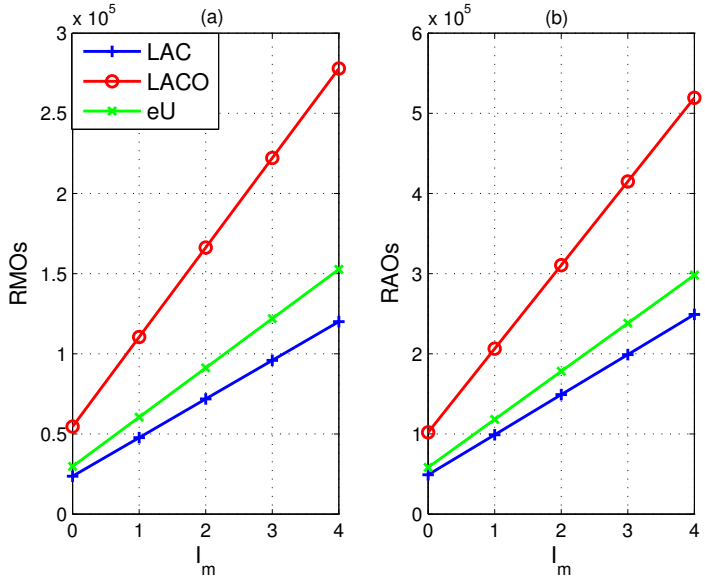

Figure 3.8: Computational complexity comparison among the pairwise iterative receivers for LAC- and LACO- and eU-OFDM for different number of iterations ($L = 4$ and $N = 1024$ are used).

receivers is denoted with $I_m = 0$ iterations. For all the pairwise iterative receivers, the computational complexity increases linearly with I_m. For a given I_m, the pairwise iterative receiver for LAC-OFDM is the least complex among the three schemes. Additionally, as I_m increases, the gap between number of RMOs (or RAOs) for the pairwise receiver for LAC-OFDM and that for LACO-OFDM increases. This also holds for the gap between the pairwise iterative receivers for LAC- and eU-OFDM.

3.5.2 BER Performance

Define the optical signal-to-noise ratio (OSNR) as $\text{OSNR} = 10\log_{10}(P_{\text{o}}/\sigma_w)$ (dB) where P_{o} is total average optical power [139]. A flat channel with AWGN is assumed in the simulation [146, 143] and QAM constellations normalized to unit average energy with Gray labelling are utilized.

Like LACO-OFDM, each layer AC-OFDM signal follows a clipped Gaussian distribution and the total average optical power is given by [86]

$$P_{\mathrm{o}} = \sum\nolimits_{l=1}^{L} \frac{\alpha_l \sigma_l}{\sqrt{2\pi}} \tag{3.5.1}$$

where $\sigma_l = \sqrt{\mathrm{E}\{|x_n^{(l)}|^2\}}$ is the standard deviation of $x_n^{(l)}$.

For the l-th layer AC-OFDM, $\mathbf{y}_c^{(l)}$ is repeated 2^{l-1} times based on (3.2.14) similar to LACO-OFDM in [74]. Thanks to this inherent repetition code, the electrical SNR at k-th subcarrier assuming the clipping distortion removed completely is given by

$$\mathrm{SNR}_k^{(l)} = 2^{l-1}\alpha_l^2 \frac{\mathrm{E}\{|X_k^{(l)}|^2\}}{2\sigma_w^2} \overset{(a)}{=} 2^{l-1}\alpha_l^2 \frac{\mathrm{E}\{|x_n^{(l)}|^2\}}{2\sigma_w^2} = \frac{2^{l-2}\alpha_l^2\sigma_l^2}{\sigma_w^2} \tag{3.5.2}$$

where (a) is due to Parseval's theorem [133]. When the power allocation factor is set as [143, 74, 86]

$$\alpha_1 : \alpha_2 : \cdots : \alpha_L = 1 : 2^{-\frac{1}{2}} : \cdots : 2^{-\frac{L-1}{2}} \text{ , and } \alpha_1 = 1, \tag{3.5.3}$$

then

$$\mathrm{SNR}_k^{(l)} = \frac{\mathrm{E}\{\|X_k^{(l)}\|^2\}}{2\sigma_w^2},\ 1 \le l \le L. \tag{3.5.4}$$

If the same constellation is used in all layers, the SNR of all data-bearing subcarriers in all layers will be the same. Using the formula for BER of QAM [141], a bound on the BER of AC-OFDM is given by

$$\mathrm{BER}_{\mathrm{AC}}^{(l)} \approx \frac{4(\sqrt{M_l}-1)}{\sqrt{M_l}\log_2 M_l} Q\left(\sqrt{\frac{3}{M_l-1}\mathrm{SNR}_k^{(l)}}\right). \tag{3.5.5}$$

Then a bound on the BER of LAC-OFDM is given by

$$\mathrm{BER}_{\mathrm{LAC}} = \frac{\sum_{l=1}^{L} \mathrm{BER}_{\mathrm{AC}}^{(l)} 2^{-l} \log_2 M_l}{\sum_{l=1}^{L} 2^{-l} \log_2 M_l}. \tag{3.5.6}$$

Since pairwise detection can at best cut the impact of noise in half at the receiver side [120, 77], $\mathrm{SNR}_k^{(l)}$ in (3.5.4) can be enhanced by at most 3-dB by using the pairwise iterative receiver. Hence, a theoretical BER approximation for the proposed pairwise iterative receiver can be obtained as

$$\mathrm{BER}_{\mathrm{LAC,\ PR}} = \frac{\sum_{l=1}^{L} \mathrm{BER}_{\mathrm{AC,\ PR}}^{(l)} 2^{-l} \log_2 M_l}{\sum_{l=1}^{L} 2^{-l} \log_2 M_l} \tag{3.5.7}$$

where

$$\mathrm{BER}_{\mathrm{AC,\ PR}}^{(l)} \approx \frac{4(\sqrt{M_l}-1)}{\sqrt{M_l}\log_2 M_l} Q\left(\sqrt{\frac{6}{M_l-1}\mathrm{SNR}_k^{(l)}}\right). \tag{3.5.8}$$

The BER performance comparison among LAC-, LACO- and eU-OFDM is shown for each layer in Fig. 3.9(a) where $N = 1024$, $L = 4$ and 16-QAM are utilized. It can be seen that all schemes have nearly the same performance. As discussed in Sec.3.3.4, the spectral efficiency of these three techniques are also nearly identical. Thus, LAC-OFDM provides the same BER performance as LACO- and eU-OFDM while remaining less complex. In addition, the theoretical BER bound of LAC-OFDM according to (3.5.6) is presented, which indicates the theoretical BER is aligned well with simulated results especially in the high OSNR regime.

The BER performance of the proposed pairwise iterative receiver of LAC-OFDM for different number of iterations is shown in Fig. 3.9(b), in which the performance of improved receiver of LACO-OFDM in [77] is also presented. In all cases, $N = 1024$, $L = 4$ and 16-QAM are utilized. The pairwise iterative receiver of LAC-OFDM

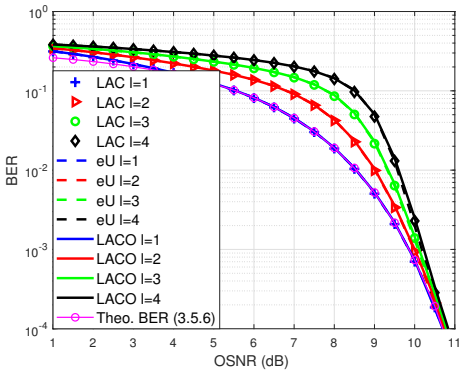

(a) BER of each layer.

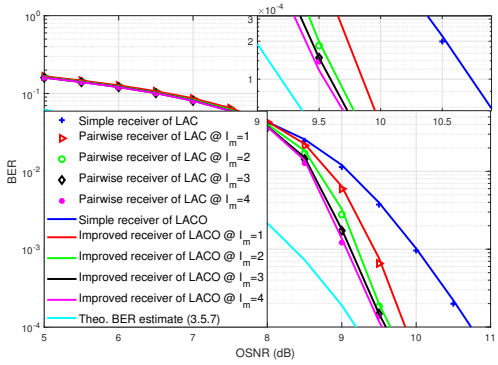

(b) BER of the pairwise iterative receiver

Figure 3.9: BER performance comparison between LAC-OFDM and its counterparts ($N = 1024$ and $L = 4$). Note 'Theo.' denotes the 'theoretical'.

achieves nearly the same performance as the improved receiver for LACO-OFDM in [77] while remaining less complex as shown in Fig. 3.8. At BER $= 10^{-4}$, for $I_m = 1,\ 2,\ 3$ and 4, the pairwise iterative receiver achieves about 0.88 dB, 1.08 dB, 1.15 dB and 1.19 dB OSNR gains compared to the simple receiver, respectively. Although the BER performance becomes better as I_m increases from 1 to 4, the relative improvement decreases with I_m. Additionally, the theoretical BER estimate according to (3.5.7) is presented, which is aligned well with simulated results in the high OSNR regime.

Consider the complexity constrained design examples in Table 3.2 where the two cases have nearly same computational complexity. In Case 1, the pairwise iterative receiver of LAC-OFDM employs one iteration while LACO-OFDM employs no iterations. Though the receivers in this scenario require approximately the same complexity, LAC-OFDM achieves a 0.88 dB OSNR gain over LACO-OFDM at BER $= 10^{-4}$. In Case 2, the pairwise iterative receiver for LAC-OFDM employs 3 iterations while LACO-OFDM employs a single iteration. In Case 2, the both schemes have nearly

Table 3.2: Comparison between pairwise receivers for LAC- and LACO-OFDM with nearly same complexity and their gain compared to corresponding simple ($I_m = 0$) receivers at BER $= 10^{-4}$ ($N = 1024$ and $L = 4$)

		RMOs	RAOs	Gain
Case 1	LAC @ $I_m = 1$	47676	98974	0.88 dB
	LACO @ $I_m = 0$	54556	101902	0 dB
Case 2	LAC @ $I_m = 3$	95868	198974	1.15 dB
	LACO @ $I_m = 1$	110396	206238	0.88 dB

the same complexity, however, the pairwise iterative receiver for LAC-OFDM achieves 0.27 dB gain over the improved LACO-OFDM receiver [77] at BER $= 10^{-4}$.

3.5.3 PAPR Performance

The PAPR of the transmitted signal $\mathbf{z}$ is defined as [142]

$$\text{PAPR} = \frac{\max\limits_{0 \le n \le N-1} z_n^2}{\text{E}\{z_n^2\}}. \tag{3.5.9}$$

The complementary cumulative distribution function (CCDF) of the PAPR is defined as [151] $\text{CCDF}(\xi) = \Pr\{\text{PAPR} > \xi\}$ where $\Pr\{\Pi\}$ denotes the probability of an event Π.

Figure 3.10 compares the CCDF of the PAPR for a variety of LAC-OFDM with related schemes where $N = 1024$. The power allocation factor is set according to (3.5.3). Notice that the PAPR performance of LAC-OFDM closely mirrors that of LACO-OFDM with the same number of layers. This is because each layer of LAC-OFDM follows the same clipped Gaussian distribution as the ACO-OFDM layers in LACO-OFDM. The total signal distribution of LAC-OFDM is thus the same as LACO-OFDM for a given number of layers. The PAPR of eU-OFDM is higher than

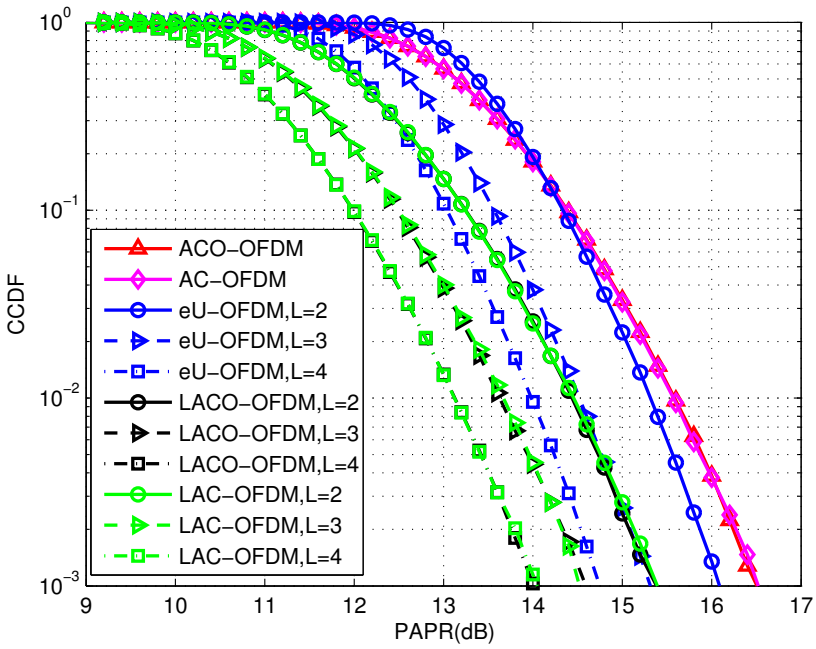

Figure 3.10: PAPR comparison between LAC-OFDM and its counterparts with $N = 1024$ subcarriers.

LAC- and LACO-OFDM for the same number of layers. Therefore, LAC-OFDM has the same PAPR as LACO-OFDM while remaining less complex to implement.

3.6 Conclusions

In this paper, a new approach for the construction of IM/DD OFDM signalling is given. Low-complexity AC-OFDM is proposed where antisymmetry is imposed in time-domain to make satisfying the non-negatively constraint straightforward. To improve spectral efficiency, LAC-OFDM is then proposed, which consists of L super-imposed layers of AC-OFDM much like traditional LACO- and eU-OFDM. Exploiting the special structure of the antisymmetry, a pairwise iterative receiver is also proposed

for LAC-OFDM, which can significantly enhance the BER performance.

Our analysis shows that for the same number of layers/streams LAC-OFDM is less complex than existing LACO- and eU-OFDM methods both for the transmitter and receiver while preserving the same BER performance. LAC-OFDM has the same PAPR performance as LACO-OFDM and a smaller PAPR than eU-OFDM. Additionally, at the same complexity, LAC-OFDM can perform more iterations than LACO-OFDM resulting in a gain in power efficiency. In particular, the pairwise iterative receiver for LAC-OFDM with one iteration requires nearly the same computational complexity as the simple receiver of LACO-OFDM while providing a 0.88 dB OSNR gain at BER = 10^{-4}. The development of low complexity optical OFDM signalling is especially important in VLC systems due to the requirement to maintain energy efficient illumination from the luminaire.

In this paper, the emphasis is on presenting the central concept of AC- and LAC-OFDM and on transceiver design and complexity analysis for LAC-OFDM for low-complexity VLC systems. Future work includes quantifying the performance on dispersive channels as well as experimental verification.

Acknowledgment

The authors would like to thank Prof. Zhaocheng Wang for helpful discussions and for providing sample code on iterative receiver for LACO-OFDM to aid in comparison with [77].

Disclosures

The authors declare no conflicts of interest.

Chapter 4

Low-Complexity Layered ACO-OFDM for Power-Efficient Visible Light Communications

Research work in this chapter appears in the following paper [75] while minor modifications are made according to thesis format.

- R. Bai and S. Hranilovic, "Low-complexity layered ACO-OFDM for power-efficient visible light communications," under major revision in *IEEE Transactions on Green Communications and Networking*, 2021.

Based on discussion in Section 1.5.1, enhancing power efficiency and decreasing the

required computational complexity are important challenges in VLC systems because of the usage of low-cost and simple LEDs that are commercially available. Considering these problems and challenges, this chapter presents low-complexity layered ACO-OFDM (L-LACO) for VLC systems.

As discussed in Chapter 2, LAC-OFDM works in a VLC LOS flat channel, however, requires complex equalization at the receiver in a VLC dispersive channel. In contrast, with the aid of a low-complexity one-tap equalizer at the receiver, L-LACO works in a VLC LOS flat channel and a VLC dispersive channel.

Mathematically, L-LACO achieves identical signals to existing LACO-OFDM while requiring only half-size IFFTs in each layer at the transmitter and requiring half-size IFFTs and FFTs at the receiver. Different from each layer in LACO-OFDM having an anti-symmetry by only modulating odd subcarriers in the frequency domain, each layer in L-LACO is directly constructed to be anti-symmetric in the time domain like LAC-OFDM. The required RMOs and RAOs are computed and compared to LACO-OFDM. Numerical results show L-LACO only requires half arithmetic operations, however, generates an identical signal as LACO-OFDM. Because identical signals are generated, L-LACO achieves the same BER performance as the existing LACO-OFDM in a VLC LOS channel and in a VLC dispersive channel as well.

Compared to LACO-OFDM, saved power for L-LACO corresponding to the reduction in arithmetic operations is analysed and verified by numerical results. The saved power increases logarithmically with the number of subcarriers and increases linearly with modulation bandwidth. As the bandwidth of VLC systems increases with new devices, such as μLEDs and LDs, the superiority of L-LACO will become increasingly essential.

Abstract Commercially available LED luminaires demand both low-complexity and high power efficiency from visible light communication (VLC) deployments. Layered asymmetrically clipped optical orthogonal frequency division multiplexing (LACO-OFDM) is attracting increasing interest due to the high spectral efficiency and high power efficiency. However, these advantages come at the price of high computational complexity at both transmitter and receiver. In this paper, we propose a low-complexity LACO-OFDM (L-LACO) to generating identical signals to conventional systems while employing a half-size IFFT/FFT and possessing low implementation complexity. The required number of real-valued multiplication operations and real-valued addition operations are quantified and compared to conventional LACO-OFDM. The saved power corresponding to the reduction in arithmetic operations is also estimated, which is shown to increase logarithmically with number of subcarriers, and to increase linearly with modulation bandwidth. Numerical results show that the proposed L-LACO requires about half the number of arithmetic operations as LACO-OFDM for both the transmitter and the receiver. The BER performance of L-LACO is estimated by Monte Carlo simulations under a VLC line-of-sight (LOS) channel and under a VLC dispersive channel that is shown to be identical to LACO-OFDM.

4.1 Introduction

Visible light communication (VLC) for indoor communications has been touted as a promising complementary link to conventional wireless radio frequency (RF) communication due to the ubiquity of solid-state illumination and large amounts of unregulated visible light spectrum [2, 3, 7]. An underlying constraint in any VLC

system based on commercial luminaires is that the complexity and power consumption of any processing must be minimized to preserve energy efficiency. As a result, intensity modulation with direct detection (IM/DD) is typically employed in VLC links thanks to its low complexity [76, 129, 152]. The data are modulated onto the instantaneous optical intensity emitted by a light-emitting diode (LED), where the average optical power corresponds to the average LED driving current. Hence, the input signal must be real-valued and non-negative [2, 3, 4, 7, 76, 129, 152]. At the receiver, a photodiode (PD) is used to convert the received optical signal to an electrical current, which is assumed to be proportional to the received optical power.

In VLC channels, orthogonal frequency division multiplexing (OFDM) has been investigated intensely to enhance data rate and power efficiency due to its inherent benefits including high spectral efficiency, resistance to frequency-selective channels, and simple one-tap equalization [153, 34, 67, 82]. In order to produce a real-valued signal compatible with IM/DD, Hermitian symmetry is generally induced in the frequency domain [51, 67, 48, 86]. Further, to achieve non-negative output amplitudes, direct current (DC) biased optical OFDM (DCO-OFDM) requires a large DC bias and all the remaining negative peaks are clipped at zero [56]. The required DC bias consumes much optical power but carries no information.

To improve optical power efficiency, asymmetrically clipped optical OFDM (ACO-OFDM) [55, 56], pulse-amplitude-modulated discrete multitone (PAM-DMT) [57], unipolar OFDM (U-OFDM) [141] and Flip-OFDM [121], antisymmetry-constructed clipped optical OFDM (AC-OFDM) [106] were proposed; however, these optical power efficient OFDM schemes have a drawback of achieving only half the spectral efficiency as DCO-OFDM. To enhance the spectral efficiency and to retain optical power

efficiency, layered spectrum efficient OFDM schemes such as enhanced U-OFDM (eU-OFDM) [141], enhanced ACO-OFDM (eACO-OFDM) [111], spectral and energy efficient OFDM (SEE-OFDM) [72], layered ACO-OFDM (LACO-OFDM) [74], and enhanced ACO-OFDM (EACO-OFDM) [154] were then proposed independently. These spectrum efficient OFDM schemes superimpose several layers/streams, which are transmitted at the same time. These multiple-layer/stream OFDM schemes are in a similar philosophy to LACO-OFDM while proposed independently.

Recently, there has been intense research on LACO-OFDM, including improved the detection performance [76, 77, 78, 79, 80, 81], reduction in peak-to-average power ratio (PAPR) [82, 83, 84, 85], capacity analysis [86, 87, 88, 89], investigation of channel coding performance [90, 91, 92, 93], dimming [94, 95, 96, 97], enhanced spectral efficiency [86, 98, 113, 99, 100, 101], experimental demonstrations [102, 100, 103, 104], decreased computational complexity [105, 72, 102, 106, 107], and explicit consideration of bandwidth constraints [108, 53]. For readability, these research papers are summarized and contrasted in Table 4.1.

Though spectrally efficient, the use of multiple layers/streams of OFDM modulation schemes suffer from increased computational complexity [149], which is especially significant for cost and power constrained VLC luminaires. Hardware-efficient layered/enhanced ACO-OFDM (L/E-ACO-OFDM) was proposed in [102], and focuses on a highly efficient implementation from a hardware perspective and creatively improves L/E-ACO-OFDM transmitter by modifying the inverse fast Fourier transform (IFFT) implementation that calculates only the bottom half in the IFFT butterfly. However, the approach only applies to the transmitter and the receiver remains highly

Table 4.1: Recent Research on LACO-OFDM.

Topics and Directions	**Relevant Recent Researches**
BER performance	[76] An improved receiver with residual clipping noise mitigation [77] An improved receiver using pairwise detection for noise cancellation [78] A receiver using diversity combining on both flat and frequency-selective channels [79] A diversity combining receiver achieving up to 2 dB electrical gains [80] A two-stage receiver realizing up to 2.43 dB gains [81] A multi-stage improved receiver to mitigate the clipping noise due to dynamic range of electrical and optical components
PAPR reduction	[82] Performance analysis & PAPR reduction [83] Layered/enhanced asymmetrically clipped optical single-carrier frequency-division multiplexing (L/E-ACO-SCFDM) with PAPR reduction up to 4.2 dB [84] Interleaved discrete-Fourier-transform-spread layered/enhanced ACO-OFDM (IDFTS-L/e-ACO) with PAPR reduction up to 7.5 dB [85] Cyclic shifted LACO-OFDM with PAPR reduction up to 2.5 dB
Capacity analysis	[86] Analyses, optimises and compares the achievable information rate of optical OFDM modulation schemes in an IM/DD channel with Gaussian noise [87] Proposes adaptive LACO-OFDM and analyses capacity with optimal layer [88] Analyses comparatively the capacity of unipolar OFDM schemes in Gaussian optical intensity channel [89] Analyses and optimises discrete-input continuous-output memoryless channel (DCMC) capacity of LACO-OFDM [53] Analyses and compares achievable rate of multi-carrier modulation schemes for bandlimited IM/DD Systems
Channel coding	[90] Pairwise coding to mitigate error propagation between layers [91] Analyses capacity and integrates forward error correction (FEC) codes to LACO-OFDM for BER improvement [92] Designs a multilayered code that trades spectral efficiency for BER improvement [93] Multilayered channel coding with experiment verification
Dimming control	[94] Dimmable LACO-OFDM with wide dimming range [95] Spatial-domain and time-domain dimming control for LACO-OFDM [96] Dimmable L/E-ACO-SCFDM [97] Dimmable reconstructed LACO-OFDM (RLACO-OFDM)
Spectrum efficient	[86, 98] Proposes ALACO-OFDM that can be more spectral efficient than LACO-OFDM with fewer layers [113] Proposes triple-layer hybrid optical OFDM (THO-OFDM) that can be more spectral efficient than LACO-OFDM with three layers [99] Proposes hybrid non-orthogonal multiple access (NOMA) and orthogonal multiple access (OMA) for LACO-OFDM performance improvement [100] Proposes hierarchical pre-distorted LACO-OFDM (HPD-LACO-OFDM) for NOMA performance improvement [101] Proposes flexible NOMA-based non-orthogonal hybrid optical OFDM (NOHO-OFDM) scheme
Experimental demo.	[102] Demonstrates an experiment based field-programmable gate arrays (FPGA) with low-complexity transmitter [100] Demonstrates a point-to-point transmission experiment [103] Demonstrates worst-case residual clipping noise power model for bit-loading in LACO-OFDM [104] Demonstrates a short-haul optical fiber link using layered/enhanced ACO-OFDM
Reduce complexity	[105, 72] Proposes a receiver with a single FFT sacrificing about $2-3$ dB power [102] focuses on a high-efficient implementation from the hardware prospect and improves L/E-ACO-OFDM transmitter [106, 107] Proposes LAC-OFDM saving half arithmetic operations while achieving same BER performance as LACO-OFDM under a VLC LOS flat channel
Bandlimited signal	[108] Simulates LACO-OFDM BER performance for a strictly bandlimited VLC system [53] Analyses achievable rate of multi-carrier modulation schemes, including SEE-OFDM, and proposes filtered SEE-OFDM (FSEE-OFDM) for bandlimited IM/DD systems

complex. A low-complexity receiver using a single fast Fourier transform (FFT) module for LACO-OFDM is investigated in [105], which reduces the complexity of the receiver at the expense of about $2-3$ dB power loss at a bit error rate (BER) of 10^{-3}. More recently, layered AC-OFDM (LAC-OFDM) is proposed for VLC line-of-sight (LOS) channels, which is low-complexity thanks to employing half-size IFFT and half-size FFT while retaining the same optical power efficiency as LACO-OFDM [106]. However, an additional N-point FFT and N-point IFFT are additionally required to implement frequency domain equalization (FDE) when LAC-OFDM is employed on a dispersive VLC channel. To summarize, only a few papers have considered the reduction of computation complexity at both the transmitter and the receiver while retaining the spectral- and power efficiency simultaneously, which is a key motivation of this work.

4.1.1 Novelty and Contributions

In this paper, we propose low-complexity ACO-OFDM (L-ACO-OFDM, termed as L-ACO hereafter), which generates identical OFDM signals as conventional ACO-OFDM while employing an IFFT that is only half the size of ACO-OFDM. To enhance the spectral efficiency, low-complexity LACO-OFDM (L-LACO-OFDM, termed as L-LACO hereafter) is proposed, which combines L layers of L-ACO signals to generate identical OFDM signals as LACO-OFDM in [74]. The size of the IFFT/FFTs employed in each layer are half the size needed in LACO-OFDM. Hence L-LACO is far less-complex as compared to LACO-OFDM at both the transmitter and receiver. The power savings due to the reduced computation compared to LACO-OFDM are estimated at both transmitter and receiver. Additionally, the BER performance of

Table 4.2: Contrast between methodology adopted in [102] and L-LACO.

	Ref. [102]	**L-LACO**
Complexity reduction at transmitter	Half	Half
Complexity reduction at receiver	Same complexity as LACO-OFDM receiver	Half
The IFFT size in the l-th layer	Same size as IFFT at LACO-OFDM transmitter	Half size as IFFT at LACO-OFDM transmitter
$\mathcal{R}$-radix IFFT butterfly	$\mathcal{R} = 2$	$\mathcal{R}$ could be any divisor of N
The need for modifying IFFT algorithm	Modifies the IFFT implementation that calculates only the bottom half in the IFFT butterfly.	No need. A common IFFT is good.

the proposed L-LACO is estimated by Monte Carlo simulations under a VLC line-of-sight (LOS) channel and a VLC dispersive channel, respectively. The simulation results show that L-LACO achieves the identical performance compared to LACO-OFDM. Therefore, L-LACO generates spectrally efficient LACO-OFDM using half-size IFFT/FFT at transmitter and receiver, which is essential for complexity and energy constrained VLC systems.

Compared to the methodology adopted in [102] that modifies the IFFT implementation by calculating only the bottom half in the IFFT butterfly, L-LACO does not need to modify any IFFT butterfly structure. In [102], a 2-radix IFFT butterfly is required to save half the complexity compared to LACO-OFDM transmitter. In contrast, a common IFFT with $\mathcal{R}$-radix butterfly could be utilized to save half-complexity where $\mathcal{R}$ could be any divisor of the number of subcarriers N. In [102], the size of IFFT in each layer remains the same as conventional LACO-OFDM. In contrast, L-LACO employs half-size IFFT as conventional LACO-OFDM in each layer.

Additionally, [102] only decreases the complexity of the L/e-ACO-OFDM transmitter. The receiver still requires as high computational complexity as conventional LACO-OFDM. In contrast, our proposed L-LACO decreases the complexity of the LACO-OFDM transmitter and the receiver by nearly half. The contrast between the methodology adopted in [102] and that adopted in L-LACO is summarized in Table 4.2.

The main contributions of this paper can be summarised as:

- Firstly, this paper proposes L-LACO to design the entire transceiver. L-LACO is shown mathematically to generate identical signals as conventional LACO-OFDM while its transceiver is less complex. The L-LACO transmitter utilizes a half-size IFFT in each layer as conventional LACO-OFDM transmitter, and L-LACO receiver utilizes half-size IFFT and half-size FFT in each iteration as conventional LACO-OFDM receiver.

- Secondly, we analyse the computational complexity of both transmitter and receiver quantitatively. This work quantifies the required number of real-valued multiplication operations (RMOs) and real-valued addition operations (RAOs) for L-LACO transceiver and conventional LACO-OFDM. Numerical results support the theoretical analysis of the computational complexity reduction.

- Thirdly, this work quantifies the saved power of the L-LACO transmitter and receiver as compared to conventional LACO-OFDM. Numerical results are aligned well with our theoretical analysis on saved power.

- Finally, this work presents the BER performance of L-LACO and conventional LACO-OFDM under both VLC LOS and dispersive channels. Numerical results

show that L-LACO has the identical BER as LACO-OFDM, however, requires about half the number of arithmetic operations.

4.1.2 Paper Structure

The remainder of this paper is organized as follows. Section 4.2 briefly introduces VLC channel model and conventional ACO-OFDM and LACO-OFDM, while the proposed L-ACO and L-LACO are presented in Sections 4.3 and 4.4, respectively. Computational complexity is analysed in Section 4.5. Numerical results are presented in Section 4.6. Finally, conclusions are drawn in Section 4.7.

Notations: In this paper, N denotes the number of subcarriers. Additionally, we use an uppercase letter, e.g, Y and its bold form, e.g., $\boldsymbol{Y}$ to denote a frequency-domain scalar and vector signal while a lowercase letter, e.g., y and its bold form, e.g., $\boldsymbol{y}$ denote a time-domain scalar and vector signal, respectively. Note Y^* denotes complex conjugate of a complex number Y. Furthermore, $\mathrm{mod}(\cdot,\cdot)$ denotes modulo operation. $|\cdot|$ denotes magnitude of a complex number or absolute value of a real number. Specifically, notation symbols with the corresponding meaning utilized throughout the paper are listed in Table 4.3.

Table 4.3: Key notations and the meaning.

Notation	Meaning
W_N	The first entry in IDFT matrix
$\boldsymbol{Y}$	Input symbol vector to N-point IFFT for ACO-OFDM
$\boldsymbol{X}$	Input symbol vector to $N/2$-point IFFT for L-ACO
$\boldsymbol{x}$	Output symbol vector of $N/2$-point IFFT for L-ACO
$\mathbf{y}$	Output symbol vector of N-point IFFT for ACO-OFDM
$\mathbf{y}_{\mathrm{c}}$	ACO-OFDM signal after clipping
$\boldsymbol{c}$	c_n, the n-th element of ACO-OFDM clipping distortion
$N_{\mathrm{AC}}(1)$	IFFT size of the first layer L-ACO
$\mathbf{Y}_L^{(l)}$	Input symbol vector to N-point IFFT for the l-th layer
$\mathbf{X}^{(l)}$	Input symbol vector to $N_{\mathrm{AC}}(l)$-point IFFT for the l-th layer
$\mathbf{x}^{(l)}$	Output symbol vector of $N_{\mathrm{AC}}(l)$-point IFFT for the l-th layer
$\mathbf{y}^{(l)}$	Anti-symmetric signal vector with length of $2N_{\mathrm{AC}}(l)$ in the l-th layer
$\boldsymbol{s}^{(l)}$	$s_n^{(l)} = \frac{1}{\sqrt{2^l}} W^n_{\frac{N}{2^{l-1}}}$, constant in the l-th layer
$\boldsymbol{v}^{(l)}$	$v_n^{(l)} = s_n^{(l)} x_n^{(l)}$, real-valued signal in the l-th layer
$\mathbf{y}_{\mathrm{c}}^{(l)}$	Symbol vector generated by clipping $\mathbf{y}^{(l)}$ at zero
$\boldsymbol{c}^{(l)}$	$c_n^{(l)}$, time-domain CD induced by the l-th layer
$\boldsymbol{C}^{(l)}$	$C_k^{(l)}$, CD falling onto k-th subcarrier induced by the l-th layer
$\mathbf{x}_{\mathrm{a}}^{(l)}$	$x_{\mathrm{a},n}^{(l)}$, absolute value of $x_n^{(l)}$
$\mathbf{X}_{\mathrm{a}}^{(l)}$	DFT of $\mathbf{x}_{\mathrm{a}}^{(l)}$
$\widetilde{\boldsymbol{X}}^{(l)}$	An estimate of $\boldsymbol{X}^{(l)}$
$\widehat{\boldsymbol{X}}^{(l)}$	An estimate of $\boldsymbol{X}^{(l)}$ after symbol detection
$\widehat{\boldsymbol{C}}^{(l)}$	An estimate of $\boldsymbol{C}^{(l)}$
$\widehat{\boldsymbol{x}}_{\mathrm{a}}^{(l)}$	An estimate of $\boldsymbol{x}_{\mathrm{a}}^{(l)}$
$\widehat{\boldsymbol{X}}_{\mathrm{a}}^{(l)}$	An estimate of $\boldsymbol{X}_{\mathrm{a}}^{(l)}$

4.2 Background

4.2.1 VLC Channel Model

For a VLC LOS link, the channel is assumed to be flat with a gain H_{LOS} as [4]

$$H_{\text{LOS}} = \begin{cases} \frac{\eta A_{\text{PD}}(m+1)}{2\pi d^2} \cos^m(\psi) \cos(\theta), & 0 \leq \theta \leq \Theta_{\text{F}}, \\ 0, & \text{Otherwise}, \end{cases} \tag{4.2.1}$$

where η is optical-to-electrical (O/E) conversion coefficient, A_{PD} is the effective collection area of the PD, ψ is the angle of irradiance with respect to LED axis, θ is the angle of incidence with respect to PD axis, Θ_{F} is field of view (FOV), d is the distance between LED and PD surfaces, and $m = -\ln(2)/\ln(\cos(\Psi_{1/2}))$ is the order of Lambertian emission and $\Psi_{1/2}$ is LED semi-angle. Without loss of generality, the receiver filter is assumed to be rectangular with optical power gain setting to unit.

Indoor VLC dispersive channels include both LOS link and diffuse components that can be well estimated by a close-form function as [4, 155]

$$h(t) = H_{\text{LOS}} \frac{\tau_0^6}{(t+\tau_0)^7} u(t) \tag{4.2.2}$$

where $u(t)$ is the unit step function, $\tau_0 = 2H/c$, H is height of room, and c is speed of light [4, 155].

4.2.2 Conventional ACO-OFDM and LACO-OFDM

In ACO-OFDM, the output time-domain signal vector has an inherent anti-symmetry due to loading data on only odd subcarriers [56]. To achieve non-negativity,

the negative parts are clipped at zero without any loss of information [56]. This clipping distortion (CD) falls onto even subcarriers, which are orthogonal to data-carrying subcarriers. Hence, symbols can be detected successfully on the odd subcarriers at the receiver [56].

To enhance the spectral efficiency, LACO-OFDM uses L layers of ACO-OFDM signals which are superimposed and transmitted simultaneously [74]. These L layers modulate symbols onto disjoint sets of subcarriers and each layer has an anti-symmetry. At the receiver, LACO-OFDM is demodulated successively layer by layer [74].

4.3 Low-complexity ACO-OFDM

For completeness, define [**?**]

$$W_N = \exp\left\{\frac{j2\pi}{N}\right\} \tag{4.3.1}$$

where N is size of IFFT and FFT and $j = \sqrt{-1}$.

Conventional ACO-OFDM with N subcarriers requires an N-point IFFT at transmitter. Hermitian symmetry is required to generate real-valued signals and only odd subcarriers are utilized to carry data leading to anti-symmetric output of an IFFT. Hence the input frequency-domain symbol vector to the IFFT for ACO-OFDM is

$$\mathbf{Y} = [0, Y_1, 0, Y_3, 0, \cdots, 0, Y_3^*, 0, Y_1^*] \tag{4.3.2}$$

where Y_k denotes M-ary quadrature amplitude modulation (QAM) symbols and $(\cdot)^*$

denotes complex conjugate. The resulting time-domain output of IFFT is thus

$$y_n = \frac{1}{\sqrt{N}} \sum_{k=0}^{N-1} Y_k W_N^{nk} \ , \ 0 \leq n \leq N-1 \ . \tag{4.3.3}$$

Notice that $\mathbf{y}$ has an inherent anti-symmetry due to the modulation of only odd subcarriers, i.e., [56]

$$y_n = -y_{n+N/2}, \ 0 \leq n \leq N/2-1 \ . \tag{4.3.4}$$

Conventional ACO-OFDM requires high computational complexity due to the usage of N-point IFFT according to (4.3.3). In the following, we show that a half-size IFFT can be employed to generate the identical signal $\mathbf{y}$ in (4.3.4). Following the philosophy of AC-OFDM [106], where anti-symmetry is introduced in the time domain, $\mathbf{y}$ can be written as

$$\mathbf{y} = [\mathbf{v}, -\mathbf{v}] \tag{4.3.5}$$

where $\mathbf{v}$ is an $\frac{N}{2}$-length vector with the n-th element given by

$$v_n = s_n x_n \tag{4.3.6}$$

where $s_n = \frac{1}{\sqrt{2}} W_N^n$ and

$$x_n = \frac{1}{\sqrt{N/2}} \sum_{q=0}^{\frac{N}{2}-1} X_q W_{\frac{N}{2}}^{nq} \ , \ 0 \leq n \leq N/2-1 \tag{4.3.7}$$

where $X_q = Y_{2q+1}$ and $q = 0, \ 1, \ldots, N/2-1$. Notice that (4.3.7) is an $\frac{N}{2}$-point IFFT. Therefore, a conventional ACO-OFDM signal $\mathbf{y}$ in (4.3.5) can be constructed

by computing $\mathbf{v}$ using an $\frac{N}{2}$-point IFFT and imposing anti-symmetry in time-domain (which requires no additional arithmetic operations). It is worth noting that v_n is a real-valued signal though x_n is not necessarily real-valued.

To satisfy the non-negativity requirement, the negative part of $\mathbf{y}$ is clipped at zero leading to $\mathbf{y}_\mathrm{c}$ with the n-th element given as [56]

$$y_{\mathrm{c},n} = \frac{1}{2} y_n + c_n \ , 0 \leq n \leq N-1 \tag{4.3.8}$$

where $c_n = \frac{1}{2}|y_n|$ is CD falling onto even subcarriers only, which is orthogonal to the data-bearing (i.e., odd) subcarriers in the frequency domain.

It is worth to noting that L-ACO signal $y_{\mathrm{c},n}$ generated by an $N/2$-point IFFT is identical to conventional ACO-OFDM signal generated by an N-point IFFT. Therefore, at the receiver side, symbols can be detected on the odd subcarriers using conventional ACO-OFDM demodulator proposed in [55].

4.4 Low-complexity LACO-OFDM

4.4.1 Transmitter Design

For conventional LACO-OFDM superimposing L layers of ACO-OFDM, an $2N_{\mathrm{AC}}(l)$-point ($1 \leq l \leq L$) IFFT is employed in the l-th layer [74], where for readability, we define

$$N_{\mathrm{AC}}(l) = \frac{N}{2^l} \ . \tag{4.4.1}$$

Here we demonstrate that extending the approach of L-ACO and inspired by LAC-OFDM [106], an identical LACO-OFDM signal can be generated by using half-sized

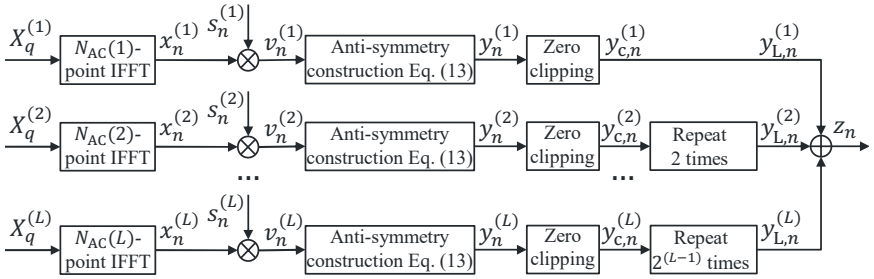

Figure 4.1: Transmitter block diagram for L-LACO.

IFFTs.

In the l-th ACO-OFDM layer, $N_{\mathrm{AC}}(l)$ symbols, after considering Hermitian symmetry, are modulated onto subcarriers with index $(2p+1)2^{l-1}$ $(p = 0\ , 1\ , \ldots , N_{\mathrm{AC}}(l))$ and the remaining subcarriers are set to zero [86], resulting in the frequency domain symbol vector

$$\begin{aligned} &\mathbf{Y}_{\mathrm{L}}^{(l)} = \\ &[0, \cdots, 0, Y_{2^{l-1}}, 0, \cdots, 0, Y_{3\cdot 2^{l-1}}, 0, \cdots, 0, Y_{2^{l-1}}^{*}, 0, \cdots, 0] \ . \end{aligned} \tag{4.4.2}$$

The output of an N-point IFFT of $\mathbf{Y}_{\mathrm{L}}^{(l)}$ has a period of $2N_{\mathrm{AC}}(l)$ with an anti-symmetry inside each period [86]. Conventional LACO-OFDM generates this output signal by employing a $2N_{\mathrm{AC}}(l)$-point IFFT and repeating the frame in time-domain $2^{(l-1)}$ times.

Consider the transmitter block diagram of L-LACO in Fig. 4.1 where an identical LACO-OFDM frame can be generated using half-size IFFTs. Generalizing the approach of L-ACO in Sec.4.3, L-LACO constructs the anti-symmetry directly in time-domain as

$$\mathbf{y}^{(l)} = [\mathbf{v}^{(l)}, -\mathbf{v}^{(l)}] \tag{4.4.3}$$

where $\mathbf{v}^{(l)}$ is an $N_{\mathrm{AC}}(l)$-length real-valued vector with the n-th element given as

$$v_n^{(l)} = s_n^{(l)} x_n^{(l)} \tag{4.4.4}$$

where $s_n^{(l)} = \frac{1}{\sqrt{2^l}} W^{n}_{\frac{N}{2^{l-1}}}$ and

$$x_n^{(l)} = \frac{1}{\sqrt{N/2^l}} \sum_{q=0}^{\frac{N}{2^l}-1} X_q^{(l)} W^{nq}_{\frac{N}{2^l}} \tag{4.4.5}$$

and $X_q^{(l)} = Y^{(l)}_{\mathrm{L},(2q+1)2^{l-1}}$, $q = 0,\ 1, \ldots, N_{\mathrm{AC}}(l)-1$, $Y^{(l)}_{\mathrm{L},(2q+1)2^{l-1}}$ is given in (4.4.2). Notice that (4.4.5) is exactly an $N_{\mathrm{AC}}(l)$-point IFFT, which indicates that a half-size IFFT can be employed in each layer to generate an identical signal to LACO-OFDM.

The negative samples of $\mathbf{y}^{(l)}$ are clipped at zero to meet the non-negativity constraint leading to $\mathbf{y}_{\mathrm{c}}^{(l)}$, denoted in Fig. 4.1 by the block 'Zero clipping'. Hence, the n-th ($0 \le n \le 2N_{\mathrm{AC}}(l)-1$) element of $\mathbf{y}_{\mathrm{c}}^{(l)}$ is given as

$$y_{\mathrm{c},n}^{(l)} = \frac{1}{2} y_{\mathrm{c},n}^{(l)} + c_n^{(l)} \tag{4.4.6}$$

where $c_n^{(l)} = \frac{1}{2}|y^{(l)}_{\mathrm{mod}(n,N_{\mathrm{AC}}(l))}|$ is CD falling on the $k2^l$-th ($k = 0, 1, \ldots, N_{\mathrm{AC}}(l)-1$) subcarriers, which is orthogonal to the data-bearing subcarriers in the l-th layer. $\mathbf{c}^{(l)}$ is a vector of length N. In each layer, $\mathbf{y}_{\mathrm{c}}^{(l)}$ is repeated 2^{l-1} times resulting in $y_{\mathrm{L},n}^{(l)}$ of length N, given by

$$\mathbf{y}_{\mathrm{L}}^{(l)} = [\underbrace{\mathbf{y}_c^{(l)}, \cdots, \mathbf{y}_c^{(l)}}_{\text{repeat } 2^{l-1} \text{ times}}] \,. \tag{4.4.7}$$

The L layers of ACO-OFDM signals are added together leading to L-LACO signal

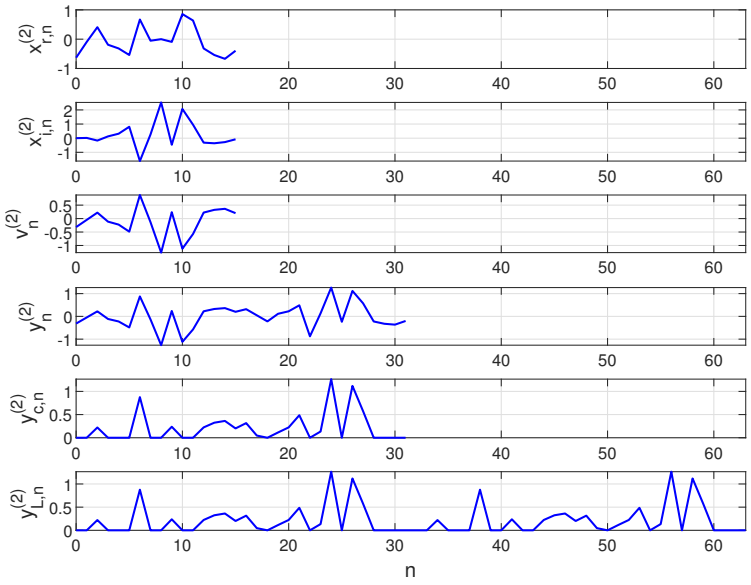

Figure 4.2: An illustration of the construction of a second layer ($l = 2$) L-ACO signal, $y^{(2)}_{\mathrm{L},n}$, for L-LACO ($N = 64$ and $M = 16$).

given by

$$\mathbf{z} = \sum_{l=1}^{L} \mathbf{y}_{\mathrm{L}}^{(l)} \ . \tag{4.4.8}$$

Thus, the L-LACO signal $\mathbf{z}$ generated using this procedure is identical to LACO-OFDM while using a half-sized IFFT used in each layer resulting in less required operations (multiplications and additions).

The signal $\mathbf{z}$ is then converted from parallel to serial (P/S) and a cyclic prefix (CP) is appended to the front of each OFDM symbol to avoid inter-symbol interference (ISI). After a digital-to-analog converter (DAC) and a low-pass filter (LPF), the resulting analog signal $z(t)$ is utilized to drive an LED.

Figure 4.2 presents an example of the signals used to construct the second layer signal, $y^{(2)}_{\mathrm{L},n}$, for L-LACO where $N = 64$ and $M = 16$. Denote $x^{(2)}_{\mathrm{r},n}$ and $x^{(2)}_{\mathrm{i},n}$ as the real

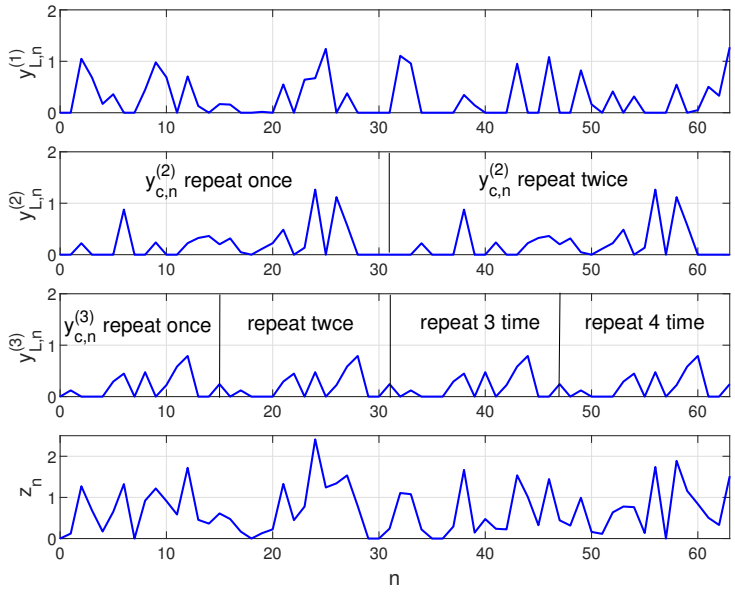

Figure 4.3: An illustration of the L-LACO signals at each layer ($y_{\mathrm{L},n}^{(l)}$) and sum (z_n) (($N = 64$, $L = 3$ and $M = 16$).

and imaginary parts of $x_n^{(2)}$, respectively. As shown in Fig. 4.2, the complex-valued output of the IFFT, $x_n^{(2)}$ is used to generate the real-valued signal, $v_n^{(2)}$ and then to construct a signal, $y_n^{(2)}$, with anti-symmetry imposed in time-domain. The signal $y_n^{(2)}$ is then clipped at zero leading to $y_{\mathrm{c},n}^{(2)}$, which is repeated twice resulting in the second layer signal, $y_{\mathrm{L},n}^{(2)}$.

Figure 4.3 shows an illustration of the construction of a complete L-LACO signal ($L = 3$, $N = 64$, $M = 16$). Notice that the first layer does not repeat while the second layer repeats two times and the third layer repeats four times. These output signals are identical to conventional LACO-OFDM, however, the size of the IFFTs used to compute each layer are half-sized.

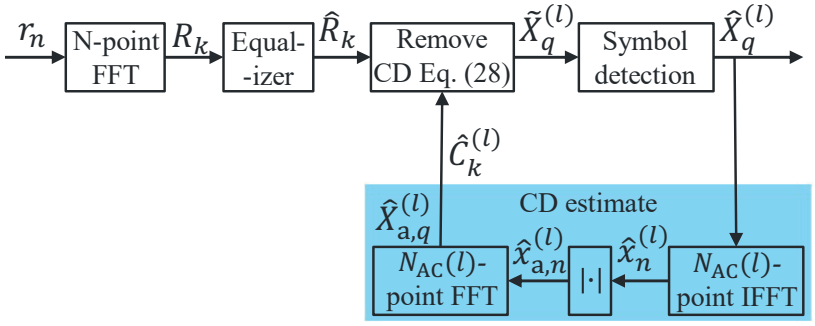

Figure 4.4: Receiver block diagram for L-LACO. Note that, in contrast to the LACO-OFDM receiver in [74], L-LACO uses half-size IFFT/FFT to estimate the CD (indicated in the shaded box).

4.4.2 Receiver Design

At the receiver side, the optical signal is first converted into an electrical current using a PD. Shot noise and thermal noise are well modelled as additive white Gaussian noise (AWGN) [4, 56, 156]. Hence, the received signal is given by

$$r(t) = h(t) * z(t) + n(t) \tag{4.4.9}$$

where $h(t)$ denotes channel impulse response, '$*$' denotes the convolution operation and $n(t)$ is the AWGN. After a low-pass filter, analog-to-digital conversion (ADC), removal of CP, and serial to parallel (P/S) conversion, the discrete received signal r_n is obtained.

Recall that the L-LACO transmitted signal $\mathbf{z}$ generated in Sec. 4.4.1 is identical to LACO-OFDM though using half-size IFFT in each layer. Hence, r_n can be demodulated using a conventional LACO-OFDM receiver designed in [74], which removes CD induced by the l-th layer using $2N_{\mathrm{AC}}(l)$-point IFFT and $2N_{\mathrm{AC}}(l)$-point FFT.

Here a low-complexity receiver is proposed for LACO-OFDM and L-LACO, which

removes CD induced by the l-th layer using $N_{\mathrm{AC}}(l)$-point IFFT and $N_{\mathrm{AC}}(l)$-point FFT that are half-size compared to conventional LACO-OFDM receiver. It is worth to noting that the proposed low-complexity receiver can also be used to demodulate LACO-OFDM.

Fig. 4.4 presents a block diagram of low-complexity receiver for L-LACO. The received signal r_n is fed into an N-point FFT followed by a one-tap equalizer. Since there is no CD affecting data-bearing subcarriers in the first layer, an estimate of X_q is obtained considering only the odd subcarriers

$$\widetilde{X}_q^{(1)} = 2\widehat{R}_{2q+1},\ q = 0,\ 1, \ldots, N/2-1 \tag{4.4.10}$$

where the factor 2 is due to zero clipping operation according to (4.4.6). Due to Hermitian symmetry, only symbols in the first half of an OFDM frame are required to be detected as

$$\widehat{X}_q^{(1)} = \arg \min_{X \in \Omega_X} |\widetilde{X}_q^{(1)} - X|,\ q = 0,\ 1, \ldots, N/4-1 \tag{4.4.11}$$

where Ω_X denotes the constellation set.

Note that the CD from lower layers only impacts higher layers [74]. Hence, prior to detecting symbols in the second layer, CD from the first layer must be removed. The CD induced by the first layer is given by $c_n^{(1)} = \frac{1}{2}|y_n^{(1)}| = \frac{1}{2\sqrt{2}}|x_{\mathrm{mod}(n,N/2)}^{(1)}|$, according to (4.4.6) and (4.4.7), which has a period of $N/2$. Hence, the discrete Fourier tranform

(DFT) of the CD induced by the first layer is given as

$$C_k^{(1)} = \frac{1}{\sqrt{N}} \sum_{n=0}^{N-1} c_n^{(1)} W_N^{-nk} \tag{4.4.12a}$$

$$= \frac{1}{2\sqrt{N}} \sum_{n=0}^{N/2-1} |y_n^{(1)}| W_N^{-nk} (1 + \cos(k\pi)) \tag{4.4.12b}$$

$$= \frac{1/2}{\sqrt{2N}} \sum_{n=0}^{N/2-1} |x_n^{(1)}| W_N^{-nk} (1 + \cos(k\pi)) \tag{4.4.12c}$$

$$= \begin{cases} \frac{1}{2} \frac{1}{\sqrt{N/2}} \sum_{n=0}^{N/2-1} |x_n^{(1)}| W_N^{-nk}, & k \in \mathbb{K}_{\text{clip}}^{(1)} \\ 0, & \text{Otherwise,} \end{cases} \tag{4.4.12d}$$

$$= \begin{cases} \frac{1}{2} X_{\text{a},q}^{(1)}, & k \in \mathbb{K}_{\text{clip}}^{(1)}, \ \& \ q = k/2 \\ 0, & \text{Otherwise,} \end{cases} \tag{4.4.12e}$$

where (4.4.12a) is definition of DFT and (4.4.12b) is due to clipping distortion $c_n^{(1)} = \frac{1}{2}|y_n^{(1)}|$ with a period of $N/2$, according to (4.4.6) and (4.4.7). (4.4.12c) is due to $|y_n^{(1)}| = \frac{1}{\sqrt{2}}|x_{\text{mod}(n,N/2)}^{(1)}|$ according to (4.4.3) and (4.4.4) with $l = 1$. In (4.4.12d), $\mathbb{K}_{\text{clip}}^{(1)} \triangleq \{k | k = 2q, \ q = 0, \ldots, N/2 - 1\}$. In (4.4.12e), $X_{\text{a},q}^{(1)}$ is given by

$$X_{\text{a},q}^{(1)} = \frac{1}{\sqrt{N/2}} \sum_{n=0}^{N/2-1} x_{\text{a},n}^{(1)} W_{N/2}^{-nq} \tag{4.4.13}$$

where $x_{\text{a},n}^{(1)} = |x_n^{(1)}|$ and $x_n^{(1)}$ is given by (4.4.5) with $l = 1$, which is an $\frac{N}{2}$-point IFFT. Additionally, note that (4.4.13) is an $\frac{N}{2}$-point FFT.

Hence, an estimate of the second layer can be estimated as

$$\widetilde{X}_q^{(2)} = 2\widehat{R}_{(2q+1)2} - 2\widehat{C}_{(2q+1)2}^{(1)}, \ q = 0, \ 1, \ldots, N/4 - 1 \tag{4.4.14}$$

where $\widehat{C}_k^{(1)}$ is an estimate of CD $C_k^{(1)}$ calculated according to (4.4.12) and replace $X_q^{(1)}$ with its estimate $\widehat{X}_q^{(1)}$. It is apparent that the factor 1/2 in (4.4.12) and 2 in (4.4.14) cancel, saving two multiplications.

Symbols in the second layer are thus detected as

$$\widehat{X}_q^{(2)} = \arg\min_{X\in\Omega_X} |\widetilde{X}_q^{(2)} - X|,\ q = 0,\ 1, \ldots, N/8 - 1\ . \tag{4.4.15}$$

More generally, according to (4.4.6) and (4.4.7), the CD induced by l-th ($1 \le l \le L$) layer is $c_n^{(l)} = \frac{1}{2}|y^{(l)}_{\mathrm{mod}(n,N/2^{l-1})}| = \frac{1}{2\sqrt{2^l}}|x^{(l)}_{\mathrm{mod}(n,N/2^l)}|$ with a period of $N_{\mathrm{AC}}(l)$. Hence, its DFT is given by

$$C_k^{(l)} = \frac{1}{\sqrt{N}}\sum_{n=0}^{N-1} c_n^{(l)} W_N^{-nk} \tag{4.4.16a}$$

$$= \frac{1}{2\sqrt{N}}\sum_{n=0}^{N/2^l-1} |y_n^{(l)}| W_N^{-nk}(1 + W_N^{-\frac{N}{2^l}k} + \ldots W_N^{-(2^l-1)\frac{N}{2^l}k}) \tag{4.4.16b}$$

$$= \frac{1/2}{\sqrt{2^l N}}\sum_{n=0}^{N/2^l-1} |x_n^{(l)}| W_N^{-nk}(1 + W_N^{-\frac{N}{2^l}k} + \ldots W_N^{-(2^l-1)\frac{N}{2^l}k}) \tag{4.4.16c}$$

$$= \begin{cases} \frac{1}{2}\frac{1}{\sqrt{N/2^l}}\sum_{n=0}^{N/2^l-1} |x_n^{(l)}| W_N^{-nk}, & k \in \mathbb{K}_{\mathrm{clip}}^{(l)} \\ 0, & \text{Otherwise,} \end{cases} \tag{4.4.16d}$$

$$= \begin{cases} \frac{1}{2}X_{\mathrm{a},q}^{(l)}\ , & k \in \mathbb{K}_{\mathrm{clip}}^{(l)},\ \&\ q = k/2^l \\ 0, & \text{Otherwise} \end{cases} \tag{4.4.16e}$$

where (4.4.16a) is DFT definition, and (4.4.16b) is due to that the CD induced by l-th ($1 \le l \le L$) layer is $c_n^{(l)} = \frac{1}{2}|y^{(l)}_{\mathrm{mod}(n,N/2^{l-1})}|$ with a period of $N/2^l$. (4.4.16c) is due to $|y^{(l)}_{\mathrm{mod}(n,N/2^{l-1})}| = \frac{1}{\sqrt{2^l}}|x^{(l)}_{\mathrm{mod}(n,N/2^l)}|$ according to (4.4.3) and (4.4.4). In (4.4.16d), $\mathbb{K}_{\mathrm{clip}}^{(l)} \triangleq \{k|q2^l\ ,\ q = 0, \ldots, N_{\mathrm{AC}}(l) - 1\}$. In (4.4.16e), $X_{\mathrm{a},q}^{(l)}$ is the DFT of $x_{\mathrm{a},n}^{(l)} = |x_n^{(l)}|$,

which is given by

$$X_{\mathrm{a},q}^{(l)} = \frac{1}{\sqrt{N/2^l}} \sum_{n=0}^{N/2^l-1} x_{\mathrm{a},n}^{(l)} W_{N/2^l}^{-nq} \tag{4.4.17}$$

where $x_n^{(l)}$ is calculated according to (4.4.5), which is an $N_{\mathrm{AC}}(l)$-point IFFT. As was noted for the first layer, note that (4.4.17) is an $N_{\mathrm{AC}}(l)$-point FFT.

As shown in [74], prior to demodulating ACO-OFDM symbols on the k-th ($k = (2q+1)2^{l-1}$) subcarrier in the l-th ($1 < l \leq L$) layer, CD from lower layers must be removed first. Hence, we obtain an estimate for $X_q^{(l)}$ as

$$\begin{gathered} \widetilde{X}_q^{(l)} = 2\widehat{R}_{(2q+1)2^{l-1}} - 2\sum_{\eta=1}^{l-1} \widehat{C}_{(2q+1)2^{l-1}}^{(\eta)}, \\ q = 0,\ 1, \ldots, N_{\mathrm{AC}}(l) - 1 \end{gathered} \tag{4.4.18}$$

where $\widehat{C}_k^{(\eta)}$ is an estimate of CD $C_k^{(\eta)}$ calculated according to (4.4.16) replacing $X_{\mathrm{a},q}^{(\eta)}$ with its estimate $\widehat{X}_{\mathrm{a},q}^{(\eta)}$.

Thanks to the Hermitian symmetry, only symbols in the first half OFDM frame are required to be detected employing symbol detection for the l-th ($1 < l \leq L$) layer as

$$\widehat{X}_q^{(l)} = \arg \min_{X \in \Omega_X} |\widetilde{X}_q^{(l)} - X|,\ q = 0,\ 1, \ldots, N_{\mathrm{AC}}(l)/2 - 1\ . \tag{4.4.19}$$

Remark 2. *Compared to the LACO-OFDM receiver in [74], the proposed L-LACO receiver is less complex. In the proposed L-LACO receiver, the CD induced by l-th layer is estimated using single $N_{\mathrm{AC}}(l)$-point FFT and single $N_{\mathrm{AC}}(l)$-point IFFT, whereas LACO-OFDM receiver utilizes one $2N_{\mathrm{AC}}(l)$-point FFT and one $2N_{\mathrm{AC}}(l)$-point IFFT.*

4.5 Computational Complexity Analysis

As described above, the transmitter and receiver of L-LACO require half-size IFFT/FFT compared to LACO-OFDM thus requires less computational complexity. In this section, we quantify the reduction in complexity for L-LACO over LACO-OFDM for a given set of modulation parameters.

4.5.1 Complexity Analysis of Low-complexity ACO-OFDM

Similar to [106], we assume in the subsequent analysis that operations such as anti-symmetry construction (4.3.5) and (4.4.3) do not require any arithmetic operations since they can efficiently implement with switching logic. Additionally, the scaled twiddle factors s_n in (4.3.6) and $s_n^{(l)}$ in (4.4.4) can be precomputed and stored in a table. Furthermore, the complexity of zero clipping in (4.3.8) and (4.4.6), and symbol detection on each carrier according to (4.4.11) and (4.4.19) are not included and will be identical for both L-LACO and LACO-OFDM.

Specifically, for conventional ACO-OFDM, a single N-point IFFT and N-point FFT are required at the transmitter and the receiver, respectively. Hence, complexity can be quantified by counting the required number of real-valued multiplication operations (RMOs) and of real-valued addition operations (RAOs) for each N-point IFFT/FFT. Based on Cooley-Tukey decomposition [133], an N-point (N a power of 2) IFFT/FFT requires $M(N)$ RMOs and $A(N)$ RAOs, which are given by

$$M(N) = 2N\log_2(N) - 4N + 4 \tag{4.5.1}$$

and

$$A(N) = 3N\log_2(N) - 2N + 2. \tag{4.5.2}$$

Notice that in the L-ACO transmitter , v_n, $0 \leq n \leq N/2-1$, is real according to (4.3.6). Hence RMOs between the real parts of s_n and x_n, and RMOs between the imaginary parts are necessary, i.e., only *two* RMOs and *one* RAO are required to generate v_n in (4.3.6). Considering signals with $N/2$ samples, N RMOs and $N/2$ RAOs are additionally required for v_n and thus y_n $(0 \leq n \leq N/2-1)$ besides the $N/2$-point IFFT in (4.3.7). Hence, the required numbers of RMOs and RAOs for L-ACO are

$$M^{(\mathrm{t})}_{\text{L-ACO}}(N) = M\left(\frac{N}{2}\right) + N = N\log_2(N) - 2N + 4 \tag{4.5.3}$$

and

$$A^{(\mathrm{t})}_{\text{L-ACO}}(N) = A\left(\frac{N}{2}\right) + \frac{N}{2} = \frac{3}{2}N\log_2(N) - 2N + 2\ . \tag{4.5.4}$$

At the receiver side, since L-ACO employs conventional ACO-OFDM receiver, its computational complexity is the same as ACO-OFDM.

4.5.2 Complexity Analysis of Low-complexity LACO-OFDM

At the transmitter of L-LACO, each ACO-OFDM layer requires an $N_{\mathrm{AC}}(l)$-point IFFT. The factors $s_n^{(l)}$ in (4.4.4) can be precomputed and stored. Similar to L-ACO, it is known a priori that $v_n^{(l)}$ and $y_n^{(l)}$ are real-valued thanks to Hermitian symmetry of the input vector according to (4.4.2). Hence RMOs between the real parts of $s_n^{(l)}$ and $x_n^{(l)}$, and RMOs between their imaginary parts are necessary, i.e., only *two* RMOs and *one* RAO are required to generate $v_n^{(l)}$ in (4.4.4). Considering that the length of $\mathbf{v}^{(l)}$ is $N_{\mathrm{AC}}(l)$, $2N_{\mathrm{AC}}(l)$ RMOs and $N_{\mathrm{AC}}(l)$ RAOs are additionally required for $v_n^{(l)}$ and

y_n $(0 \leq n \leq N_{\mathrm{AC}}(l) - 1)$ besides the $N_{\mathrm{AC}}(l)$-point IFFT in (4.4.5).

Hence, the required numbers of RMOs and of RAOs for L-LACO transmitter are

$$\begin{aligned} M^{(\mathrm{t})}_{\text{L-LACO}}(L, N) &= \underbrace{\sum_{l=1}^{L} M\left(\frac{N}{2^l}\right)}_{\text{For IFFTs}} + \underbrace{\sum_{l=1}^{L} 2N_{\mathrm{AC}}(l)}_{\text{Calculate } v_n^{(l)} \text{ in (4.4.4)}} \\ &= \left(1 - \frac{1}{2^L}\right) 2N \log_2(N) - \left(6 - \frac{L+3}{2^{L-1}}\right) N + 4L \end{aligned} \tag{4.5.5}$$

and

$$\begin{aligned} A^{(\mathrm{t})}_{\text{L-LACO}}(L, N) &= \underbrace{\sum_{l=1}^{L} A\left(\frac{N}{2^l}\right)}_{\text{For IFFTs}} + \underbrace{(L-1)N}_{\text{Sum L layers}} + \underbrace{\sum_{l=1}^{L} N_{\mathrm{AC}}(l)}_{\text{Calculate } v_n^{(l)} \text{ in (4.4.4)}} \\ &= \left(1 - \frac{1}{2^L}\right) 3N \log_2(N) - \left(8 - L - \frac{3L+7}{2^L}\right) N + 2L \ . \end{aligned} \tag{4.5.6}$$

At the receiver side of L-LACO as shown in Fig. 4.4, the N-point FFT requires $M(N)$ RMOs and $A(N)$ RAOs. When a one-tap zero-forcing equalizer (ZFE) is adopted, it requires $N/2$ complex-valued multiplications or $2N$ RMOs and N RAOs thanks to the Hermitian symmetry. It is apparent that the computational complexity induced by a ZFE is also required by LACO-OFDM. Additionally, the estimate of CD requires a single $N_{\mathrm{AC}}(l)$-point IFFT and a single $N_{\mathrm{AC}}(l)$-point FFT for l-th $(1 \leq l \leq L-1)$ layer [1]. Hence, the required numbers of RMOs and RAOs for L-LACO

[1] Note that the absolute value operation requires simple logic operation which is omitted in the complexity analysis.

receiver are

$$\begin{aligned} M^{(\mathrm{r})}_{\text{L-LACO}}(L,N) &= M(N) + \underbrace{2N}_{\text{For ZFE}} + \underbrace{2\sum_{l=1}^{L-1} M\left(\frac{N}{2^l}\right)}_{\text{Estimate CD}} \\ &= \left(6-\frac{8}{2^L}\right) N\log_2(N) - \left(18-\frac{L+3}{2^{L-3}}\right) N + 8L - 4 \end{aligned} \tag{4.5.7}$$

and

$$\begin{aligned} &A^{(\mathrm{r})}_{\text{L-LACO}}(L,N) \\ &= A(N) + \underbrace{N}_{\text{For ZFE}} + \underbrace{2\sum_{l=1}^{L-1} A\left(\frac{N}{2^l}\right)}_{\text{Estimate CD}} + \underbrace{\sum_{l=2}^{L}(l-1)\frac{N}{2^l}}_{\text{Remove CD}} \\ &= \left(9-\frac{12}{2^L}\right) N\log_2(N) - \left(16-\frac{11L+19}{2^L}\right) N + 4L - 2\,. \end{aligned} \tag{4.5.8}$$

For comparison, the required numbers of RMOs and RAOs for LACO-OFDM transmitter are [86, 106]

$$\begin{aligned} &M^{(\mathrm{t})}_{\text{LACO}}(L,N) = \\ &\left(1-\frac{1}{2^L}\right) 4N\log_2(N) - \left(12-\frac{2L+6}{2^{L-1}}\right) N + 4L \end{aligned} \tag{4.5.9}$$

and

$$\begin{aligned} &A^{(\mathrm{t})}_{\text{LACO}}(L,N) = \\ &\left(1-\frac{1}{2^L}\right) 6N\log_2(N) - \left(11-L-\frac{3L+5}{2^{L-1}}\right) N + 2L\,. \end{aligned} \tag{4.5.10}$$

For LACO-OFDM receiver, an identical ZFE is adopted. Hence, the required number of RMOs and RAOs for LACO-OFDM receiver are, respectively, given as

[106]

$$M^{(\mathrm{r})}_{\mathrm{LACO}}(L,N) = \left(1-\frac{\frac{8}{5}}{2^L}\right)10N\log_2(N) - \left(26-\frac{L+2}{2^{L-4}}\right)N + 8L - 4 \tag{4.5.11}$$

and

$$A^{(\mathrm{r})}_{\mathrm{LACO}}(L,N) = \left(1-\frac{\frac{8}{5}}{2^L}\right)15N\log_2(N) - \left(19-\frac{23L+13}{2^L}\right)N + 4L - 2\,. \tag{4.5.12}$$

4.5.3 Power Savings

VLC transmitters are constrained by complexity, i.e. transmitters must be simple and integrated into inexpensive luminaires, using low cost commercially available LEDs. Additionally, VLC transmitters must be energy efficient given that the energy efficiency of LED luminaries is a primary advantage of this illumination technology. Hence, in this section, the saved power of L-LACO over LACO-OFDM is quantified due to the reduction in number of arithmetic operations.

Following the computational complexity analysis in Section 4.5.2, the reduction in RMOs and RAOs of L-LACO transmitter over LACO-OFDM for an OFDM symbol are given as

$$\Delta^{(\mathrm{t})}_{\mathrm{Mul}} = M^{(\mathrm{t})}_{\mathrm{LACO}}(L,N) - M^{(\mathrm{t})}_{\text{L-LACO}}(L,N) \tag{4.5.13}$$

and

$$\Delta^{(\mathrm{t})}_{\mathrm{Add}} = A^{(\mathrm{t})}_{\mathrm{LACO}}(L,N) - A^{(\mathrm{t})}_{\text{L-LACO}}(L,N), \tag{4.5.14}$$

respectively.

Let the energy consumed by a single RMO and a single RAO be denoted as E_{Mul}

and E_{Add}, respectively. Then the saved energy of L-LACO transmitter over LACO-OFDM for an OFDM symbol can be computed as

$$\Delta^{(\text{t})}_{\text{Energy}} = \Delta^{(\text{t})}_{\text{Mul}} E_{\text{Mul}} + \Delta^{(\text{t})}_{\text{Add}} E_{\text{Add}}. \tag{4.5.15}$$

Assume the time length of an OFDM symbol is T_{s} and the time length of CP is T_{CP}. Hence, the saved power of the L-LACO transmitter over LACO-OFDM is

$$P^{(\text{t})}_{\text{save}}(L, N, B) = \frac{\Delta^{(\text{t})}_{\text{Energy}}}{T_{\text{s}} + T_{\text{CP}}}. \tag{4.5.16}$$

For readability, assume $T_{\text{CP}} = \beta T_{\text{s}}$ without loss of generality and assume a modulation bandwidth of the VLC system is B Hz. Then the length of an OFDM frame is $T_{\text{s}} = N/(2B)$ and $T_{\text{s}} + T_{\text{CP}} = (1+\beta)N/(2B)$. Substituting (4.5.5), (4.5.6), (4.5.9), (4.5.10), (4.5.13), (4.5.14) and (4.5.15) into (4.5.16) results in

$$P^{(\text{t})}_{\text{save}}(L, N, B) = \frac{2B}{1+\beta}(\gamma \log_2 N - \zeta) \tag{4.5.17}$$

where $\gamma \triangleq (1 - 1/2^L)(2E_{\text{Mul}} + 3E_{\text{Add}})$ and $\zeta \triangleq (6 - \frac{L+3}{2^{L-1}})E_{\text{Mul}} + (3 - \frac{3L+3}{2^L})E_{\text{Add}}$.

Using a similar approach, the saved power of L-LACO receiver over existing LACO-OFDM can be calculated as

$$P^{(\text{r})}_{\text{save}}(L, N, B) = \frac{\Delta^{(\text{r})}_{\text{Energy}}}{T_{\text{s}} + T_{\text{CP}}} \tag{4.5.18}$$

where $\Delta^{(\text{r})}_{\text{Energy}} = \Delta^{(\text{r})}_{\text{Mul}} E_{\text{Mul}} + \Delta^{(\text{r})}_{\text{Add}} E_{\text{Add}}$ is saved energy of L-LACO receiver for an OFDM symbol while $\Delta^{(\text{r})}_{\text{Mul}} = M^{(\text{r})}_{\text{LACO}}(L, N) - M^{(\text{r})}_{\text{L-LACO}}(L, N)$ denotes saved RMOs and $\Delta^{(\text{r})}_{\text{Add}} = A^{(\text{r})}_{\text{LACO}}(L, N) - A^{(\text{r})}_{\text{L-LACO}}(L, N)$ denotes saved RAOs, respectively.

Substituting (4.5.7), (4.5.8), (4.5.11) and (4.5.12) into (4.5.18) gives

$$P_{\text{save}}^{(\text{r})}(L,N,B) = \frac{2B}{1+\beta}(\psi \log_2 N - \xi) \tag{4.5.19}$$

where $\psi \triangleq (1-2/2^L)(4E_{\text{Mul}}+6E_{\text{Add}})$ and $\xi \triangleq (8-\frac{L+1}{2^{L-3}})E_{\text{Mul}} + (3-\frac{6L-3}{2^{L-1}})E_{\text{Add}}$.

Remark 3. *As L increases with B and N fixed, γ and ζ in* (4.5.17)*, ψ and ξ in* (4.5.19) *saturate to a constant, respectively as do $P_{\text{save}}^{(\text{t})}(L,N,B)$ and $P_{\text{save}}^{(\text{r})}(L,N,B)$. As N increases with B and L fixed, $P_{\text{save}}^{(\text{t})}(L,N,B)$ increases logarithmically as does $P_{\text{save}}^{(\text{r})}(L,N,B)$. As B increases with L and N fixed, both $P_{\text{save}}^{(\text{t})}(L,N,B)$ and $P_{\text{save}}^{(\text{r})}(L,N,B)$ increase linearly.*

4.6 Numerical Results

4.6.1 Computational Complexity

Numerical results for the computational complexity of L-LACO are presented and compared to LACO-OFDM [74] with realistic parameters for VLC systems.

A computational complexity comparison between transmitters of L-LACO and LACO-OFDM for different values of N and L are shown in Fig. 4.5, in which for (a) and (b) L is fixed to 4 while for (c) and (d) N is fixed to 1024. It is evident that the conventional LACO-OFDM is more complex than our proposed L-LACO in terms of the number of RMOs and RAOs. More specifically, for $L = 4$ layers and $N = 1024$ subcarriers, LACO-OFDM requires 27920 RMOs and 52620 RAOs; while our proposed L-LACO requires 13970 RMOs and 25930 RAOs. LACO-OFDM requires two times more RMOs/RAOs when compared with our proposed L-LACO.

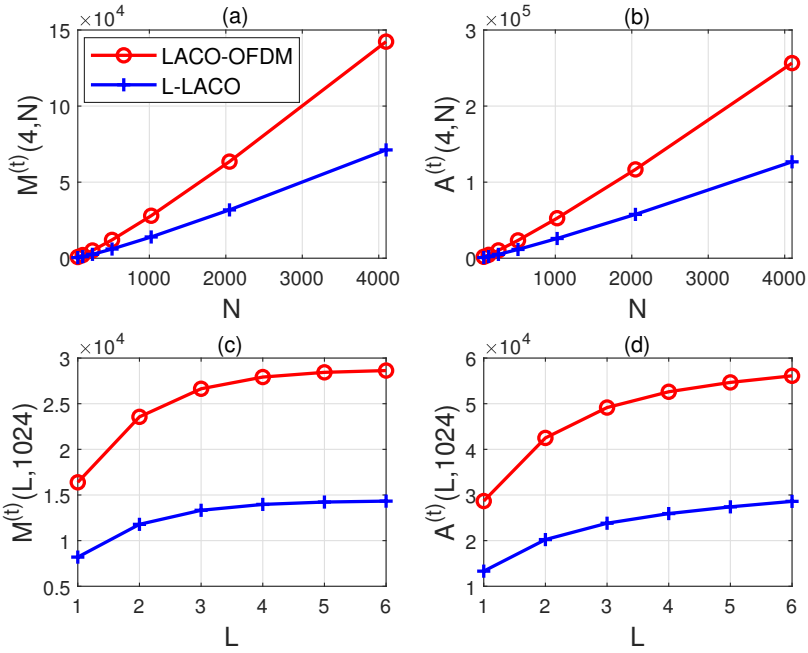

Figure 4.5: Computational complexity comparison between transmitters of L-LACO and LACO-OFDM for different values of N and L ($L = 4$ for (a) and (b), $N = 1024$ for (c) and (d)).

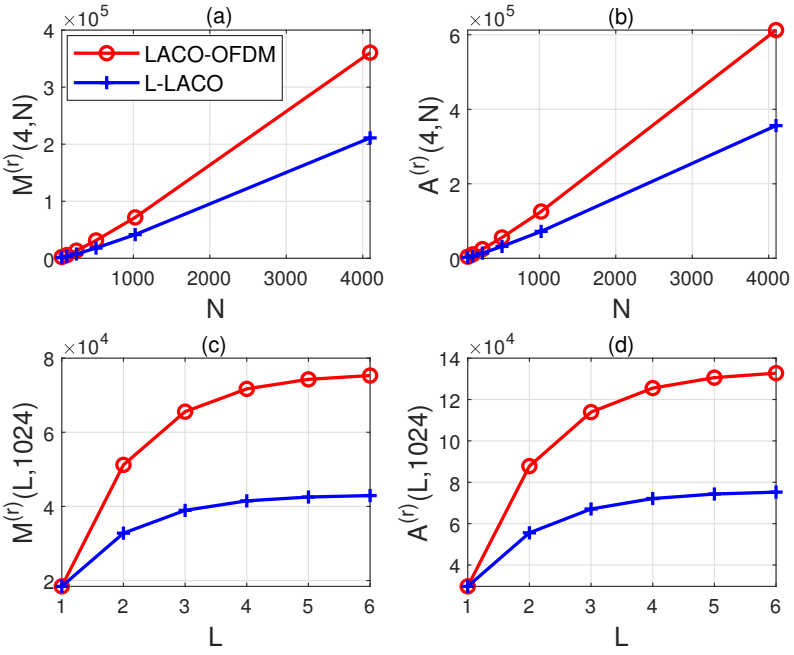

Figure 4.6: Computational complexity comparison between receivers of L-LACO and LACO-OFDM for different values of N and L ($L = 4$ for (a) and (b), $N = 1024$ for (c) and (d)).

For receivers, a computational complexity comparison between L-LACO and LACO-OFDM for different values of N and L are shown in Fig. 4.6, in which for (a) and (b) L is fixed to 4 while for (c) and (d) N is fixed to 1024. Evidently, the LACO-OFDM receiver is more complex than our proposed L-LACO in terms of the number of RMOs and RAOs since the size of IFFT/FFT used to remove CD induced by each layer are halved in L-LACO. Specifically, LACO-OFDM requires 71710 RMOs and 125518 RAOs when $L = 4$ and $N = 1024$; while our proposed low-complexity L-LACO requires 41500 RMOs and 72142 RAOs. LACO-OFDM requires nearly 1.73 times more RMOs and 1.74 times more RAOs when compared with our proposed L-LACO.

The number of RMOs and RAOs of both L-LACO transmitter and receiver increase dramatically fast as N increases. This is because the dominant term of $M^{(\mathrm{t})}_{\text{L-LACO}}(L,N)$, $A^{(\mathrm{t})}_{\text{L-LACO}}(L,N)$, $M^{(\mathrm{r})}_{\text{L-LACO}}(L,N)$, and $A^{(\mathrm{r})}_{\text{L-LACO}}(L,N)$ are respectively $\left(1-1/2^L\right)2N\log_2(N)$, $\left(1-1/2^L\right)3N\log_2(N)$, $\left(6-8/2^L\right)N\log_2(N)$ and $\left(9-12/2^L\right)N\log_2(N)$, which increase faster than linear functions of N when N is large. While the number of RMOs and RAOs increase more slowly and saturate as L increases when $N = 1024$. This is because the previously noted dominant terms, for a fixed N, saturate to limit with increasing L.

4.6.2 Saved Power

According to [157], a 32-bit floating point multiplication and a 32-bit floating point addition consume $E_{\text{Mul}} = 3.7$ pJ and $E_{\text{Add}} = 0.9$ pJ, respectively. Assume a modulation bandwidth of $B = 100$ MHz and that the length of an OFDM frame is $T_{\text{s}} = N/(2B)$ and $T_{\text{CP}} = T_{\text{s}}/16$ with $\beta = 1/16$.

The saved power of L-LACO over LACO-OFDM is then calculated according to Sec. 4.5.3 and presented for different values of L and N in Fig. 4.7. It can be seen the saved power of L-LACO receiver is higher than L-LACO transmitter when $L \geq 2$, which is aligned well given that the L-LACO receiver saved more arithmetic operations than L-LACO transmitter shown in Figs. 4.5 and 4.6. In addition, compared to LACO-OFDM, the saved power of L-LACO transmitter and receiver increase and saturate as L increases when $N = 1024$, which is aligned well with theoretical analysis in Sec. 4.5.3 and Remark 3. This is because the saved arithmetic operations increase and saturate as L increases.

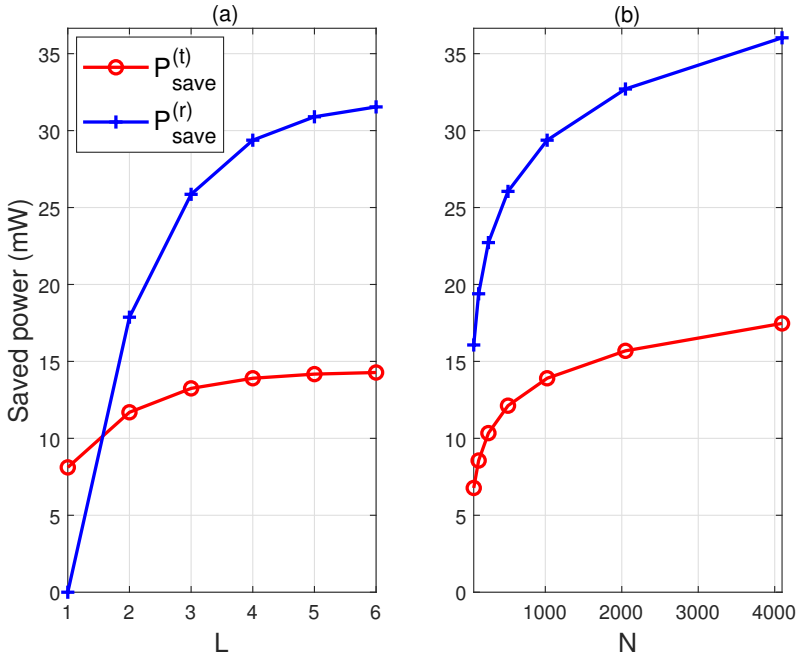

Figure 4.7: Power saving of L-LACO compared to LACO-OFDM for different values of L and N when $B = 100$ MHz ($N = 1024$ for (a) and $L = 4$ for (b)).

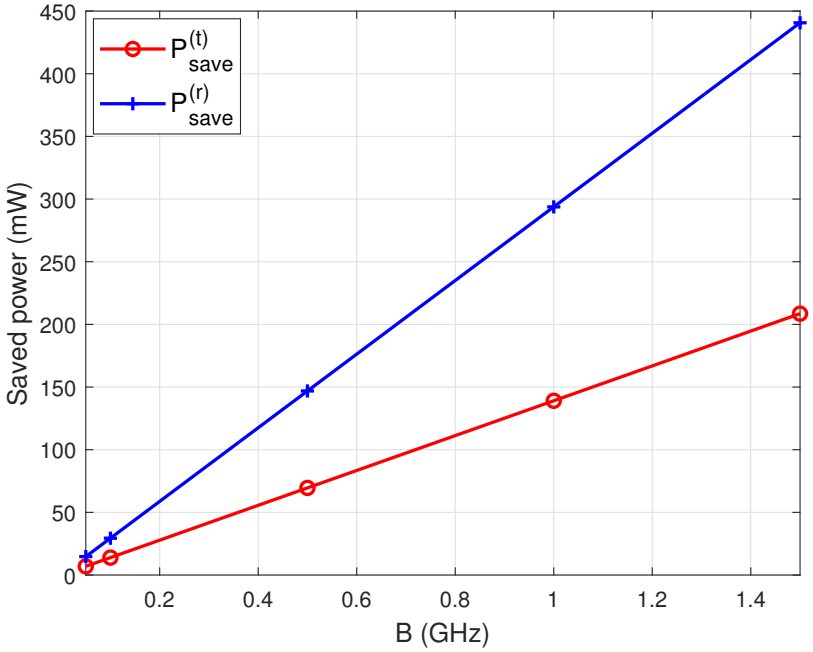

Figure 4.8: Saved power of L-LACO compared to LACO-OFDM for different values of B ($L = 4$ and $N = 1024$).

In contrast, notice that the saved power of the L-LACO transmitter over LACO-OFDM increases logarithmically with N as does the saved power of the L-LACO receiver. This trend agrees well with theoretical analysis in Remark 3.

The saved power of the L-LACO transmitter and receiver over LACO-OFDM for different values of modulation bandwidth is shown in Fig. 4.8. The saved power of the L-LACO transmitter and receiver increase linearly as modulation bandwidth B increases when $L = 4$ and $N = 1024$. This is aligned well with theoretical analysis in Remark 3. Notice that the power savings become especially significant for high-speed VLC systems realized using L-LACO.

It is worth noting that the saved power will increase linearly for larger B. For example, $B = 600$ MHz for Si-substrate LED [42], $B = 655$ MHz for micro-LED [38]

Table 4.4: Simulation Parameters

Parameters	**Values**
Room size Width × Length × Height	5m × 5m × 3m
Number of LED/PD	1 / 1
LED location	(2.5, 2.5, 2.50) m
LED semi-angle $\Psi_{1/2}$	45^o
PD location	(2.5, 2.5, 0.75) m
Optical power gain of receive filter	1
PD FOV Θ_{F}	62^o [158]
PD effective collection area A_{PD}	1 cm^2
O/E conversion coefficient η	0.54 A/W [21]
Average electrical noise power σ_w^2	-98.82 dBm [21]
Number of subcarriers N	1024
Number of layers L	3
Length of CP N_{CP}	64
Maximum delay spread $D_{\max}$	64
Modulation schemes	4-QAM, 16-QAM

and $B = 1.4$ GHz for laser diode (LD) based white-light VLC [44] are reported in recent experimental demonstrations. Thus, L-LACO becomes an even more attractive approach with the arrival of new high-bandwidth light sources envisioned for future VLC applications.

4.6.3 BER performance

In this section, the BER performance of L-LACO is evaluated by back-to-back simulations in terms of transmitted optical power P_{o} expressed in decibel milliwatts (dBm), and compared with LACO-OFDM.

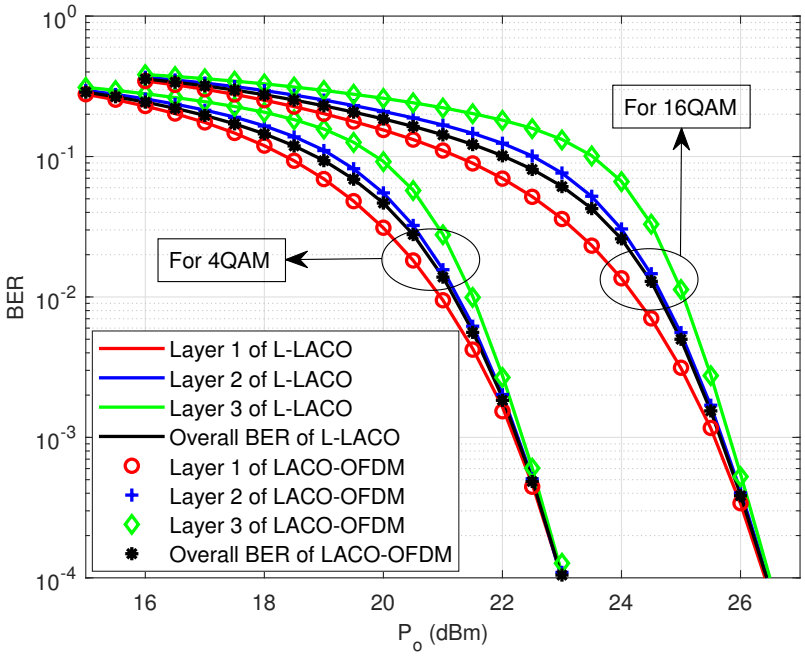

Figure 4.9: BER performance of L-LACO and LACO-OFDM under a VLC LOS channel.

BER Under a VLC LOS Link

The BER of L-LACO under a VLC LOS Link is simulated with parameters summarized in Table 4.4.

The BER performance of the proposed L-LACO and of LACO-OFDM under a VLC LOS link is shown in Fig. 4.9, where 4-QAM and 16-QAM with Gray labelling are employed in each layer. The BER of each layer are approximately the samen when operating in the high SNR regime. In addition, the BER of the proposed L-LACO is the same as existing LACO-OFDM since L-LACO generates the same OFDM symbol as LACO-OFDM, however, L-LACO requires less complexity at both the transmitter and the receiver thanks to employing half-size IFFTs/FFTs.

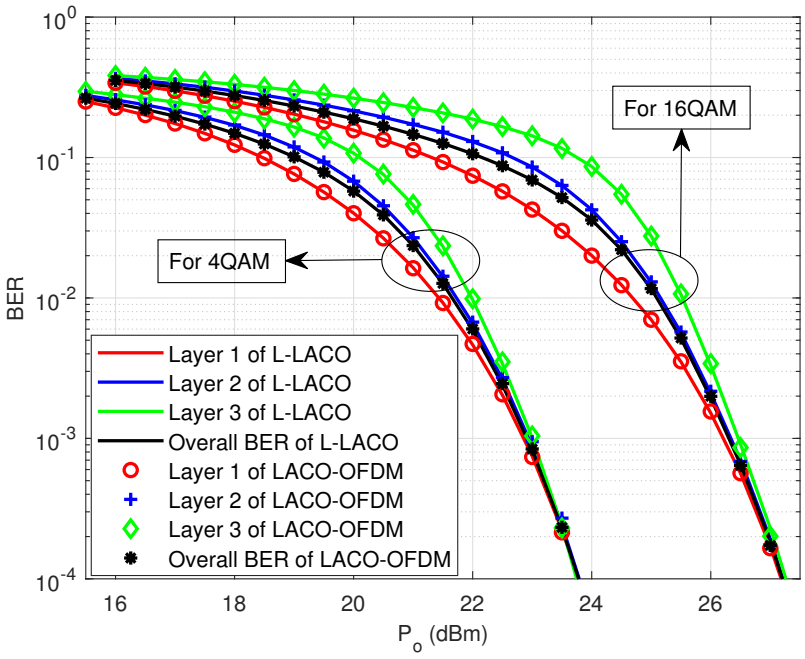

Figure 4.10: BER performance of L-LACO and LACO-OFDM under a VLC dispersive channel.

BER Under a VLC Dispersive Channel

In this section, the BER of L-LACO under a VLC dispersive channel is simulated. Here, the sampling rate for impulse response $h(t)$ in (5.4.1) is set to 300 MHz. The maximum delay span of samples of $h(t)$ is assumed to 64. Hence, the length of CP is also set to $N_{\text{CP}} = 64$.

The BER performance of the proposed L-LACO and of LACO-OFDM under a VLC dispersive channel are shown in Fig. 4.10, where the simulation parameters are summarized in Table 4.4. The BER of each layer in these Monte Carlo simulations are in close agreement especially at high SNR. Additionally, the BER of the proposed L-LACO is the same as LACO-OFDM since L-LACO generates identical signal to LACO-OFDM, however, L-LACO requires less complexity at both the transmitter

and the receiver thanks to employing a half-size IFFT/FFT.

4.7 Conclusions

In this paper, L-LACO is proposed for IM/DD systems, in which the size of IFFT and FFT used in each layer is halved compared to the existing LACO-OFDM. The proposed L-LACO generates the identical OFDM signal to LACO-OFDM and thus achieves the same spectral efficiency and optical power efficiency but retains less complexity. Numerical results show that LACO-OFDM requires two times the RMOs / RAOs as compared to the proposed L-LACO at the transmitter. At the receiver, LACO-OFDM requires 1.73 times more RMOs and 1.74 times more RAOs when compared with the proposed L-LACO. This reduction in complexity translates directly into power savings which are especially important for LED luminaires. Additionally, the proposed L-LACO achieves the same BER performance under VLC LOS and dispersive channels thanks to the identical OFDM signals generated as LACO-OFDM.

As the bandwidth of VLC systems increases with new devices, the need for low complexity, power efficient approaches, such as L-LACO, to implement spectrally efficient IM/DD modulation becomes essential. Our future work includes experimental demonstration of L-LACO including quantifying the impact of oversampling at the transmitter and receiver.

Chapter 5

Kramers-Kronig Based Optical OFDM for Bandlimited Visible Light Communications

Research work in this chapter appears in the following paper [108] while minor modifications are made according to thesis format.

- R. Bai and S. Hranilovic, "Kramers-Kronig Optical OFDM for bandlimited intensity modulated visible light communications," *Journal of Lightwave Technology*, 2021, doi: 10.1109/JLT.2021.3110661.

As discussed in Section 1.5.1, to enhance spectral efficiency and energy efficiency

are important challenges in VLC systems since commercially off-the-shelf LEDs are low-cost, simple, and have a small modulation bandwidth. Additionally, in a realistic VLC system, the links are a dispersive channel rather than an ideal flat channel due to multiple reflections of the light from the transmitter to the receiver. For such a practical VLC dispersive channel, transmit signal is required to be strictly bandlimited to avoid in-band distortion. Before being fed into an LPF, interpolation with $\text{sinc}(t)$ pulse can be utilized to make the transmit signal bandlimited. However, for ALACO-OFDM in **Chapter 2**, LAC-OFDM in **Chapter 3**, and **L-LACO** in Chapter 4, the transmit signal will not be non-negative at all time instants when interpolation with $\text{sinc}(t)$ pulse is used. Alternatively, interpolation with a non-negative rectangular pulse can be employed to generate an analog signal; however, the transmit signal is no longer bandlimited.

To solve these problems and challenges, this chapter introduces KKO-OFDM that directly generates bandlimited non-negative OFDM signals that are constrained in the mean. In KKO-OFDM, a single-sideband minimum phase signal is employed to carry information. Then the squared modulus of this signal is utilized as LED drive current to modulate the light intensity. Mathematically, the transmit signal is constructed to be real-valued, non-negative and strictly bandlimited, thus is suitable for VLC channels. At the receiver, the phase of the information-carrying signal is retrieved according to the Kramers-kronig relations.

For KKO-OFDM, the required DC bias is analysed and designed theoretically and is verified by numerical results. The theoretical analysis on the electrical signal-to-noise ratio, bit-error rate, and data rate is supported by Monte Carlo simulations. Our analysis shows KKO-OFDM achieves as high spectral efficiency as DCO-OFDM,

however, realizes about 1 dB optical gain at a BER= 10^{-4} in a VLC line-of-sight (LOS) flat channel, and realizes about 1.3 dB optical gains in a VLC dispersive LPF channel. KKO-OFDM achieves about 1.4 dB optical gains over bandlimited LACO-OFDM in a VLC LOS flat channel and achieves about 1.8 dB optical gains in a VLC dispersive LPF channel. What is more, KKO-OFDM transmitter requires less complexity compared to LACO-OFDM. The PAPR for KKO-OFDM is also smaller than LACO-OFDM. These advantages support a ascendancy of KKO-OFDM over DCO-OFDM and LACO-OFDM for a realistic bandlimited VLC system.

Abstract Visible light communication (VLC) operates on optical intensity channels that are inherently limited in bandwidth. Though Kramers-Kronig (KK) receivers have been considered as a lower complexity alternative for coherent fiber optic communication (FOC) systems, in this paper we extend this concept to bandlimited IM/DD VLC channels and propose KK optical OFDM (KKO-OFDM). In KKO-OFDM the optical power of a low-cost LED is directly modulated by the double-sideband (DSB) squared modulus of a minimum phase single-sideband (SSB) signal. This results in a real-valued, non-negative and strictly bandlimited transmit signal which is suitable for VLC channels. At the receiver, the phase of the transmitted SSB signal is reconstructed via the KK relations. The required DC bias, average electrical signal-to-noise ratio (SNR), bit error rate (BER), and capacity are analyzed with approximate closed-forms and through simulation. Numerical results show that KKO-OFDM achieves the same spectral efficiency as the existing DC biased optical OFDM (DCO-OFDM), however, realizes approximately 1 dB optical SNR gain at a BER= 10^{-4} while simultaneously having a small peak-to-average power ratio.

5.1 Introduction

Visible light communication (VLC) systems are emerging complementary links to radio due to the ubiquity of solid-state illumination as well as the availability of unregulated optical spectrum [3, 4, 159, 48, 139, 86]. For a VLC system, a light-emitting diode (LED) is used as a transmitter and its optical intensity is modulated to carry information (i.e., intensity modulation (IM)). The receiver is typically a photodiode (PD) which produces an electrical current in proportion to the intensity of light (i.e., direct detection (DD)). Such IM/DD systems must drive the LED with a

real-valued and non-negative electrical current signal, while maintaining a constraint on the average amplitude (i.e., intensity) [3, 4, 159, 48, 139, 86].

The low-cost white LEDs employed in IM/DD VLC systems have a low-pass characteristic and have a typical modulation bandwidth of only several tens of MHz [160]. Orthogonal frequency division multiplexing (OFDM) has been considered as a candidate modulation scheme for such systems due to its high spectral efficiency, resistance to inter-symbol interference (ISI), simple one-tap equalization and extensive usage in wired and wireless broadband communications [56, 160, 86, 161, 106, 101]. Direct current (DC) biased optical OFDM (DCO-OFDM) is a popular OFDM scheme for IM/DD systems due to its simplicity and high spectral efficiency. In order to generate a transmittable signal, a real output is guaranteed by imposing Hermitian symmetry in frequency domain and a DC bias is added to ensure non-negativity. If a fixed DC bias is selected, there is a risk of clipping the DCO-OFDM signals resulting in out-of-band (OOB) distortion which is not bandlimited [53]. Alternatively, the DC bias can be varied symbol-by-symbol to ensure non-negativity, resulting in no OOB distortion [54]. However, this method can cause flickering and is not suitable for VLC systems that are required to provide stable illumination. Asymmetrically clipped optical OFDM (ACO-OFDM) is another popular scheme for VLC systems, in which only odd subcarriers are modulated [56]. Using the anti-symmetric property of such signals, the negative parts are clipped at zero directly without any loss of information. However, OOB clipping distortion still exists due to sharp transition caused by this zero clipping [53]. Alternative approaches have also been considered, namely spectrally factorized optical OFDM (SFO-OFDM) [63] which considers the generation of bandlimited IM signals directly through the autocorrelation of a complex

data sequence to guarantee non-negativity. However, the demodulation requires high computational complexity for a practical SFO-OFDM system with many subcarriers.

In related coherent fiber-optic communication (FOC) systems, data are transmitted in both the amplitude and the phase of an electric field of a laser. Recently, low complexity receivers for such FOC coherent links have been proposed which can recover both the amplitude and phase from measurements of the intensity using a PD at the receiver [162, 163, 164, 165, 166]. These systems require that the transmitted complex signal is a minimum phase waveform and rely on the Kramers-Kronig (KK) relations to recover the phase [162].

In this paper, we extend the application of the KK relations to develop a strictly bandlimited IM/DD optical OFDM modulation format termed as *KK Optical*-OFDM (KKO-OFDM). In KKO-OFDM, a minimum phase single-sideband (SSB) complex signal is employed to carry information and its squared modulus is utilized to directly modulate the optical power emitted from a low-cost LED. Mathematically, the squared modulus of an SSB signal is necessarily non-negative and strictly bandlimited and has no OOB clipping distortion as compared to conventional DCO- and ACO-OFDM. At the receiver, a PD is used to detect the received optical power and the KK relations are used to infer the phase information to reconstruct the original SSB signal. Unlike related work on coherent FOC channels, where the KK relations are used to reconstruct the phase of an electric field, here the squared modulus of an SSB signal is used to directly modulate the optical power emitted by the white LEDs in a VLC system and the KK relations are used to infer the phase of this SSB signal at the receiver. Compared to recent work in VLC optical single side-band OFDM (SSB-OFDM) [160], KKO-OFDM does not require upsampling and up-conversion

at the transmitter, resulting in less complexity, which is attractive to VLC systems employing low-cost simplicity LEDs.

The paper provides a design guide for KKO-OFDM for VLC channels. A theoretical bit error rate (BER) is derived which shows a small gap to the simulated results and thus can be employed to evaluate the performance conveniently. The capacity of KKO-OFDM is analysed and a small gap is found compared to capacity bounds of IM/DD OWC channels in existing literature. The computation complexity of KKO-OFDM is comparable to DCO-OFDM at the transmitter, however requiring greater complexity at the receiver. Monte Carlo simulation results show that KKO-OFDM is more power efficient compared to DCO-OFDM and LACO-OFDM for a bandlimited VLC systems achieving a 1.0 dB gain over bandlimited DCO-OFDM and 1.4 dB gain over bandlimited LACO-OFDM at BER= 10^{-4}. The peak-to-average power ratio (PAPR) of KKO-OFDM signals is shown to be smaller than DCO-OFDM and LACO-OFDM, indicating the increased robustness of KKO-OFDM to LED nonlinear transfer characteristics.

The balance of the paper is organized as follows. Sec. 5.2 describes bandlimited IM/DD optical OFDM schemes and introduces the transceiver for KKO-OFDM. KKO-OFDM design and signal analysis are presented in Sec. 5.3. Numerical results are analysed in Sec. 5.4. Finally, conclusions are drawn in Sec. 5.5.

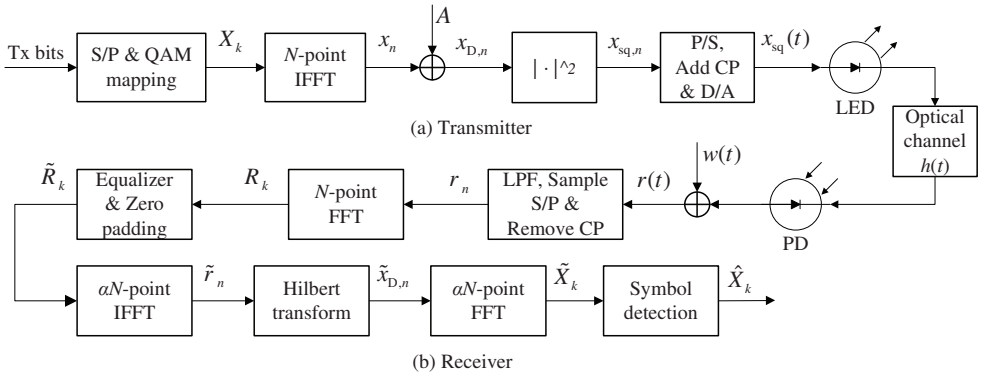

Figure 5.1: Transmitter (a) and receiver (b) block diagrams for KKO-OFDM.

5.2 Bandlimited KK Optical-OFDM Definition

5.2.1 Conventional Bandlimited Optical OFDM

For comparison and completeness, in this subsection we define two conventional strictly bandlimited optical OFDM approaches. A continuous, finite energy signal $s(t)$ is defined as bandlimited to frequency range $[-B, B]$ if the support of its Fourier transform is limited to $[-B, B]$.

In DCO-OFDM with N subcarriers, the 0-th and $N/2$-th subcarriers are set to zero with data symbols modulated onto the remaining subcarriers. Hermitian symmetry, i.e., $X_k = X^*_{N-k}$, is imposed on each OFDM symbol to ensure the output of inverse fast Fourier transform (IFFT), x_n, a real-valued signal [56]. Assuming the available bandwidth of the LED is B, consider constructing the strictly bandlimited data bearing signal $x(t)$ via Nyquist-Shannon interpolation as [137]

$$x_{\text{DCO}}(t) = \underbrace{\sum_{n=-\infty}^{\infty} x_n \text{sinc}\left(2Bt - n\right)}_{x(t)} + D_{\text{DCO}} \tag{5.2.1}$$

where $\text{sinc}(\zeta) = \sin(\pi\zeta)/(\pi\zeta)$, $x(t)$ is the data-bearing signal and D_{DCO} is a DC bias added to satisfy the non-negativity constraint. To improve power efficiency, consider adaptively setting the DC bias per OFDM frame as the minimum required to ensure non-negativity [54]

$$D_{\text{DCO}} = -\min\{x(t)\} \, . \tag{5.2.2}$$

In ACO-OFDM, data symbols are only modulated onto the odd subcarriers with even subcarriers set to zero while imposing Hermitian symmetry in the frequency domain. The resulting output of IFFT x_n is anti-symmetric and clipping the negative parts to zero results in no loss of information leading to [56]

$$x_{\text{clip},n} = \frac{1}{2}x_n + \frac{1}{2}|x_n|, \; 0 \leq n \leq N-1 \tag{5.2.3}$$

where $\frac{1}{2}|x_n|$ is clipping distortion only onto even subcarriers.

Similar to DCO-OFDM in (5.2.1), consider constructing a bandlimited signal with samples $x_{\text{clip},n}$ using Nyquist-Shannon interpolation leading to $x_{\text{clip}}(t)$. Though $x_{\text{clip},n} \geq 0$, after interpolation, $x_{\text{clip}}(t)$ may no longer satisfy the non-negativity constraint, hence a sufficiently large DC bias must be added to $x_{\text{clip}}(t)$ as in [53, 54] leading to

$$x_{\text{ACO}}(t) = x_{\text{clip}}(t) + D_{\text{ACO}} \tag{5.2.4}$$

where $D_{\text{ACO}} = -\min\{x_{\text{clip}}(t)\}$.

To enhance the spectral efficiency, LACO-OFDM simultaneously transmits the sum of L layers of ACO-OFDM signals in the time domain [74]. These ACO-OFDM layers employ disjoint sets of subcarriers, with each layer satisfying an anti-symmetric property. Define similarly, $x_{\text{L,clip},n}$ as sum of samples of the L layers of ACO-OFDM

and $x_{\mathrm{L,clip}}(t)$ as the bandlimited signal arising from Nyquist-Shannon interpolation. To ensure non-negativity a sufficiently large DC bias, $D_{\mathrm{LACO}} = -\min\{x_{\mathrm{L,clip}}(t)\}$, is adaptively added to each LACO-OFDM symbol, resulting in a non-negative bandlimited signal $x_{\mathrm{LACO}}(t)$.

5.2.2 KKO-OFDM Transmitter

The transmitter block diagram for KKO-OFDM with N subcarriers is shown in Fig. 5.1(a). For convenience, assume N is a power of 2. The bits to be transmitted are first mapped to quadrature amplitude modulation (QAM) symbols. These QAM constellation symbols are modulated onto subcarriers with index number of $k = 1, \ldots, N/2-1$ with remaining subcarriers set to zero to form the SSB frequency-domain symbol as

$$\mathbf{X} = \left[0, X_1, X_2, X_3, \ldots, X_{N/2-1}, \underbrace{0, \ldots, 0}_{N/2 \text{ zeros}}\right]. \tag{5.2.5}$$

Notice that different from DCO-OFDM, KKO-OFDM does not require Hermitian symmetry.

The frequency-domain symbol $\mathbf{X}$ is fed into an N-point IFFT module leading to time-domain signal $\mathbf{x}$, of which the n-th element is given by

$$x_n = \frac{1}{\sqrt{N}} \sum_{k=0}^{N-1} X_k \exp\left(j\frac{2\pi}{N}nk\right), \ 0 \le n \le N-1 \tag{5.2.6}$$

where x_n is a complex-valued signal.

Consider adding a real DC bias $A > 0$ to the SSB-signal x_n to ensure that resulting

$x_{\mathrm{D},n}$ is a minimum phase waveform [162, 163], given by

$$x_{\mathrm{D},n} = x_n + A \; . \tag{5.2.7}$$

An SSB signal is a minimum phase waveform for which all roots are outside the unit circle [162]. In this work, in order to avoid flickering in VLC systems, A is set as a constant. The selection of A is discussed at length in Sec. 5.3.2.

For a minimum phase signal such as $x_{\mathrm{D},n}$, the phase and the natural logarithm of its amplitude form a Hilbert transform pair [162]. Thus, only intensity of $x_{\mathrm{D},n}$ need be transmitted over the channel without any loss of information. The phase can be recovered completely from the measurements of the intensity at the receiver. Thus, define the driving signal for the LED as

$$x_{\mathrm{sq},n} = \|x_{\mathrm{D},n}\|^2 \tag{5.2.8}$$

where $\|\cdot\|$ denotes the magnitude of a complex value.

Notice that while $x_{\mathrm{D},n}$ is a complex-valued single-sideband signal, $x_{\mathrm{sq},n}$ is a real-valued, double-sideband (DSB) signal with support over discrete frequency indices $\{0, \ldots, N-1\}$ [162].

After parallel-to-serial (P/S) and padding a CP, the transmitted intensity signal $x_{\mathrm{sq}}(t)$ is formed using Nyquist-Shannon interpolation as

$$x_{\mathrm{sq}}(t) = \sum_{n=-\infty}^{\infty} x_{\mathrm{sq},n} \mathrm{sinc}(2Bt - n) \; . \tag{5.2.9}$$

Notice that $x_{\mathrm{sq}}(t)$ is real, strictly bandlimited to frequencies $[-B, B]$ and $\forall t$, $x_{\mathrm{sq}}(t) \geq 0$

since it arises as the magnitude square of a single-sideband signal [63]. That is, $x_{\text{sq}}(t)$ is a strictly bandlimited signal satisfying the non-negativity constraint without the need of clipping or additional bias.

Unlike coherent FOC systems where the electric field of a laser is modulated by a complex-valued signal [162, 163, 165], here KKO-OFDM produces a real-valued, non-negative, bandlimited signal $x_{\text{sq}}(t)$ as LED drive current to directly modulate the optical power of the light emitted by an LED for VLC systems.

The average optical power of KKO-OFDM signal is proportional to the mean of $x_{\text{sq}}(t)$, which is given by

$$P_{\text{o}} = \text{E}\{x_{\text{sq}}(t)\} = \text{E}\{(x_{\text{r},n} + A)^2 + x_{\text{i},n}^2\} = \text{E}\{\|x_n\|^2\} + A^2 \tag{5.2.10}$$

where $x_{\text{r},n}$ and $x_{\text{i},n}$ are real and imaginary parts of x_n, respectively and $\text{E}\{\cdot\}$ denotes expectation.

5.2.3 KKO-OFDM Receiver

The KKO-OFDM receiver block diagram is shown in Fig. 5.1(b). A PD is utilized to convert the received optical intensity into a photocurrent, which is assumed proportional to the received instantaneous optical power. The optical bandwidth of the PD response, B_{PD} is generally much greater than the bandwidth of an LED, i.e., $B_{\text{PD}} \gg B$. The detected photocurrent, $r(t)$, is contaminated by high-intensity shot noise and thermal noise and is given by [4, 129, 158]

$$r(t) = h_{\text{VLC}}(t) \otimes x_{\text{sq}}(t) + w(t) \tag{5.2.11}$$

where $h_{\mathrm{VLC}}(t)$ is impulse response (IR) for the VLC channel. The combination thermal noise and high-intensity shot noise, $w(t)$, can be well modelled as signal-independent additive white Gaussian noise (AWGN) [4, 129, 158].

The front end of the receiver consists of an ideal low pass filter (LPF) to B Hz followed by Nyquist rate sampling, and removal of the cyclic prefix (CP). Equalization is performed in frequency domain by a single complex multiplication in each frequency bin after an N-point FFT. Since r_n is real, its DFT R_k has a Hermitian symmetry. Thanks to this Hermitian symmetry, only $N/2$ complex-valued multiplications are required to implement the one-tap equalization. As is conventional in KK receivers for FOC systems, up-sampling is required for subsequent steps [162]. Let $\alpha \geq 1$ denote the up-sampling factor, i.e., αN samples per symbol. Here, up-sampling is accomplished by zero padding in frequency domain in prior to performing an αN-point IFFT to yield signal $\widetilde{r}_n$.

Recall that for a minimum phase waveform, the phase and the natural logarithm of amplitude form a Hilbert transform pair [162, 163]. Define $\widetilde{x}_{\mathrm{D},n}$ as a minimum phase waveform with phase $\widetilde{\phi}_n$ so that $\|\widetilde{x}_{\mathrm{D},n}\|^2 = \|\widetilde{r}_n\|$ which can be shown to always exist [162]. Hence, $\widetilde{\phi}_n$ can be estimated through the Hilbert Transform block in Fig. 5.1(b) as

$$\widetilde{\phi}_n = \mathcal{H}\left(\log\left(\sqrt{\|\widetilde{r}_n\|}\right)\right) \tag{5.2.12}$$

where $\mathcal{H}$ denotes the Hilbert transform. Subsequently, $\widetilde{x}_{\mathrm{D},n}$ is estimated as

$$\widetilde{x}_{\mathrm{D},n} = \sqrt{\|\widetilde{r}_n\|}\exp\{j\widetilde{\phi}_n\}\ . \tag{5.2.13}$$

Taking the DFT of $\widetilde{x}_{\mathrm{D},n}$, an estimate of X_k can be obtained as

$$\widetilde{X}_k = \frac{1}{\sqrt{\alpha N}} \sum_{n=0}^{\alpha N-1} \widetilde{x}_{\mathrm{D},n} \exp\left(-j\frac{2\pi}{\alpha N} nk\right). \tag{5.2.14}$$

Finally, symbol detection is employed to detect the modulated QAM symbols as

$$\widehat{X}_k = \arg\min_{X\in\Omega_X} \|X - \widetilde{X}_k\|,\ k = 1, \cdots, N/2-1 \tag{5.2.15}$$

where Ω_X denotes the constellation set of symbols.

5.3 KKO-OFDM Design & Analysis

5.3.1 Spectral Efficiency

The spectral efficiency is defined as the transmitted bit rate divided by bandwidth usage. Assume N_{CP} is the length of CP used and constellation size is M for each subcarrier. For KKO-OFDM, $N/2-1$ subcarriers out of N are employed to modulate QAM symbols, hence the spectral efficiency is

$$\Upsilon_{\mathrm{KKO}} = \frac{N/2-1}{N+N_{\mathrm{CP}}} \log_2(M) \ \text{ bits/s/Hz}. \tag{5.3.1}$$

Note that (5.3.1) is also the spectral efficiency of DCO-OFDM [56].

For ACO-OFDM, the spectral efficiency is given by [56]

$$\Upsilon_{\mathrm{ACO}} = \frac{N/4}{N+N_{\mathrm{CP}}} \log_2(M) \ \text{ bits/s/Hz} \tag{5.3.2}$$

while the spectral efficiency of LACO-OFDM with L layers is given by [106, 74]

$$\Upsilon_{\text{LACO}} = \left(1 - \frac{1}{2^L}\right) \frac{N/2}{N + N_{\text{CP}}} \log_2(M) \text{ bits/s/Hz.} \tag{5.3.3}$$

Based on comparison among these OFDM schemes, the spectral efficiencies of DCO- and KKO-OFDM are the highest while ACO-OFDM is the smallest. As L increases, the spectral efficiency of LACO-OFDM approaches that of DCO- and KKO-OFDM.

5.3.2 Selection of DC bias A

Given that KKO-OFDM only transmits the squared modulus of the data signal, $x_{\text{D}}(t)$ must be a minimum phase in order to recover the phase exactly. From [164], $x_{\text{D}}(t)$ is minimum phase if and only if the DC bias A is large enough to ensure that the winding number of the trajectory of $x_{\text{D}}(t)$ in complex plane is zero. Define $\mathcal{M}$ as the event that $x_{\text{D}}(t)$ is minimum phase. A more tractable sufficient condition for a given signal $x_{\text{D}}(t)$ to be minimum phase is to set $A \geq A_{\max}$ where [162]

$$A_{\max} = \max_t \|x(t)\|. \tag{5.3.4}$$

Define $\mathcal{S}$ as the event that for a fixed bias A the sufficient condition holds, i.e., that $A \geq A_{\max}$ for a random selection $x(t)$. In the following, the likelihood of $\mathcal{S}$ will be used to lower bound the probability of $\mathcal{M}$ when using a fixed value of DC bias A.

For a given OFDM symbol, (5.3.4) can be approximated as

$$A_{\max} \approx \max_{0 \leq n \leq N-1} \|x_n\| . \tag{5.3.5}$$

According to central limit theorem (CLT) [110], the real and imaginary parts of x_n are distributed as $x_{\mathrm{r},n} \sim \mathcal{N}(0, \sigma_x^2/2)$ and $x_{\mathrm{i},n} \sim \mathcal{N}(0, \sigma_x^2/2)$ where $\sigma_x^2 = \mathrm{E}\{\|x_n\|^2\}$. In addition, $x_{\mathrm{r},n}$ and $x_{\mathrm{i},n}$ are statistically independent resulting in the amplitude $\|x_n\|$ following a Rayleigh distribution. The complementary cumulative distribution function (CCDF) of $A_{\max}$ is thus

$$\begin{aligned} F_{A_{\max}}(a) &= \Pr\{A_{\max} > a\} = 1 - \Pr\{\cap_{\forall n}\{\|x_n\| \leq a\}\} \\ &= 1 - \left(1 - \exp\left(-\left(\frac{a}{\sigma_x}\right)^2\right)\right)^N . \end{aligned} \tag{5.3.6}$$

Notice that $F_{A_{\max}}(A) = \Pr\{\mathcal{S}^c\}$ where the superscript 'c' indicates the set complement. Noting the form of (5.3.6), for readability, define $\mu_{\max} = A_{\max}/\sigma_x$ where

$$F_{\mu_{\max}}(\mu) = \Pr\{\mu_{\max} > \mu\} = 1 - \left(1 - \exp\left(-\mu^2\right)\right)^N . \tag{5.3.7}$$

Consider selecting a fixed bias $A = \mu\sigma_x$ for some μ in order to ensure that the resulting $x_{\mathrm{D}}(t)$ is minimum phase with a sufficiently high probability. Figure 5.2 presents $\Pr\{\mathcal{S}^c\}$ using the closed-form CCDF (5.3.7) based on the sufficient condition (5.3.4) as well as $\Pr\{\mathcal{M}^c\}$ using the definition in Sec. 5.2.2 and simulated for $N = 1024$ and 16-QAM.

Notice that the closed-form on $\Pr\{\mathcal{S}^c\}$ aligns well with simulated results and can be used as a convenient, but loose, upper bound on $\Pr\{\mathcal{M}^c\}$. For example, for $\mu = 3$, $\Pr\{\mathcal{M}^c\} = 0.03$ while $F_{\mu_{\max}}(3) = 0.11$. Interestingly, numerical results in Sec. 5.4.2 indicate KKO-OFDM with $\mu = 3$ can achieve BER $< 10^{-4}$ when employing 16-QAM. That is, the proposed KKO-OFDM receiver is able to correctly detect the transmitted symbols even when $x_{\mathrm{D}}(t)$ is *not* a minimum phase. Increasing A will cause smaller

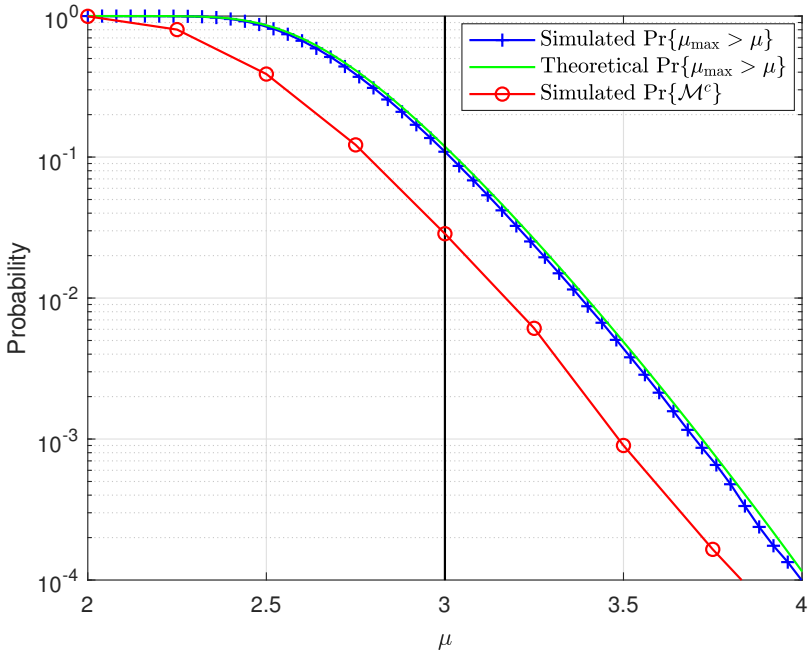

Figure 5.2: CCDF of $\mu_{\max}$ for KKO-OFDM signals ($N = 1024$ and 16-QAM).

$\Pr\{\mathcal{M}^c\}$ at the expense of reduced optical power efficiency. Therefore, the selection of A, and equivalently μ, must be carefully tuned to balance optical power efficiency with the probability of $x_{\mathrm{D}}(t)$ being a minimum phase. The theoretical bound from (5.3.7) serves as a useful starting point for the selection of μ.

From (5.2.10),

$$P_{\mathrm{o}} = (\mu^2 + 1)\sigma_x^2. \tag{5.3.8}$$

Dimming of the illumination of the VLC-enabled luminaire is closely related to the average optical power P_{o}. The values of μ and of σ_x^2 can be carefully set to achieve a specific dimming target. From Sec. 5.4.2, the optimal value of μ is fixed for a specific constellation size. Hence, $\sigma_x^2 = P_{\mathrm{o}}/(\mu^2 + 1)$ is carefully adjusted to satisfy the required dimming target.

Define the optical signal-to-noise ratio (OSNR) as [139, 86]

$$\text{OSNR} = \frac{P_{\text{o}}}{\sigma_w} \ . \tag{5.3.9}$$

5.3.3 Effective Average Electrical SNR

In order to obtain insight on the performance of KKO-OFDM, in this subsection an analytical estimate of the end-to-end electrical SNR is computed under the assumption of high OSNR, which is typical in many VLC applications [139, 167, 158]. An additional assumption of this analysis is that a sufficiently large bias A is added so that $x_{\text{D},n}$ is minimum phase.

Consider rewriting the received signal in (5.2.12) as

$$\|\widetilde{r}_n\| = \left(\|x_{\text{D},n}\|^2\right)\left(\|1 + 2v_n\|\right) \tag{5.3.10}$$

where

$$v_n = \frac{w_n}{2\|x_{\text{D},n}\|^2} \ , \quad \|x_{\text{D},n}\| > 0 \ . \tag{5.3.11}$$

Substituting (5.3.10) into (5.2.12) gives

$$\widetilde{\phi}_n = \phi_n + \phi_{\text{e},n} \tag{5.3.12}$$

where ϕ_n is the phase of $x_{\text{D},n}$ and $\phi_{\text{e},n}$ is the error in phase estimation given by

$$\phi_{\text{e},n} = \mathcal{H}\left(\log\left(\sqrt{\|1 + 2v_n\|}\right)\right) \ . \tag{5.3.13}$$

Substituting (5.3.10) and (5.3.12) into (5.2.13) gives

$$\begin{aligned}\widetilde{x}_{\mathrm{D},n} &= \|x_{\mathrm{D},n}\|\sqrt{\|1+2v_n\|}\exp\{j(\phi_n+\phi_{\mathrm{e},n})\} \\ &= x_{\mathrm{D},n}\sqrt{\|1+2v_n\|}\exp\{j\phi_{\mathrm{e},n}\}\ .\end{aligned} \tag{5.3.14}$$

When OSNR is large, $\|v_n\| < \epsilon$, for small real ϵ, with a high probability, and $\phi_{\mathrm{e},n}$ in (5.3.13) is equivalently small such that symbols can be detected successfully. Hence, using a first-order Taylor series approximation yields

$$\widetilde{x}_{\mathrm{D},n} \approx x_{\mathrm{D},n}\,(1+v_n)\exp\{j\phi_{\mathrm{e},n}\} = x_{\mathrm{D},n} + \widetilde{w}_n \tag{5.3.15}$$

where $\widetilde{w}_n$ is an equivalent additive noise given by

$$\begin{aligned}\widetilde{w}_n &= x_{\mathrm{D},n}\left((\exp\{j\phi_{\mathrm{e},n}\}-1) + v_n\exp\{j\phi_{\mathrm{e},n}\}\right) \\ &\approx x_{\mathrm{D},n}\left(j\phi_{\mathrm{e},n} + v_n(1+j\phi_{\mathrm{e},n})\right) \\ &= x_{\mathrm{D},n}\left(v_n + j\phi_{\mathrm{e},n}\,(1+v_n)\right)\ .\end{aligned} \tag{5.3.16}$$

From (5.3.13), using the first-order Taylor series approximation of the argument gives

$$\phi_{\mathrm{e},n} \approx \mathcal{H}\,(v_n)\ . \tag{5.3.17}$$

Substituting (5.3.17) into (5.3.16) gives

$$\widetilde{w}_n \approx x_{\mathrm{D},n}\left(v_n + j\mathcal{H}\,(v_n)\,(1+v_n)\right)\ . \tag{5.3.18}$$

Hence, at high OSNR, the average power of noise can be approximated as

$$\begin{aligned} P_{\widetilde{w}} &= \mathrm{E}\{\|\widetilde{w}_n\|^2\} = \mathrm{E}\left\{\|x_{\mathrm{D},n}\|^2 \left(v_n^2 + \mathcal{H}^2\left(v_n\right)\left(1+v_n\right)^2\right)\right\} \\ &\approx \mathrm{E}\left\{\|x_{\mathrm{D},n}\|^2 v_n^2\right\} + \mathrm{E}\left\{\|x_{\mathrm{D},n}\|^2 \mathcal{H}^2\left(v_n\right)\right\} \ . \end{aligned} \tag{5.3.19}$$

Given that typically $A \gg \|x_n\|$ (to ensure $x_{\mathrm{D},n}$ is minimum phase) and w_n is independent of $x_{\mathrm{D},n}$, v_n in (5.3.11) can be approximated as

$$v_n \approx \frac{w_n}{2A^2} = \frac{\mu^2+1}{2\mu^2}\frac{w_n}{P_{\mathrm{o}}} \ . \tag{5.3.20}$$

Substituting (5.3.20) into (5.3.19) gives

$$P_{\widetilde{w}} = \frac{\left(\mu^2+1\right)^2\sigma_w^2}{4\mu^4 P_{\mathrm{o}}} + \frac{\left(\mu^2+1\right)^2 \mathrm{E}\left\{\mathcal{H}^2\left(w_n\right)\right\}}{4\mu^4 P_{\mathrm{o}}} \overset{(a)}{=} \frac{\left(\mu^2+1\right)^2\sigma_w^2}{2\mu^4 P_{\mathrm{o}}}. \tag{5.3.21}$$

where (a) arises since the Hilbert transform changes only the phase in the frequency domain, and the power remains the same, thus $\mathrm{E}\left\{\mathcal{H}^2\left(w_n\right)\right\} = \mathrm{E}\left\{w_n^2\right\} = \sigma_w^2$.

An underlying assumption of this analysis is that $\widetilde{x}_{\mathrm{D},n}$ and $x_{\mathrm{D},n}$ are minimum phase SSB signals. Hence $\widetilde{w}_n$ is an SSB signal according to (5.3.15). Let $\widetilde{W}_k$ denote the DFT of $\widetilde{w}_n$. Following Parseval's theorem, the electrical power of the signal and equivalent noise at each frequency bin can be approximated as

$$P_{\widetilde{W}} = \mathrm{E}\{\|\widetilde{W}_k\|^2\} = 2\mathrm{E}\{\|\widetilde{w}_n\|^2\} = 2P_{\widetilde{w}} \ . \tag{5.3.22}$$

and

$$P_{\mathrm{X}} = \mathrm{E}\{\|X_k\|^2\} = 2\sigma_x^2 = \frac{2P_{\mathrm{o}}}{\mu^2+1} \ . \tag{5.3.23}$$

Notice that in general $\widetilde{w}_n$ is dependent on the signal $x_{\mathrm{D},n}$ via (5.3.16). However, in

practice and as shown in [168], after the FFT at the receiver in Fig. 5.1 the resulting time-domain signal-dependent noise is well approximated as being signal-independent. Hence, the average electrical SNR at each subcarrier can be estimated as

$$\mathrm{SNR_e} = \frac{P_{\mathrm{X}}}{P_{\widetilde{W}}} \approx \frac{2\mu^4}{(\mu^2+1)^3}\frac{P_{\mathrm{o}}^2}{\sigma_w^2} = \frac{2\mu^4}{(\mu^2+1)^3}\mathrm{OSNR}^2 \,. \tag{5.3.24}$$

The BER of KKO-OFDM can thus be estimated as [141, 169],

$$\mathrm{BER} \approx \frac{4(\sqrt{M}-1)}{\sqrt{M}\log_2 M} Q\left(\sqrt{\frac{6\mu^4}{(\mu^2+1)^3(M-1)}}\mathrm{OSNR}\right) \tag{5.3.25}$$

where M is the rectangular QAM constellation size.

5.3.4 Capacity Analysis

Assuming $x_{\mathrm{r},n}$ and $x_{\mathrm{I},n}$ are accurately modelled as independent and Gaussian distributed, notice that $x_{\mathrm{sq},n} = (x_{\mathrm{r},n}+A)^2 + x_{\mathrm{i},n}^2$ follows a (scaled) noncentral chi-squared distribution with two degrees of freedom [170] and has probability density function (PDF)

$$f(\xi) = \frac{1}{\sigma_x^2}\exp\left\{-\frac{\mu^2\sigma_x^2+\xi}{\sigma_x^2}\right\} I_0\left(\sqrt{\frac{4\mu^2\xi}{\sigma_x^2}}\right),\ \xi > 0 \tag{5.3.26}$$

where $I_\nu(y) = (y/2)^\nu \sum_{j=0}^{\infty} \frac{(y^2/4)^j}{j!\Gamma(\nu+j+1)}$ is a modified Bessel function of the first kind and $\Gamma(z)$ is the gamma function [170]. In the special case of $\mu = 0$, $f(\xi)$ is exponential. The theoretical and simulated PDF of KKO-OFDM signal with uniformly selected 16-QAM constellation points are depicted in Fig. 5.3. It can be seen the theoretical PDF follows closely the simulated PDF.

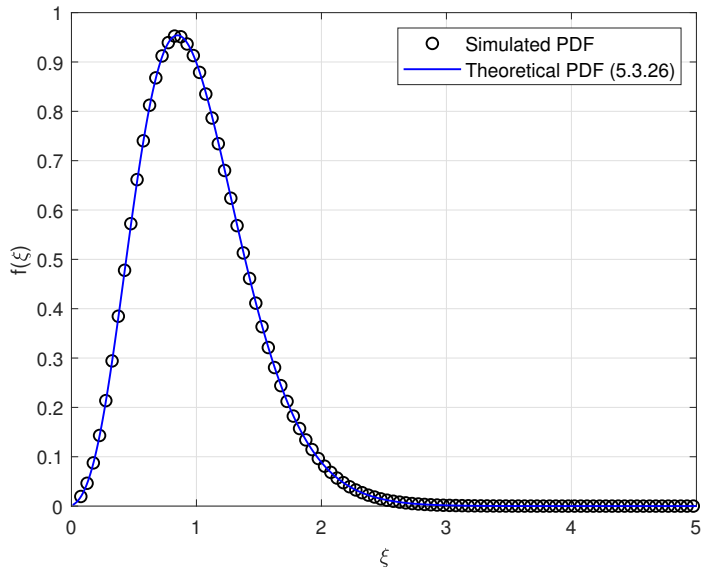

Figure 5.3: Theoretical and simulated PDF of KKO-OFDM signal with QAM symbols ($\mu = 3$ and $P_{\mathrm{o}} = 1$, $M = 16$, $N = 1024$).

The capacity of the bandlimited average amplitude-constrained IM/DD channel can be lower bounded by the mutual information between $x_{\mathrm{sq},n}$ and r_n denoted as I_{KKO}

$$I_{\mathrm{KKO}} = h(r_n) - h(r_n|x_{\mathrm{sq},n}) = h(r_n) - h(w_n) \tag{5.3.27}$$

where $h(\cdot)$ denotes the differential entropy of a continuous random variable. The PDF of r_n can be calculated by convolving the PDF of $x_{\mathrm{sq},n}$ in (5.3.26) with the Gaussian noise distribution of w_n. The resulting I_{KKO} in (5.3.27) can thus be obtained numerically, though there is no closed-form is available.

On the other hand, a closed-form estimate of the information rate can be computed using the approximation for electrical SNR in (5.3.24) and Shannon's famous capacity expression for the AWGN channel [137].

Since the approximation in (5.3.24) relates the optical power constraint to an

electrical power constraint, the resulting KKO-OFDM system can be treated as $N/2-1$ parallel independent complexed-valued AWGN channels or $N-2$ real-valued AWGN channels with an electrical SNR, $\mathrm{SNR_e}$ according to (5.3.24). The resulting estimate on the information rate of KKO-OFDM is

$$R_{\mathrm{KKO}} = \frac{1}{2}\log\left(1+\frac{2\mu^4}{(\mu^2+1)^3}\mathrm{OSNR}^2\right) \text{ bits/channel use} \tag{5.3.28}$$

for large N.

Figure 5.4 presents the information rate of KKO-OFDM versus OSNR for bandlimited IM/DD channels with an average amplitude constraint. Additionally, an upper bound on the capacity of discrete-time IM/DD OWC channels [130] and lower bounds (using the entropy power inequality, exponential input distribution and LACO-OFDM [86]) are added as benchmarks. Notice that these bounds apply only to discrete-time IM/DD channels and do not simultaneously consider non-negativity and a strict bandwidth constraint.

The lower bound on the capacity of bandlimited IM/DD channels via I_{KKO} is close to the closed-form approximation R_{KKO} at each specific value of OSNR for $\mu = 3$. There is a gap between the information rate of KKO-OFDM and the bounds on the capacity of the discrete-time IM/DD OWC channel. This is not surprising given that KKO-OFDM is by construction bandlimited and earlier bounds are computed for discrete-time channels, which do not consider an explicit bandwidth limit. Indeed, discrete-time IM/DD channels can be made compatible with bandlimited channels via the Nyquist-Shannon interpolation formula at the expense of requiring an additional, and often large, DC bias as discussed in Sec. 5.2.1 and shown numerically in Sec. 5.4. The information rate of DCO-OFDM with a fixed DC bias $D_{\mathrm{DCO}} = 3\sigma_x$ is also

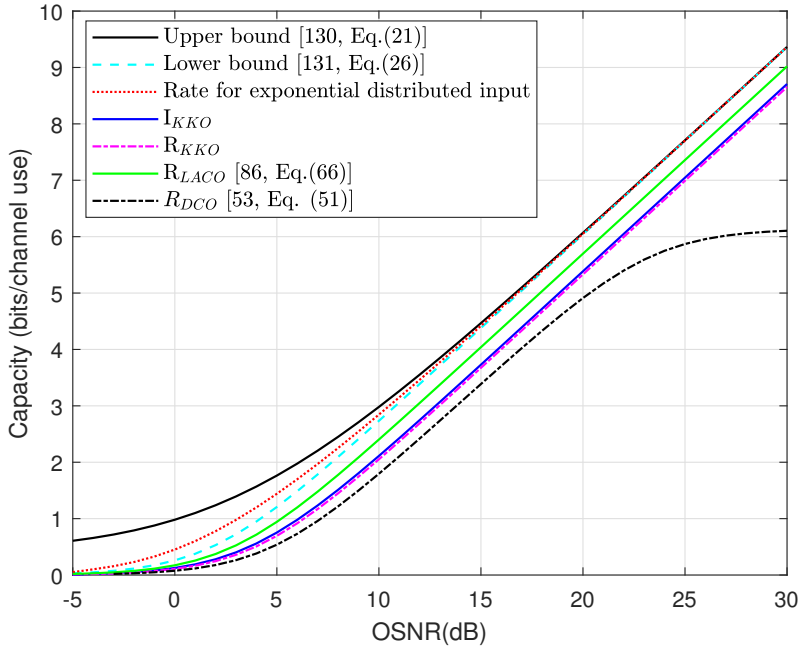

Figure 5.4: Capacity bounds on data rate of KKO-OFDM ($\mu = 3$).

presented in Fig. 5.4 according to Eq. (51) [53]. Due to the fixed bias, clipping distortion is unavoidable and results in a saturated rate in the high OSNR regime [53]. Notice that R_{KKO} is greater than R_{DCO} and the gain of KKO-OFDM over DCO-OFDM increases with OSNR.

5.3.5 Computational Complexity Analysis

At the transmitter, KKO-OFDM requires only a single N-point IFFT module, which is same as DCO-OFDM. The computational complexity of the transmitter is thus $\mathcal{O}(N \log_2 N)$ [48]. In LACO-OFDM, L-IFFT modules are needed for L layers, resulting in a complexity of $(2 - 1/2^{L-1})\mathcal{O}(N \log_2 N)$ [74]. Hence, DCO- and KKO-OFDM transmitters are less complex than LACO-OFDM, which makes them more

suitable for low-cost LED luminaries in VLC systems.

At the receiver, DCO-OFDM requires an N-point FFT module, resulting in a computational complexity of $\mathcal{O}(N \log_2 N)$ [48]. LACO-OFDM is demodulated recursively and the complexity can be estimated as $(5 - 1/2^{L-3})\mathcal{O}(N \log_2 N)$ [74]. KKO-OFDM requires digital up-sampling, which employs an N-point FFT module and an αN-point IFFT module. Additionally, KKO-OFDM requires an additional Hilbert transform module, which can be achieved in frequency domain using an αN-point FFT module and an αN-point IFFT module [162]. In addition, an αN-point FFT is used before symbol detection. Hence, in total, the computational complexity can be estimated as $\mathcal{O}(\alpha N \log_2(\alpha N))$. Indeed the receiver of KKO-OFDM is more complex that DCO-OFDM, however, given the availability of computational resources at mobile receivers this complexity may be acceptable given the achieved gains quantified in the next section.

5.4 Numerical Results

5.4.1 Bandlimited Optical OFDM and KKO-OFDM Waveforms

Examples time-domain waveforms for bandlimited IM/DD DCO-, ACO-, and KKO-OFDM are shown in Fig. 5.5 where the average optical power of all signals are normalized to unity.

Figure 5.5(a) shows an example of DCO-OFDM time-domain waveform, from which it can be seen that all samples of DCO-OFDM $x_n + D_{\text{DCO}}$ fall onto $x_{\text{DCO}}(t)$ after Nyquist-Shannon interpolation using (5.2.1). Similarly, Figure 5.5(b) shows an

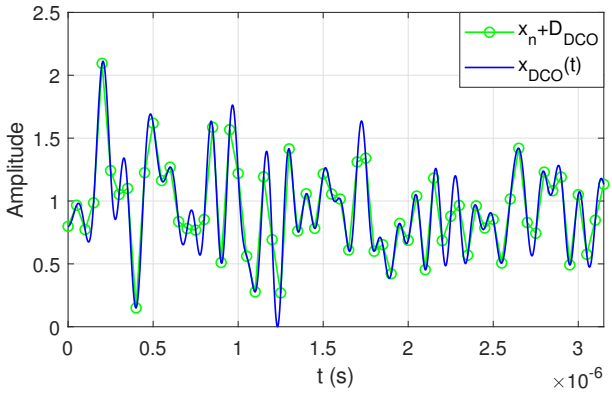

(a) Bandlimited DCO-OFDM

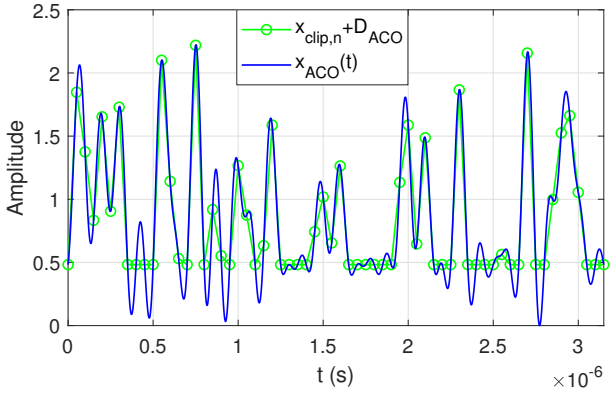

(b) Bandlimited ACO-OFDM

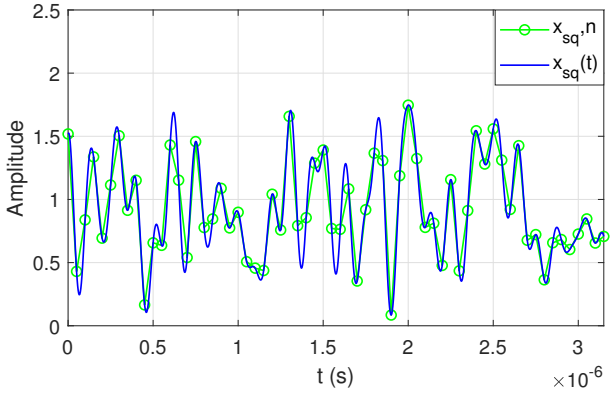

(c) KKO-OFDM

Figure 5.5: Signals of DCO-, ACO-, and KKO-OFDM with/without Nyquist-Shannon interpolation normalized to have unit optical power ($N = 64$, $M = 16$ and $B = 10$ MHz).

ACO-OFDM waveform where the minimum bias D_{ACO} is added to avoid clipping of the bandlimited Nyquist-Shannon interpolated signal (5.2.4).

Figure 5.5(c) shows the KKO-OFDM time-domain waveform where $\mu = 3$. All samples of KKO-OFDM $x_{\text{sq},n}$ fall onto the signal $x_{\text{sq}}(t)$ constructed via Nyquist-Shannon interpolation using (5.2.9). In addition, $x_{\text{sq}}(t)$ is a non-negative and strictly bandlimited signal falling into $[-B,\ B]$. This result arises directly since the squared magnitude of a complex SSB signal is necessarily real, non-negative and remains bandlimited in $[-B,\ B]$. The bandlimited signal, $x_{\text{sq}}(t)$ is completely determined by the samples spaced $1/(2B)$ seconds apart [137].

5.4.2 BER Performance

In the case of line-of-sight (LOS) VLC links, and to aid in comparing with earlier work, a good model is to consider a flat channel response [56]. In the following, and without loss of generality, channel is assumed flat in the band of interest and the DC gain between the transmitter and receiver is assumed to be unity [56]. The number of subcarriers are set to $N = 1024$ and QAM constellations with gray labelling are employed. The bandwidth is set to $B = 10$ MHz in all simulations.

BER versus α

The BER performance of KKO-OFDM for different values of up-sampling factor α is shown in Fig. 5.6, in which 16-QAM and $\mu = 3$ are used. It can be seen that the BER performance of KKO-OFDM improves and approaches the theoretical BER as α increases. From (5.2.12), notice that though $x_{\text{sq}}(t)$ is bandlimited, $\log(x_{\text{sq}}(t))$ is not necessarily bandlimited. As the up-sampling factor α increases, more information

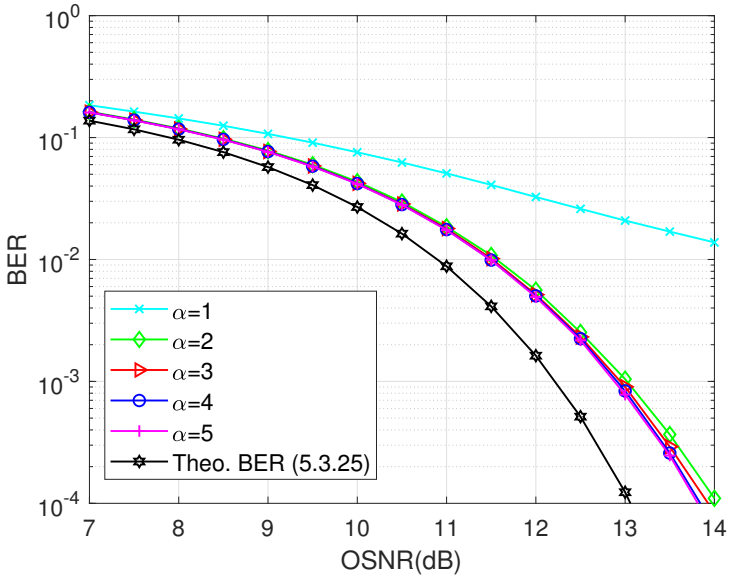

Figure 5.6: BER performance of KKO-OFDM for different values of up-sampling factor with $\mu = 3$.

about $\log(x_{\text{sq}}(t))$ is collected and improved BER performance is achieved. However, increasing the up-sampling factor comes at the expense of increasing the computational complexity. From Fig. 5.6, the performance of the KKO receiver saturates at $\alpha = 4$ and small gains are available for further increases in α. Hence, $\alpha = 4$ is employed to balance performance versus complexity in subsequent simulations.

Notice that the theoretical BER is loose at higher OSNRs. This gap arises primarily due to the fact that the theoretical BER given by (5.3.25) is based on a first-order Taylor series approximation, which holds only for large A and $x_{\text{D}}(t)$ remaining a minimum phase signal. Additionally, limited oversampling results in inaccuracies in the logarithmic (5.2.12) and exponential (5.2.13) operations which are nonlinear. Thus, the theoretical BER according to (5.3.25) can be treated as an estimate of performance.

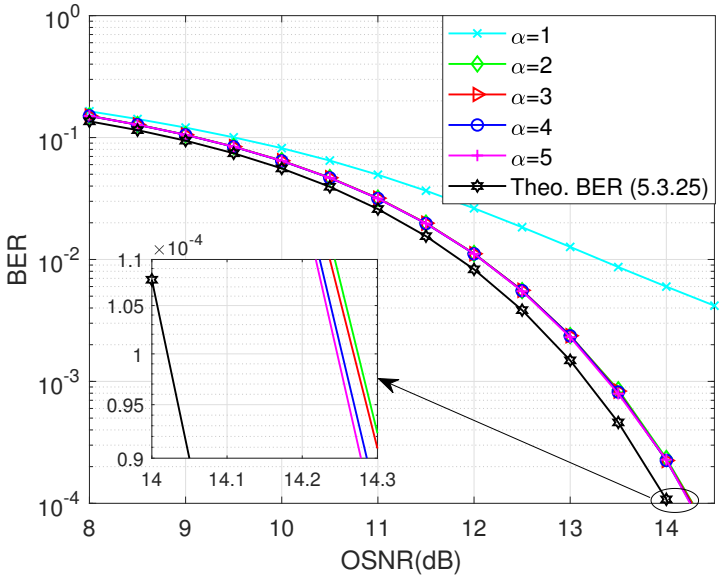

Figure 5.7: BER performance of KKO-OFDM for different values of up-sampling factor with $\mu = 4$.

Similar KKO-OFDM BER results are shown in Fig. 5.7 with $\mu = 4$ for various α. In this case, the theoretical BER approximation in (5.3.25) is much tighter to the numerical results. This can be explained by the fact that when μ is large so too is A and the first-order Taylor series approximations used to compute (5.3.25) are more accurate. Notice also that for $\mu = 4$, the BER curves saturate for smaller values of α as compared to the case $\mu = 3$ illustrated in Fig. 5.6. This is because the first-order Taylor series approximation for the log of the received signal is more accurate as μ and equivalently A increases. Thus, increasing μ and A will cause power inefficiency while allowing for a decrease in α leading to a decrease computational complexity. Therefore, there exists a trade-off between α and μ.

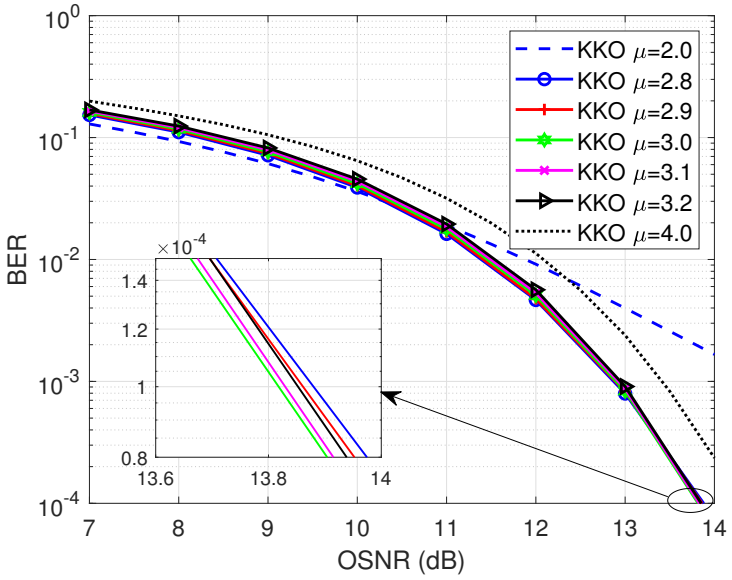

Figure 5.8: BER performance of KKO-OFDM for different values of μ ($M = 16$ and $\alpha = 4$).

BER versus μ

Figure 5.8 presents the BER performance of KKO-OFDM for different values of μ using 16-QAM and $\alpha = 4$. Notice from Fig. 5.2 that $\mu \approx 3$ ensures that $x_{\mathrm{D},n}$ is minimum phase with high probability. As seen in the figure, if $\mu = 2$, $x_{\mathrm{D},n}$ is minimum phase with $\Pr\{\mathcal{M}\} = 0.004$ which dominates the overall BER regardless of OSNR. However, when $\mu = 4$, $x_{\mathrm{D},n}$ is minimum phase with high probability at the expense of reduced optical power efficiency (5.3.24) due to conservatively large choice of A resulting in worse BER performance than the case with $\mu = 3$.

Thus, $\mu = 3$ is used as the starting point to search for the optimal value for each OSNR for each constellation employed. Table 5.1 presents the optimal values of μ for various QAM constellations which minimize the OSNR required to achieve a BER= 10^{-4}. Notice that the optimal value of μ also increases with the order of

Table 5.1: Optimal μ for BER=10^{-4} over constellation sizes

M-QAM	4	16	64	128	256
Optimal μ	2.7	3.0	3.3	3.4	3.4

QAM formats. For normalized constellations, the minimum distance decreases as the constellation size increases requiring a higher likelihood of $x_{D,n}$ being minimum phase to meet the SNR requirements at a given BER. Therefore, the optimal value of μ increases slightly as the order of QAM format increases.

In all cases, the values remain near $\mu = 3$ and balance the impact of increases P_{o} in (5.3.8) with the likelihood that the transmitted waveform is not minimum phase. The values of μ in Table 5.1 were found through extensive simulations are used in subsequent simulations.

Received Constellations

The received scatter plot of constellation points is shown in Fig. 5.9, where the OSNR= 18 dB, $\alpha = 4$ and 1000 OFDM symbols are simulated. Notice that the individual constellation points are easily discernible. In practice, SNRs in VLC channels often operation and OSNRs significantly exceeding 18 dB [167].

BER Comparison

Figure 5.10 presents the BER comparison between KKO-OFDM and DCO-OFDM operating the same spectral efficiency. Notice that both KKO- and DCO-OFDM have the same spectral efficiency for a given M. In particular, constellation sizes of $M = 4,\ 16,\ 64$ and 256 are employed yielding spectral efficiencies of $\Upsilon_{\text{KKO}} = 1,\ 2,\ 3$ and 4 bits/s/Hz, respectively. It can be seen that KKO-OFDM outperforms

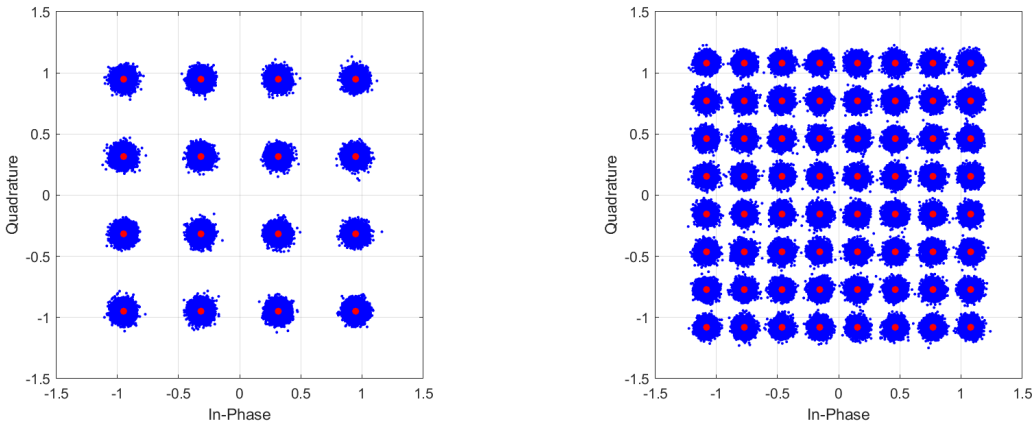

(a) 16-QAM (b) 64-QAM

Figure 5.9: Scatter constellation plots of KKO-OFDM.

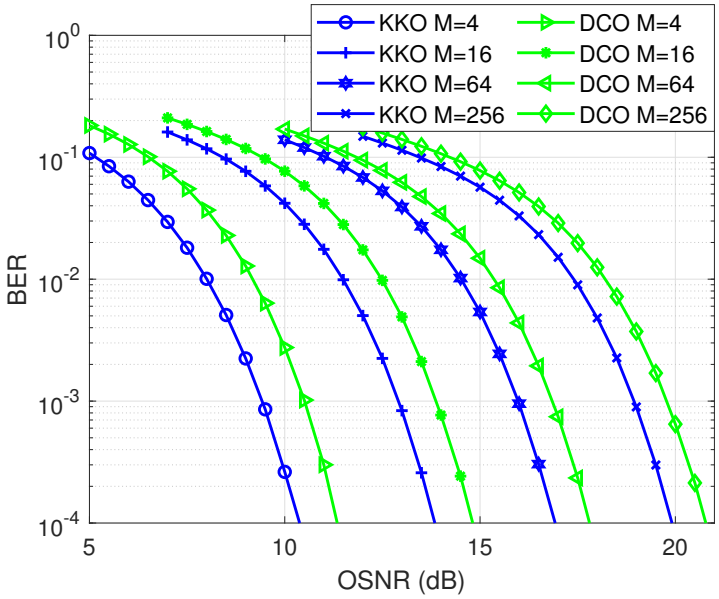

Figure 5.10: BER comparison between KKO-OFDM and DCO-OFDM at the same constellation size and hence spectral efficiency (μ selected according to Table 5.1).

DCO-OFDM at these four spectral efficiencies at BER= 10^{-4}. Compared to DCO-OFDM, KKO-OFDM achieves about 1.0 dB OSNR gain at BER= 10^{-4}.

Notice that KKO-OFDM modulates a SSB signal and constrains its energy to

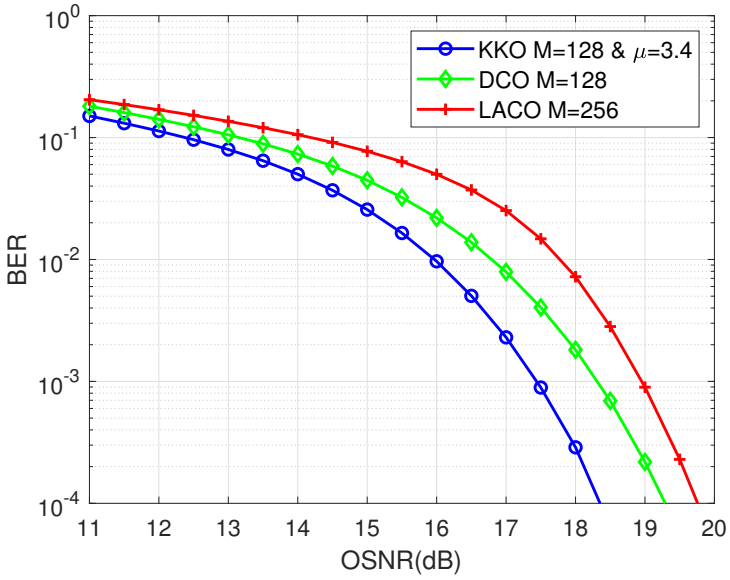

Figure 5.11: BER comparison between KKO-OFDM, DCO-OFDM and LACO-OFDM at a spectral efficiency of 3.5 bits/s/Hz.

signal carriers only, while DCO-OFDM modulates DSB signal requiring Hermitian symmetry. Additionally after Nyquist-Shannon interpolation, by construction there exist no negative peaks in KKO-OFDM. However, the large negative peaks in DCO-OFDM require a comparably large DC bias to meet the non-negativity constraint leading to optical power inefficiency.

A BER comparison between KKO-OFDM, DCO-OFDM and LACO-OFDM all operating at the same spectral efficiency of 3.5 bits/s/Hz is shown in Fig. 5.11. For KKO-OFDM and DCO-OFDM, 128-QAM is utilized while for LACO-OFDM, the number of layers is set to $L = 3$, and 256-QAM is utilized. It can be seen that KKO-OFDM achieves the best BER performance at the BER of 10^{-4} and achieves about 1.0 dB and 1.4 dB OSNR gains compared to DCO-OFDM and LACO-OFDM respectively.

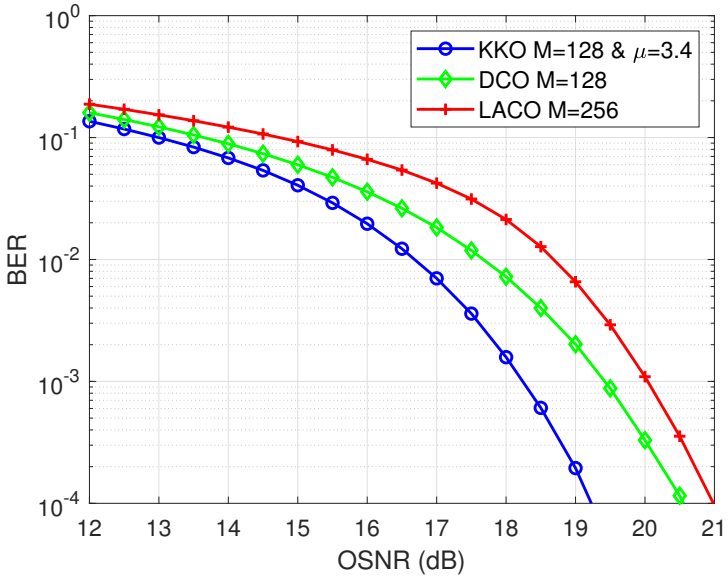

Figure 5.12: BER comparison between KKO-OFDM, DCO-OFDM and LACO-OFDM under a VLC LPF channel at a spectral efficiency of 3.5 bits/s/Hz.

BER in a VLC Lowpass Channel

In this section, BER performance of KKO-OFDM is evaluated in a VLC lowpass dispersive channel, which includes line-of-sight (LOS) path and diffuse reflections. The impulse response of this channel is well estimated by a close-form function as [4]

$$h_{\mathrm{VLC}}(t) = H_{\mathrm{DC}} \frac{\tau_0^6}{(t+\tau_0)^7} u(t) \tag{5.4.1}$$

where channel DC gain H_{DC} is assumed to be unity without loss of generality, $u(t)$ is the unit step function, $\tau_0 = 12\sqrt{11/13}\tau_{\mathrm{rms}}$, and τ_{rms} is root-mean-square (rms) delay spread typically assumed to be 10 ns [4]. Here, the sampling rate to simulated the impulse response $h(t)$ is set to 60 MHz.

Figure 5.12 presents BER comparison between KKO-OFDM, DCO-OFDM and LACO-OFDM in the lowpass VLC channel at the same spectral efficiency of 3.5 bits/s/Hz.

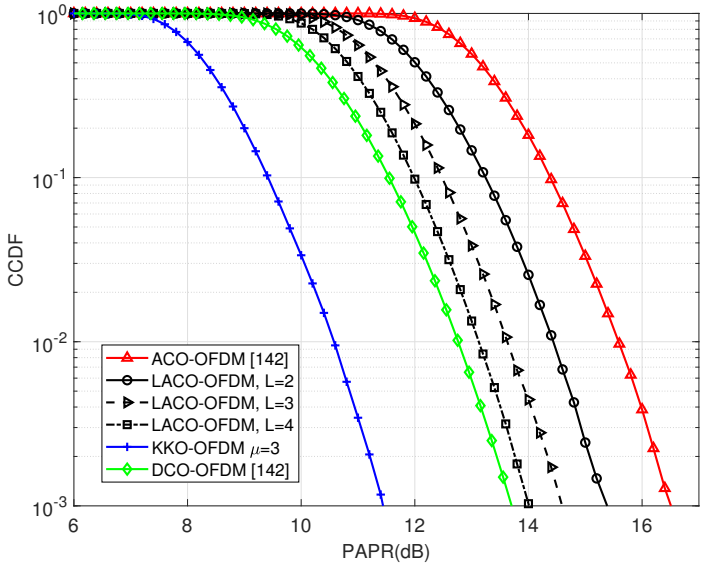

Figure 5.13: PAPR comparison between KKO-OFDM, DCO-OFDM and LACO-OFDM ($N = 1024$).

For simplicity, a zero forcing equalizer is employed, which only requires $N/2$ complex-valued multiplications as discussed in Sec. 5.2.3. It is apparent the proposed receiver in this paper can successfully demodulate KKO-OFDM under a VLC lowpass dispersive channel. When BER= 10^{-4}, KKO-OFDM achieves a 1.3 dB and 1.8 dB optical gains compared to DCO-OFDM and LACO-OFDM with $L = 3$, respectively.

5.4.3 PAPR Performance

The CCDF comparison of PAPR for KKO-OFDM, DCO-OFDM and LACO-OFDM is shown in Fig. 5.13, where $N = 1024$ subcarriers is assumed. For ACO-OFDM and DCO-OFDM, the CCDF of PAPR is calculated using [142] while the CCDF of PAPR in LACO-OFDM is evaluated by simulation [86, 106]. For KKO-OFDM, $\mu = 3$ is used. It is worth noting that increasing μ will decrease PAPR,

however it may degrade the BER performance.

As can be seen, the PAPR CCDF of KKO-OFDM is significantly lower than other approaches. In particular, at a CCDF value of 10^{-3}, the PAPR of KKO-OFDM is 2.3 dB and 5.1 dB smaller than DCO-OFDM and ACO-OFDM, respectively. This more compact PAPR distribution for KKO-OFDM suggests that it is more robust in the presence of nonlinear LED transfer characteristics.

5.5 Conclusions

In this paper, KKO-OFDM is introduced which produces an inherently real-valued, non-negative amplitude and strictly bandlimited signal well suited to IM/DD VLC systems. Relying on the KK relations, KKO-OFDM modulates an SSB signal and requires no Hermitian symmetry. Indeed, KKO-OFDM is the first inherently bandlimited IM/DD modulation format suitable for lowpass optical wireless channels. Unlike earlier work in optical fiber channels where the KK relations are used to retrieve the phase of a coherent laser emission, here we extend the use of the KK relations to develop an IM/DD system suited to bandwidth constrained VLC systems.

Numerical results are aligned well with analysis and show that KKO-OFDM outperforms DCO-OFDM and LACO-OFDM when operating at the same spectral efficiency and with a strict bandwidth limitation. We present a design guide for the selection of parameters for KKO-OFDM as well as closed-form approximations for the resulting electrical SNR and achievable information rates for the first time explicitly taking into account bandlimited channels. Numerical results show that an optical power gain of 1 dB over DCO-OFDM and 1.4 dB gains over LACO-OFDM are readily obtainable. On a low pass VLC channel, KKO-OFDM was able to realize

a larger gain of 1.3 dB in optical SNR over DCO-OFDM. As an additional benefit, the PAPR distribution of KKO-OFDM signal is significantly more compact than DCO- and LACO-OFDM indicating an improved resilience to LED nonlinear characteristics.

Our future investigations include experimental demonstrations of this approach in realistic VLC channels.

Chapter 6

Conclusions and Future Work

6.1 Conclusions

While visible light communications are integrating into the ubiquitously employed illumination LEDs, there are several problems and challenges for OFDM-based VLC systems, including enhancing spectral and power efficiency and decreasing computational complexity. This thesis introduces novel spectrum- and power-efficient, and low-complexity optical OFDM schemes compatible with IM/DD VLC channels to solve these problems and challenges.

Leveraging all the subcarriers, ALACO-OFDM is introduced to enhance spectral efficiency and energy efficiency. Compared to the existing LACO-OFDM and eU-OFDM, ALACO-OFDM can achieve higher spectral efficiency and information rate even with fewer layers. Thanks to fewer layers, the required computational complexity is slightly lower. Additionally, optical power allocation is optimized based on convex optimization techniques to enhance energy efficiency and information rate further.

ALACO-OFDM is shown to be more energy-efficient compared to existing LACO-OFDM and eU-OFDM in a VLC LOS flat channel. Furthermore, ALACO-OFDM is more robust to LED non-linear transferring thanks to lower PAPR compared to its counterparts.

By constructing an anti-symmetry directly in the time domain, this thesis introduces AC-OFDM as a low-complexity modulation scheme, unlike ACO-OFDM having an anti-symmetry by modulating odd subcarriers only. AC-OFDM is shown to achieve the same spectral efficiency and PAPR as conventional ACO-OFDM, however, is less complex to implement thanks to employing half-size IFFT/FFT. This thesis introduces LAC-OFDM to enhance spectral efficiency, consisting of L layers of AC-OFDM signals and transmitting them simultaneously. The computational complexity of LAC-OFDM, eU-OFDM and LACO-OFDM are analyzed, which shows that LAC-OFDM enjoys lower complexity at both the transmitter and the receiver compared to LACO-OFDM and eU-OFDM while achieving nearly the same BER performance in a VLC LOS flat channel. Furthermore, a pairwise iterative receiver is presented for LAC-OFDM to enhance the power efficiency, which employs pairwise detection in each iteration.

Given a practical VLC dispersive channel, L-LACO is introduced with simple one-tap equalization while LAC-OFDM makes the receiver equalization complex. L-LACO mathematically generates identical signals to LACO-OFDM; however, it requires half-size IFFT and FFT in each layer at the transmitter and receiver. Different form LACO-OFDM classically achieving anti-symmetry in each layer by modulating data onto odd subcarriers, L-LACO constructs anti-symmetry in the time domain directly. Consequently, LACO-OFDM requires about two times RMOs and RAOs

more than the proposed L-LACO at both transmitter and receiver, respectively. L-LACO generates an identical signal to LACO-OFDM mathematically, thus achieving the same performance requiring half arithmetic operations. Additionally, the power saving thanks to the saved arithmetic operations is analyzed. Furthermore, the BER of L-LACO is simulated under a VLC LOS flat channel with AWGN and under a VLC dispersive LPF channel, respectively, which are identical to LACO-OFDM.

Finally, for practical bandlimited VLC channels, KKO-OFDM is presented based on KK relations to enhance spectral and power efficiency. In KKO-OFDM, a minimum phase signal's squared modulus is employed to modulate the light intensity emitted by an LED. Mathematically, the transmit signal is constructed to be real-valued, non-negative and strictly bandlimited, suitable for VLC channels. The KKO-OFDM transmitter is shown to be low complexity and fits low-cost, simple LEDs. At the receiver, the phase of the minimum phase signal is retrieved according to KK relations. Additionally, the required DC bias is analyzed and designed. The theoretical analysis of electrical SNR, BER, and data rate is supported by Monte Carlo simulations. Furthermore, KKO-OFDM realizes better BER performance over DCO-OFDM and LACO-OFDM in bandlimited VLC LOS AWGN channels and VLC dispersive LPF channels.

6.2 Future Work Plan

This thesis introduces novel optical OFDM schemes to enhance spectral and energy efficiency and decrease the required computational complexity. This thesis's potential future work includes spectrum- and energy-efficient optical OFDM considering dimming, secured optical OFDM, and experimental demonstrations.

6.2.1 Optical OFDM Considering Dimming

VLC adds a secondary communication functionality to ubiquitous LED luminaires while providing illumination simultaneously. Illuminating a room is the primary role of LEDs. Additionally, there require different dimming levels in different offices, in different cases and by different people. Hence, a VLC system needs to support dimming and keep communication least suffered. Hence, spectrum- and energy-efficient OFDM-based VLC systems will be investigated to support dimming in the future.

6.2.2 Physical Layer Security for Optical OFDM

Internet security is becoming increasingly essential and frequently comes to people's minds. VLC systems are much more secure than conventional RF if eavesdroppers are in the next-door office since light cannot inherently penetrate a wall while low-frequency electromagnetic waves can easily hang out in an office. Although VLC systems enjoy such an advantage, VLC systems cannot be secure enough when legitimate users are close to unauthorized eavesdroppers inside an office due to the broadcast nature of the wireless medium. Therefore, it is essential to investigate methods to secure spectrum- and energy-efficient OFDM-based VLC systems.

6.2.3 Experimental Demonstrations

This thesis has massive theoretical analyses considering a realistic indoor case supported by Monte Carlo simulations. Simulation results are shown to be pretty close to actual experimental results; however, experimental demonstrations are straightforward to verify a VLC system successful in the real world. In the future, experiments will be implemented to demonstrate the proposed spectrum- and energy-efficient

OFDM-based VLC systems.

Appendix A

Proof of the achievable information rate of the absolute-value Gaussian channel

This appendix develops the achievable information rate of the absolute-value Gaussian channel. The following proof is used to prove **Theorem 1.** in Chapter 2.

Given $y = |x|$ and $x \sim N(0, \sigma_x^2)$, y follows a truncated Gaussian distribution. Given y and w are independent, $z = y + w$ has PDF

$$f_z(z) = \int_{-\infty}^{\infty} f_w(w) f_y(z-w) dw = 2\left(1 - Q\left(\frac{z\sigma_x}{\sigma_w \sigma}\right)\right) \frac{1}{\sqrt{2\pi}\sigma} \exp\left\{-\frac{z^2}{2\sigma^2}\right\} \quad \text{(A.0.1)}$$

where $\sigma \stackrel{\triangle}{=} \sqrt{\sigma_w^2 + \sigma_x^2}$ and $Q(x) = \int_x^{\infty} \frac{1}{\sqrt{2\pi}} \exp\{-\frac{t^2}{2}\} dt$. The differential entropy of z is thus

$$h(z) = -\int_{-\infty}^{\infty} f_z(z) \log f_z(z) dz = \frac{1}{2} \log 2\pi e\sigma^2 - (1 - D) \quad \text{(A.0.2)}$$

where

$$\begin{aligned} D &= -\int_{-\infty}^{\infty} f_z(z) \log\left(1 - Q(\frac{z\sigma_x}{\sigma_w \sigma})\right) dz \\ &\overset{(a)}{=} -2\int_{-\infty}^{\infty} (1 - Q(t\gamma)) \log(1 - Q(t\gamma)) \frac{1}{\sqrt{2\pi}} \exp\left\{-\frac{t^2}{2}\right\} dt \\ &\overset{(b)}{=} -2\int_{0}^{\infty} (1 - Q(t\gamma)) \log(1 - Q(t\gamma)) \frac{1}{\sqrt{2\pi}} \exp\left\{-\frac{t^2}{2}\right\} dt \\ &\quad - 2\int_{0}^{\infty} Q(t\gamma) \log Q(t\gamma) \frac{1}{\sqrt{2\pi}} \exp\left\{-\frac{t^2}{2}\right\} dt \\ &\overset{(c)}{=} 2\int_{0}^{\infty} \mathcal{H}(Q(t\gamma)) \frac{1}{\sqrt{2\pi}} \exp\left\{-\frac{t^2}{2}\right\} dt \end{aligned} \tag{A.0.3}$$

where $\mathcal{H}(p)$ is the entropy of a Bernoulli random variable with probability p. Step (a) is based on integration by substitution $t = z/\sigma_w\sqrt{\gamma^2+1}$ while step (b) is based on $1 - Q(-t\gamma) = Q(t\gamma)$ and

$$\begin{aligned} &\int_{-\infty}^{0} (1 - Q(t\gamma)) \log(1 - Q(t\gamma)) \frac{1}{\sqrt{2\pi}} \exp\left\{-\frac{t^2}{2}\right\} dt \\ &\overset{u=-t}{=} \int_{0}^{\infty} Q(u\gamma) \log Q(u\gamma) \frac{1}{\sqrt{2\pi}} \exp\left\{-\frac{u^2}{2}\right\} du. \end{aligned} \tag{A.0.4}$$

Step (c) arises from the definition of the entropy of a Bernoulli random variable.

Hence, the capacity of this absolute-value Gaussian channel is found by substituting $h(z)$ and $h(w) = \frac{1}{2}\log 2\pi e\sigma_w^2$ into

$$C_{\text{v}} = I(z;y) = h(z) - h(z|y) = h(z) - h(w) \tag{A.0.5}$$

to give

$$C_{\text{v}} = \frac{1}{2}\log\left(1 + \frac{\sigma_x^2}{\sigma_w^2}\right) - (1 - D) \text{ bits/channel use.} \tag{A.0.6}$$

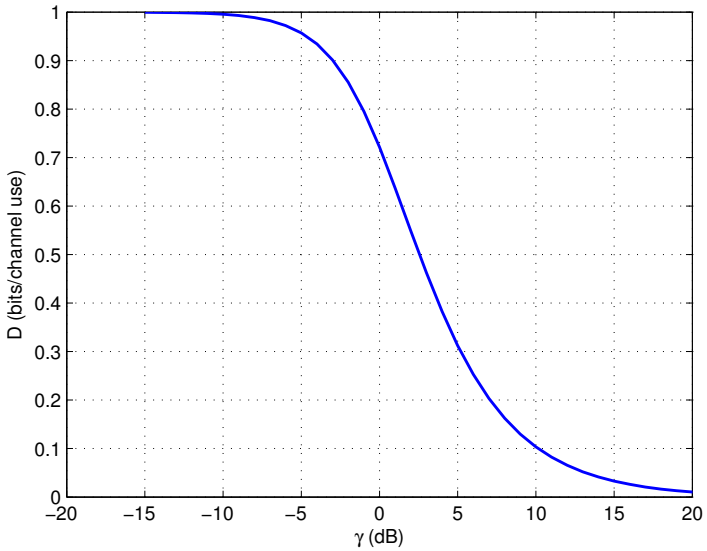

Figure A.1: D as a function of γ.

Note that $0 < \mathcal{H}\left(Q\left(t\gamma\right)\right) \leq 1$. Hence, we have

$$0 < D \leq 2\int_0^\infty \frac{1}{\sqrt{2\pi}} \exp\left\{-\frac{t^2}{2}\right\} dt = 1 \tag{A.0.7}$$

where the upper bound can be achieved when $\gamma = 0$.

For $t > 0$, if $0 \leq \gamma_1 < \gamma_2$ then $0 < Q\left(t\gamma_2\right) < Q\left(t\gamma_1\right) \leq 1/2$ and thus $\mathcal{H}\left(Q\left(t\gamma_1\right)\right) > \mathcal{H}\left(Q\left(t\gamma_2\right)\right)$. Hence, we have

$$D(\gamma_1) - D(\gamma_2) = 2\int_0^\infty \left(\mathcal{H}\left(Q\left(t\gamma_1\right)\right) - \mathcal{H}\left(Q\left(t\gamma_2\right)\right)\right) \frac{1}{\sqrt{2\pi}} \exp\left\{-\frac{t^2}{2}\right\} dt > 0 \tag{A.0.8}$$

which indicates $D(\gamma)$ is monotonically decreasing in γ and $D \longrightarrow 0$ as $\gamma \longrightarrow \infty$. Fig. A.1 shows D for different values of γ.

Bibliography

[1] Cisco, "Cisco annual Internet report (2018–2023) white paper." [Online]. Available: https://www.cisco.com/c/en/us/solutions/collateral/executive-perspectives/annual-internet-report/white-paper-c11-741490.pdf

[2] H. Haas, J. Elmirghani, and I. White, "Optical wireless communication," *Philosophical Transactions of the Royal Society A*, vol. 378, no. 2169, p. 20200051, 2020.

[3] L. Hanzo, H. Haas, S. Imre, D. O'Brien, M. Rupp, and L. Gyongyosi, "Wireless myths, realities, and futures: from 3G/4G to optical and quantum wireless," *Proceedings of the IEEE*, vol. 100, no. Special Centennial Issue, pp. 1853–1888, 2012.

[4] J. M. Kahn and J. R. Barry, "Wireless infrared communications," *Proceedings of the IEEE*, vol. 85, no. 2, pp. 265–298, 1997.

[5] H. Elgala, R. Mesleh, and H. Haas, "Indoor optical wireless communication: potential and state-of-the-art," *IEEE Communications Magazine*, vol. 49, no. 9, pp. 56–62, 2011.

[6] Z. Xu and B. M. Sadler, "Ultraviolet communications: potential and state-of-the-art," *IEEE Communications Magazine*, vol. 46, no. 5, pp. 67–73, 2008.

[7] P. H. Pathak, X. Feng, P. Hu, and P. Mohapatra, "Visible light communication, networking, and sensing: A survey, potential and challenges," *IEEE Communications Surveys & Tutorials*, vol. 17, no. 4, pp. 2047–2077, 2015.

[8] C. Elliott, "Energy savings forecast of solid-state lighting in general illumination applications." [Online]. Available: https://www.osti.gov/biblio/1607661

[9] L. Lampe, A. M. Tonello, and T. G. Swart, *Power Line Communications: Principles, Standards and Applications from multimedia to smart grid*. John Wiley & Sons, 2016.

[10] M. S. Mossaad, S. Hranilovic, and L. Lampe, "Amplify-and-forward integration of power line and visible light communications," in *2015 IEEE Global Conference on Signal and Information Processing (GlobalSIP)*. IEEE, 2015, pp. 1322–1326.

[11] H. Meng, S. Chen, Y. Guan, C. Law, P. So, E. Gunawan, and T. Lie, "A transmission line model for high-frequency power line communication channel," in *Proceedings. International Conference on Power System Technology*, vol. 2. IEEE, 2002, pp. 1290–1295.

[12] Y.-J. Lin, H. A. Latchman, M. Lee, and S. Katar, "A power line communication network infrastructure for the smart home," *IEEE Wireless Communications*, vol. 9, no. 6, pp. 104–111, 2002.

[13] H. Meng, S. Chen, Y. Guan, C. Law, P. So, E. Gunawan, and T. Lie, "Modeling of transfer characteristics for the broadband power line communication channel," *IEEE Transactions on Power delivery*, vol. 19, no. 3, pp. 1057–1064, 2004.

[14] K. Warmerdam, A. Pandharipande, and D. Caicedo, "Connectivity in IoT indoor lighting systems with visible light communications," in *2015 IEEE Online Conference on Green Communications (OnlineGreenComm)*. IEEE, 2015, pp. 47–52.

[15] S. Hranilovic, L. Lampe, and S. Hosur, "Visible light communications: The road to standardization and commercialization (Part 1)[Guest Editorial]," *IEEE Communications Magazine*, vol. 51, no. 12, pp. 24–25, 2013.

[16] F. G. Osorio, M. Xinran, Y. Liu, P. Lusina, and E. Cretu, "Sensor network using Power-over-Ethernet," in *2015 International Conference and Workshop on Computing and Communication (IEMCON)*. IEEE, 2015, pp. 1–7.

[17] R. V. White, "Electrical isolation requirements in Power-over-Ethernet (PoE) power sourcing equipment (PSE)," in *Twenty-First Annual IEEE Applied Power Electronics Conference and Exposition, 2006. APEC'06.* IEEE, 2006, pp. 4–pp.

[18] S.-K. Lim, K. G. Ruling, I. Kim, and I. S. Jang, "Entertainment lighting control network standardization to support VLC services," *IEEE Communications Magazine*, vol. 51, no. 12, pp. 42–48, 2013.

[19] T.-J. Park and S.-H. Hong, "Experimental case study of a BACnet-based lighting control system," *IEEE Transactions on Automation Science and Engineering*, vol. 6, no. 2, pp. 322–333, 2009.

[20] F. Sánchez Sutil and A. Cano-Ortega, "Smart public lighting control and measurement system using LoRa network," *Electronics*, vol. 9, no. 1, p. 124, 2020.

[21] A. Mostafa and L. Lampe, "Physical-layer security for MISO visible light communication channels," *IEEE Journal on Selected Areas in Communications*, vol. 33, no. 9, pp. 1806–1818, 2015.

[22] S. Ma, Z.-L. Dong, H. Li, Z. Lu, and S. Li, "Optimal and robust secure beamformer for indoor MISO visible light communication," *Journal of Lightwave Technology*, vol. 34, no. 21, pp. 4988–4998, 2016.

[23] F. Yang, K. Zhang, Y. Zhai, J. Quan, and Y. Dong, "Artificial noise design in time domain for indoor SISO DCO-OFDM VLC wiretap systems," *Journal of Lightwave Technology*, vol. 39, no. 20, pp. 6450–6458, 2021.

[24] T. V. Pham and A. T. Pham, "Energy efficient artificial noise-aided precoding designs for secured visible light communication systems," *IEEE Transactions on Wireless Communications*, vol. 20, no. 1, pp. 653–666, 2020.

[25] O. I. Younus, H. Le Minh, P. T. Dat, N. Yamamoto, A. T. Pham, and Z. Ghassemlooy, "Dynamic physical-layer secured link in a mobile MIMO VLC system," *IEEE Photonics Journal*, vol. 12, no. 3, pp. 1–14, 2020.

[26] S. Ma, M. Hong, E. Song, X. Wang, and D. Sun, "Outage constrained robust secure transmission for MISO wiretap channels," *IEEE Transactions on Wireless Communications*, vol. 13, no. 10, pp. 5558–5570, 2014.

[27] N. Holonyak Jr and S. F. Bevacqua, "Coherent (visible) light emission from $Ga(As_{1-x}P_x)$ junctions," *Applied Physics Letters*, vol. 1, no. 4, pp. 82–83, 1962.

[28] S. Nakamura, T. Mukai, and M. Senoh, "Candela-class high-brightness InGaN/AlGaN double-heterostructure blue-light-emitting diodes," *Applied Physics Letters*, vol. 64, no. 13, pp. 1687–1689, 1994.

[29] G. Pang, K.-L. Ho, T. Kwan, and E. Yang, "Visible light communication for audio systems," *IEEE Transactions on Consumer Electronics*, vol. 45, no. 4, pp. 1112–1118, 1999.

[30] Y. Tanaka, S. Haruyama, and M. Nakagawa, "Wireless optical transmissions with white colored LED for wireless home links," in *11th IEEE International Symposium on Personal Indoor and Mobile Radio Communications. PIMRC 2000. Proceedings (Cat. No.00TH8525)*, vol. 2, 2000, pp. 1325–1329 vol.2.

[31] T. Komine and M. Nakagawa, "Integrated system of white LED visible-light communication and power-line communication," *IEEE Transactions on Consumer Electronics*, vol. 49, no. 1, pp. 71–79, 2003.

[32] H. Le Minh, D. O'Brien, G. Faulkner, L. Zeng, K. Lee, D. Jung, Y. Oh, and E. T. Won, "100-Mb/s NRZ visible light communications using a postequalized white LED," *IEEE Photonics Technology Letters*, vol. 21, no. 15, pp. 1063–1065, 2009.

[33] J. Vučić, C. Kottke, K. Habel, and K.-D. Langer, "803 Mbit/s visible light WDM link based on DMT modulation of a single RGB LED luminary," in *2011 Optical Fiber Communication Conference and Exposition and the National Fiber Optic Engineers Conference*. IEEE, 2011, pp. 1–3.

[34] A. Khalid, G. Cossu, R. Corsini, P. Choudhury, and E. Ciaramella, "1-Gb/s transmission over a phosphorescent white LED by using rate-adaptive discrete multitone modulation," *IEEE Photonics Journal*, vol. 4, no. 5, pp. 1465–1473, 2012.

[35] G. Cossu, A. Khalid, P. Choudhury, R. Corsini, and E. Ciaramella, "3.4 Gbit/s visible optical wireless transmission based on RGB LED," *Optics Express*, vol. 20, no. 26, pp. B501–B506, 2012.

[36] D. Tsonev, H. Chun, S. Rajbhandari, J. J. McKendry, S. Videv, E. Gu, M. Haji, S. Watson, A. E. Kelly, G. Faulkner *et al.*, "A 3-Gb/s Single-LED OFDM-Based Wireless VLC Link Using a Gallium Nitride μLED," *IEEE Photonics Technology Letters*, vol. 26, no. 7, pp. 637–640, 2014.

[37] X. Huang, Z. Wang, J. Shi, Y. Wang, and N. Chi, "1.6 Gbit/s phosphorescent white LED based VLC transmission using a cascaded pre-equalization circuit and a differential outputs PIN receiver," *Optics Express*, vol. 23, no. 17, pp. 22 034–22 042, 2015.

[38] M. S. Islim, R. X. Ferreira, X. He, E. Xie, S. Videv, S. Viola, S. Watson, N. Bamiedakis, R. V. Penty, I. H. White *et al.*, "Towards 10 Gb/s orthogonal frequency division multiplexing-based visible light communication using a GaN violet micro-LED," *Photonics Research*, vol. 5, no. 2, pp. A35–A43, 2017.

[39] R. Bian, I. Tavakkolnia, and H. Haas, "15.73 Gb/s visible light communication with off-the-shelf LEDs," *Journal of Lightwave Technology*, vol. 37, no. 10, pp. 2418–2424, 2019.

[40] Z. Yu, C. Gong, J. Wei, N. Huang, and Z. Xu, "3-Gb/s Visible Light Communication over 5 m Distance Based on Imaging System with Low Transmission Power and Off-the-Shelf LEDs," in *2021 International Wireless Communications and Mobile Computing (IWCMC)*. IEEE, 2021, pp. 2109–2114.

[41] H. Chen, W. Niu, Y. Zhao, J. Zhang, N. Chi, and Z. Li, "Adaptive deep-learning equalizer based on constellation partitioning scheme with reduced computational complexity in UVLC system," *Optics Express*, vol. 29, no. 14, pp. 21 773–21 782, 2021.

[42] F. Hu, S. Chen, G. Li, P. Zou, J. Zhang, J. Hu, J. Zhang, Z. He, S. Yu, F. Jiang *et al.*, "Si-substrate LEDs with multiple superlattice interlayers for beyond 24 Gbps visible light communication," *Photonics Research*, vol. 9, no. 8, pp. 1581–1591, 2021.

[43] D. Tsonev, S. Videv, and H. Haas, "Towards a 100 Gb/s visible light wireless access network," *Optics Express*, vol. 23, no. 2, pp. 1627–1637, 2015.

[44] H. Chun, A. Gomez, C. Quintana, W. Zhang, G. Faulkner, and D. O'Brien, "A wide-area coverage 35 Gb/s visible light communications link for indoor wireless applications," *Scientific Reports*, vol. 9, no. 1, pp. 1–8, 2019.

[45] S. Haruyama, "Japan's Visible Light Communications Consortium and its standardization activities," 2010. [Online]. Available:

https://mentor.ieee.org/802.15/dcn/08/15-08-0061-00-0vlc-japan-s-visible-%20light-communications-consortium-and-its.pdf

[46] J.-P. Javaudin, M. Bellec, D. Varoutas, and V. Suraci, "OMEGA ICT project: Towards convergent Gigabit home networks," in *2008 IEEE 19th International Symposium on Personal, Indoor and Mobile Radio Communications*. IEEE, 2008, pp. 1–5.

[47] "IEEE standard for local and metropolitan area networks-Part 15.7: short-range wireless optical communication using visible light," *IEEE Std*, vol. 802, pp. 7–2011, 2011.

[48] R. Bai, Q. Wang, and Z. Wang, "Asymmetrically clipped absolute value optical OFDM for intensity-modulated direct-detection systems," *Journal of Lightwave Technology*, vol. 35, no. 17, pp. 3680–3691, 2017.

[49] S. Fine and E. Klein, "Biological effects of laser radiation," *Advances in Biological and Medical Physics*, vol. 10, pp. 149–226, 1965.

[50] K. Lee, H. Park, and J. R. Barry, "Indoor channel characteristics for visible light communications," *IEEE Communications Letters*, vol. 15, no. 2, pp. 217–219, 2011.

[51] J. Armstrong, "OFDM for optical communications," *Journal of Lightwave Technology*, vol. 27, no. 3, pp. 189–204, 2009.

[52] Z. Wang, Q. Wang, S. Chen, and L. Hanzo, "An adaptive scaling and biasing scheme for OFDM-based visible light communication systems," *Optics Express*, vol. 22, no. 10, pp. 12 707–12 715, 2014.

[53] S. Mazahir, A. Chaaban, H. Elgala, and M.-S. Alouini, "Achievable rates of multi-carrier modulation schemes for bandlimited IM/DD systems," *IEEE Transactions on Wireless Communications*, vol. 18, no. 3, pp. 1957–1973, 2019.

[54] S. Hranilovic and D. A. Johns, "A multilevel modulation scheme for high-speed wireless infrared communications," in *1999 IEEE International Symposium on Circuits and Systems (ISCAS)*, vol. 6. IEEE, 1999, pp. 338–341.

[55] J. Armstrong and A. J. Lowery, "Power efficient optical OFDM," *Electronics Letters*, vol. 42, no. 6, pp. 370–372, 2006.

[56] S. D. Dissanayake and J. Armstrong, "Comparison of ACO-OFDM, DCO-OFDM and ADO-OFDM in IM/DD systems," *Journal of Lightwave Technology*, vol. 31, no. 7, pp. 1063–1072, 2013.

[57] S. C. J. Lee, S. Randel, F. Breyer, and A. M. Koonen, "PAM-DMT for intensity-modulated and direct-detection optical communication systems," *IEEE Photonics Technology Letters*, vol. 21, no. 23, pp. 1749–1751, 2009.

[58] D. Tsonev and H. Haas, "Avoiding spectral efficiency loss in unipolar ofdm for optical wireless communication," in *2014 IEEE International Conference on Communications (ICC)*. IEEE, 2014, pp. 3336–3341.

[59] N. Fernando, Y. Hong, and E. Viterbo, "Flip-OFDM for unipolar communication systems," *IEEE Transactions on Communications*, vol. 60, no. 12, pp. 3726–3733, 2012.

[60] A. Weiss, A. Yeredor, and M. Shtaif, "Iterative symbol recovery for power-efficient DC-biased optical OFDM systems," *Journal of Lightwave Technology*, vol. 34, no. 9, pp. 2331–2338, 2016.

[61] J. Lian and M. Brandt-Pearce, "Clipping-enhanced optical OFDM for IM/DD communication systems," in *2018 IEEE International Conference on Communications Workshops (ICC Workshops)*. IEEE, 2018, pp. 1–6.

[62] ——, "Clipping-enhanced optical OFDM for visible light communication systems," *Journal of Lightwave Technology*, vol. 37, no. 13, pp. 3324–3332, 2019.

[63] K. Asadzadeh, A. A. Farid, and S. Hranilovic, "Spectrally factorized optical OFDM," in *2011 12th Canadian workshop on information theory*. IEEE, 2011, pp. 102–105.

[64] R. Bai, R. Jiang, T. Mao, W. Lei, and Z. Wang, "Iterative receiver for ADO-OFDM with near-optimal optical power allocation," *Optics Communications*, vol. 387, pp. 350–356, 2017.

[65] R. Bai, J. Chen, T. Mao, and Z. Wang, "Enhanced asymmetrically clipped DC biased optical OFDM for intensity-modulated direct-detection systems," *Journal of Communications and Information Networks*, vol. 2, no. 4, pp. 36–46, 2017.

[66] X. Huang, F. Yang, X. Liu, H. Zhang, J. Ye, and J. Song, "Subcarrier and power allocations for dimmable enhanced ADO-OFDM with iterative interference cancellation," *IEEE Access*, vol. 7, pp. 28 422–28 435, 2019.

[67] B. Ranjha and M. Kavehrad, "Hybrid asymmetrically clipped OFDM-based IM/DD optical wireless system," *Journal of Optical Communications and Networking*, vol. 6, no. 4, pp. 387–396, 2014.

[68] N. Wu and Y. Bar-Ness, "A novel power-efficient scheme asymmetrically and symmetrically clipping optical (ASCO)-OFDM for IM/DD optical systems," *EURASIP Journal on Advances in Signal Processing*, vol. 2015, no. 1, pp. 1–10, 2015.

[69] Q. Wang, Z. Wang, and L. Dai, "Asymmetrical hybrid optical OFDM for visible light communications with dimming control," *IEEE Photonics Technology Letters*, vol. 27, no. 9, pp. 974–977, 2015.

[70] M. S. Islim, D. Tsonev, and H. Haas, "A generalized solution to the spectral efficiency loss in unipolar optical OFDM-based systems," in *2015 IEEE International Conference on Communications (ICC)*. IEEE, 2015, pp. 5126–5131.

[71] ——, "Spectrally enhanced PAM-DMT for IM/DD optical wireless communications," in *2015 IEEE 26th Annual International Symposium on Personal, Indoor, and Mobile Radio Communications (PIMRC)*. IEEE, 2015, pp. 877–882.

[72] H. Elgala and T. D. Little, "SEE-OFDM: Spectral and energy efficient OFDM for optical IM/DD systems," in *2014 IEEE 25th Annual International Symposium on Personal, Indoor, and Mobile Radio Communication (PIMRC)*. IEEE, 2014, pp. 851–855.

[73] E. Lam, S. K. Wilson, H. Elgala, and T. D. Little, "Spectrally and energy efficient OFDM (SEE-OFDM) for intensity modulated optical wireless systems," *arXiv preprint arXiv:1510.08172*, 2015.

[74] Q. Wang, C. Qian, X. Guo, Z. Wang, D. G. Cunningham, and I. H. White, "Layered ACO-OFDM for intensity-modulated direct-detection optical wireless transmission," *Optics Express*, vol. 23, no. 9, pp. 12 382–12 393, 2015.

[75] R. Bai, S. Hranilovic, and Z. Wang, "Low-complexity layered ACO-OFDM for power-efficient visible light communications," *major revision in IEEE Transactions on Green Communications and Networking*, 2021.

[76] Z. Zhang, A. Chaaban, and M.-S. Alouini, "Residual clipping noise in multilayer optical ofdm: Modeling, analysis, and applications," *IEEE Transactions on Wireless Communications*, vol. 19, no. 9, pp. 5846–5859, 2020.

[77] Q. Wang, Z. Wang, X. Guo, and L. Dai, "Improved receiver design for layered ACO-OFDM in optical wireless communications," *IEEE Photonics Technology Letters*, vol. 28, no. 3, pp. 319–322, 2015.

[78] M. M. Mohammed, C. He, and J. Armstrong, "Diversity combining in layered asymmetrically clipped optical OFDM," *Journal of Lightwave Technology*, vol. 35, no. 11, pp. 2078–2085, 2017.

[79] T. Q. Wang, H. Li, and X. Huang, "Diversity combining for layered asymmetrically clipped optical OFDM using soft successive interference cancellation," *IEEE Communications Letters*, vol. 21, no. 6, pp. 1309–1312, 2017.

[80] ——, "Interference cancellation for layered asymmetrically clipped optical OFDM with application to optical receiver design," *Journal of Lightwave Technology*, vol. 36, no. 11, pp. 2100–2113, 2018.

[81] ——, "Analysis and mitigation of clipping noise in layered ACO-OFDM based visible light communication systems," *IEEE Transactions on Communications*, vol. 67, no. 1, pp. 564–577, 2018.

[82] X. Zhang, Q. Wang, R. Zhang, S. Chen, and L. Hanzo, "Performance analysis of layered aco-ofdm," *IEEE Access*, vol. 5, pp. 18 366–18 381, 2017.

[83] J. Zhou, Q. Wang, Q. Cheng, M. Guo, Y. Lu, A. Yang, and Y. Qiao, "Low-PAPR layered/enhanced ACO-SCFDM for optical-wireless communications," *IEEE Photonics Technology Letters*, vol. 30, no. 2, pp. 165–168, 2017.

[84] R. Bai, Z. Wang, R. Jiang, and J. Cheng, "Interleaved DFT-Spread Layered/Enhanced ACO-OFDM for Intensity-Modulated Direct-Detection Systems," *Journal of Lightwave Technology*, vol. 36, no. 20, pp. 4713–4722, 2018.

[85] W. Hu, "Design of a cyclic shifted LACO-OFDM for optical wireless communication," *IEEE Access*, vol. 8, pp. 76 708–76 714, 2020.

[86] R. Bai and S. Hranilovic, "Absolute value layered ACO-OFDM for intensity-modulated optical wireless channels," *IEEE Transactions on Communications*, vol. 68, no. 11, pp. 7098–7110, 2020.

[87] F. Yang, Y. Sun, and J. Gao, "Adaptive LACO-OFDM with variable layer for visible light communication," *IEEE Photonics Journal*, vol. 9, no. 6, pp. 1–8, 2017.

[88] J. Zhou and W. Zhang, "A comparative study of unipolar OFDM schemes in Gaussian optical intensity channel," *IEEE Transactions on Communications*, vol. 66, no. 4, pp. 1549–1564, 2017.

[89] X. Zhang, S. Chen, and L. Hanzo, "On the discrete-input continuous-output memoryless channel capacity of layered ACO-OFDM," *Journal of Lightwave Technology*, vol. 38, no. 18, pp. 4955–4968, 2020.

[90] B. Song, B. Corcoran, Q. Wang, L. Zhuang, and A. J. Lowery, "Subcarrier pairwise coding for short-haul L/E-ACO-OFDM," *IEEE photonics technology letters*, vol. 29, no. 18, pp. 1584–1587, 2017.

[91] X. Zhang, Z. Babar, R. Zhang, S. Chen, and L. Hanzo, "Multi-class coded layered asymmetrically clipped optical OFDM," *IEEE Transactions on Communications*, vol. 67, no. 1, pp. 578–589, 2018.

[92] Z. Babar, X. Zhang, P. Botsinis, D. Alanis, D. Chandra, S. X. Ng, and L. Hanzo, "Near-capacity multilayered code design for LACO-OFDM-aided optical wireless systems," *IEEE Transactions on Vehicular Technology*, vol. 68, no. 4, pp. 4051–4054, 2019.

[93] C. Lacava, Z. Babar, X. Zhang, I. Demirtzioglou, P. Petropoulos, and L. Hanzo, "High-speed multi-layer coded adaptive LACO-OFDM and its experimental verification," *OSA Continuum*, vol. 3, no. 9, pp. 2614–2629, 2020.

[94] Q. Wang, Z. Wang, L. Dai, and J. Quan, "Dimmable visible light communications based on multilayer ACO-OFDM," *IEEE Photonics Journal*, vol. 8, no. 3, pp. 1–11, 2016.

[95] T. Wang, F. Yang, L. Cheng, and J. Song, "Spectral-efficient generalized spatial modulation based hybrid dimming scheme with LACO-OFDM in VLC," *IEEE Access*, vol. 6, pp. 41 153–41 162, 2018.

[96] T. Zhang, Y. Qiao, J. Zhou, Z. Zhang, Y. Lu, and F. Su, "Spectral-efficient L/E-ACO-SCFDM-based dimmable visible light communication system," *IEEE Access*, vol. 7, pp. 10 617–10 626, 2019.

[97] B. Li, W. Xu, S. Feng, and Z. Li, "Spectral-efficient reconstructed LACO-OFDM transmission for dimming compatible visible light communications," *IEEE Photonics Journal*, vol. 11, no. 1, pp. 1–14, 2019.

[98] R. Bai and S. Hranilovic, "Absolute value layered ACO-OFDM for intensity-modulated optical wireless channels," in *ICC 2019 - 2019 IEEE International Conference on Communications (ICC)*, 2019, pp. 1–6.

[99] S. Feng, R. Zhang, W. Xu, and L. Hanzo, "Multiple access design for ultra-dense VLC networks: Orthogonal vs non-orthogonal," *IEEE Transactions on Communications*, vol. 67, no. 3, pp. 2218–2232, 2018.

[100] H. Li, Z. Huang, Y. Xiao, S. Zhan, and Y. Ji, "A power and spectrum efficient NOMA scheme for VLC network based on hierarchical pre-distorted LACO-OFDM," *IEEE Access*, vol. 7, pp. 48 565–48 571, 2019.

[101] X. Huang, F. Yang, C. Pan, and J. Song, "Flexible NOMA-based NOHO-OFDM scheme for visible light communication with iterative interference cancellation," *Optics Express*, vol. 29, no. 4, pp. 5645–5657, 2021.

[102] Q. Wang, B. Song, B. Corcoran, D. Boland, C. Zhu, L. Zhuang, and A. J. Lowery, "Hardware-efficient signal generation of layered/enhanced ACO-OFDM for short-haul fiber-optic links," *Optics Express*, vol. 25, no. 12, pp. 13 359–13 371, 2017.

[103] Z. Zhang, A. Chaaban, C. Shen, H. Elgala, T. K. Ng, B. S. Ooi, and M.-S. Alouini, "Worst-case residual clipping noise power model for bit loading in LACO-OFDM," in *2018 Global LIFI Congress (GLC)*. IEEE, 2018, pp. 1–6.

[104] B. Song, C. Zhu, B. Corcoran, Q. Wang, L. Zhuang, and A. J. Lowery, "Experimental layered/enhanced ACO-OFDM short-haul optical fiber link," *IEEE Photonics Technology Letters*, vol. 28, no. 24, pp. 2815–2818, 2016.

[105] X. Liu, J. Li, J. Li, and Z. Huang, "Analysis of the single-FFT receiver for layered ACO-OFDM in visible light communications," *Journal of Lightwave Technology*, vol. 38, no. 17, pp. 4757–4764, 2020.

[106] R. Bai and S. Hranilovic, "Layered antisymmetry-constructed clipped optical OFDM for low-complexity VLC systems," *Optics Express*, vol. 29, no. 7, pp. 10 613–10 630, 2021.

[107] ——, "Layered antisymmetry-constructed clipped optical OFDM for IM/DD systems," in *2019 IEEE Global Communications Conference (GLOBECOM)*. IEEE, Nov. 2019, pp. 1–6.

[108] ——, "Kramers-Kronig Optical OFDM for bandlimited intensity modulated visible light communications," *Journal of Lightwave Technology*, vol. 39, no. 22, pp. 7135–7145, 2021. 10.1109/JLT.2021.3110661.

[109] L. Chen, B. Krongold, and J. Evans, "Successive decoding of anti-periodic OFDM signals in IM/DD optical channel," in *2010 IEEE International Conference on Communications*. IEEE, 2010, pp. 1–6.

[110] ——, "Performance analysis for optical OFDM transmission in short-range IM/DD systems," *Journal of Lightwave Technology*, vol. 30, no. 7, pp. 974–983, 2012.

[111] M. S. Islim, D. Tsonev, and H. Haas, "On the superposition modulation for OFDM-based optical wireless communication," in *2015 IEEE Global Conference on Signal and Information Processing (GlobalSIP)*. IEEE, 2015, pp. 1022–1026.

[112] A. J. Lowery, "Enhanced asymmetrically-clipped optical OFDM," *CoRR*, vol. abs/1510.04771, 2015. [Online]. Available: http://arxiv.org/abs/1510.04771

[113] T. Zhang, H. Ji, Z. Ghassemlooy, X. Tang, B. Lin, and S. Qiao, "Spectrum-efficient triple-layer hybrid optical OFDM for IM/DD-based optical wireless communications," *IEEE Access*, vol. 8, pp. 10 352–10 362, 2020.

[114] R. Islam and M. R. H. Mondal, "Hybrid DCO-OFDM, ACO-OFDM and PAM-DMT for dimmable LiFi," *Optik*, vol. 180, pp. 939–952, 2019.

[115] Y. Sun, F. Yang, and J. Gao, "Novel dimmable visible light communication approach based on hybrid LACO-OFDM," *Journal of Lightwave Technology*, vol. 36, no. 20, pp. 4942–4951, 2018.

[116] S. K. Wilson and J. Armstrong, "Transmitter and receiver methods for improving asymmetrically-clipped optical OFDM," *IEEE Transactions on Wireless Communications*, vol. 8, no. 9, pp. 4561–4567, 2009.

[117] L. Chen, B. Krongold, and J. Evans, "Diversity combining for asymmetrically clipped optical OFDM in IM/DD channels," in *GLOBECOM 2009-2009 IEEE Global Telecommunications Conference*. IEEE, 2009, pp. 1–6.

[118] S. D. Dissanayake and J. Armstrong, "Novel techniques for combating DC offset in diversity combined ACO-OFDM," *IEEE Communications Letters*, vol. 15, no. 11, pp. 1237–1239, 2011.

[119] J. Dang, Z. Zhang, and L. Wu, "Frequency-domain diversity combining receiver for ACO-OFDM system," *IEEE Photonics Journal*, vol. 7, no. 6, pp. 1–10, 2015.

[120] K. Asadzadeh, A. Dabbo, and S. Hranilovic, "Receiver design for asymmetrically clipped optical OFDM," in *2011 IEEE GLOBECOM Workshops (GC Wkshps)*. IEEE, 2011, pp. 777–781.

[121] N. Fernando, Y. Hong, and E. Viterbo, "Flip-OFDM for Unipolar Communication Systems," *IEEE Transactions on Communications*, vol. 60, no. 12, pp. 3726–3733, 2012.

[122] J. Dang, Z. Zhang, and L. Wu, "A novel receiver for ACO-OFDM in visible light communication," *IEEE Communications Letters*, vol. 17, no. 12, pp. 2320–2323, 2013.

[123] N. Huang, J.-B. Wang, J. Wang, C. Pan, H. Wang, and M. Chen, "Receiver design for PAM-DMT in indoor optical wireless links," *IEEE Photonics Technology Letters*, vol. 27, no. 2, pp. 161–164, 2014.

[124] N. Huang, J.-B. Wang, C. Pan, J.-Y. Wang, Y. Pan, and M. Chen, "Iterative

receiver for Flip-OFDM in optical wireless communication," *IEEE Photonics Technology Letters*, vol. 27, no. 16, pp. 1729–1732, 2015.

[125] J. Dang, Z. Zhang, and L. Wu, "Improving the power efficiency of enhanced unipolar OFDM for optical wireless communication," *Electronics Letters*, vol. 51, no. 21, pp. 1681–1683, 2015.

[126] Q. Wang, Z. Wang, and L. Dai, "Iterative receiver for hybrid asymmetrically clipped optical OFDM," *Journal of Lightwave Technology*, vol. 32, no. 22, pp. 4471–4477, 2014.

[127] R. Garnaut, *The Garnaut Climate Change Review: the Final Report*. Cambridge, UK, Cambridge University Press, 2008.

[128] A. Tsiatmas, C. P. Baggen, F. M. Willems, J.-P. M. Linnartz, and J. W. Bergmans, "An illumination perspective on visible light communications," *IEEE Communications Magazine*, vol. 52, no. 7, pp. 64–71, 2014.

[129] S. Hranilovic, *Wireless Optical Communication Systems*. Springer, 2004.

[130] S. Hranilovic and F. R. Kschischang, "Capacity bounds for power-and band-limited optical intensity channels corrupted by Gaussian noise," *IEEE Transactions on Information Theory*, vol. 50, no. 5, pp. 784–795, 2004.

[131] A. Lapidoth, S. M. Moser, and M. A. Wigger, "On the capacity of free-space optical intensity channels," *IEEE Transactions on Information Theory*, vol. 55, no. 10, pp. 4449–4461, 2009.

[132] H. Elgala and T. D. Little, "SEE-OFDM: Spectral and energy efficient OFDM

for optical IM/DD systems," in *2014 IEEE 25th Annual International Symposium on Personal, Indoor, and Mobile Radio Communication (PIMRC)*. IEEE, 2014, pp. 851–855.

[133] B. Porat, *A Course in Digital Signal Processing*. John Wiley & Sons, Inc., 1996.

[134] X. Li, R. Mardling, and J. Armstrong, "Channel capacity of IM/DD optical communication systems and of ACO-OFDM," in *2007 IEEE International Conference on Communications*. IEEE, 2007, pp. 2128–2133.

[135] X. Zhang, Z. Babar, R. Zhang, S. Chen, and L. Hanzo, "Multi-class coded layered asymmetrically clipped optical OFDM," *IEEE Transactions on Communications*, vol. 67, no. 1, pp. 578–589, 2018.

[136] Y. Sun, F. Yang, and L. Cheng, "An overview of OFDM-based visible light communication systems from the perspective of energy efficiency versus spectral efficiency," *IEEE Access*, vol. 6, pp. 60 824–60 833, 2018.

[137] C. E. Shannon, "A mathematical theory of communication," *The Bell System Technical Journal*, vol. 27, no. 3, pp. 379–423, 1948.

[138] J. Grubor, S. Randel, K.-D. Langer, and J. W. Walewski, "Broadband information broadcasting using LED-based interior lighting," *Journal of Lightwave Technology*, vol. 26, no. 24, pp. 3883–3892, 2008.

[139] M. S. Mossaad, S. Hranilovic, and L. Lampe, "Visible light communications using OFDM and multiple LEDs," *IEEE Transactions on Communications*, vol. 63, no. 11, pp. 4304–4313, 2015.

[140] A. A. Farid and S. Hranilovic, "Capacity bounds for wireless optical intensity channels with Gaussian noise," *IEEE Transactions on Information Theory*, vol. 56, no. 12, pp. 6066–6077, 2010.

[141] D. Tsonev, S. Videv, and H. Haas, "Unlocking spectral efficiency in intensity modulation and direct detection systems," *IEEE Journal on Selected Areas in Communications*, vol. 33, no. 9, pp. 1758–1770, 2015.

[142] J. Wang, Y. Xu, X. Ling, R. Zhang, Z. Ding, and C. Zhao, "PAPR analysis for OFDM visible light communication," *Optics Express*, vol. 24, no. 24, pp. 27 457–27 474, 2016.

[143] D. Tsonev and H. Haas, "Avoiding spectral efficiency loss in unipolar OFDM for optical wireless communication," in *2014 IEEE International Conference on Communications (ICC)*, 2014, pp. 3336–3341.

[144] M. Z. Chowdhury, M. K. Hasan, M. Shahjalal, M. T. Hossan, and Y. M. Jang, "Optical wireless hybrid networks: Trends, opportunities, challenges, and research directions," *IEEE Communications Surveys & Tutorials*, vol. 22, no. 2, pp. 930–966, 2020.

[145] H. G. Olanrewaju, J. Thompson, and W. O. Popoola, "Pairwise coding for MIMO-OFDM visible light communication," *IEEE Transactions on Wireless Communications*, vol. 19, no. 2, pp. 1210–1220, 2019.

[146] S. D. Dissanayake and J. Armstrong, "Comparison of ACO-OFDM, DCO-OFDM and ADO-OFDM in IM/DD systems," *Journal of Lightwave Technology*, vol. 31, no. 7, pp. 1063–1072, 2013.

[147] M. S. Islim, D. Tsonev, and H. Haas, "On the superposition modulation for OFDM-based optical wireless communication," in *2015 IEEE Global Conference on Signal and Information Processing (GlobalSIP)*. IEEE, 2015, pp. 1022–1026.

[148] X. Zhang, S. Chen, and L. Hanzo, "On the discrete-input continuous-output memoryless channel capacity of layered ACO-OFDM," *Journal of Lightwave Technology*, vol. 38, no. 18, pp. 4955–4968, 2020.

[149] A. J. Lowery, "Spectrally efficient optical orthogonal frequency division multiplexing," *Philosophical Transactions of the Royal Society A*, vol. 378, no. 2169, p. 20190180, 2020.

[150] T. Zhang, L. Sun, C. Zhao, S. Qiao, and Z. Ghassemlooy, "Low-complexity receiver for HACO-OFDM in optical wireless communications," *IEEE Wireless Communications Letters*, pp. 1–1, 2020.

[151] M. Gao, C. Li, and Z. Xu, "Optimal transmission of VLC system in the presence of LED nonlinearity and APD module saturation," *IEEE Photonics Journal*, vol. 10, no. 5, pp. 1–14, 2018.

[152] Z. Ghassemlooy, W. Popoola, and S. Rajbhandari, *Optical Wireless Communications: System and Channel Modelling with Matlab®*. CRC press, 2019.

[153] R. Zhang and L. Hanzo, "Multi-layer modulation for intensity-modulated direct-detection optical OFDM," *Journal of optical communications and networking*, vol. 5, no. 12, pp. 1402–1412, 2013.

[154] A. J. Lowery, "Enhanced asymmetrically clipped optical ODFM for high spectral efficiency and sensitivity," in *2016 Optical Fiber Communications Conference and Exhibition (OFC)*. IEEE, 2016, pp. 1–3.

[155] J. B. Carruthers and J. M. Kahn, "Modeling of nondirected wireless infrared channels," *IEEE Transactions on Communications*, vol. 45, no. 10, pp. 1260–1268, 1997.

[156] M.-A. Khalighi, S. Long, S. Bourennane, and Z. Ghassemlooy, "PAM-and CAP-based transmission schemes for visible-light communications," *IEEE Access*, vol. 5, pp. 27 002–27 013, 2017.

[157] M. Horowitz, "1.1 computing's energy problem (and what we can do about it)," in *2014 IEEE International Solid-State Circuits Conference Digest of Technical Papers (ISSCC)*. IEEE, 2014, pp. 10–14.

[158] L. Zeng, D. C. O'Brien, H. Le Minh, G. E. Faulkner, K. Lee, D. Jung, Y. Oh, and E. T. Won, "High data rate multiple input multiple output (MIMO) optical wireless communications using white LED lighting," *IEEE Journal on Selected Areas in Communications*, vol. 27, no. 9, pp. 1654–1662, 2009.

[159] A. A. Purwita, M. D. Soltani, M. Safari, and H. Haas, "Terminal orientation in OFDM-based LiFi systems," *IEEE Transactions on Wireless Communications*, vol. 18, no. 8, pp. 4003–4016, 2019.

[160] H. Kazemi and H. Haas, "On the performance of single side-band ofdm for band-limited visible light communication," in *2020 IEEE International Conference on Communications Workshops (ICC Workshops)*. IEEE, 2020, pp. 1–6.

[161] X. Zhang, Z. Babar, P. Petropoulos, H. Haas, and L. Hanzo, "The evolution of optical OFDM," *IEEE Communications Surveys & Tutorials*, 2021.

[162] A. Mecozzi, C. Antonelli, and M. Shtaif, "Kramers–Kronig receivers," *Advances in Optics and Photonics*, vol. 11, no. 3, pp. 480–517, 2019.

[163] ——, "Kramers–Kronig coherent receiver," *Optica*, vol. 3, no. 11, pp. 1220–1227, 2016.

[164] A. Mecozzi, "A necessary and sufficient condition for minimum phase and implications for phase retrieval," *arXiv preprint arXiv:1606.04861*, 2016.

[165] X. Chen, C. Antonelli, S. Chandrasekhar, G. Raybon, A. Mecozzi, M. Shtaif, and P. Winzer, "Kramers–Kronig receivers for 100-km datacenter interconnects," *Journal of Lightwave Technology*, vol. 36, no. 1, pp. 79–89, 2018.

[166] T. Harter, C. Füllner, J. N. Kemal, S. Ummethala, J. L. Steinmann, M. Brosi, J. L. Hesler, E. Bründermann, A.-S. Müller, W. Freude *et al.*, "Generalized Kramers–Kronig receiver for coherent terahertz communications," *Nature Photonics*, vol. 14, no. 10, pp. 601–606, 2020.

[167] T. Fath and H. Haas, "Performance comparison of MIMO techniques for optical wireless communications in indoor environments," *IEEE Transactions on Communications*, vol. 61, no. 2, pp. 733–742, 2012.

[168] M. Safari, "Efficient optical wireless communication in the presence of signal-dependent noise," in *2015 IEEE International Conference on Communication Workshop (ICCW)*. IEEE, 2015, pp. 1387–1391.

[169] F. Xiong, *Digital Modulation Techniques*. Norwood, MA, USA: Artech House, Inc., 2006.

[170] R. J. Muirhead, *Aspects of multivariate statistical theory*. New York: Wiley, 1982.